Improvement of Crash Worthiness of Structure of Three Wheeler Vehicle

Daniel Hambissa Datti

Office of Graduate Studies

Adama Science and Technology University

December, 2021

Adama, Ethiopia

Improvement of Crash Worthiness of Structure of Three Wheeler Vehicle

Daniel Hambissa Datti

A Thesis Submitted to

The Department of Mechanical Engineering

School of Mechanical, Chemical and Materials Engineering

Presented in Partial Fulfillment of the Requirement for Master of Science in Automotive Engineering

Office of Graduate Studies

Adama Science and Technology University

December, 2021

Adama, Ethiopia

Improvement of the Crash Worthiness of Structure of Three Wheeler Vehicle

Daniel Hambissa Datti

Advisor: Dr. Ramesh Babu Nallamothu

A Thesis Submitted to

The Department of Mechanical Engineering

School of Mechanical, Chemical and Materials Engineering

Presented in Partial Fulfillment of the Requirement for Master of Science in Automotive Engineering

Office of Graduate Studies

Adama Science and Technology University

December, 2021

Adama, Ethiopia

DECLARATION

I hereby declare that this Master Thesis entitled **"**Improvement of the Crash Worthiness of Structure of Three Wheeler Vehicle" is my original work. That is, it has not been submitted for the award of any academic degree, diploma or certificate in any other university. All sources of materials that are used for this thesis have been duly acknowledged through citation.

Daniel Hambissa Datti		
Name of student	Signature	Date

RECOMMENDATION

We, the advisors of this thesis, hereby certify that we have read the revised version of the thesis entitled "Improvement of the Crash Worthiness of Structure of Three-Wheeler Vehicle" prepared under our guidance by Daniel Hambissa submitted in partial fulfillment of the requirements for Master of Science in automotive engineering. Therefore, we recommend the submission of revised version of the thesis to the department following the applicable procedures.

Dr. Ramesh Babu Nallamothu	______________	____________
Major Advisor	Signature	Date

APPROVAL PAGE

The advisors of the thesis entitled "Improvement of the Crash Worthiness of Structure of Three-Wheeler Vehicle" and developed by Daniel Hambissa, hereby certify that the recommendation and suggestions made by the board of examiners are appropriately incorporated into the final version of the thesis.

Major Advisor	Signature	Date

We, the undersigned, members of the Board of Examiners of the thesis by Daniel Hambissa have read and evaluated the thesis entitled "Improvement of the Crash Worthiness of Structure of Three-Wheeler Vehicle" and examined the candidate during open defence. This is, therefore, to certify that the thesis is accepted for partial fulfilment of the requirement of Master of Science in Automotive Engineering.

Chairperson	Signature	Date
Internal Examiner	Signature	Date
External Examiner	Signature	Date

Finally, approval and acceptance of the thesis is contingent upon submission of its final copy to the Office of Postgraduate Studies (OPGS) through the Department Graduate Council (DGC) and School Graduate Committee (SGC).

Department Head	Signature	Date
School Dean	Signature	Date
Office of post Graduate studies, Dean	Signature	Date

ACKNOWLEDGMENT

First of all I would like to express my special thanks of gratitude and appreciation to my instructor and advisor Dr. Ramesh Babu Nallamothu who gave me the golden advice to do this wonderful project, and also helped me in doing a lot of research. He is always happy and willing to help me to solve confusion, patient to help me out with questions, and direct me to the final result of the thesis. On top of that, he is an easy-going and open-minded person, whom is also like a good friend to me. Without his encouragement, and guidance this project would not have materialized and finished. Finally, apart from the efforts of me, the success of any project depends largely on the encouragement and guidelines of many others. I take this opportunity to express my gratitude to the people who have been instrumental in the successful completion of this project. Specifically, I would like to thank my parents and friends who helped me a lot in finalizing this thesis.

TABLE OF CONTENTS

LIST OF TABLES

LIST OF FIGURES

ACRONYMS

ANSYS	Analysis of systems
C1, BMW	Class. Scooter Bayerische motoren werke
CAD	Computer-aided design
CATIA	Computer aided three dimensional interactive application
CRIS	Controlled rollover impact system
FEA	Finite element method
FMVSS	The federal motor vehicle safety standard
HAZ	Heat affected zone
HIC	Health insurance community
JRS	Jordan rollover system
LS-DYNA	Liver more dynamic simulation
MBD	Movable deformable barrier
TWV	Three-wheel vehicles
TST	Three wheeled scooter taxi
NACP	New car assessment program
NHTSA	National highway traffic safety administration
IGES	Initial graphics exchange specification model
IIHS	Insurance institute for highway safety
WHO	World health organization
LWV	Light weight vehicles
SID	Side impact dummy
SWR	Strength to weight ratio

NOMENCLATURE

A	Acceleration (mm/s^2)
$E_{i,}$	Internal energy (kJ)
E_{11}	Young's modulus (MPa)
E_{22}	Young's modulus (MPa)
E_d	Damping energy (kJ)
E_h	Hourglass energies (kJ)
E_{ke}	Kinetic energy (kJ)
E_s	Interface sliding (dissipated contact energy) (kJ)
F	Force of vehicles (N)
G	Acceleration Due to Gravity (m/s^2)
G_{12}/G_{31}	Shear modulus
G_{23}	Shear modulus
M	Momentum (kg.m/s)
M	Mass (kg)
SL	Shear strength
V	Velocity of vehicles (m/s)
W_{ext}	Work done by the external forces (kJ)
XC	Longitudinal compressive strength (MPa)
XT	Longitudinal tensile strength (MPa)
YC	Transverse compressive strength (MPa)
YT	Longitudinal tensile strength (MPa)
ρ	Mass density(kg/m^3)
μ_{12}/μ_{13}	Poisson's ratio (minor)
ϵ_{11C}	Strain at longitudinal compressive strength (MPa)
ϵ_{22C}	Strain at transverse compressive strength (MPa)
ϵ_{11T}	Strain at longitudinal tensile strength (MPa)
ϵ_{22T}	Strain at transverse tensile strength (MPa)
γ_{12S}	Engineering strain at shear strength (MPa)

ABSTRACT

Three wheeled motor vehicles, popularly termed as auto rickshaws or Bajaj, are gaining popularity in the commuting world due to the driving conditions prevailing all over the world. With the increase in traffic every year, the number of road accident injury risk and deaths by type of vehicles (percentage share), of which three-wheeler accidents contributes is increasing. These vehicles haven't subjected to any crash safety specifications and are not evaluated for crash worthiness. So, it is now time to consider safety features/modification of three-wheelers to reduce the grave consequences of its users. Improvements should be made on the structure of TWV in order to improve the structure strength, stability, crashworthiness, safety etc. This thesis work was aimed to improve the crashworthiness of the existing three-wheeled to minimize crash injuries. The frontal, side, rollover and rear impact collision of the existing TWV analyzed. Human dummies are incorporated in the analysis to study the response of occupants at event of crushes. Based on the analysis results obtained from the existing model of TWV then modifications are made by means of a stable frame structure, energy absorbing components and a restraint system. Then the modified TWV was analyzed under the same condition as the existing one. Software like that of CATIA was used for 3d modeling and LS-DYNA for simulation and FEM analysis. The result of the simulations shows that with the modification, 80mm more living space, 630 N reduction of impact force, and 0.8 kJ of additional energy is absorbed during side collision. The rear structure of the modified model also provided 30% more protection for rear parts. In addition, the energy absorption at the rear is increased with 1.6 kJ of energy. Moreover, the force of impact was also reduced by 22%. On another hand, during the front crush, the existing model proved better performance in terms of energy absorption and impact force. Since for the modified model, the structural deformation is less and occupants were fitted with lap belts, so the disadvantage of low absorption and high impact force during frontal crush was overcome. So it can be concluded that with the modified model, The safety and crashworthiness of the TWV was greatly improved without affecting the appearance and weight of the existing models. In addition, the safety and rate of death of passengers on the existing three-wheeler vehicles are reduced. so that the existing model of TWV should be fitted with the designed crashworthiness futures implemented on this paper.

Keywords: Crash worthiness, Finite element analysis, LS-DYNA, *Structure, Three- wheeled vehicle.*

CHAPTER ONE
INTRODUCTION

1.1 Background of Study

Transportation industry plays a major role in the economic development of many nations. The automotive or vehicle industry is facing tremendous engineering challenges over several years to meet the requirements generated by the fuel shortage, stability, crashworthiness, fuel cost, pollution control, raw material cost, and weight and costumer safety.

In meeting these challenges a wide variety of new models has been emerged or entered into the market in search for better strength and safety and fuel efficiency. As a result, three wheeled motor vehicles have been developed for the purpose of public and private transport, all over the world and in particular in developing countries. Three wheeled motor vehicles (TWV), popularly termed as auto rickshaws or Bajaj, are gaining popularity in the commuting world due to the driving conditions prevailing all over the world**,** they are typically used in India and most of the developing countries like Ethiopia . They have their front steering with one wheel similar to those of motor cycles and motor scooters and the two rear wheels are driving wheels with a differential and suspension, which are similar to those of automobiles. They are popular means of transportation in Ethiopia because of their low priced have initial purchase, small-sized, and low fuel consumption. One problem of these vehicles is the lowest strength of the frame and main structure (Eromo, 2017).

They are generally characterized by a sheet-metal body or open-frame resting and have one wheel in front and two wheels in their rear. a frontal geometry consisting of a mudguard with an attached headlamp, an upright body And windscreen, a canvas roof, and a small cabin, with a maximum velocity of 55 km/h, the driver is placed in a small cabin in the front of the vehicle and the passengers sit in the rear. The total weight of the vehicle is around 650 kg including the driver and three passengers (Milind, 2015). Three-wheel vehicles (TWV) are preferred in place of four-wheeled vehicles because they can negotiate narrow lanes; maneuverability in small turn radii road is better and they are easy to handle on crowded roads. In the case of 4-wheeled vehicles moving with a small turn radius, all wheels do not execute pure rolling motion because of geometric steering constraints. This leads to wheel skid, resistance to the turning action, and accentuated tire wear. The wheels of TWV do not skid during low-speed maneuvers. Therefore, maneuverability in small radii turns is more for TWVs as compared to 4-wheelers.These low cost vehicles will remain a major mode of travel in the South Asian region and might move on to Africa as well (Mukherjee, 2017). Even now a day, their frames are being assembled in our country, Ethiopia. Also their market demand is increasing fast (Enawgew, 2013). With the traffic increasing every, the proportion of three wheelers on the road is also increasing, in view of their maneuverability, easy drive through narrow lanes and operating cost considerations. Moreover, as the average speed of travel of these vehicles increases, but at the same time, the design objective is for a low cost, light weight and high payload, and greater acceleration capacity three wheelers, makes a concern for safety. Other than some basic safety features, three wheelers are not evaluated for crash worthiness. It may be noted that the crash regulations were mostly for car segment, and as such the regulation for a three wheeler is not in existence (Srikanth, 2009).

The TST chassis is made by the manufacturer and the body is fabricated by local body-makers. The body frame work is constructed by joining together thin-welded closed-section members, and where these are subjected to particularly large torsion and bending stresses, such as in the case of body sills, they may be reinforced by the inclusion of longitudinal partitions (Eromo, 2017), the vehicle is not subject to any crash safety specifications .Because of their low mass, TWV's will remain at a disadvantage in head on crash situations unless the law mandates crash-compatible heavier vehicles. Otherwise the number of accidents, injuries and damage caused due to the crush of this vehicle are increasing on the world. In their Global Status Report for Road Safety 2013, the World Health Organization (WHO) has ranked road traffic crashes as the eighth leading cause of death in the world, and the leading cause of death for people aged 15-29. Despite technological advances, and the introduction of many safety features into motor vehicle designs in the recent past, the number of road traffic crash deaths remains at about 1.2 million per annum globally. Of these deaths, 80% occur in middle income countries, where the majority of the road users were found to be vulnerable road users (motorized two or three wheeled vehicle users and pedestrians) (WHO, 2013).

In India it was reported that 5% of Road accidents were caused due to crushes of 3 wheeler vehicles and some studies done between July 2007 to June 2012 on traffic accident in East

Wollega, Ethiopia shows that around 12% vehicle crush accidents occurs accounts for Cycle/motor cycle/ Bajaj (Mama Gasu, 2019) and also between Akaki and Adama about 14% road traffic collisions occurs due to the collation of those vehicles (Asefa et al., 2014). Figure 1.1(a) and 1.1(b) show the accidents occurred in front of Adama science and Technology University.

(a) (b)

Figure 1.1. Front collision with pickup car and roof crush of TWV

Several hundred of motorcycle accidents analyzed at BMW also show that in considering the nature of the collision, the clear leader was the frontal collision, accounting for around 42%. Side and rear collisions at 4% and 2% may be regarded as being of relatively minor significance. Moreover the most frequently struck object in a motorcycle accident is the car, which accounts for 50% of cases (Osendorfer & Rauscher, 2001). In addition, the poor safety structure of the three-wheeler plays a major role in injuries to different part of the occupants.

Studies done In Sri Lanka and South Asian countries Shows that the occupants of three-wheelers sustain a different pattern of injuries compared to occupants of other vehicles, which cause a fatal outcome. The commonest site of fatal injury was head (78.8%), which was more common in passengers. The commonest skull fracture was on base (70.5%). The majority had brain contusion (36.4%) and subarachnoid haemorrhage (31%) was the commonest type of intracranial haemorrhage. Chest injuries directly contributed to death in 57 cases while rib fractures were seen in all such cases. Spinal injuries were seen in 41 (31%) cases where cervical spine injuries were the commonest which was seen in 30 (73.2 %) cases. In the study, 65.2% of deaths have taken place within the first hour following the incident. Out of all the fatal cases, 84.8% of the victims were trapped inside the vehicle and others (15.2%) were thrown away. Toppling of the three-wheeler was seen in 27.3% of cases (Vadysinghe et al., 2018). The inherent lack of crash protection to TW riders and passengers puts them at a higher risk for traffic-related injuries and deaths. The injuries sustained tend to be more serious in PTW users than car occupants because of this lack of protection (Global Road Safety Partnership, 2007).

So, it is now time to consider safety features modification of three-wheelers to reduce the grave consequences of its users.improvements should be made on the structure of TWV in order to improve the structure strength, stability, crashworthiness, safety etc. With increased customer demand and government regulation, more and more attention has been recently drawn to improvement of structural crashworthiness for reducing occupant fatalities and injuries. Primarily, the crashworthiness has been studied by testing, supported by analytical methods that consider simple linear strength of the material. Crash worthiness experimentation is very expensive but, with the advancement of computer hardware and software, several analytical design capabilities have evolved, providing engineers with a variety of tools to design modern vehicle structures that can meet the growing Customer demands for better crashworthiness performance (Srikanth, 2009).

Theses paper aimed to solve and improve the crashworthiness of the existing three-wheeled vehicle by remodeling in such way that crash injuries are minimized. Therefore, the first task carried out in this paper was modeling and analysis of the existing three-wheeled vehicle structure. After that the result will be interpreted and then depending on the results, the new model was created to avoid the shortcomings of the existing three wheeled vehicle. To do so, different software's like that of CATIA, for 3D modeling and LS-DYNA, for FEM analysis were used.

1.1.2 Survey on vehicle impact and safety risks in riding TWV

Liable to turn turtle, due to a shunt from another vehicle, a bump in the road, or overly rapid Caused by the drivers, with the passengers being thrown against the sparse, hard metal interior, whose sole soft surfaces are the rear passenger bench and the driver's seat. The lack of doors means that the occupants could be thrown onto the road, with the potential for serious injury, even at low speed (Elmardi Suleiman Khayal, 2019).

It also poses a significant risk to pedestrian safety due to the poor impact energy absorption of its structures and materials (These vehicles run at maximum speeds of 50 km/h. Impact speeds are typically of the order of 25-30 km/h. As a result sometimes the severities of injuries caused are low. This is in spite of the fact that typically the TSTs are not equipped with seat belts. A different paradigm was hence needed to augment safety in these vehicles. Computer simulations suggest for injury evaluation, thorax, head, and knees are areas of concern. Additionally, soft tissue injuries in abdominal region could be possible in severe crushing events. To cope with the increasing demands of the customer, the modern auto rickshaws are driven at higher speed and hence safety is a concern, as accidents can be fatal (Anoop Chawla et al., 2001). In reality, vehicle collisions are unique dynamic events where the vehicle may collide with another vehicle of similar or different shape, stiffness and mass; or it may collide with another stationary object. Some of the three wheeler auto rickshaws collisions are classified and shown below.

Frontal Collision: A frontal collision is one where the front ends of two vehicles hit each other. This has the potential for the highest crash energy. In the case shown in Figure 2.1, the vehicle is hit through its front wheel steering system.

Figure 1.2.Frontal Impact (Srikanth, 2009).

Frontal Offset Impact: A typical frontal offset impact for an auto rickshaw is shown in the Figure 2.2. Due to the impact, the front cowl along with the floor has intruded into the driver leg room compartment.

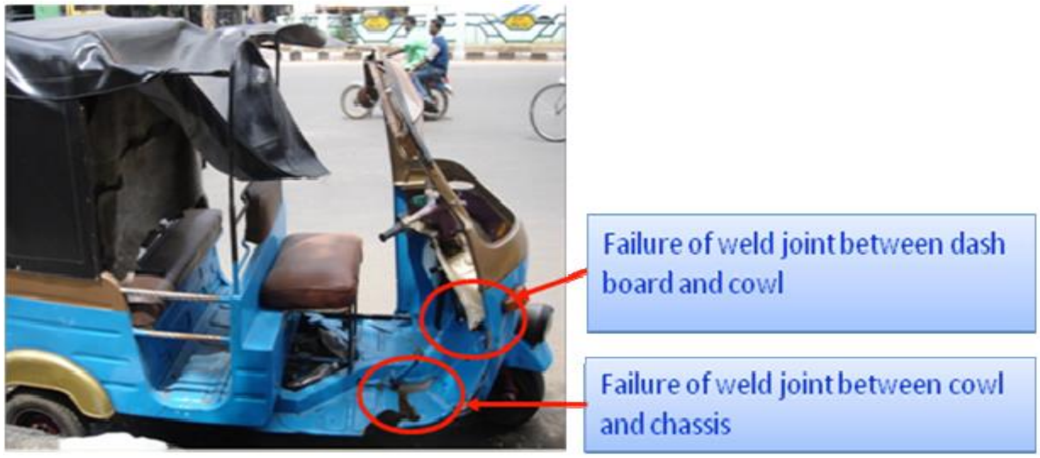

Figure 1.3.Frontal offset impact (Srikanth & Prakash, 2009).

Rear impact collisions: Occur when a slower moving or stationary vehicle is struck from behind by a vehicle moving at a faster rate of speed. For cases of rear impact, the seats should be designed with high back rests and integrated head rests to help keep the head, neck and upper torso in safe alignment during the dynamics of a crash.

Side Impact: Side impact mechanisms come into play when the vehicle is involved in an intersection collision or when the vehicle veers off the road and impacts sideways utility pole, tree or other obstacle on the roadside.

Rollover Impact Analysis: A rollover is a type of vehicle crash in which a vehicle tips over on to its side or roof. Rollovers have a higher fatality rate than other types of vehicle collisions Vehicle rollovers are divided into two categories: tripped and un-tripped. Tripped rollovers are caused by forces from an external object, such as a curb or a collision with another vehicle. Un-tripped crashes are the result of steering input, speed and friction with the ground.

1.2 Statement of problem

With the increase in traffic every year, the proportion of three wheelers on road is also getting increased. The number of road accident injury risk and deaths by type of vehicles (percentage share) of which three-wheeler accidents contributes is increasing. As it is stated In Global Status of the World Health Organization (WHO), most of the traffic accident deaths, in middle income countries are due motorized two or three wheeled vehicle. Most of the time that is due to the instability, structural strength, and deformation characteristics of the TWV body under crash. Most of the passive safety standards for the passengers and drivers which are compulsory for any vehicle structure crashworthy are not well designed and implemented on the existing three wheeler vehicle model. The TWV chassis is made by the manufacturer and the body is fabricated by local body-makers. The vehicle is not subjected to any crash safety specification. As result, the existing TWV does not fulfill this basic safety requirement as other vehicles. So, the structure or crashworthiness of existing three wheeler vehicle models should be modified in such a way that the damage and injures which are occurring due to different crush or impact condition were minimized.

1.3 Objectives

1.3.1 General objective

The general objective of this thesis work is to improve the Crashworthiness of three wheeler vehicle.

1.3.2 Specific objectives

In order to achieve the main objective of this thesis, the following activates s can be done sequentially.

- To study the structural details of the existing three-wheeler (auto rickshaws) Vehicles.
- To model and analyze the structure of existing three-wheeler using finite element methods (FEA)
- To modify the structure with crashworthiness features and analyze it.
- To compare the crashworthiness of the improved structure with that of the existing vehicle structure.

1.4 Significance of the Study

This work is expected to:

- Improve the strength of the vehicle.
- Reduce the rate of accidents i.e. rate of injures and death.
- Improve the safety and comfort of the passengers.
- Provide premises for further study

- Increase the market acceptance of TWV

Beneficiaries: TWV owners, drivers, Passengers, Automobile industries, Companies, Society, and Country as a whole.

1.5 Scope of the study

Theses study were aimed to solve and improve the crashworthiness of the existing three-wheeled vehicle by remodeling in such a way that crash injuries are minimized. Here the intention was achieved by the means of a stable frame structure, energy-absorbing components and a restraint system. The frontal, side, rollover and rear impact collision of TWV was analyzed. The analysis incorporate human dummies to study the response of the occupants at events of crush. It also includes the modification of the body structure to improve crashworthiness. To accomplish these goals CATIA software will be used for modeling, and simulation and strength analysis will be done by FEA (Finite element analysis) and LS-DYNA. The dynamic analysis of TWV using LS-DYNA software is presented, based on the obtained values some alternative modifications were proposed in order to increase the collision behavior and toughness of the body structure without affecting the total weight and stability. The scope of this work includes only Bajaj three wheeler structures. Other three wheelers vehicles were not included. In addition to this the injuries to occupants were not analyzed.

1.6 Limitation

Through conducting this study the following challenges were encountered;

- Due to high cost of experimental crashworthiness test, this paper focus on the numerical aspects of TWV crashworthiness improvement.

- The usage of numerical method also required a high performance computer. Since it was very challenging to get such kind of machines, so with the use of low performance computer the required results were obtained by waiting for more than a week.

1.6 Organization of the study

This thesis is organized into six chapters. The **First Chapter** introduce the background of the study which mainly focus on giving information about three wheeler vehicles, and stated the statement of the problem, objective, significance, limitation and scope of the thesis. Comprehensive review on previous researches works related to safety issues of vehicles were included in chapter two. The pros and cons of previous researches were stated and it also includes the gaps observed from those researches. **Chapter Three** elaborates on the materials and methodology of the work including data collection. **Chapter Four** presented the detail of the modeling and analysis procedures used for analyzing the existing and modified TWV. It also described the methods and material used for developing the safety development of TWV. In **Chapter Five,** the result of different computational simulation were imported and discussed. It shows the result and discussion of the modifications, existing and modified model of TWV. **Chapter Six** presents the major conclusions of the work conducted in this thesis, highlighting the findings and concluding with recommendations for further work.

CHAPTER TWO
LITERATURE REVIEW

2.1 Vehicle crashworthiness

From an engineering perspective, crashworthiness is the ability of the vehicle to prevent occupant injuries in the event of an accident. It measure of the ability of a structure and any of its components to protect the occupants in survivable crashes. Crashworthiness connotes a measure of the vehicle's structural ability to plastically deform and yet maintain a sufficient survival space for its occupants in crashes involving reasonable deceleration loads (Georgiou, 2018). It is one of the core topics in the passive safety of vehicles and plays an important role in the condition that the impact cannot be avoided. Generally, the analysis of crashworthiness is based on the related crash responses, i.e. the displacement, velocity and acceleration, of critical parts of a vehicle in full car crash tests (Waghmare, 2013).

2.1.1 Crashworthiness Requirements

Some of the general structural crashworthiness requirements are;

- Sufficiently stiff in bending and torsion for proper ride and handling.
- Minimize high frequency fore-aft vibrations that give rise to harshness.
- Accommodate for a range of occupant sizes, ages, and crash speeds for both genders.
- Deformable, yet stiff, front structure with crumple zones to absorb the crash kinetic energy.
- Deformable rear structure to maintain integrity.
- Properly designed side structures and doors to minimize intrusion.
- Strong roof structure for rollover protection.
- Properly designed restraint systems that work in harmony with the vehicle structure.
- Accommodate various chassis designs for different power train locations and drive configurations.

Crashworthiness mainly depends on the position, cross-section and material of the intrusion barrier (Kumar et al., 2019).

2.2 Various Crash Test

A crash test is a form of destructive testing usually performed in order to ensure safe design standards in crashworthiness and crash compatibility for various types of vehicle like small,medium and heavy duty and its related systems and components for the sake of getting the performance of the vehicle under the different conditions of crash at different angles with taking certain object like rigid wall, cables specially three-strand cable, concrete barriers, guardrail systems etc., (Yadav & Pradhan, 2014). It will be performed either by numerical simulations or experimentally.

There are different types of crash test, in Frontal Impact test, a fully front structure of the vehicle collides with another object like another vehicle, rigid wall etc. at a given speed. On another hand In Offset Test**,** only a part of front portion of the vehicle strikes on some barrier usually a Vehicle at a given speed. In addition, in Small Overlap Test only a small portions of the vehicle strikes an object like tree, pole or if a car were to clip another. This situation loads a maximum value of force into the vehicle structure at a particular given speed. This test usually comprises of 15% to 20% of the front structure (Yadav & Pradhan, 2014). More over in side Impact Test sometimes the vehicle is in static condition or in dynamic and another vehicle or an object collide at the side surface having some speed. On another hand in Roll-Over Test a vehicle is in rollover condition having certain angle by which they tests ability (specifically the pillars holding the roof) to support itself in a dynamic impact. It is also done for the static crash testing condition. There are also Roadside Hardware test which is performed to ensure that the crash barriers and crash cushions will protect vehicle occupants from roadside hazards. There is also old versus new test which is done between old car against a new car and the big car against a small car; it is performed to show the advancements in crashworthiness.

Among this the most common types of crash tests shown on Figure 2.3, Front impact test, Front offset crash test, Side impact test and Roll over test. Among this the most common types of crash tests are, Front impact test, Front offset crash test, Side impact test and Roll over test (Ambati et al., 2012). Safety organizations have different methods of testing vehicles before assigning their ratings. The two main players are the National Highway Traffic Safety Administration (NHTSA) and the Insurance Institute for Highway Safety (IIHS) (Alex Ogana, 2009).

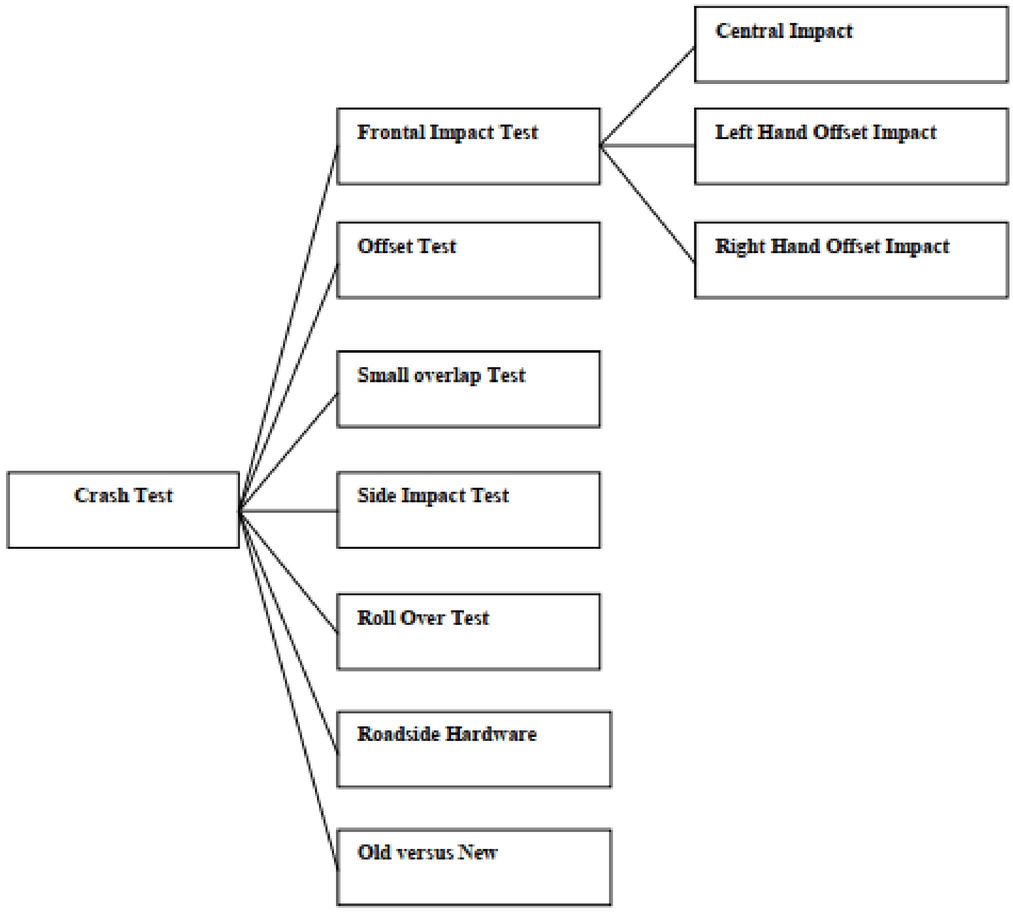

Figure 2.1. Classification of various crash test used in testing (Ambati et al., 2012)

2.2.1 Head on full frontal fixed barrier

The Full Frontal Fixed Barrier Crash test (or Rigid Barrier test) represents a vehicle-to-vehicle full frontal engagement crash with each vehicle moving at the same impact velocity. The test is intended to represent most real world crashes (both vehicle-to-vehicle and vehicle-to-fixed object) with significant frontal engagement in a perpendicular impact direction (Hollowell et al., 2009).

NHTSA's front-crash test accelerates a car straight into a rigid barrier at 35 mph, with the entire width of a vehicle's front end hitting the barrier. Instrument-bearing, seat-belted crash-test dummies in the two front seats record the level of crash forces on the head, neck, chest, and legs. Those measurements correlate with injury, but formerly only the head and chest results formed the basis of the star rating. Individual star ratings are assigned to the driver and the front passenger. Some automotive experts have criticized NHTSA's full-frontal, rigid-barrier test as unrealistic because such head-on crashes into a flat, solid wall are relatively rare. Others argue that real-world or not, flat-barrier testing is a good way to gauge the effectiveness of the restraint systems, primarily the safety belts and air bags (NHTSA Crash Test - Consumer Reports, 2021).

The Insurance Institute for Highway Safety (IIHS) front-crash tests are quite different from NHTSA's in that they're designed to highlight the vehicle's structural integrity, as well as restraint performance. Vehicles are rated as Good, Acceptable, Marginal, or Poor based on what happens to vehicle structure, as well as forces on the dummies. IIHS now conducts two series of front-crash tests, one that engages 40 percent of a vehicle's front and a newer test, inaugurated in 2012, that uses a smaller overlap, engaging just 25 percent of the car's front. Both simulate what would happen if two cars of the same weight and type crashed head-on, partially overlapping. The older test, with the 40-percent offset, engages the portion straight ahead of the driver. The newer test is more like a head-on crash where two cars hit left-headlight to left-headlight or a single-vehicle crash into a fixed object like a utility pole or tree. These are very different from the full-width crash NHTSA uses.

Both the IIHS front-crash scenarios use an impact speed of 40 mph instead of 35 mph; and only the left front of the car hits the barrier. The 40-percent overlap test uses a deformable barrier while the 25-percent overlap test uses a rigid barrier (NHTSA Crash Test - Consumer Reports, 2021). In this research by keeping the standards and regulation in mind, it has been decided to investigate car crashing into TWV. The differences that would appear between the Vehicles crashing into rigid wall and a rigid truck are;

- The truck was either flexible, that means that it could be deformed during the crash, or the truck was rigid and therefore not deformed during the crash.
- Also, the truck was in some cases free to be pushed backward by the car during the crash, simulating a 12 tones truck. In other simulations, the rear of the truck has been fixed in order to simulate an infinitely loaded truck since it was restrained from behind (Lefer & Rebolloso, 2012).

2.2.2 Side impact test standard

Side impact crashes are the second most common reason for vehicle passenger deaths after frontal crashes. To reduce the number of passenger deaths occurring in accidents, several crash

Tests have been established to ensure safety standards of cars and encourage automobile manufacturers to make safety improvements. The Federal Motor Vehicle Safety Standard (FMVSS) 214 Side Impact Protection was enhanced in 1990. In 1997, the National Highway Traffic Safety Administration (NHTSA) introduced a side impact crash test with a Moving Deformable Barrier (MDB), representing the front end of a car from the early 1980s, within the New Car Assessment Program (NCAP).

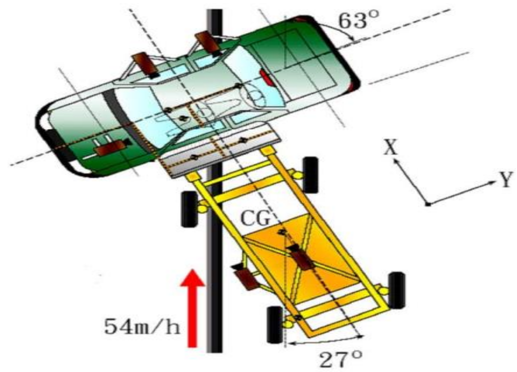

Figure 2.2. The test setup of FMVSS 214 (Sheldon, 2018).

In this test, a MDB with a mass of 1,368 kg hits a stationary vehicle at a 90° angle with a crabbed wheel angle of 27°. The velocity of the MDB is 54 km/h, see Figure 2.4 .The deformable part of the barrier is 838 mm high, measured from the ground (Sheldon, 2018). Such a scenario mimics what could happen if you were hit on the side at an intersection. Individual side-impact star-rating scores are assigned to the driver and left-rear passenger. For pre-2011 models, only a chest-injury measure dictated the score. For 2011 and later models, the score factors in head, chest, abdomen, and pelvis data for the driver and injury to the head and pelvis for the rear-seat passenger (NHTSA Crash Test - Consumer Reports, 2021).

As there is a much greater risk of head injuries from impacts with taller bullet vehicles, the Insurance Institute for Highway Safety (IIHS) decided to start its own side impact crash test in 2003 with a modified MDB as show on Figure 2.5. In the IIHS side impact crash test, the modified MDB hits the driver side of a stationary target vehicle at 50 km/h. The IIHS MDB has the geometry, shape, and height of a typical midsize SUV. The mass of the IIHS MDB (1,500 kg) is comparable to a small SUV or midsize car. The deformable part of the barrier is 1,138 mm high, measured from the ground. The IIHS side impact rating is based on different aspects, including injury risk assessment, restraint system, and structural performance (Sheldon, 2018).

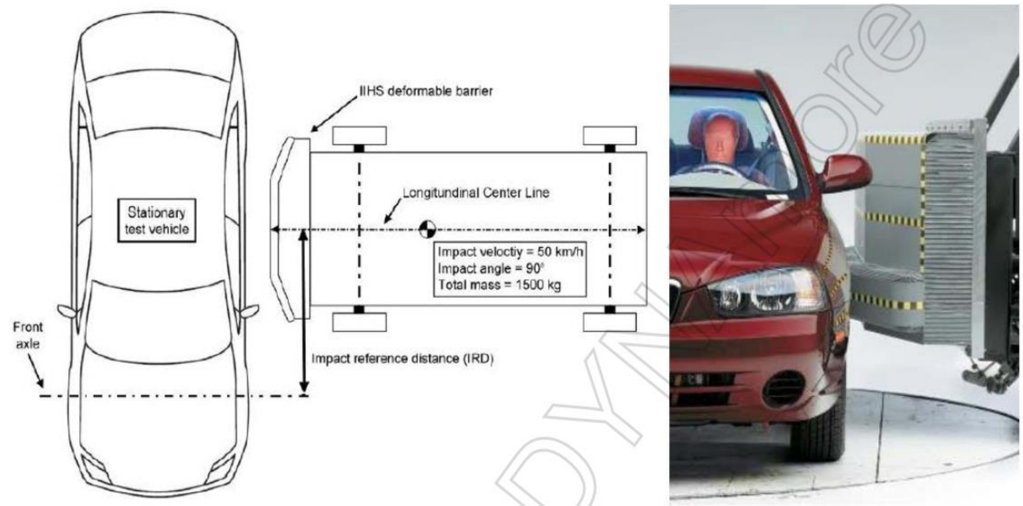

Figure 2.3. IIHS side impact configuration (NHTSA Crash Test - Consumer Reports, 2021).

The IIHS side-impact test is more severe than NHTSA's. The IIHS bases its scores on head, neck, chest, abdomen, pelvis, and leg injury. The two dummies in the IIHS side-crash test represent a small adult female or a 12-year-old adolescent. One is the driver, the other a left-rear passenger (NHTSA Crash Test - Consumer Reports, 2021).

2.2.3 Lateral NCAP Pole Test

This test is done to simulate what happens if a driver slides off a road and crashes into an object such as a utility pole. NHTSA and IIHS Crash Test Safety Ratings Explained A vehicle in the NCAP side pole test is sent into a fixed, rigid pole 254 mm (10 inches) in diameter, at a speed of 32 km/h (20 mph). Figure 2.6 (a) shows the pole. A 5th percentile female dummy is positioned in the front seating position (Singh, 2012). The complete test set-up is illustrated in Figure 2.6 and Figure 2.7.

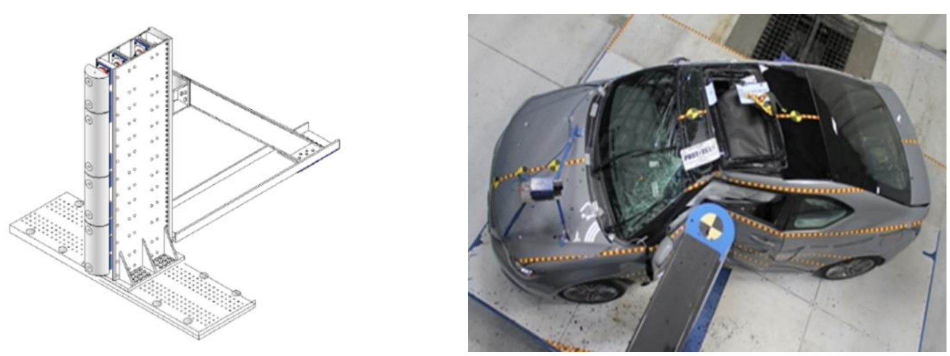

(a) (b)

Figure 2.4. Fixed, rigid pole, used for NCAP pole test and experimental test

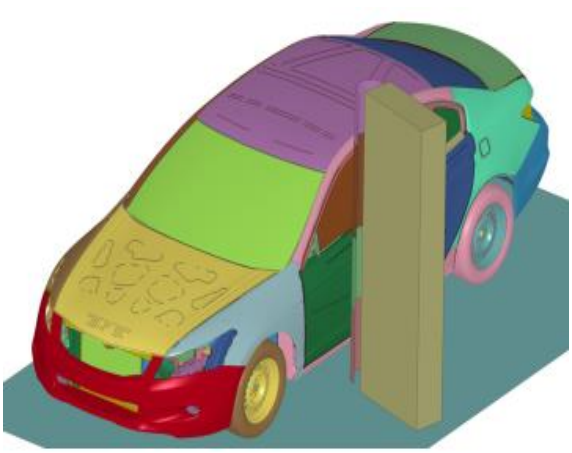

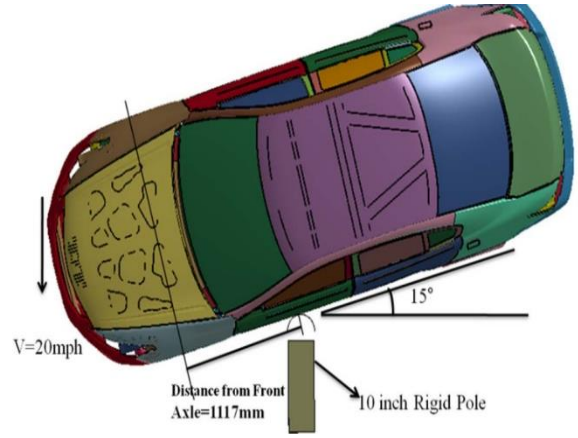

(a) (b)

Figure 2.5. The isometric and top view of the NCAP FEA method used for side pole test

Figure 2.6 (a) shows the pole used for NACP side pole test and Figure 2.6 (b) implies the experimental set up. Whereas Figure 2.7 show the FEA method for NACP side pole test with side and top view.

Procedure

In this test the LWV 1.2 impacts the rigid pole laterally at a speed of 32 km/h such that its line of forward motion forms an angle of 75 degrees with the vehicle's longitudinal axis, simulating areal-world crash in which the vehicle hits a tree while sliding on the road. The rigid pole is vertically oriented metal structure with:

- Diameter of 254 mm.
- Beginning no more than 102 mm above the lowest point of the tires on the struck side of the fully loaded test vehicle.
- Extending at least 150 mm above the highest point of the roof of the test vehicle.
- The direction of vehicle motion is such that the pole is always aligned with the CG of the head of the driver (Singh, 2012).

2.3.4 Rollover test standards

Rollover accidents of a vehicle are one among the most occurring accidents that we see in our daily lives.it is considered to be a long-duration event compared to other accidents such as with frontal, rear or side impacts.as a result the passengers experience major injuries like neck, head and spine injuries for a longer period of time (Cassia et al., 2015). The rollover accidents are characterized by deformation of the roof and its supporting structures. So, to reduce the injuries and major the car must have high strength to resist the crush force. Strengthening of the roof is suggested as an appropriate countermeasure for such injuries (V.Teja, J.Goutham raj, 2019). Generally during rollovers, the injuries are caused by occupant ejection and roof crush.

Occupant ejection is due to the movement of the occupants and would be reduced by using seat belt use, improved side curtain air bags and advanced window glazing. The roof crush due to the low strength and high deformation of the vehicle roof into an occupant compartment and could be reduced by a stronger roof structure. The need for stronger vehicle roof structure led to creation of the vehicle safety standard for roof crush resistance (Kweon, 2020). The purpose of the standard is to reduce deaths and injuries due to the crushing of the roof into the passenger compartment in rollover accidents.

2.2.4 Roof Crush Resistance Standard and Rating

To improve occupant safety in rollover accidents Efforts have been continuing by both Federal and private institutions. The standards and their relevant information are summarized here as follows.

A) Controlled Rollover Impact System (CRIS)

It involves a semi-tractor and trailer at the back of which is mounted a fixture holding the vehicle as shown in Figure 2.8. The fixture can be adjusted to cause the vehicle to drop from a given height giving it a defined vertical velocity. However, there is no direct measurement of the horizontal or vertical speed of the vehicle at impact. The traveling speed of the semi-tractor/trailer controls the horizontal speed of the vehicle at impact. Figure 2.9 shows the FEA model of a vehicle with dummy for CRIS (Friedman & Hutchinson, 2009) .

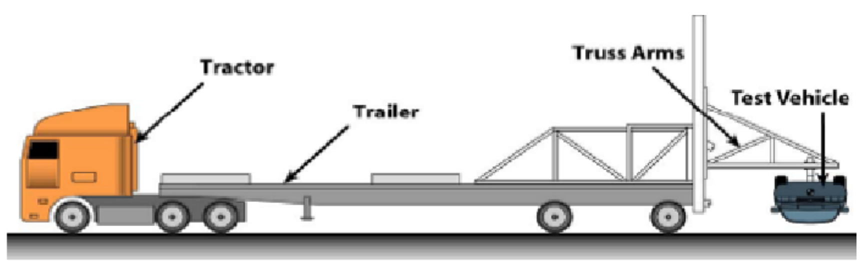

Figure 2.6. Schematic of CRIS (experimental) (Friedman & Hutchinson, 2009).

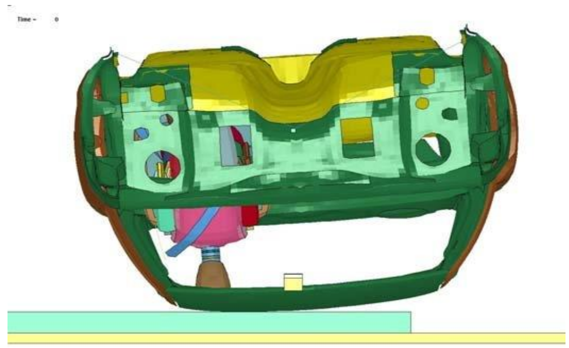

Figure 2.7. FEA model for CRIS (Friedman & Hutchinson, 2009).

B*) Jordan Rollover System (JRS)*

The system consists of a pneumatic dynamic impact sled upon which is mounted a platform representing the road surface. The pneumatic system drives pistons connected to cables that move the platform and cause the vehicle to rotate. The rotation rates are controlled through a pulley system connecting the pistons to the rotational drive system; the pistons are disconnected from the rotational drive system at impact allowing the vehicle to roll freely during impact. Figure 2.10 (a) and (b) shows, the actual laboratory test and FE test model. As the vehicle is rotated by means of pneumatic system, a roadway segment is run underneath and the vehicle is dropped so that its roof strikes the road as it would in an actual rollover. After both sides of the roof have impacted the roadway, the vehicle is then lifted by the spit so that it will sustain no further damage to the vehicle sides or undercarriage (Friedman & Hutchinson, 2009).

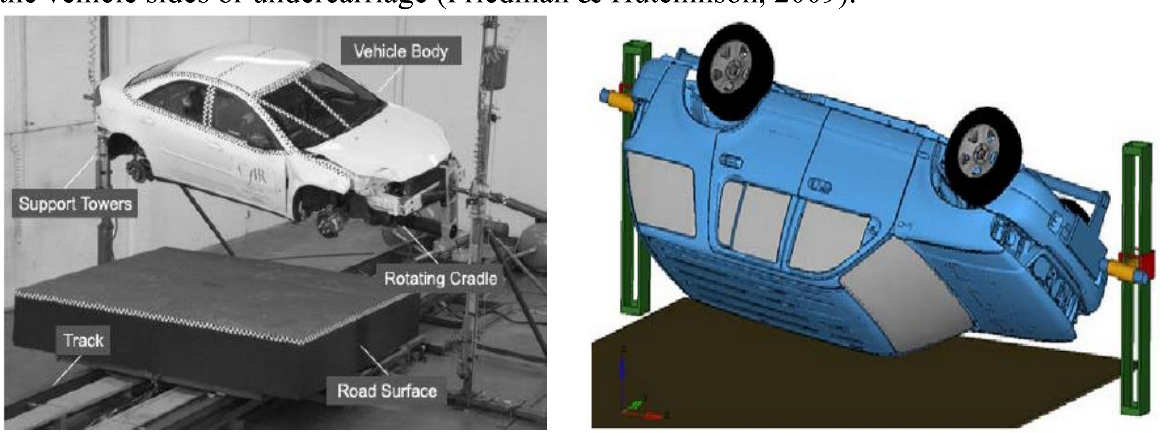

(a) (b)

Figure 2.8 . The actual laboratory test and FE test model (Friedman & Hutchinson, 2009)

C) Federation of Motor Vehicle Safety Standards AND IIHS No.216 (FMVSS 216)

FMVSS No. 216a is most common are which regulates minimal roof strength design in

Vehicles. To FMVSS No. 216a to encourage manufacturers to improve roof designs. The standards and their relevant information are summarized here as follows.

FMVSS No. 216a

The first standard for testing vehicles strength at event of rollover accident is called FMVSS no. 216a (Federal motor vehicle safety standard). Prior to FMVSS No. 216a, it is called the FMVSS 216, in the early 1970s. The code determines the strength of passenger car based on the ratio of the vehicle gross weight and resistance force (SWR). The rating was applicable for (GVWR) of 2,722 kg (6,000 lb.) or less and the SWR specified in FMVSS No. 216 was 1.5, meaning that a passenger car roof should withstand a load of at least 1.5 times the vehicle unloaded weight. The standard has been amended several times since its inception, such as extending to multipurpose passenger vehicles (MPV) and modifying the quasi-static testing procedure and then finally it has been upgraded to FMVSS No. 216a which is the most noteworthy recent upgrade in 2009. Some of the major changes in the 2009 upgrade includes:

- Raising the SWR threshold of 1.5 to 3.0 for passenger cars.
- Changing from a one-sided to a two-sided test.
- Expanding to heavier passenger vehicles (GVWR greater than 6,000 lb to 10,000 lb or less) with the SWR threshold of 1.5.
- Introducing headroom maintenance criteria.

FMVSS No. 216a became final on April 30, 2009, and laid out a multi-year phase-in compliance requirement beginning in 2012 through 2015, implying that full compliance should be satisfied for all noted vehicle fleets with the model year of 2016. One of the important requirements specified in the standard involves roof strength measured in the strength-to-weight ratio (SWR). The SWR is a unit less metric measuring vehicle’s roof strength by its own weight. For example, a 3.0 SWR means that a vehicle’s roof structure is capable of withstanding 3.0 times the vehicle’s unloaded weight under the test conditions specified in FMVSS No. 216a.

Non-Federal Safety Rating

The Insurance Institute for Highway Safety (IIHS) introduced a rating system for vehicle roof strength in 2009, based on the peak SWR from a roof crush test similar to what FMVSS No. 216a specifies. There are several differences between the IIHS and FMVSS No. 216a tests, Such as

- The number of sides to be tested (i.e., one side for IIHS and both sides for FMVSS No. 216a)
- No headroom maintenance criterion in IIHS's test.

The roof strength rating of IIHS falls into one of the four levels based on the peak SWR (good, acceptable, marginal, and poor) as shown on Figure 2.11. The highest rating, "Good," requires at least an SWR of 4.0 (IIHS, 2016). IIHS has been testing about 20 to 30 new vehicles for roof strength and other safety characteristics each year to promote safer vehicle designs (Kweon, 2020). This standard does not apply to school buses and passenger cars that conform to the dynamic rollover test requirements of FMVSS 208, occupant crash protection, and 5.3 by means that require no action by passenger car occupants. It also does not apply to convertibles, except for optional compliance with the standard as an alternative to the rollover test requirements in 5.3 of FMVSS (Patil et al., 2018).

The test setup condition for FMVSS and IIHS ratings

The basic setups followed in both standards are the same and presented on the following section as follow. Figure 2.12 shows the testing procedure. As it is shown the vehicle is fixed to the ground and rectangular block with 762 millimeters by 1,829 millimeters.

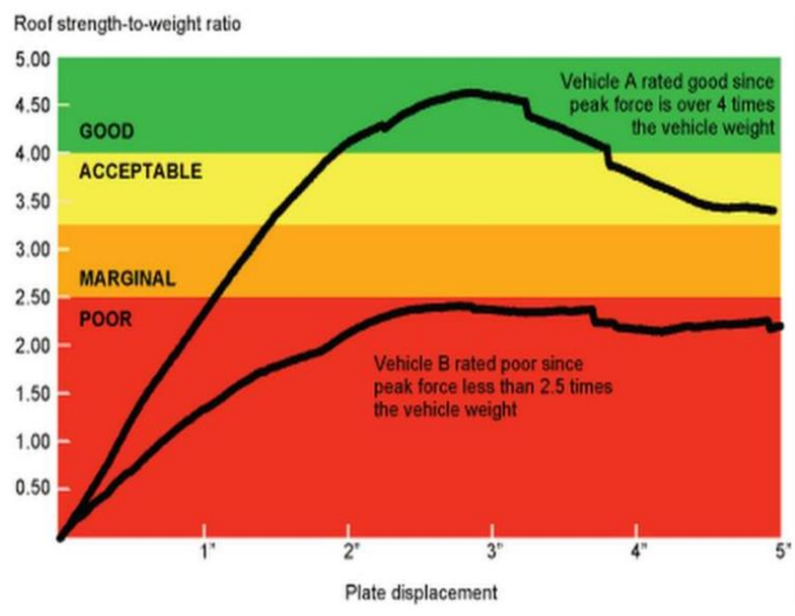

Figure 2.9. IIHS rating system for strength to ratio(SWR) (Patil et al., 2018)

It is placed on roof top with 25° roll angle and 5° pitch angle. The rigid rectangular block or loading device is allowed to move 127 millimeters to achieve the specified resistive load when applied to the forward edge of a vehicle's roof. This procedure is named as quasi-static test where load is applied to frontal edge of roof structure to determine whether 1.5 times of vehicle weight can be tolerated within 127 mm displacement of the load device (Cassia et al., 2015).

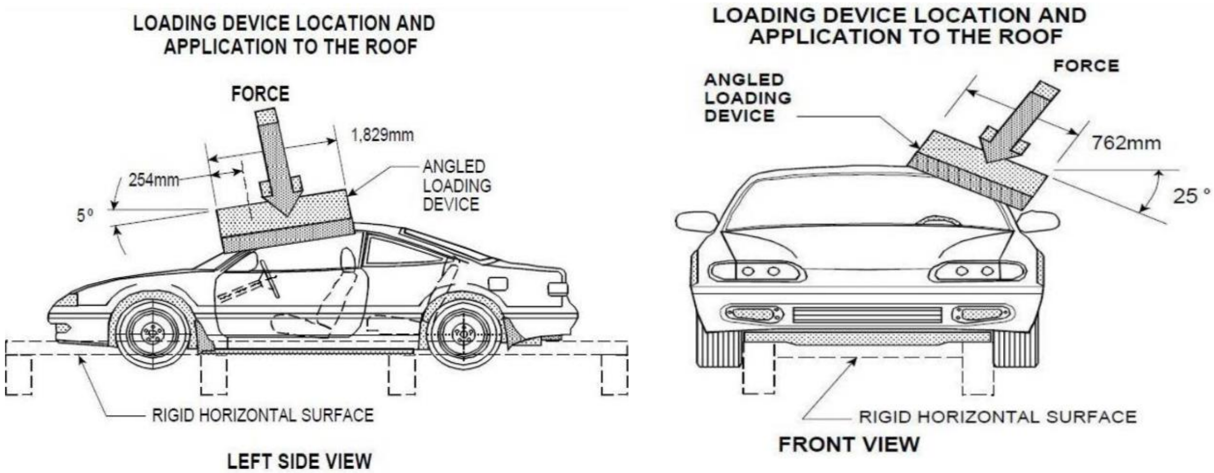

Figure 2.10. Schematic view of test set up for FMVSS 216 (Jeong et al., 2008)

Figure 2.12 shows the IIHS roof crush setup used according to the above procedure, Figure 2.13 (a) shows the FEA method and Figure 2.13 (b) indicates the experimental method used.

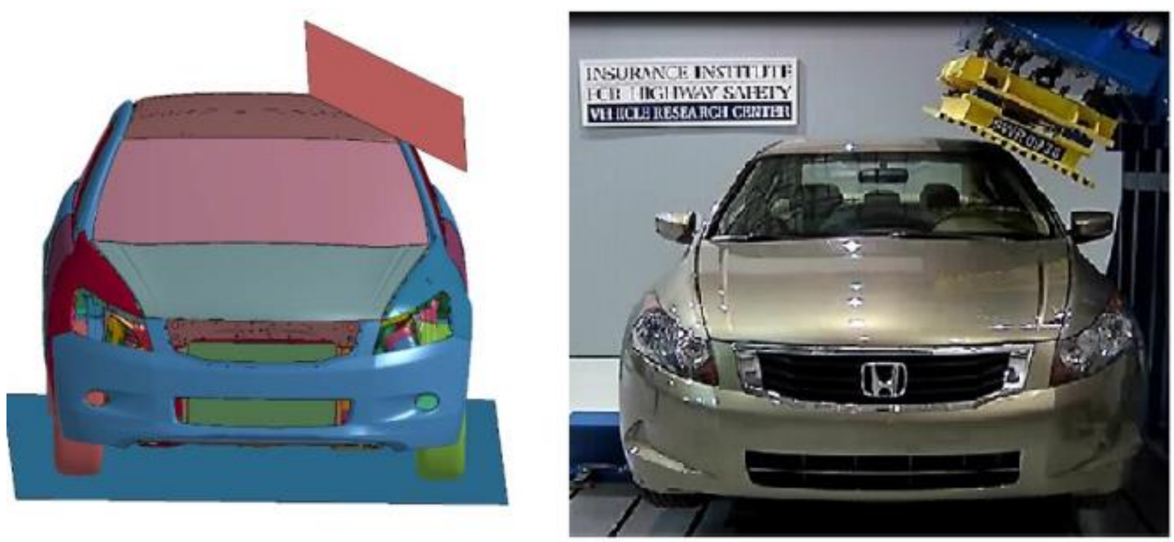

(a) (b)

Figure 2.11. The IIHS roof crush setup FOR FEA and experimental method

Roof Crush Resistance

One measure of vehicle roof strength is the SWR, calculated from results of a laboratory roof crush test. The roof crush test pushes a metal plate against a side of the forward edge of vehicle's roof at a constant rate to a certain distance and the force applied to the metal plate is continuously recorded throughout the test. An SWR value is calculated by dividing an applied force by an unloaded vehicle weight as follows,

$$\mathrm{SWR} = \frac{\text{Applied Force}}{\text{Unloaded Vehicle Weight}} \tag{2.1}$$

Where: applied force and unloaded vehicle weight are measured in the same unit such as Newton (N), or pounds-force (lbf) and, thus a calculated SWR is unit less.

The SWR is devised to represent how much a vehicle's roof structure could withstand its own weight reflecting a rollover event in a crash. A larger SWR value indicates a stronger roof and less occupant compartment intrusion. A vehicle with a larger SWR is more likely to maintain an occupant's survival space when a vehicle rolls, resulting in a higher survivability and occupant injuries that are less serious. At each crush test continuously pushing the plate, many SWR values can be calculated from the tested vehicle using Equation 2.1, one for each applied force being recorded. Among those SWR values, the maximum SWR value corresponding to the largest applied force occurring within the *5 inches* of platen travel distance is the peak SWR (see Equation 2.2). The peak SWR corresponds to the maximum resistance capacity of a vehicle's roof structure against crushing and thus represents the strength of a vehicle's roof.

$$\mathrm{SWR} = \frac{\text{Maximum Applied Force}}{\text{Unloaded Vehicle Weight}} \tag{2.2}$$

Where: the maximum applied force is obtained within 5 (127mm) inches of the platen displacement. The peak SWR is the officially designated test result for any vehicle (Kweon, 2020).On this paper the standard used for rating the roof strength of TWV is IIHS. All the set ups and the procedures are according to the standards mentioned in IIHS.

2.2.5 Rear end collision

A rear-end collision, or simply a rear-end is a car crash scenario in which a vehicle collides with another vehicle in front of it. Rear crashes are the third most frequent type of accidents

Standing behind the front and side collisions in the United States (NHTSA, 2016). Though common, not many rear-impact crashes are fatal. But they do cause many injuries, especially whiplash trauma to the neck injuries are the most common type of injuries to the occupants in rear-end collision. Thoracic injuries are far less common in rear-end collisions, and so are lumbar injuries (Vedantam, 2018). Rear-end collisions can occur in four types as shown in Figure 2.14 (NHTSA, 2015). It can be observed that the most occurred rear-end crash is the rear offset collision. Coincidentally, The FMVSS 301R regulation also uses a similar scenario for the test where the occupant's response can be studied.

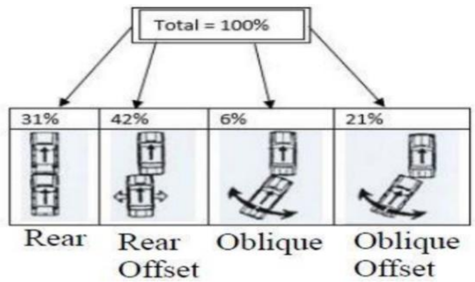

Figure 2.12. Rear crush distribution (NHTSA 2015).

Federal Motor Vehicle Safety Standard (FMVSS) No. 301 specifies a rear-impact test. The rear-impact test is designed to promote the crashworthiness of the body structure and fuel tank. In this test a moveable deformable barrier (MDB) impacts at 80 km/h (50 mph) into the rear of a stationary vehicle with an overlap of 70% as shown in Figure 2.15. The MDB used in the rear-impact test weighs 1380 kg (Singh, 2012).

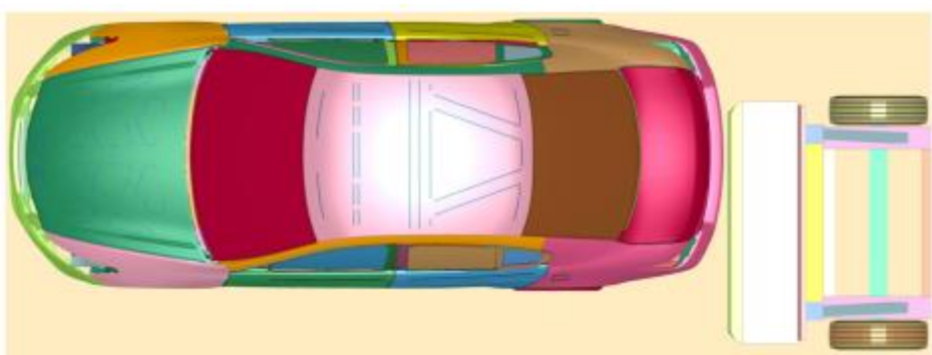

Figure 2.13. FE Test setup for FMVSS No.301.

The IIHS evaluates rear impacts with physical inspections and crash testing. The crash test, which is conducted with the vehicle seat attached to a moving sled, simulates a rear-end crash about equivalent to a stationary vehicle being struck at 20 mph by a vehicle of the same weight. The key to rear-impact protection is head-restraint design. Restraints need to be high enough and positioned close enough to the back of the head to cradle an occupant's head in a rear collision. those restraints that are clearly too low or ill-designed automatically receive a poor rating from IIHS, while those with a chance of providing decent protection are crash-tested (Alex Ogana, 2009).

2.3 Passenger and driver model

The diverse group of dummies helps us to understand and measure the human body's movement during a crash, and see how it fares with various vehicle safety features. A lot of research goes into these dummies before they are put into use. Each of us differs in size and weight, so each crash test dummy is designed differently too. Development. In 1949, the first dummy was used in the air force; after years of development, the dummies have been widely used as substitutes for human body in car crash tests. According to the type used for collision, the dummies can be categorized as frontal impact dummy, side impact dummy, and rear impact dummy. Figure 2.16 lists crash test dummy types and their application conditions. In order to better understand the development of mechanical dummies, the following describes in detail the development process of each series of dummy

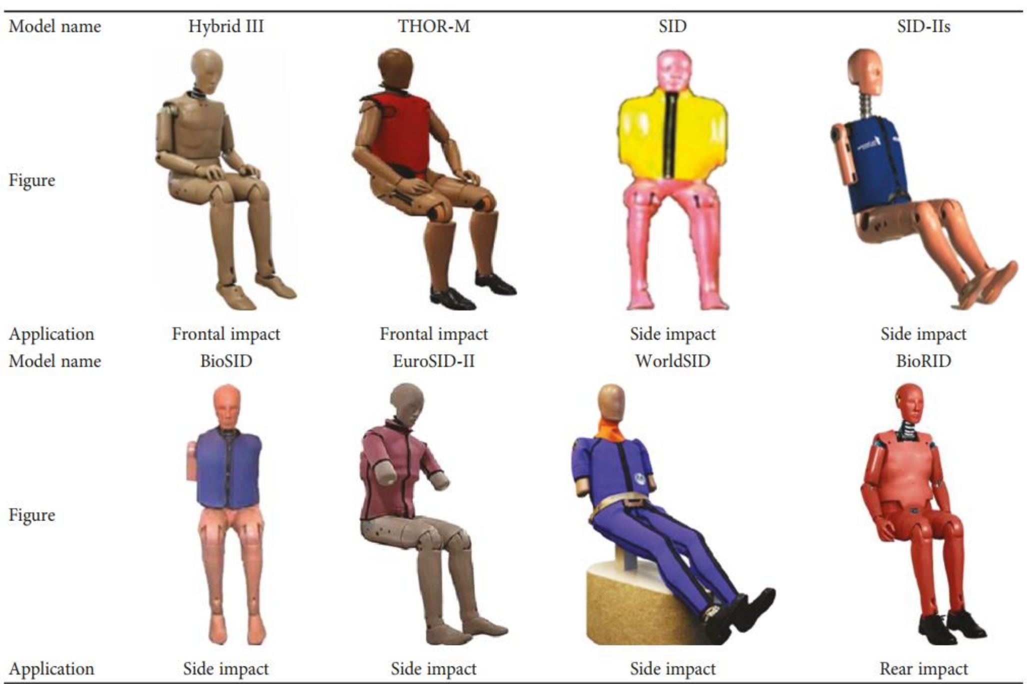

Figure 2.14. Dummies and their application (Haslegrave, 1974)

2.3.1 Frontal Impact Dummy

In 1971, ARL and Sierra collaborated to develop the Hybrid I dummy. This dummy can be used to measure head and chest Tri axial acceleration and femur load. After that many parts had been redesigned by different organization to achieve better results: the head/neck interface was more anatomical, the improved neck mount model facilitated the reproducibility of head kinematics, the self-centering shoulders and improved shoulder load distribution yielded more repeatable responses, and lower torso with butyl rubber lumbar spine improved overall repeatability. Nowadays, the Hybrid III dummy has been widely used in the field of car crash tests, including the 50th adult male dummy, the 95th adult male dummy, and the 5th adult female dummy. The Hybrid III 50th adult male dummy is currently the most widely used dummy in various countries. The Federal Motor Vehicle Safety Standard (FMVSS 208) clearly stipulates that the Hybrid III 50th dummy is designated as frontal impact dummy in car crash tests. In the frontal impact, the most vulnerable parts of the body are the head, neck, chest, and knee. The Hybrid III is the most widely used frontal impact dummy around the world, and it has been done in various parts of rigorous tests to validate the bio fidelity of dummy (Xu et al., 2018).

2.3.2 Side Impact Dummy

When the car is subjected to a side collision, the most vulnerable parts of the human body are the head, neck, shoulders, chest, abdomen, and pelvis, and each part needs to be validated. In the late 1970s, the University Of Michigan and the NHTSA jointly developed the world's first side impact dummy SID which was developed according to 50th American male. Its head and neck retained the structure in Hybrid II, and foam parts are used instead of the omitted arms in the torso. The chest of the SID cannot simulate the chest response of human for its material had no elasticity in the horizontal direction. After the different improvements on SID was done and upgraded from the original structure, for example, a load sensor was added to the head-neck contact surface, reducing the coefficient of friction between the clavicle and the mounting plate, added a new backplane with load cell, and so on. In 1997, the ISO initiated the development of a more bio fidelic side impact dummy: the World SID dummy. World SID dummy was based on the medium size of men worldwide (Lst et al., 2009). There predictability, the durability, and the sensitivity have been greatly improved compared to other dummies.

In addition to the above dummies, in the 1990s, a consortium consisted of Chalmers University, Volvo Car Corporation, and Saab Automobile AB develop the new Rear impact Dummy the dummy was designed to represent a 50th male in Europe and its vertebral column curve fitted well with that of human. The vertebral column consisted of 24 separate vertebrae; the vertebral column will perform realistic movements when faced with impact load. Compared with Hybrid III dummy, Bio RID dummy is more closely related to human characteristics on the neck and vertebrae .Therefore, it is more realistic to simulate the human response after a rear-end collision in a rear collision accident. It can be seen from the development of the dummies that all kinds of dummies have undergone continuous improvement, so that the response of each part of the dummy can be more and more close to the human body response. However, most of these dummies are designed based on the Male size in Europe and America. But the size of the human body varies greatly from country to country. The dummy may have limited ability to predict the injury of people who are not European and American (Haslegrave, 1974).

2.3.3 Dummy FE model

Currently, the Livermore Software Technology Corporation (LSTC) developed and validated a variety of dummies including the 50th, 5th, and 5th percentile male female dummies and Side Impact Crash Test Dummy. The model was developed by LSTC in the LS-DYNA finite element code. Component level tests and assembly level tests were utilized for validation of the model. All these dummies each have both a rigid and a deformable version. Since these dummies were first released in the 90s a number of shortcomings have been identified including difficulty in positioning, difficulty in injury/response extraction, and lack of documentation (Guha et al., 2011).

Efforts are now underway to update the full set of dummies to address the problems listed above and also to take full advantage of advancements in both LS-DYNA and LS-Pre Post. The dummy selected for this research are two types, these are, Frontal and rear impact dummies and Side impact dummies the dummies used for rear and front impact are the same which is lstc.h3_5th_fast.111130_v2.0 and for side impact the selected dummy model is LSTC SID-IIs_D_FAST.110923_V0.100.

This file is available online and downloaded from the official LSTC website. The Model is distributed free of charge to licensees of LSTC's LS-DYNA software who are current with their

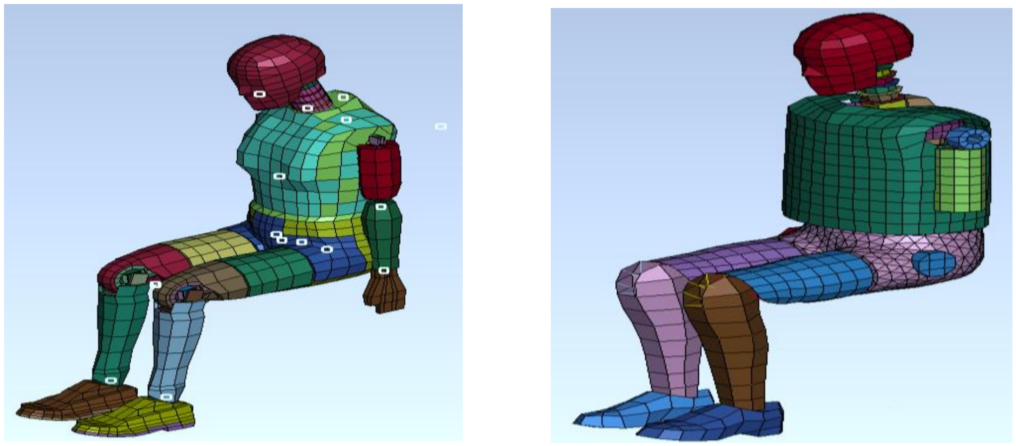

(a) (b)

Figure 2.15. FEA dummy model (Guha et al., 2011).

Table 2.1 Specification of the dummies

	Frontal and rear dummy	Side dummy
Number of nodes	4313	4,860
Number of solid elements	2644	5,593
Number of shell elements	376	1624
Number of beam elements	447	3

annual license fees (Annual License) or maintenance fees (Paid-up License) (Lst et al., 2009). Figure 2.17 and Table 2.1 shows a brief overview over the basic statistics of the current version of the front and side dummy FEA model.

2.4 Previous studies

Significantly less research has been dedicated to three wheeled vehicles, in particular auto-rickshaws. In order to bring significant change in their overall activity and improve body and structure of three-wheeler vehicles, the existing vehicle frame structure was redesigned and the results were compared with the already existing ones. It was found that 24.6% of the total drag of the original (Model-1) was reduced on the model-2 that is equivalent to 4.93 kW of an engine brake power at 60 km/h in speed. Also 8.1% of fuel can be saved for every 60 km/h. Also, for impact analysis such as frontal, rear, side and rollover static impact analysis finite element analysis software was used and on the result it is showed that the modified model is much better than that of the existing model but the research work did not include the vehicle to vehicle crash of frontal, rear, side and rollover frame structures collation. The weight could also further reduce by means of shape optimization and structural analysis (Eromo, 2017).

And also, another research was done to strengthen analysis of the existing three-wheeled vehicle and to remodel a new three-wheeled vehicle for the Ethiopia market. Various load analysis on chassis and optimization has been achieved by changing the chassis type and by increasing its resistance to loads. The chassis and body frame were designed so as the vehicle can withstand better crash and static types of loads and is capable of moving on bumpy road. The frame has been improved by optimizing the number of bars and tubes that are part of it and repeating over and over FEA analyses. In this way could reduce the weight of our vehicle and increase its strength. During crash the maximum von-misses stress obtained in the existing model was about 70 times larger than the results obtained in the new model. This shows that the new model can withstand impact loads so as the risk level has been minimized. But the modified model Stability analysis the TWV structure considering individual members and the dynamic response of the model was not performed (Enawgew, 2013).

This instability was studied using a multi-body dynamic (MBD) model and with experiments conducted on a prototype three wheeled vehicle (TWV) on a test track. In an initial model, all components including main structures like frame, steering column and rear forks are assumed to be rigid bodies. A linear eigenvalue analysis, carried out at different speeds, reveals a mode that has a predominantly steering oscillation, also called a Wobble mode, with frequency around 5 to 6 Hz. The analysis result shows that the damping of this mode is low but positive up to the maximum speed of the TWV. However, the experimental study shows that the mode is unstable at speeds below 8.33 m/s. To predict and study this instability in detail, a more refined model of the TWV, with flexibility in three important bodies, was constructed in ADAMS-CAR. With flexible bodies, three modes of a steering oscillation were observed. Two of them are well damped and the other is lightly damped with negative damping at lower speeds. It was found that structural flexibility modeling is essential to capture the wobble mode instability that is observed experimentally. Also, it was found that steering column flexibility may be one of the main reasons for these instabilities so it suggested that experimental study of wobble with steering column flexibility and study of modal interactions of various modes that may lead to instabilities at particular vehicle speeds should be performed (Karanam & Ghosal, 2013).

The rollover propensity of a three-wheeled scooter taxi is analyzed on another study. A rigid body mathematical model was used to simulate increasing steer, NHTSA, J-turn, and Road Edge Recovery maneuvers. The anomaly between public perception of the rollover susceptibility and available crash data has been resolved through finite element (FE) simulation. The optimum configuration of the vehicle and seating arrangement for varying numbers of passengers was determined. The safety of occupants and pedestrians in impact events was analyzed through simulation in MADYMOTM and Cost-effective solutions to improve safety were identified. Simulations for pedestrian impact with frontal and side of the vehicle were developed and run with varying offset at vehicle speeds of 10, 20 and 30 km/h with braking of 0·2 g. The injury severity of different body parts for pedestrian as well as occupant was estimated through these simulations. Analysis indicates that small design changes could significantly enhance safety of occupants and pedestrians. Pedestrian injuries become significant at impact speeds above 30 km/h in direct impacts when the pedestrian impacts near the centerline of the vehicle. It also indicated that In case of frontal rigid barrier impacts at 30 km/h, both the driver and the passenger have a very high probability of suffering serious head and upper leg (femur) injuries. The knees of passengers and the driver impact rigid surfaces inside the vehicle. It is possible to significantly reduce severity of upper leg injuries by providing padding at the contact points. Head injury severity can be reduced by providing less stiff impact surfaces at the contact point for the passengers and with similar modifications in the driver cabin windshield area. Provision of lap belts does not seem to benefit either the driver or the passenger however; provision of lap and shoulder belts for both the driver and the passenger show major safety benefits (A Chawla et al., 2001).

Biomechanics issues in two and three-wheeler vehicles under different impact conditions were highlighted by the use of computer simulations. It was mentioned that these vehicles run at maximum speeds of 50 km/h. And impact speeds are typically of the order of 25-30 km/h. As a result, the severities of injuries caused were low. This is in spite of the fact that typically the TSTs are not equipped with seat belts. A different paradigm is hence needed to augment safety in these vehicles. Computer simulations suggest for injury evaluation, thorax, head, and knees are areas of concern. Additionally, soft tissue injuries in abdominal region could be possible in severe crushing events. With low cost changes, the interiors of the TSTs can be redesigned to minimize these impacts. Enclosing the partially open structure to prevent the occupant being ejected during a crash is also suggested. TST's are not fitted with a bumper. The first impact with the pedestrian is thus often with the upper thigh or the pelvis region as against the lower leg. This reduces knee injuries and whole body rotation. There is scope to modify the fronts of TSTs further to reduce injuries to pedestrians (Anoop Chawla et al., 2001).

FE models were developed to study the crash of the TSTs and study the safety of the occupants, namely the passengers and importantly, the driver. The effect of the front mudguard appears to be critical. Thus the simulations carried out have two basic models, one without the front mudguard and the other comprising a front mudguard. This is being done specially because some models of TSTs have a front wheel guard that rotates with the steering column, and the mudguard then does not play a significant role in absorbing the energy. The simulations have been carried out at impact velocities of 30kmph. The accelerations experienced by the head nodes and chest nodes of the driver dummy during impact. It is important to note that in the unmodified TST accelerations are around 150 g which is clearly very dangerous. Also the HIC value for the head comes out to be around 1200. This value is higher than the acceptable limit of 1000. The deformations of the front shield have also been observed. They also some preliminary simulations with the mudguard. The results show that the mudguard affects the dynamics of the impact. In the absence of a mudguard, there is a significant shearing of the front shield and the contact between the knee-joint and the front shield is delayed.

This knee contact with the front shield is suspected to be a major source of injury. The prime reason being that the knee-joint in a three-wheeler is much closer to the impacting surface and thus more susceptible to injury than say, in a car. In the presence of front mudguard, there is no shearing action and hence the deformations in the shield are greater. The mudguard in this case plays an important by absorbing a significant amount of energy in the process of getting crushed. It is also observed from the initial studies that upon impacting against the windshield, the head tends to bend backwards and, as a result the neck is subjected to elongation. Further studies would help in quantifying the severity of neck injuries and the injury to head. The above findings lead to believe that in the present form the TST is very dangerous especially, for the occupants. The driver. However, it was believe that with small and low-cost changes the vehicle can be made much safer for the driver. These changes could include appropriate padding cushions at the impacting surfaces and addition of a lap belt for the driver. Further studies will quantify the effect of these modifications on the behavior of the TST (A Chawla et al., 2001).

Another attempt was done to study the crash characteristics of TSTs using crash simulation computer software (MADYMO) with the objective of developing practical guidelines to make the vehicle safer in collisions with other motorized road users and pedestrians. Impact modeling was done for the standard and modified TST occupied by a driver and one passenger at impact velocities of l0-30 km/h crashing with a pedestrian and a bus front. The results showed that the existing TST were not safe for the driver, the passenger or the pedestrian even at low impact velocities of about 15-20 km/h. They can sustain high HICs, face/head contact forces and tibia/knee contact forces in crashes with buses at velocities 20 km/h and greater. There is a lot of scope in changing its design to make it safer. Minor modifications like adding padding at suitable locations and altering the front of the TST can make a significant difference to safety of the occupants as well as the pedestrians. These modifications significantly reduce the risk of injury in the TST up to impact V's of about 20 km/h. Changes of the design of the TST, like changing the orientation of the passengers and introducing stiffer floor structure combined with redesigning of the bus front to be more compatible in a crash event can reduce the risk of injury for the passenger at speeds of 25-30 km/h. However, in order to reduce injury risk to acceptable levels for the driver at higher speeds of around 30 km/h more modifications in the design of the TST would be needed. These could be in the form of lap and shoulder belts for the driver, or other structural changes in the TST. Pedestrian impact simulations indicate that it may be possible to reduce the impact forces by changing the shape of the front of the TST. The results indicate that it should be possible to improve the crash safety properties of vehicles indigenously designed in Asian and African countries by the use of crash simulation models like MADYMO (A. chawla, S. mukherjee, D. mohan, Jasvinder singh, 1997). Another paper reports the rigid body-based simulations for frontal impact of Three Wheeled Scooter Taxi (TST) with a rigid barrier and those of a TST with a pedestrian in different spatial configurations.

The simulations have been carried out in MADYMO. The paper described the development of the TST model, assesses the scale of injuries to the driver, occupant and pedestrian during the occurrence of these impacts and analyses the crashworthiness of TST. It was observed that even with small changes in the TST there is significant improvement in the injury indices. It believes that there is a considerable scope of improvement of the crashworthiness of the TST. The TST can give serious injuries to its occupants when it is running at 30kmph and impacts into a rigid barrier. Adding seat belts improves the crashworthiness of the TSTs further. In fact, with the seatbelts it can be ensured that the driver and passenger head does not come into contact with any hard surface. This contributes significantly to the crashworthiness of these vehicles. Passenger safety can also be significantly increased by making rear facing passenger seats. In rear facing passenger seats the passenger does not hit any hard surface during a frontal crash (A Chawla et al., 2001).

Another simulation was done using a MADYMO model, the three knee-cushion variants were investigated under varying conditions. Results show that the knee-cushions originally proposed for the zero Emission Downsized Improved Safety urban vehicle (three wheeler) prototypes do not offer satisfactory protection for pelvis and legs. Although using numerical and experimental simulations, the study shows that a knee airbag in combination with a knee-cushion clearly reduces the loads on the pelvis and femurs during a frontal impact situation (Gehre et al., 2001).

In general auto rickshaws (three wheeler vehicles) are low speed vehicles with a maximum speed of 60 km/h with reasonable acceleration. The international standard for crashworthiness is normally evaluated at 48 km/h. However, at the time of accident, especially, during frontal impact, the vehicle speed is normally reduced due to the driver braking action, and the instantaneous speed is around 20 km/h. taking the above into the account, the crashworthiness analysis was done at two speeds of 20 km/h and 48 km/h. The drive away chassis and all other components in the system were modeled and meshed in order to make a precise model using HYPERMESH pre-processor. P1-shell element with average element size of 10–15 was used in the present model. Johnson-Cook type material model Type 2 is used in the analysis. Strain rate sensitivity is accounted for in the model. The material properties used in the analysis was IS513 steel. From analysis result, it can be observed the frontal crash modulus is only 1/10th of the crash modulus for a mid-size car segment at 20 km/h. The crash modulus is double at speed of 48 km/h. Unlike cars, there is no front bumper for the auto rickshaws and hence no frontal energy absorbing member. This can be improved either by having foam filling in between cowl bottom and reinforcement (closed section) or having a corrugated section inside the long members.

To improve the crash worthiness, the initial slope of the force curve has to be high, which in turn gets reflected in the crash modulus. The initial force transition has to be increased by providing an energy absorbing zone. The coefficient of restitution for frontal impact is more when compared to rear impact. The rear crash modulus is much higher than frontal crash. The initial slope is high thereby higher force is absorbed. The coefficient of restitution for rear impact is having good inelastic collision when compared to front impact. It is also suggested that this work can be extended to evaluate the crash behavior for the whole vehicle, including windshield assembly, cabin assembly and soft top assembly i.e. lumped mass analysis can be made to set of independent parts. The safeties of the vehicle due to fuel tank leakage during rear impact, effect of HAZ (Heat affected zone) due to welding in the crash behavior were other area which needs to be considered (Ljungberg et al., 2015).

The potential protection for the rider results from a high-stability frame structure, the quality of the deformation characteristics, high-performance restraint systems and the manner in which these features are harmonized with one another. This harmonization of components was achieved through crash testing. Considering this with C1, BMW launched a new class of two wheeler vehicle. With the C1 a new class of two wheeled vehicle was conceived with the aim of transferring passive safety measures from the rider’s clothing to the vehicle structure and components. New test methods have been developed (lateral fall) or adapted (roof indentation) and the ISO 13232 motorcycle crash standard have been used to prove the concept during development. The early positive results of the accident analysis confirm the safety concept. As a result of the restraints, the rider is held inside the protective frame structure. The measures applied to the vehicle have prevented head contact with the striking vehicle or with the road surface. A comparison was made between a two-wheeler with safety system and one without .The comparison vehicle used in this case was a C1 without roof frame, safety belt or deformation elements (C0).

The dummy riding the C1 was modelled without a helmet and that on the C0 with a helmet. The simulation was validated on the basis of the 7 crash tests described in ISO 13232, Part 2 and carried out with the C1 .Thereafter, for the risk/benefit analysis, 200 different types of collision with a passenger car over a period of up to 5000 ms were simulated and evaluated. The 200 configurations were based on accident analysis data and are likewise described in the ISO 13232 motor cycle crash standard. At 5000 ms, the lateral fall following the initial collision was also taken into account. For conventional passenger car, the benefit ratio for restraint systems lies between 3 and 7 percent. For the C1, the resulting injury risk/benefit ratio was 10%. Included in the 10% are AIS 1 injuries caused by the belt at higher impact speeds. Yet, despite the promising results, one should not overlook the fact that there are limits to this development. Even the C1 cannot offer 100% protection against serious or even fatal injuries. The design represents a previously unknown level of safety for a two-wheeler. Nevertheless, the C1 remains a motorized two-wheeled vehicle and its smaller dimensions alone place it at a disadvantage compared with a motor car. The restraint system is not capable of holding all of the rider's limbs within the passenger cell. Its characteristics and its passive safety are not transferable to other two-wheelers. It was not the intention and nor is it possible, to turn every motorcycle into a C1 (Osendorfer & Rauscher, 2001).

(Inani & Bisen, n.d.), Design the body design of the TW vehicle aesthetically. To achieve their goal THEY redesign the initial CAD model in order to improve the manufacturing process and meet the mechanical requirements demanded. They recommends that More design of e rickshaw body are to be analyzed in order to reduce the cost of chassis and to suggest alternative design for higher strength with aesthetically designed which provide more comfortable and safer.

On another study a parametric and comparative analysis of auto-rickshaw-related pedestrian impacts and pedestrian-ground impacts by computational simulation was done using a Finite Element model of an auto-rickshaw and LS-DYNA, 50_{th} percentile adult male and six-year-old child Hybrid III Anthropometric Test Devices (dummies). The comparative study explored the kinematic responses and injury metrics associated with both adults and children impacted by an auto-rickshaw, as well as the most commonly impacted areas of an auto-rickshaw and the injury metrics for the adult pedestrian produced by primary and secondary impacts. The results suggest that adult pedestrians are subjected to a relatively high risk of head, neck and chest injuries during primary impacts at 10, 20 and 35km/h, respectively, and the 6YO-child pedestrians are at risk of serious head and neck injury at 10 and 15km/h, respectively. Vehicle impact response was investigated and Aluminium-6016-T4 and magnesium-AZ31B windscreen frame materials and a polycarbonate windscreen were found to produce the lowest injury risk of all the materials investigated whilst offering the greatest safety at the lowest cost (Kunle et al., 2019).

Another work intends to provide the validation for an Auto rickshaw model by comparing frontal crash simulation with a random head-on crash video. MATLAB video processing tool has been used to process the crash video, and the impact velocity of the frontal crash was obtained. The vehicle modelled in CATIA is imported in the LS-DYNA software simulation environment to perform frontal crash simulation at the captured speed. The simulation is compared with the crash video at 5, 25, and 40 milliseconds respectively. The comparison shows that the crash pattern of simulation and real crash video are similar in detail (Ljungberg et al., 2015).

2.5 Research gap

From the above reviews it can be observed that most of the study focuses on the analysis of the structure of the existing three-wheeler vehicles emphasizing on their strength, stability issues, and biometrics problem and modifying the shape aerodynamically. Most of the problems existing with the three-wheeler vehicle are assessed. More over their results focus on suggesting modification should be made in order to improve the safety of TWV. On some papers, modification was also made and analyzed for different TWV crush aspects but the modifications and crush analyzing aspects are limited to only front and rear impacts, In addition the modifications were not satisfactory to protect the occupant and the driver at the event of crush. Moreover, there was no research work which was directly related to improvement of crashworthiness of TWV. This thesis work focused on the improvement of the crashworthiness of the existing three-wheeled vehicle by remodeling the in such way that crash injuries are minimized.

CHAPTER THREE
MATERIALS AND METHODS

3.1 Introduction

3.1.1 Crush theory

A moving vehicle has a massive amount of kinetic energy and momentum force and if these occur in a crash, this massive amount of momentum force needs to be absorbed, which can be very deadly and causes a lot of damages. The amount can vary based on the speed and mass of the car and the speed and mass of whatever it hits. The heavier the vehicle, the faster the speed and the greater the amount of momentum energy that needs to be absorbed in case of a crash. Another major consideration on the amount of the momentum force and impact of the crash is whether the car comes to a sudden stop or comes to stop gradually (driverseducationusa.com, 2021).

If the car running at a faster speed and have an accident that causes it to come to a sudden stop when hitting the other object, the momentum force will have much more forceful impact and therefore more damage to the vehicle and more injuries to occupant body. If it can slow down before hitting the object, or there is a longer time involved for the vehicle to come to a stopping point, the momentum force will have less forceful impact and therefore less damage to the vehicle or less injuries to occupant body.

If you have a head-on collision with another vehicle, or if you hit a solid object that is not movable such as a building, a concrete structure, a big rock or a tree, the momentum force will have a much stronger and forceful impact because it needs to be absorbed instantly. And also if the vehicle hit another vehicle with the same opposite angle and speed, the larger, heavier vehicle will have a greater momentum force and, therefore, will cause more damage to the smaller, lighter vehicle. The larger, heavier vehicle may push the smaller, lighter vehicle backward and even crush the smaller vehicle. Generally, The best way to reduce the initial force in a crash with a given amount of mass and speed is to slow down the deceleration in a collision, slowing down the deceleration by even a few tenths of a second can create a drastic reduction in the force involved.

Physicists measure this force as acceleration even when moving from a high speed to a lower speed, any change in speed over time is scientifically referred to as acceleration. To avoid confusion, we will refer to crash acceleration as deceleration**.** The second law of motion, formulated by Sir Isaac Newton between (1642 and 1727), is the fundamental law for most vehicle dynamic analyses:

$$Force\ (F)\ =\ m\ a \tag{2. 1}$$

Where F is the applied vehicle force; a is the resulting acceleration of the vehicle and m is the vehicle mass.

In most impact cases high momentum is generated by the vehicle in the travelling direction, which can be defined as the extent to which it is difficult to stop a moving object, such as a vehicle. According to the following formula:

$$Momentum\ (M)\ =\ m\ v \tag{2. 2}$$

Where m is the vehicle mass and v is the vehicle travelling velocity.

In addition, the applied vehicle motion converts the potential energy (PE) to kinetic energy (KE), and depends exclusively on the vehicle mass and velocity, as shown in the following formula:

$$Kinetic\ Energy\ (KE)\ =\ 1/2\ m\ v^2 \tag{2. 3}$$

Where m is the vehicle mass associated with vehicle type and size and v is the vehicle travelling velocity, which is significantly important, as the velocity is incorporated in the energy formula by a square power.

Both the momentum and kinetic energy of the vehicle, during the vehicle-to-vehicle impact are transferred to the impacted both cars, which causes the motion response (kinematic) and injury risk level for different injury criteria. Moreover, the structure of a vehicle will absorb energy by undergoing deformation; however, it must do so in a controlled manner to also protect the occupants of the vehicle. During impact the material will undergo initial elastic deformation before beginning to deform plastically Automotive structures primarily rely on plastic deformation for absorption of kinetic energy. It is important that the materials do not require significant impact forces to plastically deform. As the vehicle impacts other vehicle, some of its kinetic energy is absorbed as internal energy in the vehicles deforming structure, with the remaining energy being the sum of the kinetic energies of the vehicles In a head-on collision involving two vehicles, the total initial (before collision) kinetic energy (Ek,i) can be determined (Kunle et al., 2019). The mass and speed of the vehicle A and B are respectively called m_A, v_{A_1} and m_B, v_{B_1}. Then the initial kinetic energy is given by

$$E_{Before} = \left(\frac{1}{2}\left(m_A v_{A_1}{}^2\right) + m_B v_{B_1}{}^2\right)\Big)_{intial}$$

$$E_{After} = \left(\frac{1}{2}\left(m_A v_{A_2}{}^2 + m_B v_{B_2}{}^2\right)\right)_{after}$$

After collision according to the conservation of energy, the following equation can be written:

$$\left(\frac{1}{2}\left(m_A v_{A_1}{}^2\right) + m_B v_{B_1}{}^2\right)\Big)_{before} = \left(\frac{1}{2}\left(m_A v_{A_2}{}^2 + m_B v_{B_2}{}^2\right)\right)_{after} + E_{absorbed} \qquad (2.4)$$

Assuming that after crashing the two vehicles is moving together with the same residual speed v3;

$$\frac{1}{2}\left(m_A v_{A_1}{}^2 + m_B v_{B_1}{}^2\right) = \frac{1}{2}\left(m_A + m_B\right) v_3^2$$

From the conservation of momentum principle, the following equation can be written:

$$\left(m_A V_{A1} + m_B V_{B1}\right)_{before} = \left(m_A V_{A2} + m_B V_{B2}\right)_{after} \qquad (2.5)$$

Assuming that after crashing the two vehicles are moving together with the same residual speed v3;

$$\left(m_A V_{A_1} + m_B V_{B_1}\right)_{before} = (m_A + m_B) V_3$$

$$V_3 = \frac{m_A V_{A_1} + m_B V_{B_1}}{(m_A + m_B)} \qquad (2.6)$$

From these three equations, the dissipated energy used to deform both vehicles can be calculated. It is equal to the difference between the initial and residual energy.

$$\Delta E = E_{Before} - E_{After}$$

$$\Delta E = \frac{m_A m_B}{m_A + m_B}\left(v_{A_1} + v_{B_1}\right)^2 \qquad (2.7)$$

In this study, both the truck and TWV was assumed to be move with same velocity after impact therefore the energy that needs to be absorbed is depending on the truck and TWV speed before impact (v) and the mass of both vehicles. This energy is dissipated by both the deformation of the car front and the truck front. The work done by the average force arising during the collision in crushing the car is;

$$\Delta E = F.S$$

Where: F = average force acting during the impact (N)

s = car crush distance (m)

$$F = \frac{\Delta E}{s} = \frac{m_A m_B}{(m_A + m_B)s}\left(v_{A_1} + v_{B_1}\right)^2 \tag{2.8}$$

This shows that the average force acting during the impact is function of the truck and TWV masses, closing speed and car crush distance. Energy dissipated by the TWV deformation can be estimated to be;

$$E_{TWV} = \frac{1}{2} F_{max} d_{max}$$

The force reaches a maximum value, F_{max}, while the displacement increases to a maximum deflection, d_{max}.

The velocities after impact may be determined with the coefficient of restitution (e). The coefficient of restitution (COR) is the ratio of speed of separation to speed of approach in a collision.

$$e = \frac{(V_{B_1} - V_{A_1})after}{(V_{A_1} - V_{B_1})before} \tag{2.9}$$

An object with a COR equal to 1 collides elastically, while an object with a COR of 0 will collide in elastically, effectively sticking to the object it collides with, not bouncing at all. The coefficient of restitution is a number which indicates how much kinetic energy (energy of motion), remains after a collision of two objects. If the coefficient is high (very close to 1), it means that very little kinetic energy was lost during the collision. If the coefficient is low (close to 0), it suggests that a large fraction of the kinetic energy was converted into the heat or was otherwise absorbed through deformation (Dange et al., 2015).

3.3 Materials

To conduct the numerical analysis of the three-wheeler vehicle. The following FEA tools are used.

CATIA V5

The CATIA V5 is geometric modeling software developed by Dassault Systems. It is the leading commercial computer program used in product development solutions for wide variety of industries, such as aerospace, automotive, electrical, electronic etc. which provides greater flexibility in modeling of the irregular contours. CATIA V5 is the only solution capable addressing the complete product development process, from product concept specifications through product-in-service, in a fully integrated an associative manner. It facilitates the true collaborative engineering across the multi-disciplinary extended enterprise, including style from design, mechanical design and equipment and systems engineering, managing digital mock-up, machining, analysis, and simulation (Basavaraju, 2005). It capability of Sketch tracer Generation, Surface Generation, Component assembly and so on.

LS-DYNA

LS-DYNA is a general purpose transient dynamic finite element program capable of simulating complex real-world problems. It is optimized for shared and distributed memory UNIX, Linux, and Windows based, platforms. It is an explicit 3-D finite element program for analyzing the large deformation dynamic response of the elastic and inelastic solids and structures (Livermore & Corp, Software, 2021). LS-DYNA allows switching between explicit and different implicit time stepping schemes. Disparate disciplines, such as coupled thermal analyses, Computational Fluid Dynamics (CFD), fluid-structure interaction, Smooth Particle Hydrodynamics (SPH), Element Free Galerkin (EFG), Corpuscular Method (CPM), and the Boundary Element Method (BEM) can be combined with structural dynamics (predictive engineering Goods, 2020).

LS-DYNA has been developed in California for more than 20 years. It is the most frequently used code for many complex applications in structural nonlinear dynamics. Its usage is growing rapidly due to LS-DYNA's flexibility, enabling it to be applied to new disciplines. The new developments are driven in co-operation with leading universities from all over the world and new requirements requested by the vast customer base. The program is extensively used by many top automobile, aerospace and research organizations. A wide range of material types and interfaces enable the efficient mathematical modeling of many engineering problems (Livermore

& Corp, Software, 2021). The code's origins lie in highly nonlinear, transient dynamic finite element analysis using explicit time integration.

"Nonlinear" means at least one (and sometimes all) of the following complications:

- Changing boundary conditions (such as contact between parts that changes over time).
- Large deformations (for example the crumpling of sheet metal parts).
- Nonlinear materials that do not exhibit ideally elastic behavior (for example thermoplastic polymers).

"Transient dynamic" means analyzing high speed, short duration events where inertial forces are important. Typical uses include:

- Automotive crash (deformation of chassis, airbag inflation, seatbelt tensioning)
- Explosions (underwater Naval mine, shaped charges).
- Manufacturing (sheet metal stamping).

The detail on the procedures mentioned under the method hierarchy is discussed in detail in the next chapter four.

3.2 Methods

To achieve the project general and specific objectives, a series of steps or methodology are to be followed. Various steps included in the methodology are listed and summarized in Figure 3.1.It shows the procedure used for accomplishing the study. Among the procedures the modeling and analysis stage have a more detail explanation and it is stated in detail on chapter four.

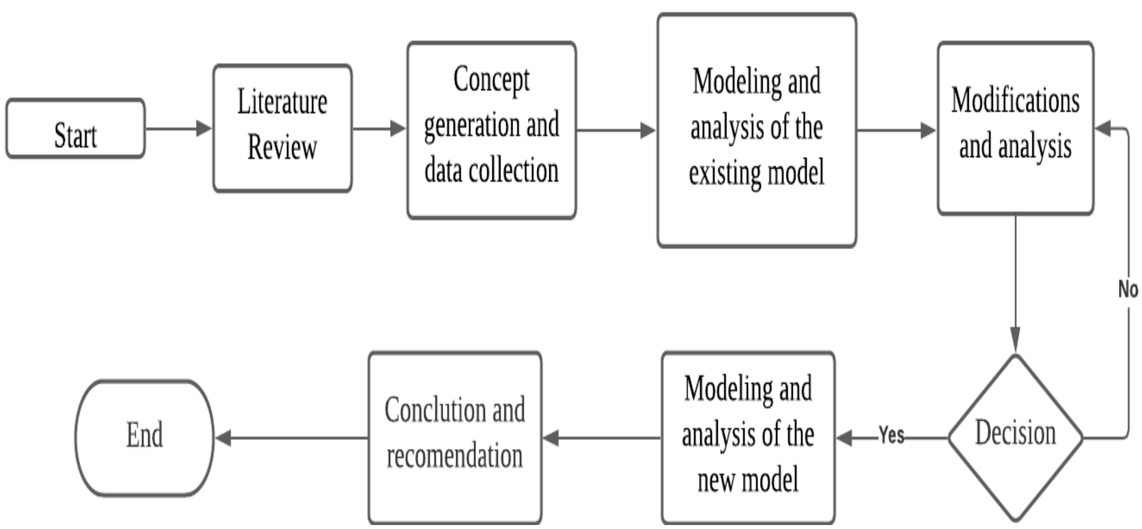

Figure 3.1. Block diagram of the thesis methodology.

3.2.1 Literature review and problem identification

In order to have full image of the project such as what other done on this area, their drawbacks and gaps literature surveys were carried. Latest reviews and research works in area related to development, modification, design and analysis of TWV is collected and surveyed.

3.2.2 Data collection

In order to do the Numerical analysis the necessary data about the existing three wheel vehicle is collected. Different data were collected to understand the present status of research, and Methodology of TWV which can also help in developing or modifying structural crashworthiness of TWV, the data are presented as follow.

Specification of three-Wheeler Vehicle (Bajaj RE)

Technical specification and necessary data of the existing three wheeler vehicle has been collected from (Enawgew, 2013) & (kunle et al., 2019). All necessary information of three-wheeler vehicle is shown in Table 3.1. In addition to this, when dealing with crash worthiness, the mass of the vehicle parts plays vital role (kokate et al., 2020). The weight of the major parts of the three wheel vehicle which are critical for the crash analysis were listed on Table 3.2. Table 3.2 will give information on auto rickshaw parts with major components.

Table 3.1. The technique Specification of three-wheeler vehicle

Engine	
Engine	Four stroke, spark ignition, forced air cooled
No of cylinders	One
Bore	63.5 mm
Stroke	62.8 mm
Engine displacement	198.88 CC
Maximum net power	7.45 kW at 4500 + 250 RPM
Maximum net torque	17.30 Nm at 3500 + 250 RPM
Compression pressure	12+ 0.5 kg/cm^2
Compression ratio	9:1
Idling speed	1200+150 RPM
Ignition system	Electronic, D.C type
Ignition timing	3o BTDC up to 1500 RPM and 17o BTDC up to 2500 RPM
Onward Lubrication	Pressurized Lubrication by Separate Oil Sump

Fuel	Petrol
Fuel Tank Capacity	Full: 8 liters and Reserve: 1.5 liters
Carburetor	Side draft 18mm equivalent venture
Spark plug	2 nos
Spark plug gap	0.6 up to 0.8 mm
Starting	Electric Start
Transmission	
Clutch	Wet, multi disk type
Transmission (gear)	4-speed forward+ 1reverse
Overall gear ratios	
1st gear	32.558:1
2nd gear	19.065:1
3rd gear	11.862:1
4th gear	8.25:1
Reverse gear	28.59:1
Differential	Integral with Engine
Differential gear ratio	Forward 2.192:1, Reverse 1.925:1
Suspension	
Front	Anti-drive type, constant rate coil spring and double acting
Rear	Independently sprung wheels by trailing arms with helical
Chassis and Body	
Frame type	Constructed from pressed steel sheets and sections welded
Brakes	
Front	Hydraulic expanding shoe type size 170 mm × 29.5 wide
Rear	Hydraulic expanding shoe type size 170 mm × 29.5 wide
Hand	Hydraulic expanding shoe type size
Parking	Mechanically operated on rear brakes
Wheel outer diameter	400 mm
Wheel rims	8 in×3 in
Tire Size	4-8,4P.R.
Tire pressure	
Front	2.1 kg/cm^2 (30 psi)
Rear	2.4 kg/cm^2 (34 psi)
Weight	
Kerb weight	280 kg
play-load including driver	310 kg
front axle weight	210 kg

rear axle weight	430kg
Performance	
Maximum speed	65 km/h
Climbing ability	18% maximum

Table 3.2. Weight of the major parts of auto Rickshaws

NO	Components	Weights(kg)
1	Glass and frame	25
2	Seats (Passenger and driver) Including assembly	9
3	Sunroof and supporting bar	5
4	Engine	45
5	Chassis	65
6	Tire (including rim)	6
7	Brakes	20
8	Fork	12
9	Body	45
10	Shock absorber (rear +front)	9
11	Head and tail lamp	1.5
12	Gas cylinder	38
13	Total weight	@280

Vehicle dimension

The model has been done using the overall dimensions length is 2625 mm, width 1345 mm and height is 1730 mm of the vehicle structure is steel (Eromo, 2017).

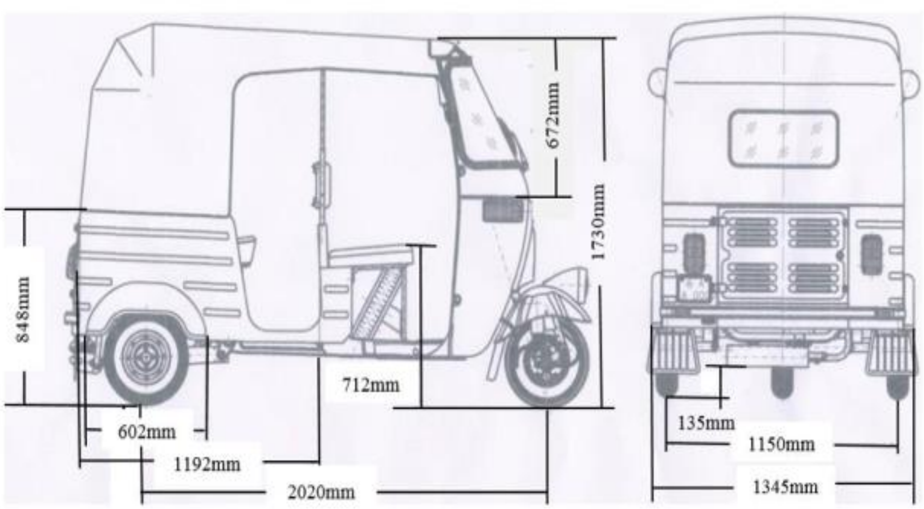

Figure 3.2. Dimensional specification of TWV

Figure 3.2 shows 2D drawing of existing vehicle structure. The main material Bars with circular cross sections and diameters of 25 mm and 2-3 mm thickness (Eromo, 2017). Since here dealing with a linear direct impact, each component model geometry was less important so several of the components of the car were not modeled finally each part assembled together before going to finite element analysis (Kokate et al., 2020).

3.2.3 Concept generation

The concept generation process results in a set product concepts from which we make the final specification and design. Different concepts towards the crashworthiness improvement of three-wheeler structure is generated. This includes safety development concepts and structure modification methods. This will be discussed more on next chapter.

3.2.4 Modeling and analysis of the existing model

The modeling analysis of the structure of the existing model of TWV will be carried out by using software. Achieve this aim the vehicle is first modeled in on CATIA software and model quality is cheeked by ANSYS and Ls-pre post and finally the analysis will be done using ls-dyna processor.

3.2.5 Modifications and analysis

After carefully observing the crashworthiness behavior of the existing model, modifications and designs were made on critical points of the vehicle. Then the modified parts were analyzed separately.

3.2.6 Decision

At this point, the response of modifications is examined using engineering analysis and decision methods. If the result were satisfactory the next stage of the project will take place but if not, the modification is re-designed.

3.2.7 Design and analysis of the new model

The safety developments or modifications which increase the crashworthiness of vehicles are fitted in to the existing model and further analyzed using LS-DYNA.

Lastly but not least the numerical comparison between the existing model and modified model is done using different crashworthiness determinant parameters such as energy absorbing ability, impact force, deformation and so on. The detail of the above-mentioned procedures is discussed on the next chapter.

3.2.8 Verification parameters

Without experimental data, the appropriateness of the values obtained on a computational model accurately represented by verification process. In case LS DYNA simulation, verification can be made by checking the quantity of energy balance, deformations, kinematics, kinetics and other quantities (Gulavani et al., 2014), the most common and logical ways are listed below:

- Energy balance
- Energy Ratio
- Ratio of hourglass energy (HE) to IE

Energy Balance Curve

The energy balance of a system in an impact is governed by the law of conservation of energy. According to the law of conservation of energy, Energy can neither be created nor be destroyed, but it can be converted from one form of energy to another form. Applying the same principle to crash analysis, the amount of kinetic energy lost during impact must be converted to other forms of energy such as internal energy, sliding energy and hourglass energy.

Kinetic energy is the work input and internal energy is the work output. Internal energy is the energy absorbed by the system and is directly proportional to the product of force and deformation. It is also noted that, there may be negligible errors in calculating energy ratio because all the processes in this universe are irreversible and some losses are always included which deviates energy ratio slightly from one.

- The total applied energy should be constant throughout the simulation.
- Total energy is the sum of kinetic energy and potential energy of the complete system.
- The kinetic energy should be decreasing and internal energy should be increasing; and ideally the sum of kinetic energy and internal energy should be equal to total energy
- The Hourglass energy should be less than 5% of total energy.

Energy ratio: The energy balance for an explicit time integration scheme is given by:

$$\underbrace{E_i + E_s + E_d +}_{\text{Total energy}} E_{ke} + \underbrace{E_h = W_{ext} + E_i^0}_{\text{initial total energy}} + E_{ke}^o \tag{5.1}$$

Where: E_i : internal energy E_h : hourglass energies

E_d : damping energy W_{ext} : work done by the external forces

E_{ke} : kinetic energy, E_S : interface sliding (dissipated contact energy)

And the superscript 0 denotes the initial values.

The total sum of energies in the left-hand side of the equation represent the total energy of the system, and terms on the right-hand side of the equation represent the initial total energy plus the work done by the external forces (W_{ext}). The ratio of the 'total energy' to the sum of 'initial total energy' and 'external work done 'is called the energy ratio. The energy ratio is also known as the 'energy balance'.

$$e = \frac{E_i+E_s+E_d+E_{ke}+E_h}{W_{ext}+E_i^0+E_{ke}^o} \tag{5.2}$$

An energy ratio with value of equal to 1 shows more stable and reliable FEA result, but most of it is difficult to achieve such value. This is due to the modelling error which may increases or decreases the total energy. There are two causes which can be considered when checking the energy ratio:

If e>1, which mean that artificially energy is added in the model and rises the total energy values, as a results instability occur, most of the time the rises of total energy is due to a numerical instability or through initial penetration.

If e<1, which indicates that the total energy reduces because of artificially absorbed energy, either by excessive hour-glassing or during stabilization of an ill-conditioned contact surface (LS-DYNA Support Site, 2021).

Generally, energy ratio simply is different from unity, and then there are high probability FE results to contain errors. Since it is difficult to obtain energy ratio equal to unity so, the acceptable value of the ratio is 1.00 +/- 0.07 the discrepancies in the ratio are due to spurious energy produced in the system and simulation error (Pezzucchi, 2016).

Ratio of TE/HE: Through analyzing the energy curves, the validity of the finite element model can also be determined using the ratio between the total energy to hourglass energy. Hourglass energy can cause a zero-energy model. If the hourglass Energy is less than 5% of the total energy, the finite element model is reliable (Gulavani et al., 2014).

The above mentioned verification method are implemented at each simulation results report. The accuracy of the FEA model is checked by examining the different pattern exhibited by the simulation results. Following checkpoints are considered for simulation.

1. The results of Simulations of existing TWV frontal, rear, side rollover impact and occupant responses for respective simulations are imported and discussed.
2. The analysis results of the modifications are presented.
3. The results of Simulations of modified TWV frontal, rear, side rollover impact and occupant responses for respective simulations are imported and discussed.

At each section the main parameter which are going to be examined are the energy balance, absorbed energy, impact force, deformations, structural response and occupant response. The simulation reports at each crush scenarios are presented below.

CHAPTER FOUR

MODELING AND ANALYSIS

Under this section the method used for analyzing and modifying the existing three wheeler vehicle are discussed. The work flow used were shown on Figure 4.1. These steps were used on the analyzing frontal, rear, side and roof impact of the existing and modified model.

4.1 Work flow of modeling and analysis

In performing the design and analysis of the three-wheeler vehicle, the followed steps were developed and were listed on Figure 4.1**.**

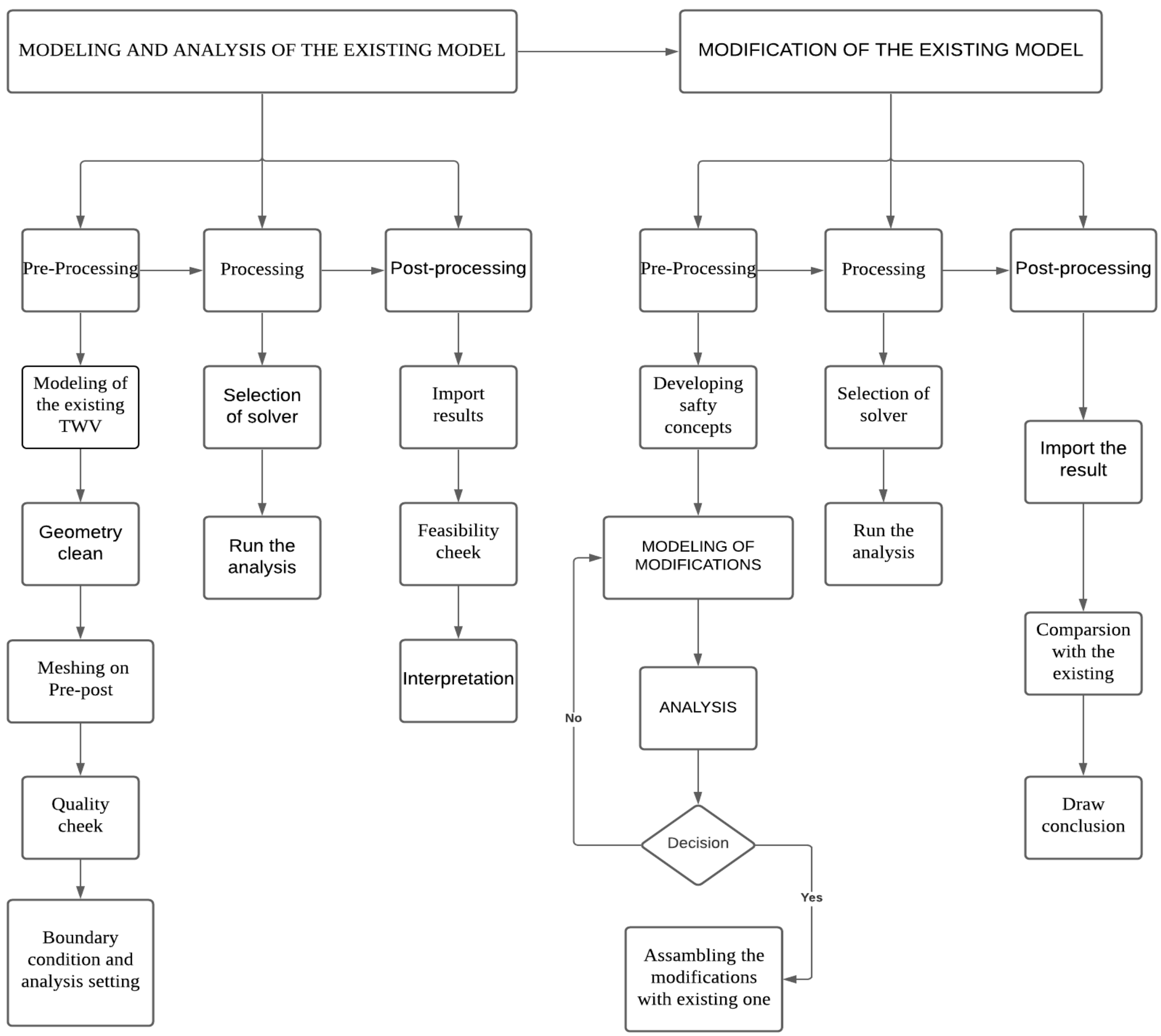

Figure 4.1. Work flow for modeling and analysis

CATIA V 5 is used for modeling and then model was imported in to ANSYS and surface cleaning of the model is done using ANSYS workbench and then LS-PREPOST. The crash analysis is being done in LS DYNA post process. The detail of each of the steps mentioned above are discussed on the following section.

4.2 Modeling and analyzing of the existing structure

4.2.1 Modeling of TWV

Geometry model of three wheeled Vehicle is modeled based specification obtained from data collection. Before attaching the geometry to LS DYNA several steps are performed during modeling in CATIA. These are shown on Figure 4.2.

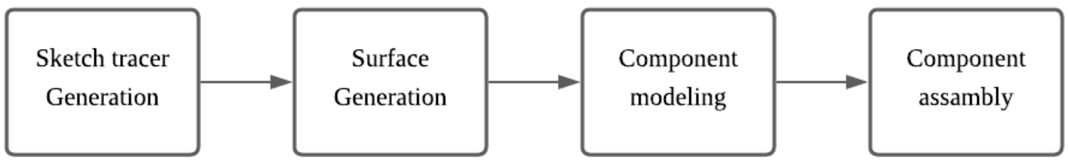

Figure 4.2. Modeling procedure

Sketch tracer Generation is the initial stage of modeling in which the basic profile or part of the TWV is formed by tracing from image. After that, the surface is generated, and the corresponding extruding thickness was given for each part. Finally, the parts are assembled. The parts were named separately and assembled in CATIA; the whole assembly of an auto-rickshaw is as shown in Figure 3.5. The lists of parts modeled assembled are listed below:

1. Rear structure body structure: covers the rear parts and used as passengers' compartment.

2. Front structure body structure and Windshield: it is driver compartment consists of dashboards head light and covers steering linkage and others.

3. Steering and mudguard: used for steering used for maneuvering and consists of steering linkages and suspension components at front and the mudguard cover the front tire.

4. Seats: includes the passenger's front and driver.

6. Chassis: supports the weight of whole vehicle and occupants and includes all rear suspension components and linkages.

7. Roof support frame: have function of supporting the roof structure.

8. Roof: cover the occupants from external factor such as sun.

9: engine and other Components: this is modelled to consider the mass and space of the engine, gas cylinder and other missing rear parts.

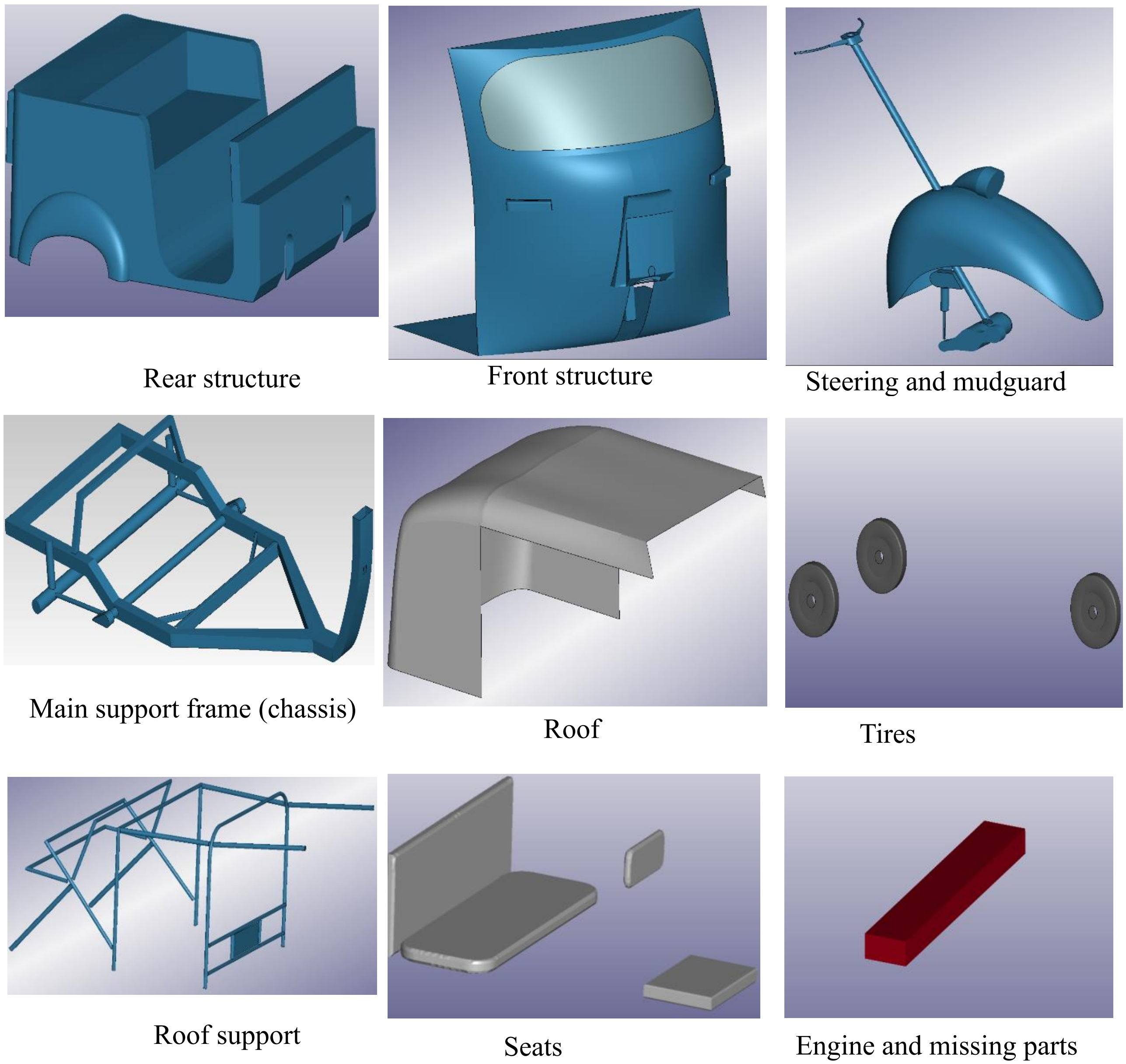

Figure 4.3. Modeled components of TWV

After modeling the above main components, the next procedure is to assemble the separated components in to one full model. The assembled 3D modeling of the three structure is shown on Figure 4.4.


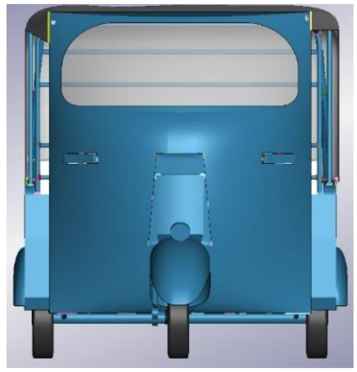
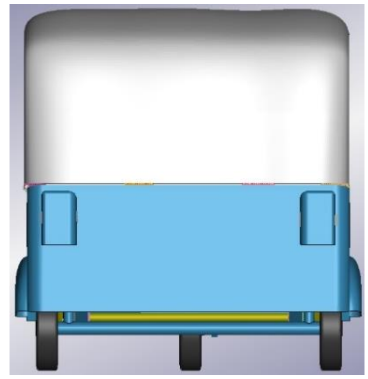

(a) (b) (c)

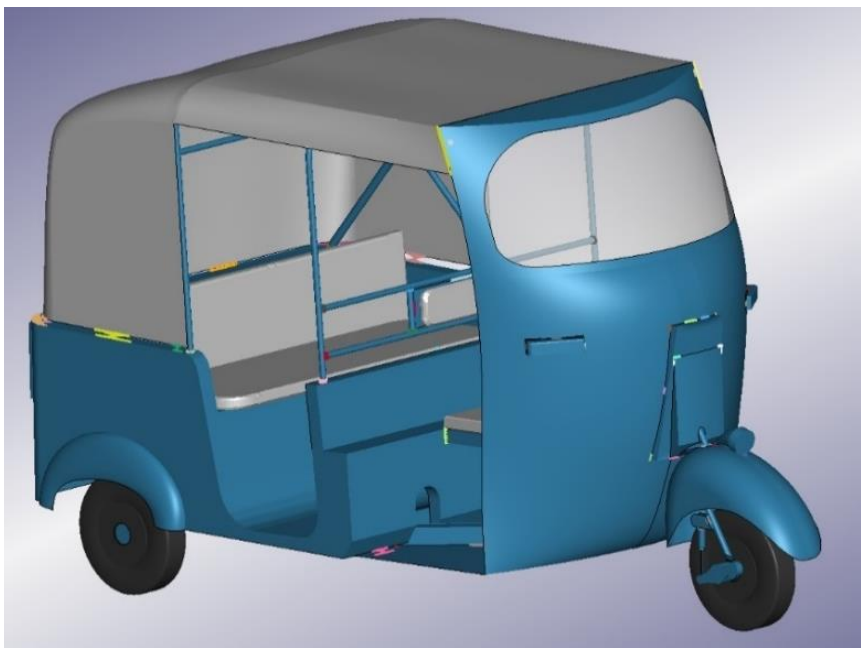

(d)

Figure 4.4. Auto rickshaw model; (a) side view; (b) front view. (c) Rear view; (d) 3D view

4.2.2 Model cheek and surface clean

After modeling Getting Model 'Right' or model Checking consist of three basic stages and this are before, during and after analysis (Krishnamoorthy et al., 2011).

Pre-analysis checking: Any checks to do before running your analysis in LS-DYNA.

Checking during the analysis: Any checks you may want to do whilst the model is running.

Post-analysis checking: Checks on your models after the analysis is complete. This includes feedback to access initial model data.

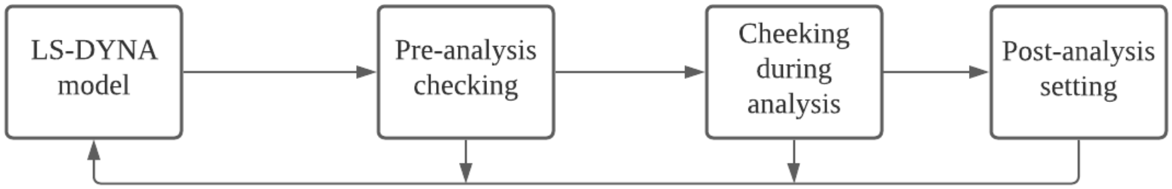

Figure 4.5. Model checking procedures

4.2.2.1 Pre-analysis checking

Before meshing the: Computer Aided Design (CAD) of an auto rickshaw model was converted by ANSYS software in to an Initial Graphics Exchange Specification (IGES) model. Then, the model was cheeked for whether modeling errors are available or not. Duplicated surfaces, unwanted lines, edges and part to part penetration etc., are cheeked and removed from the imported model. The next stage is to export the model to ls dyna pre-post meshing and for further deep checking's LS dyna Pre-Analysis Checking includes:

Simple and detailed checks

- Checks on curves referenced by particular material types.
- Rigid body constraint clash checks.
- Tied (or not tied) contact checks/penetration checks.

Element quality checks.

Incorrect values in certain fields (for example a negative value when this is not valid).This errors usually leads to usually errors like the above will result in LS-DYNA not running, and a termination so when running in LS-DYNA it is important that the issue is picked up at the pre-analysis checking stage, as it may go unnoticed. This is arguably the most important step of the checking process. Having confidence in the model you are submitting into LS-DYNA is important, and having a common process in place for checking before submission can lead to consistently "healthy" models across a larger team.

Normal cheeks

This interface is for reviewing and reversing shell, segment, and thick shell normal. Consistent normal in a part may be required to meet mesh quality standards, for contact definitions in LS DYNA, and also for post-processing shell results at various integration points. Uniformly aligned normal are also required before performing a shell offset operation.

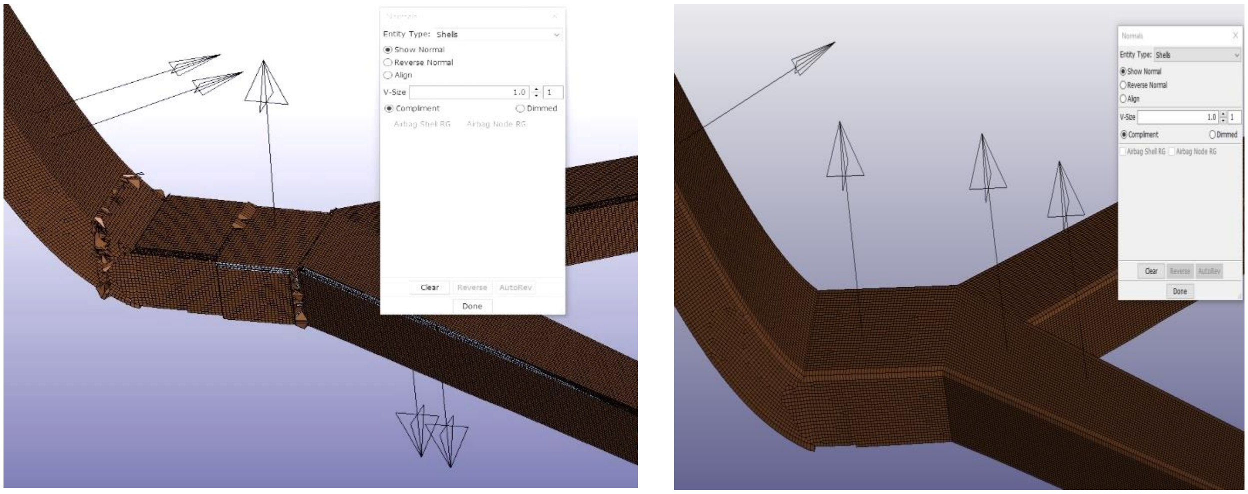

(a) (b)

Figure 4.6. Shell Normal before (a) and after fixing the problems (b)

Figure 4.6 shows the problem occurred on the chassis frame in which the shell normal were misaligned (Figure 4.6.a) create problem by deforming at some intersection and then after correcting the problem (Figure 4.6. b) by reversing the shell direction.

Check for crossed edges

The first thing to do is to ensure that no crossed edges exists. The case where an edge of an element crosses another shell element mid surface, or face on a solid element, is not a penetration in a classical sense in LS-DYNA. But these mesh errors might lead to severe problems when running an analysis in LS-DYNA so, it is very important that such modeling is avoided (Redscan, 2017).

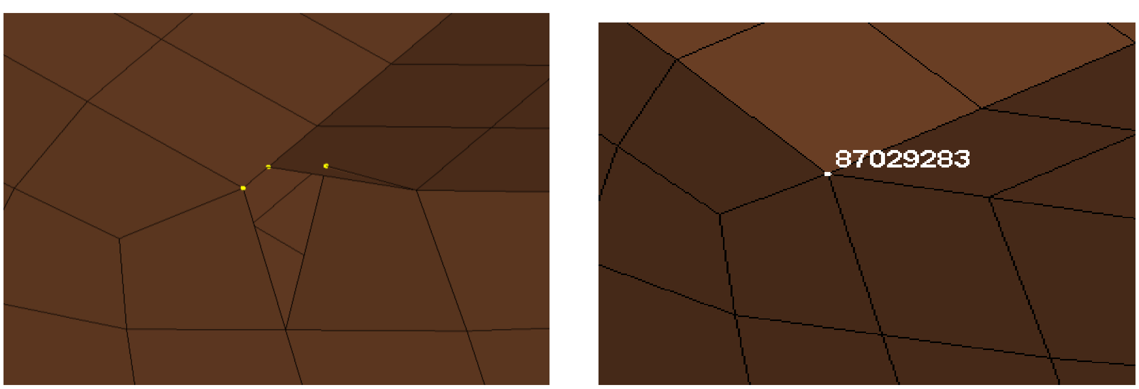

a b

Figure 4.7. Crossed edges problem before and after fixing

Initial Penetration

Initial penetration is a term used frequently to describe the amount of penetration that exists between a node and its closest master segment (in the case of classic node/ segment treatment) or between two interacting segments (in the case of `segment-based` treatment) during the initialization of the problem. This is shown in Figure 4.8 by considering only the thickness on the master segment for simplicity. The most obvious recommendation would be to have no initial penetrations at all. However, this is rather difficult due to the nature of the model building process and the number of design changes that usually occur during the course of the product lifecycle. Penetrations are checked for shell, beam and solid elements in LS DYNA, Penetration check by "Select Parts" and check by CONTACT. Penetration check by "Select Parts" (Dynasupport.com, 2021). Figure 4.8 shows penetration cheek by part. The arrow shown on the model shows the penetration and the magnitude is shown on the vector plot at right side of the model.

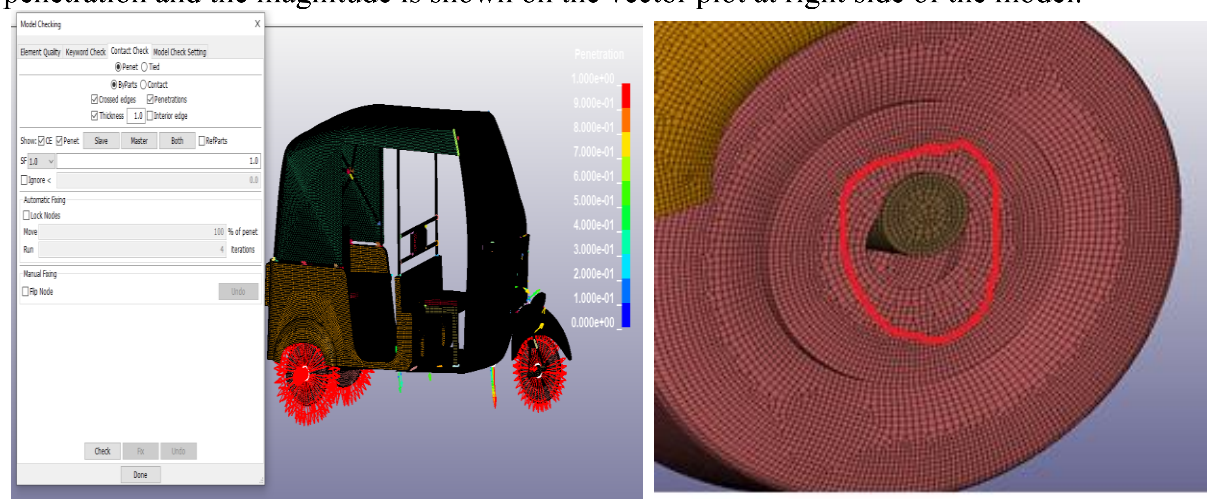

Figure 4.8. Initial Penetration

This option is useful if you not yet have created any contact definitions. Contact thickness for this check is taken from section card data unless the "Thickness" toggle is activated. If "Thickness" is toggled, all shell and beam elements will get the user-specified contact thickness, solid elements have zero thickness. The check that is performed follows the same rules as *CONTACT_GENERAL would do, i.e. it will check for node-to-surface, free-edge-to-free-edge and node to edge penetrations for all parts to all parts.

Penetration cheek by contact

By selecting a contact from the list of defined contact in the model, the elements included in the contact are displayed and the check is performed by taking care of all parameters that affects the contact thickness (SST, MST, SFST, SFMT, SHLTHK, SLDTHK, SSTHK, OPTT, SFT, TH, THSF) and which nodes/elements is to be checked against penetration to which elements.

Need for Penetration-Free Simulation Model at First Cycle

Existence of penetration at the first cycle in non-interference contact definitions, which is after the Initialization of the problem, has several adverse effects on the quality of the simulation. LS-DYNA attempts to remove any penetration that may exist at the first cycle by applying forces to the nodes involved. This initial force can in some instances be very large which may have adverse effects on the stability of the model. These forces could also lead to localized initial stresses and strains that may be non-physical. Additionally, if the penetrations were unable to be removed completely at the first cycle, they tend to be carried over to the subsequent cycles leading to a `negative energy` condition altering the numerical accuracy of the simulations. Experience with large and complicated models show that any existence of penetration at the first cycle effects repeatability and robustness when the model is run using multiple combinations of software and hardware. These shortcomings of initial penetrations motivate both the developers and the users to find a method that not only eliminate the issues but they do that in a way that requires minimum user effort (Dynasupport.com, 2021).

Keyword check

Another way to tackle problems on the modeling process is to look for keyword cheek.

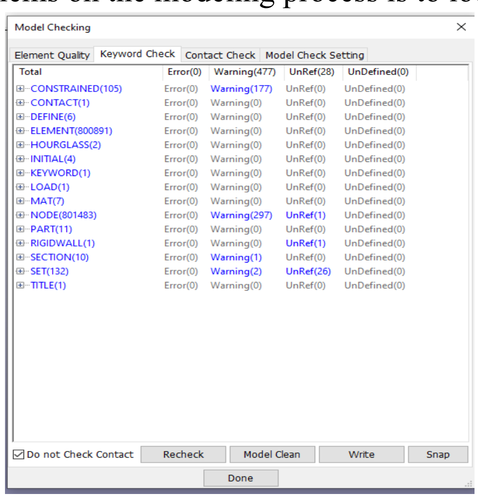

Figure 4.9. Keyword cheeks

Here the model is cheeked for keyword input error such as section, material and constraints. Figure 4.9. Shows the Model keyword report in which all the errors are removed and left with some warnings.

During analysis

Under this section, penetrations and modeling error etc., were reported. So that a user can fix the problem by reading *Warning* in message file or on the running LS DYNA command window.

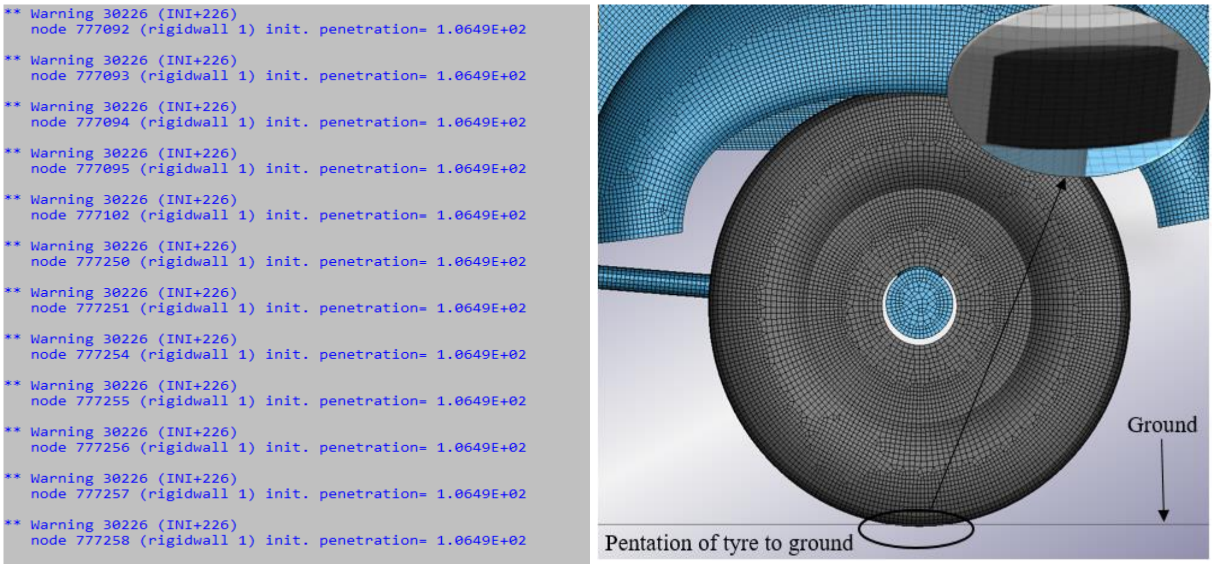

Figure 4.10. Warring during analysis

Figure 4.10, shows the reported waring message .it reports the penetration detected between the ground and tire

Post-analysis checking

Post-checking provide information about the model deformations, energy balance and other results. The deformations can also be reviewed from the test video. This information is useful for model checking especially for those parts with large permanent deformations. Although the relation of energy balance, hourglass energy and energy ratio is also cheeked (Cheng et al., 2001). On this paper this cheeks are presented on result and discussion chapter.

4.2.3 Computational vehicle model

Computer Aided Design (CAD) of an auto rickshaw model from ANSYS software was imported to LS DYNA in form of Initial Graphics Exchange Specification (IGES) model format. Then, the FE model was created by LS DYNA software using dimensions from the real vehicle, as shown in Figure 4.11 with top (a) and isometric view (b). The accuracy and efficiency of finite element simulations are highly reliant on mesh quality Therefore, a fine mesh of acceptable quality was required to produce accurate results and furthermore, avoid error terminations, such as a negative volume in the solid element.

Mesh generation

Mesh generation includes mesh type, size and geometrical attributes. There are three different mesh types, 1D, 2D and 3D, relevant to element dimension.

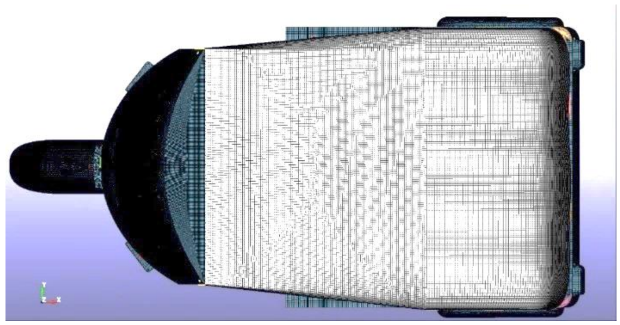

(a)

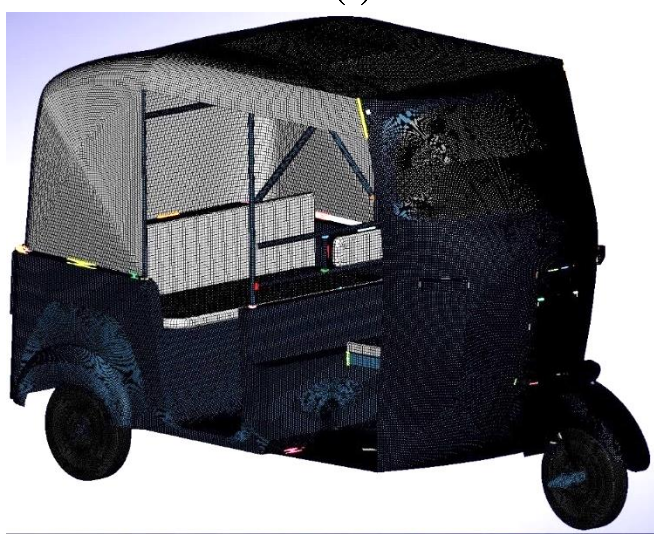

(b)

Figure 4.11. FE model of the auto rickshaw

Mostly, auto rickshaw components were a shell plate, which means that the length and width of the structure is considerably larger than its thickness. Therefore, 2D mesh type was used. The three-wheel vehicle geometry was meshed by LS DYNA software using mixing of linear quadrilateral 97.7% and triangular elements 0.295%. The element size for the whole model between 2mm and 6mm. The total number of elements for the whole meshed model were

1292983 and node 1311326. So, the whole meshed model is very complex and computationally "expensive", see Figure 4.11.

Quality cheek

Different quality parameters like skew, aspect ratio, included angles, Jacobian, stretch etc., are the measures of how far a given element deviates from ideal shape. Square means all angles 900 and equal sides, while equilateral triangle is all angles 600 and equal sides. Some of the quality checks are based on angles (like skew, included angles) while others on side ratios and area (Rahman & Babu, 2019). Table 4.1 shows the quality of the existing TWV model.

Table 4.1. Element quality check summary

Quality Name	Minimum. Value	Maximum. value	Allowable	#Violated(%)
Min side length	0	0	3	0(0%)
Max side length	0	0	30	0(0%)
Aspect Ratio	1	9.77	5	10(0.000818%)
Warpage	0	180	15	331(0.0271%)
Min Quad Angle	20	90	45	214(0.0175%)
Max Quad Angle	0	0	135	0(0%)
Min Tria Angle	0	0	30	0(0%)
Max Tria Angle	0	0	120	0(0%)
Taper	0	0	0.7	0(0%)
Skew	0	58.6	45	44(0.0036%)
Jacobian	-0.0617	1	0.6	643(0.0526%)
Char. length	0	0	1	0(0%)
Area	0	0	5	0(0%)
Feature angle	0	0	30	0(0%)
Time Step	0	0	1.00E-06	0(0%)
#quads (%) :1218224(99.7%) #trias (%):3609(0.295%), #total of failed (%):0(0%)				

4.2.4 Analysis setting

A) Part Material properties and thicknesses of the vehicle components

Material Definition

Vehicle material types and properties are the most important factors, which effect significantly the accuracy of the impact simulation. Moreover, material types and properties should fulfil the automotive criteria, such as safety, environment, lightweight, fuel consumption, cost and design. Mostly, the vehicle model consists of shells, which need to identify thicknesses for every single shell besides mechanical material properties.

Table 4.2. Material mechanical properties for vehicle part set

Vehicle item	Mass density (kg/mm^3)	Young's Modulus (KN/mm^3)	Poisson's ratio	Yield Stress (KN/mm^3)	Shear Modulus (KN/mm^3)	Tangent modulus
Vehicle structure	7.80e-006	210	0.3	0.25		1
Chassis and roof support	7.80e-006	210	0.3	0.25		
Wind screen	2.500e-006	76	0.3	0.138		1
road	7.86e-0012	2e5	0.3			
Roof	6.800e-006	135	0.35		5	
Seat(cushion)	1.010e-007	0.00416	0.35			
tire	1.700e-006	24.61	0.32			

However, it has two solid parts. The vehicle components materials were selected by the ls-dyna material library. The keyword used for tire was modeled by MAT_ELASTIC. While, MAT_PIECEWISE_LINEAR_PLASTICITY Was used for windscreen and vehicle structures the roof was modeled by MAT_FABRIC. Since some parts are not subjected to deformation so they were modeled by MAT_RIGID, these are seat, axles and engine components representation. Most vehicle components thicknesses were defined by section shell and the rest with solid element. For shell elements the value of the thickness are determined based on their density and mass value listed on above data collections. The material mechanical properties and shell thicknesses of the vehicle components are shown in Table 4.2 and Table 4.3.

Table 4.3. Thicknesses of the vehicle component

vehicle component	Thicknesses(mm)
Vehicle structure	1
Seat(cushion)	0.5
Frame or chassis	6
Roof support	2
Road	0.5
Roof	0.15
Windscreen	3
Tire	5

Missing Components

To simplify the model, several of the components of the car were not modeled, but rather were represented as point masses and rigid bodies. The components acted mainly in series progressing from the front of the car to the middle, all interconnected to each other. This component representation was done to preserve the inertial properties of these components, which would be very important to create an accurate impact simulation of the TWV. These point masses were created in LS-DYNA by creating a single node, and adding a mass using ELEMENT_MASS and the node is connected to any of the rigid part in the model using *CONTRAINED_EXTRA NODE. Masses were at both of the front wheels to represent the mass of the wheel and brake component assembly. Engine part and steering assembly mesh were only added for visualization purposes. Additionally one very large point mass (accounting for roughly 20% of the total mass of the simulation) was attached to the frame body to represent the mass of all components behind the monocoque including the engine, transmission, and suspension, and other miscellaneous components.

Element Formulation

This paper adopts default element formulation. Belytschko-tsay element formulation is used for shell element with 3 point integration point and constant stress for solid.

Constraints

After meshing the individual parts, interactions have been defined between them. These interactions are defined between the surfaces of different parts and control the transmission of forces and moments between individual members. Kinematic joints have been defined for different parts of the vehicle. In LS-DYNA, The constraint between two deformable parts was given by the keyword CONSTRAINED_NODAL_RIGID_BODY in Entity creation. Also to connect rigid to deformable body CONSTRAINED_EXTRA_NODE_SET is used by creating node set from deformable body. This type of constraint connects a single node or multiple node of deformable part to another rigid part. And constrained rigid body is another keyword used to connect rigid bodies with another rigid body. In addition, JOINT_REVOLUTE was used to constrain tire with the vehicle components.

Contact Definition

The contact between two parts is given to prevent penetration during the crash. There are a lot of contact types are available in the keyword manager. In this case, the contact is directly in within the components of the TWV like windshield, the front portion, driver seat, etc., and between the road and the tires, between the dummy and various parts of the TWV, and also used to define the interaction between the impacting surfaces (TWV and external part).

Table 4.4. Master and slave parts

Contact type	Slave	Master
Automatic surface to surface	Tire	ground
Automatic surface to surface	Whole vehicle	Other external part
Automatic single surface	Whole vehicle	non

In order to define the interaction between different parts of the TWV, a set of parts (PART_SET) is defined then, the keyword CONTACT_AUTOMATIC_SINGLE_SURFACE used. The master and slave parts are listed in Table 4.4. Considering the difficulties in using any external pre-processor to remove initial penetrations, the option of using the IGNORE used on the contact definitions. This method handle the presence of initial penetrations. Using IGNORE=1 causes LS-DYNA to skip the geometry update step thereby preserving the geometry while considering size changes.

4.2.5 The occupant restraint system

The TWV model used were equipped with Hybrid III dummy models therefore direct improvements on occupant injury protection could be seen the dummy finite element model, which was used to emulate, is completely based on the test of 5th percentile Hybrid dummy frontal crush and side dummy. The key parts, such as chest and neck, are mounted with the quality of flexible, so as to judge of the injury after crash. For each of the crash condition their response of their body is studied.

Dummy positioning

Before positioning, units of the dummies are changed to the desired unit system using unit transformation key and also dummy model components are renumbered. As the dummy was imported in to LS PRE-POST, the dummy was in the position shown on Figure 4.12 (a).

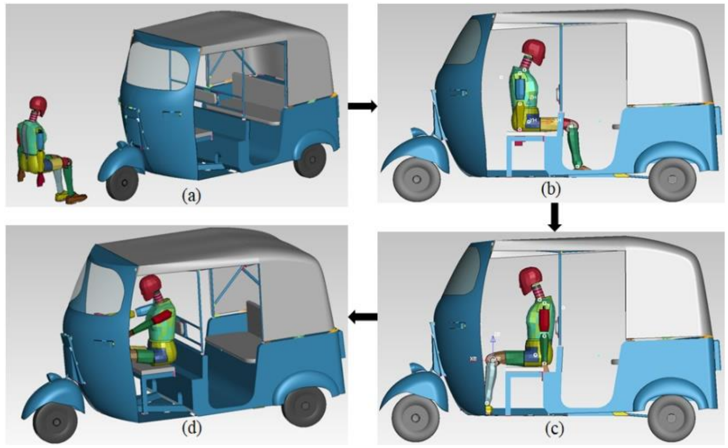

Figure 4.12. Dummy positioning steps

Starting from this point, a positional change, from imported to desired (driver sit in this case) was made using dummy position tool in LS-PREPOST software. The changes did not disturb the integrity of any of the dummy joints (Kunle et al., 2019). The dummy is translated in X,Y,Z direction to reach the desired position as it shown Figure (b). Then it is rotated 180 degree to achieve the correct direction as it is shown Figure (c). Finally the body part of the dummy are set in to the appropriate driver condition. Other dummies (side dummies) which are used on this paper follows the same procedure except their body parts positioning.

Simplifying the model

To minimize the computational run time, vehicle simplification was required thus, among the passenger dummies only the right side dummy was considered. However to meet the total mass of the occupants and TWV, their center of gravity is measured and sum of their mass is applied at that point. To do so, all the components of the auto rickshaw, driver and right passenger were removed to measure the mass, center of gravity and the moment of inertia of the two dummies, by LS-DYNA software (LS-Pre-Post), as shown in Figure 4.13 (b).

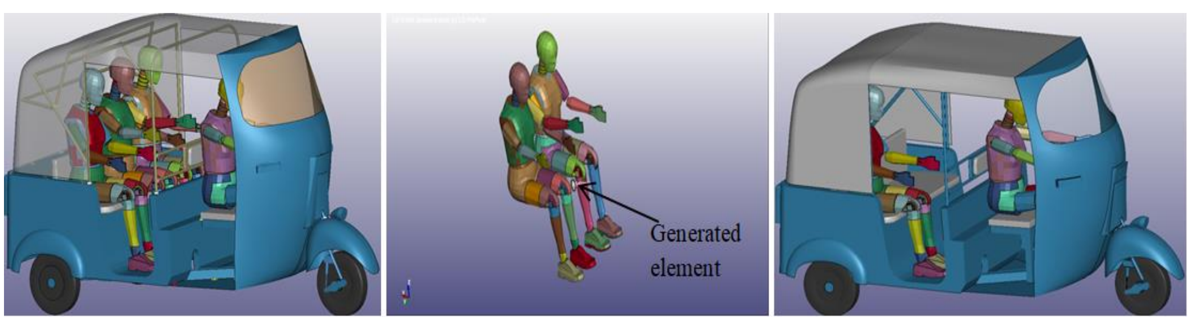

Figure 4.13 Method for simplifying the model

The occupants inside the TWV were simplified, such that only one element was generated to represent the same mass, center of gravity and moment of inertia, see Figure 4.13 (C). The simplified model of vehicle, therefore, has fewer occupants than the full model. The new model consists of a one rear passenger, and driver, as shown in Figure 4.13(c).

4.2.6 Boundary Conditions and Simulation environment

The function of the boundary conditions is to create and define constraints and loads on finite element models. To simulate a full vehicle crash, all loads and boundary conditions that occur in the actual crash event need to be modeled. Just as a vehicle is subjected to gravitational loads in real life, the simulated model should have a representative gravity force applied. Friction forces between the tires and the road surface play an important role in how the vehicle behaves on impact, so these have to be accounted for in the simulation. A velocity has to be applied to the vehicle in a manner as to not impart any unrealistic acceleration or cause the simulation to run for an extended amount of time. Fortunately, Ls-Dyna provides methods to simulate all of these requirements (Liu, 2013). In this section the setups for the simulation of front, side, rear and roof impact test will be presented. The Boundary condition and set up follows the standards indicted on literature. The detail of set ups and boundary condition in each of the crush scenarios are discussed as follow.

Case 1. Front Impact

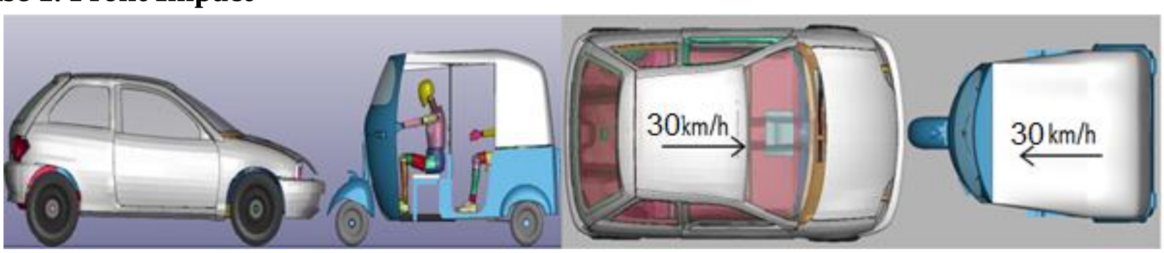

(a) (b)

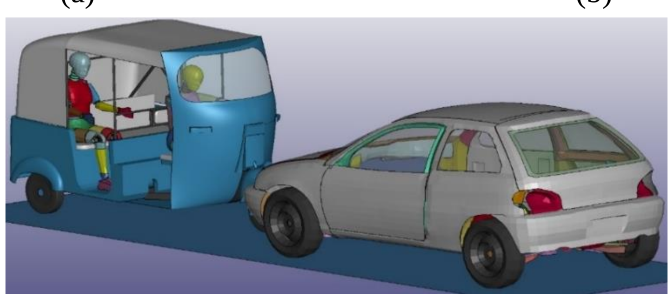

(c)

Figure 4.14. Simulation set ups and boundary condition of frontal crush

In front impact test, THE TWV with dummy inside is crashing with another car which is moving on opposite side with the speed of 30 km/h and the main purpose is to clarify the damages to TWV front body and driver and passenger. Figure 4.14 front impacts SET UP IS shown in three different views which we will analyze in the following section.

Boundary condition

To simulate the Frontal (Head on) impact, the TWV vehicle is subject to an initial velocity of 25 km/h and along the horizontal direction towards the car. The mass of the two cars and the TWV, dummies and car are given velocity of 25 km/h and TWV and the simulation takes 0.1ms.

Case 2.Lateral Test

In this test the A three wheeler vehicle impacts the rigid pole laterally at a speed of 25 km/h such that its line of forward motion forms an angle of 75 degrees with the vehicle's longitudinal axis, simulating a real-world crash in which the vehicle hits a tree while sliding on the road. The rigid pole is a vertically oriented metal structure with:

- Diameter of 254 mm.
- Beginning no more than 102 mm above the lowest point of the tires on the struck side of the fully loaded test vehicle.
- Extending at least 150 mm above the highest point of the roof of the test vehicle. The direction of vehicle motion is such that the pole is always aligned with the CG of the head of the driver. This impact set up is shown in Figure 4.15 (a) and (b).

The direction of vehicle motion is such that the pole is always aligned with the CG of the head of the driver(Singh, 2012). The LS-DYNA set-up for the side impact crash test of the TWV model with a pole is shown in Figure 4.15.

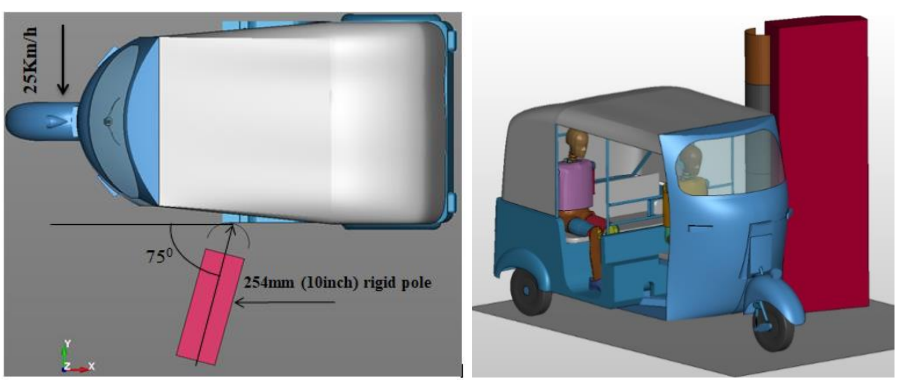

(a) (b)

Figure 4.15. FEA set up for Lateral Test

Case 3. Roof Crush Resistance Test

Set up

As it is stated on the standard the FEA model represents a quasi-static analysis that can virtually simulate realistic conditions of real rollover accidents. The boundary conditions and set ups used are discussed below.

The roof crush test device

The Finite Element model OF roof crush test (PLATE) device which is developed by NHTSA is RIGID WALL_GEOMERIC_FLAT_MOTION AND downloaded from NHTSA website.

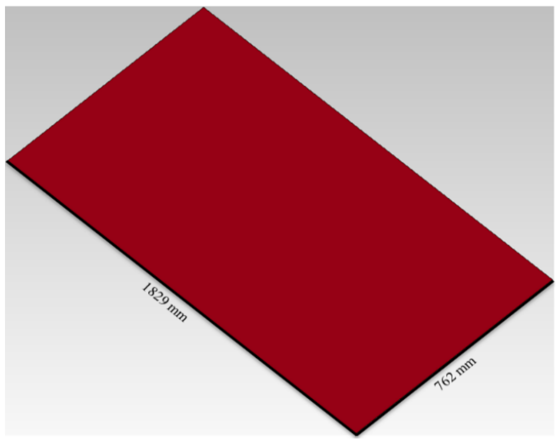

Figure 4.16. Impactor plate

The plate have rectangular a flat surface with 762 mm and 1,829 mm length as shown in Figure 4.16. It is imported in to LS-DYNA and placed on the TWV with 25° roll angle and 5° pitch angle using KEWORD_INCLUDE_TRANSFORM as shown on Figure 4.17.

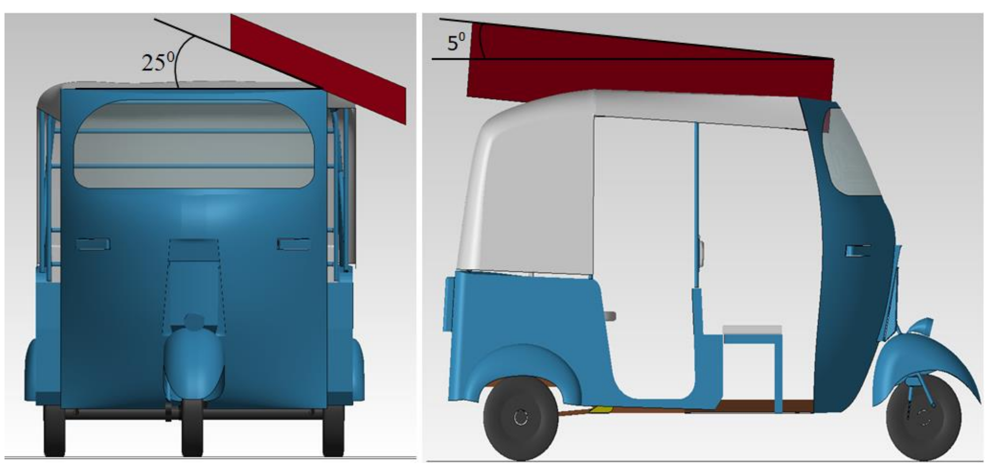

Figure 4.17. Setup for roof crush test

THE Plate 1mm Shell thickness and material is defined using *SECTION_SHELL and *MAT_ELASTIC keyword card. The material Properties are defined on Table 4.5

Table 4.5. Plate material

Mass Density (Ton/mm3)	Young's Modulus (MPa)	Poisson's Ratio
7.890e-12	2.100e+05	0.3

Boundary condition

The vehicle tire is constrained in all degree of freedom using Keyword *Boundary_spc_set. The velocity of the rest of the vehicle parts are set to zero. In another hand X, Y, Z translational degrees of freedom is set for the motion of rigid plate. The displacement is defined in the desired vector direction using *BOUNDARY_PRESCRIBED_MOTION_SET (i.e. translational motion only in direction given by the vector. Movement on plane normal to the vector is permitted). *DEFINE_CURVE keyword is used to define displacement curve of the plate. The plate should move distance of 5 inches (127mm) with 0.2s as per FMVSS standards. The defined curve relation of time vs displacement is shown on Figure 4.17.

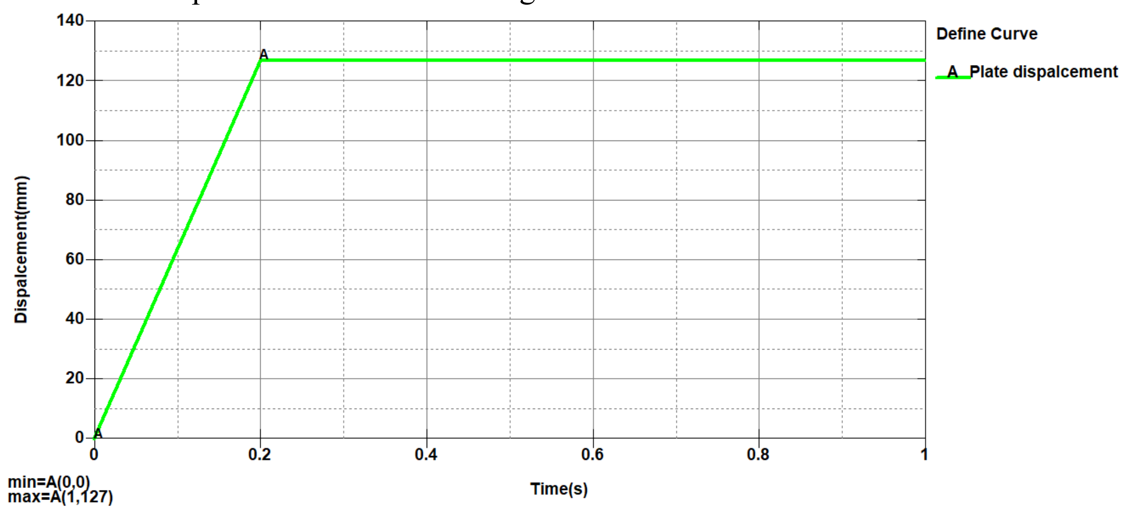

Figure 4.18. Displacement curve for plate motion

As mentioned on previous sections *CONTACT_AUTOMATIC_SINGLE_SURFACE is used for vehicle self-contact. *CONTACT_AUTOMATIC_SURFACE_TO_SURFACE card is used to create the contact between rigid plate and TWV structure. Termination time of 0.2s is activated using CONTROL_TERMINATION keyword. So that the pate is expected to move 127mm with 0.2s and the TWV roof structure should respond with reaction force at least 1.5 of its curb weight (FMVSS 216) or 3.5 (IIHS) to be safe .

Case 4. Rear-End Crash Scenario Modeling

Federal Motor Vehicle Safety Standard (FMVSS) No. 301 specifies a rear-impact test. The rear-impact test is designed to promote the crashworthiness of the body structure and fuel tank. In this test a moveable deformable barrier (MDB) impacts at 25 km/h into the rear of stationary vehicle with an offset of 70% as shown in Figure 19 (a) and (b). The MDB used in the rear-impact test weighs 1380 kg. Moving Deformable Barriers (MDB) are the most widely used barrier, however, not all the crash tests use the same kind of barrier. The barrier specific to FMVSS 310R is downloaded from LSTC's website (Livermore Software Technology Corporation, 2018). The MDB face assembly has a bumper which is constructed of honeycomb 1690 kPa sandwiched between thick aluminum plates (Kalaga, 2018). The barrier the specifications are shown in Table 4.6.

Table 4.6. MDB specification

Model	Deformable Barrier
version	170920_v4.3
model	LTSC shell barrier
Weight,Kg	1380
Wheel Base,mm	2591
Total number of element	549,509

It is simulated in LS-Dyna solver for 0.1 seconds with the barrier located almost at the point of contact to reduce simulation time. The setup is shown in Figures 4.18 (a) and (b).

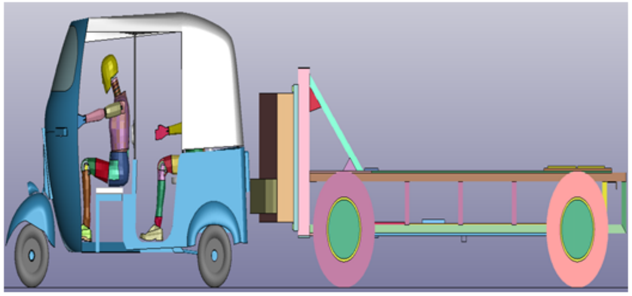

a

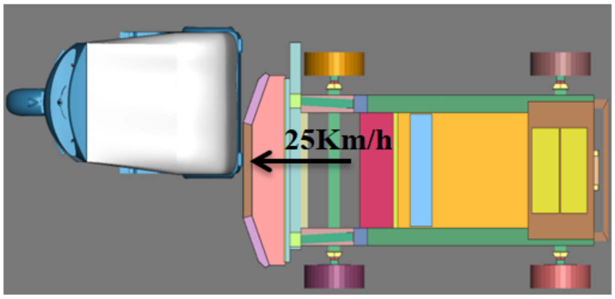

b

Figure 4.19. Rear end collision set ups

A node set for the entire barrier is created and the input velocity is given using*INTIAL VELOCITY_GENERATION data group in the *INITIAL keyword interface. This is used by creating a *SET_PART. The contacts among the parts are modeled using a single surface sliding interface AUTOMATIC_SINGLE_SURFACE and the contacts between the car and the barrier are given using the keyword AUTOMATIC_SURFACE_TO_SURFACE. While giving the contacts, the car, which is a stationary target, is assigned master and the barrier, which is the impactor entity, is assigned as slave. The termination time has been set to 0.14 seconds in *CONTROL_TERMINATION keyword with a time step of -4e-7 using *CONTROL_TIMESTEP keyword. Other analysis setting which helps for the simulation are listed below.

Impact velocity

In general auto rickshaws are low speed vehicles with a maximum speed of 60 km/h with reasonable acceleration. The international standard for crashworthiness is normally evaluated at 48 km/h. However, at the time of accident, especially. for during frontal impact, the vehicle speed is normally reduced due to the driver braking action (Srikanth & Prakash, 2009). These velocities tend to be in the range of 20-30 km/h (A Chawla et al., 2001). Hence, the simulations have been done based on this range for different crush scenarios mentioned above INITIAL_VELOCITY_GENERATION was used to define varied vehicle impact velocity.

Control cards

Solution control has a significant influence on simulation stability and accuracy. CONTROL_TERMINATION was used to define the simulation termination time. It is used to control the time step and run time of the file. These cards are necessary to control the duration of simulation time.

1. DT min
2. DT The

Run time of file is 0.1s. The results are plotted for the energies absorbed by the fascia in 15 ms. DT min is the interval in which the codes are generated in processing the file in ls-dyna. DT is the time step value. It is the minimum time taken by the sound wave for travelling from one end to other of the shortest element. It is also used in plotting the graph i.e. for every 0.001 interval a point on the graph is plotted. Decreasing the value below 0.001 increasing the smoothness of The curve but at the same time increases time.

Other control cards are defined, these are control are:

- CONTROL_ACCURACY: control parameters that can improve the accuracy of the calculation.
- CONTROL_CONTACT: Change defaults for computation with contact surfaces.
- CONTROL_ENERGY: Provide controls for energy dissipation options.
- CONTROL_HOURGLASS: control zero energy formation.

Database cards

Database cards are given to obtain the output i.e. to generate results and to interpret plots. database was used to define the expected results using American Standard Code for Information Interchange (ASCII) to define specific functions such as NODOUT, JNFORC, JSTIFR and DEFORC (Kunle et al., 2019). Generally, they are used to analyze the energy absorption characteristics that are discussed in next chapter namely result and discussions. Some of the database plots used are:

- D3PLOT (database for complete output states)
- D3DUMP (complete database for restart)
- ASCII options (material energies (MATSUM), wall force (RWFORC), Resultant interface forces (RCFORC) and so on

4.3 Modification on the existing three-wheeler vehicle

4.3.1 Introduction

For years now, the vehicles safety has become more and more important in the car development. The World Health Organization has synthesized evidence-based measures called **Save LIVES** that can significantly reduce road traffic fatalities and injuries. Among the 6 strategies listed to reduce injuries and deaths from road crashes the first Standards states that, at event of frontal and side impact the vehicle should with stand a frontal or side impact crash and protect the occupants when tested at specific speeds (Desapriya, 2011). By keeping that in mind modification were mode for three-wheeler vehicle. Generally, modifications are done by vehicles owners to give them a distinctive appearance, to improve their performance, to add desired features, change the engine (alternate or replacement engines), suspension, or to add a long-range fuel tank. Others modify their vehicles so that they are better suited to a specialised purpose.in another hand, Excessive modifications can affect the road handling of the vehicles, such as, it may distract the original vehicle stability, fuel consumption due to addition of too much weight and other safety regulations which may result in wrong side of the law and perhaps insurance company. So staying safe and legal is extremely important when modifying car. So that the improvement which were going to made on TWV should meet the following additional criteria:

- The vehicle must not have any rust or deficiencies in the areas to be modified or in the areas already modified.
- The vehicle must be structurally sound, without need of mechanical repairs and able to support/accommodate the needed adaptation (For & Vehicle, 2021).
- Do not affect the level of safety, strength or reliability of vital systems, like brakes steering and occupant protection systems.
- Have little or no impact on the vehicle's compliance with mandatory vehicle standards (Nsw.gov.au/topics/Government, 2021).

4.3.2 Safety development

The first thing to consider when making the modification is the driver and the occupants should be extensively protected from direct contact with obstructions and free from, uncontrolled flight. In another word the driver and occupants must receive moderately and retired force or momentum occurred due to the collision. In modern vehicles safety equipment such as seatbelts, side door beams, airbags, or other active safety systems have been integrated to protect their occupants for different crash configurations as side impact frontal impact, side impact, and rear impact or from rollover.

To achieve this goal, the car body structure is also designed to be as safe as possible with some crushing zones to absorb energy but also a stiff protective cell for the occupants so called safety cage, the aim of this section is to modify and design TWV body structure as safe as possible with some crushing zones to absorb most of the impact energy but, also a stiff protective cell for the occupants. Here the intention is to achieve this aim by means of an energy absorbing component (deformation elements), a restraint system and stable frame structure. The modifications were based on the study done on previous section of the existing model. The study indicates that small design changes could significantly enhance safety of TWV occupants.

1) Deformation elements

To keep the load on the driver and occupants to a minimum, deformable beam elements are

Mounted at different places of the TWV frame structure. The location in which the modification were fitted are shown in Figure 4.20. The location of mountings is based on the study done on the existing model.the twv is fitted with three main energy-absorbing zones, these were front, side and rear parts of the TWV, see Figure 4.20. The added energy absorbing parts are designed in order to have a controlled deformation. This deformation is used to absorb the maximum kinetic energy during a crash. The equation (2.4) discussed was used to determined absorbed energy. This deformation zones not only absorbed the kinetic energy of impactor, but also the kinetic energy of the TWV itself, for example when the TWV fully crushed into full into a rigid wall. The beam element were act as a bumper beam and designed in such way that that are capable of deformation and together with other linkages. They acts in the same way as the bumper beam of other commercially vehicles. By doing so they will significantly help during collisions of the TWV (Srikanth, 2009) & (Chawla A, 2020) .In addition the support were added and have function of linking the beams with other part of the existing structure and supporting the beam. The side beams have been designed to meet the requirements of beams at event of side crush. They absorbed the side collation energy, reduce intrusion in to the TWV and reduce the force of impact transferred in to the occupants and drivers.

The rear bumper is responsible for protecting the engine, fuel tank, and exhaust systems as well as other safety related components at event of rear crush. This can be achieved by reducing any intrusion into the vehicles compartment. The front bumper have functionality of reduce kinetic energy, lessening the stress on the drivers and occupants body. It should deform and absorbed the impact energy without affecting the occupants. In addition to the added bumper beams in the front, the tire covering structure is converted in to energy absorbing unit by changing its material property. So that the modified tire cover have the function of absorbing energy in addition to covering the front tire. (Kunle et al., 2019), suggested that the combination of Aluminum 6016-T4 windscreen frame and polycarbonate windscreen have the potential reduce impact energy and relatively similar to the current design and cost. The TWV model before and after modification is shown on Figure 4.19 and 4.20.

2) Restraint systems

With low cost changes, the interiors of the TSTs can be redesigned to minimize these impacts (A.C. & S. Mukherjee, 2003).

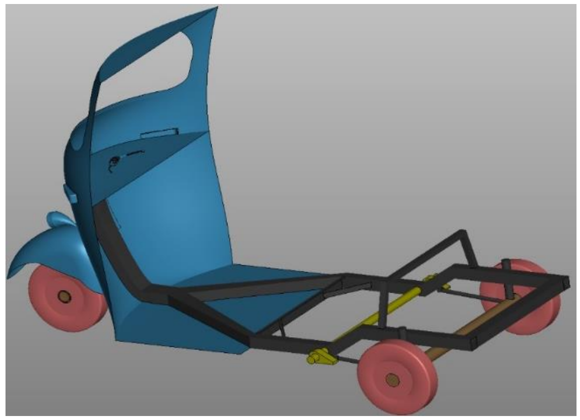

Figure 4.20. Existing structure before modification

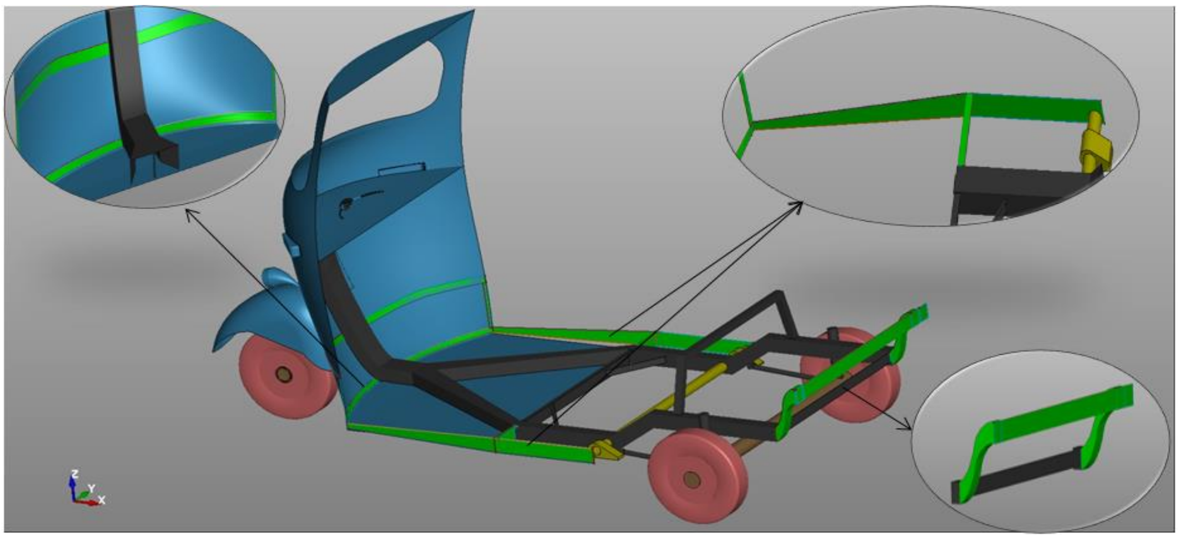

Figure 4.21. After modification (modified model)

A) Padding the critical points of the TWV

With changes in Stiffness of the areas where the occupants are in direct contact with TWV injury level can be reduced significantly. For instance, in case of frontal crushes less than 30 km/h, The knees and head of passengers and the driver impact relatively more stiff surfaces inside the TWV. As a result, both the driver and the passenger have a very high probability of suffering serious head and upper leg (femur) injuries (A Chawla et al., 2001). The injuries mentioned can be reduced by padding or covered with cushion the contact points of driver cabin and passenger compartments with soft material.

B) Seat Belts for driver and Passenger

The driver and occupants must be protected from sliding out to left or right, so they have to couple with the passenger cell via safety belts. Fitting seat belts for the driver and passenger in another solution used to increase safety benefits of two. As a result of the belts, the driver and the occupant are restrained to move and impact with interior part of TWV. Depending on how they are designed and used, seat belts are different. The major types are:

- Lap belts
- Shoulder belts
- Three-point belts
- Automatic seat belts
- Bet-in-seat (BIS)
- Five-point harness

Lap Belt it is also referred to a 2-point seat belt. The belt attached at two-end points over a person’s lap and has no shoulder harnesses. This type of seatbelt is commonly seen in airplanes and in older vehicles. A 3-point seat belt has a sash that goes over the shoulder of the user, and then crosses their lap. They distribute the force of an impact across the chest, pelvis, and shoulders, decreasing the risk of injury for users in an accident. The design prevents more injury than the lap belt alone. As a result, the 3-point belt is the type most commonly used. As the law now mandates that all motor vehicles have seat belts, the 3-point belt is the one predominantly installed by auto manufacturers. A 4-point seat belt has two shoulder straps instead of one. This custom style belt is also known as a racing car seat belt (Belts et al., 2021). Among this 3 seat belt is used for the TWV. The dummy is constrained by three-spot style seatbelt. As shown in Figure 4.22. The seatbelt finite element models include seatbelt, slip ring, pretension, retractor and the sensor element that can make pretension and retractor working.

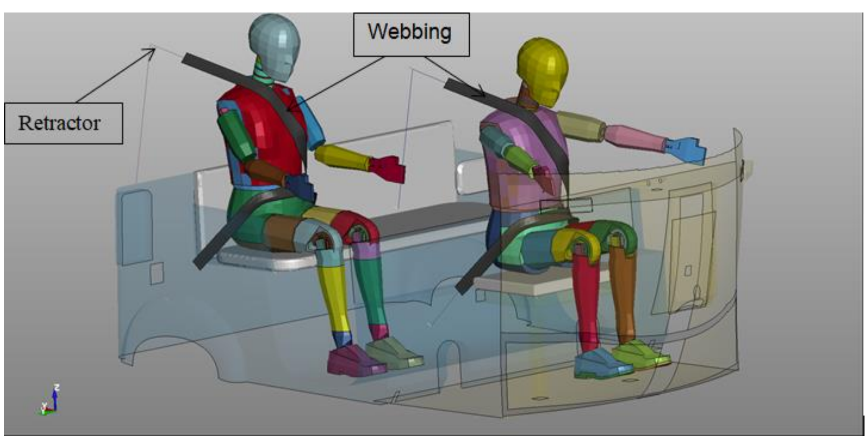

Figure 4.22. Seat belt fitting for the occupants

In LS-DYNA the Seatbelt Fitting command is supplied in Occupant Safety module to easily execute the process. In place of using the command APPLICATION _SEAT_ BELT_ FITTING, from LSTC website the complete belt model is downloaded and imported in to the exiting TWV and fitted into the occupants. After positioning the belt, constrained _rigid body is used to connect the anchor points of the belts with the vehicle components. This reduces the time required for modeling the seat belts. The dummies with seat belts are shown in Figure 4.22.

The retractor also has a mechanism designed to lock the belt into place if the car comes to a sudden stop, which causes the webbing to hold firmly against the wearer. Consequently, this prevents uncontrolled movement inside the vehicle during an accident. The webbing is the flexible part of the seat belt system that is pulled around the person and is tightened to support the occupant body upon impact. The webbing model is consisting of different seat belt: segment belt or single-Line belt (1-D Beam) and Fabric belts (2-D Shells) the segment belt elements are characterized by *SECTION_SEATBELT and *MAT_SEATBELT

The *SECTION_SEATBELT is a keyword that allows model single-line belt elements. density, minimum allowable length for belt elements, load curve for loading and unloading are inputs specified for belt material (Nilesh Dhole, 2012).

C) Stable frame structure

Maintaining the safety cell required to protect the driver and occupants makes high demands on the frame structure, particularly in the case of serious accidents.

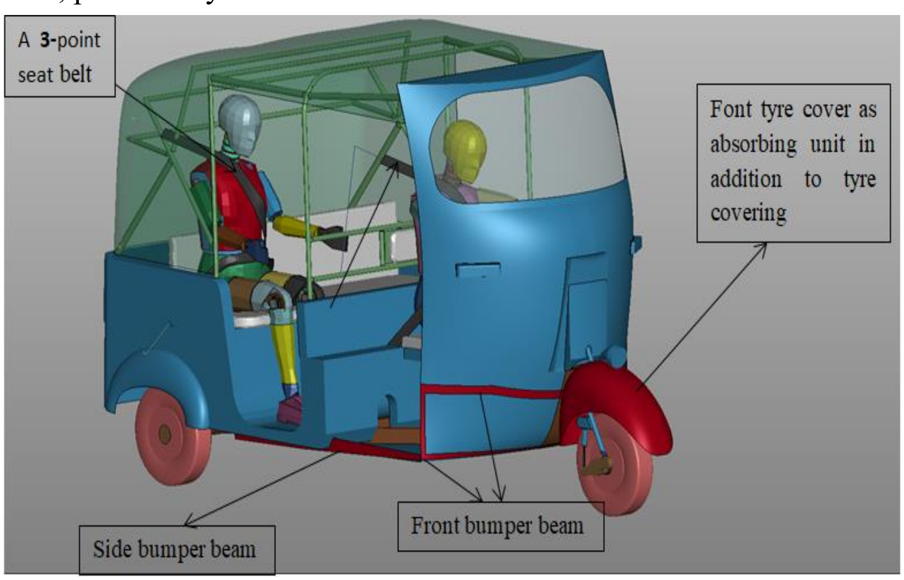

Figure 4.23. TWV isometric view of the modification

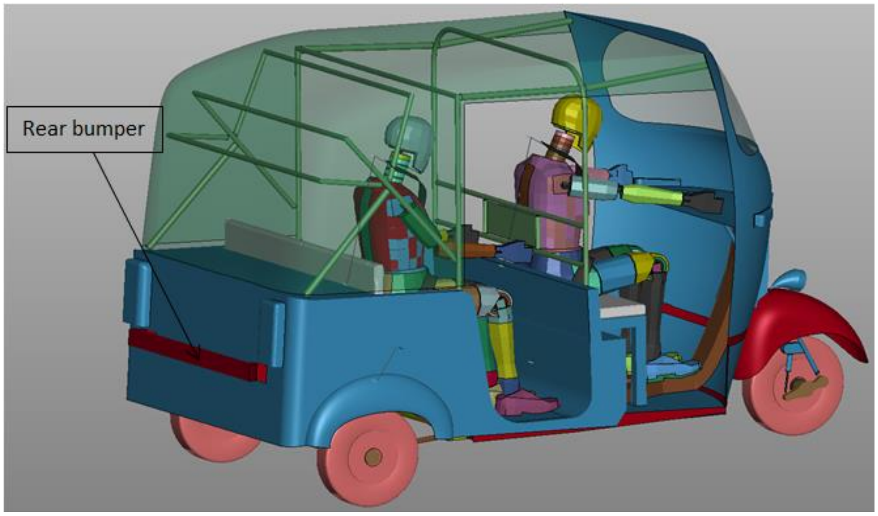

Figure 4.24. TWV isometric rear view of after modification

In case of roll overs accidents the roof frame of the TWV should withstand the loads acting from outside. The final 3D model of the modified TWV is shown Figure 4.23.in addition to the above safety development, the new model have the same fuel consumption with the existing TWV because the total mass of the new model was made the same with the exiting by introducing the use of lightweight material. Since modifications were done symmetrically so the stability of the vehicle is not also affected by the modifications.

4.4 Bumper beam design

To improve the performance of vehicles at event of crash many technological development is needed towards designing a successful lightweight energy absorbing units. During crash, the energy absorbing members of the vehicle are expected to fold progressively, so as to absorb more energy and to ensure enough passenger space (Babu et al., 2020).

Automobile bumper beam is a structural component or part of vehicle, which is mounted at rear, front or side (side doors) for improving crashworthiness or occupant protection during different crash cases. In low speed collision, it used to prevent or reduce damage to the vehicle by absorbing the shock or impact forces. Most of the time, they are not designed as structural components that would significantly contribute to vehicle crashworthiness at high speed. Several design factors are considered on selecting a bumper beam (Babu et al., 2020). The most important factors is:

- The ability of the bumper system to absorb shocks.

- To stay intact at high speed impacts.
- Weight, manufacturing process ability and cost are also the factors design phase.
- Both initial bumper cost and repair cost are also important.

Based on reading of a large number of references, a conclusion is drawn that materials with different thicknesses can gain different performance. So, The purpose of this section is select the best material for the side, rear and front bumper beams and to cheek the selected material strength, energy absorbing capabilities and deformation by varying the thickness of the cross section.

4.4.1 Bumper beam material

On different surveys, it was observed that the performance of the bumper beam at event collision is greatly depending on the material used. If it is properly selected, it produces a great impact on the vehicle performance by minimizing the weight (high fuel efficiency) without sacrificing the strength. Since, most of the fuel consumption (75%) due to the weight of the vehicle. It is also mentioned that, 6%–8% increase in fuel economy can be realized for every 10% reduction in weight. So the use of Lightweight material especially for three wheeler vehicle provide opportunities for reducing vehicle weight, thus increasing fuel efficiency and reducing emission of harmful pollutants. So, for the bumper beams carbon fiber composite material are taken into consideration to achieve the required performance (Wang & Li, 2015). The advantages of composites compared to steels for automobiles are;

- Since their densities are very less, weight reduction of 20%–40% achieved.
- 40%–60% reduced tooling cost.
- Less assembly Cost and time.
- Resistance to corrosion and scratches, reduced noise vibration harshness (NVH), and higher damping.
- Materials and process innovations capable of adding value while providing cost savings.
- Safer structures due to higher specific energy absorption.

Carbon fiber composites are one of 21st century automotive materials. It has mostly known by its properties such as low density, high strength, high modulus, corrosion resistance, selflubricating, high temperature resistance, low thermal expansion coefficient, and good conductivity/thermal performance. However, the price of the carbon fiber composites too expensive to be widely used in the automobile manufacturing as compared to materials such as steel or aluminum. Since a lot of researches and efforts are on-going by researchers and research institutions to reduce the manufacturing cost of carbon fiber composites, the commercialization and use of carbon fiber composites with minimized cost for automobiles will come true in the near future. So in this paper, the bumper beams are additionally mounted on the TWV for safety purposes so that the increase in weight due to the addition of those part should be kept to minimum. Therefore, carbon fiber composites bumper beam material is preferred and used instead of other material. With the given material property data obtained from literatures (Mahadevan & Liu, 1996), the properties will be directly used as the physical parameters in LS-DYNA material cards, and they are summarized in Table 4.7. The type of the carbon fiber composite used is unidirectional IM7/8552 whose density is 1.58 kg/m^3. The Poisson's ratio (y12 and y13) of the carbon fiber composite is 0.0185 and y23 (0.5). Other mechanical properties are shown on Table 4.7.

Table 4.7. Composite material properties for LS-DYNA material cards

Properties	Units	Value
Mass density ρ	kg/mm^3	1.58E-06
Young's modulus, E_{11}	MPa	165000
Young's modulus, E_{22}	MPa	9000
Poisson's ratio(minor), μ_{12}/μ_{13}	-	0.0185
Poisson's ratio, μ_{23}	-	0.5
Shear modulus, G_{12}/G_{31}	MPa	5600
Shear modulus, G_{23}	MPa	2800
Longitudinal compressive strength, XC	MPa	1590
Longitudinal tensile strength, XT	MPa	2560
Transverse compressive strength, YC	MPa	185
Transverse tensile strength, YT	MPa	73
Shear strength, SL	MPa	90
Strain at longitudinal compressive strength, ϵ_{11C}	-	0.011
Strain at longitudinal tensile strength, ϵ_{11T}	-	0.01551

Strain at transverse compressive strength, ϵ_{22C}	-	0.032
Strain at transverse tensile strength, ϵ_{22T}	-	0.0081
Engineering strain at shear strength, γ_{12S}	-	0.05

4.4. Material and thickness definition

The geometric modelling bumper beam is done by using LS-DYNA modelling tools and mesh, boundary conditions, material properties and section properties are defined using on the Ls-pre-post. The beam is uniformly meshed with 10 mm element size. The beam is meshed with shell elements. The ends of the beam are constrained in all the directions both in translational and rotational. The material model or keyword used to define the material is*MAT_ENHANCED_COMPOSITE_DAMAGE or *MAT_054 or *MAT_055. This material model used to define unidirectional thin shell. The card assumes when the material is undamaged, the material is considers be orthotropic and linear elastic and when the damage occurs nonlinearity is introduced into the material (Chatla, 2012). This material card has special measures to failure under compression.

Material 54 is suggested by Chang which is called Chang matrix failure criterion and material 55 is suggested by Tsai-Wu which is called Tsai-Wu matrix failure criterion and these two models have very similar formulation. In material model 54 and 55, ultimate failure can occur in any four different ways:

1) Chang-Chang failure criterion is satisfied in tensile fiber mode.
2) Maximum fiber tensile strain is met.
3) Maximum effective failure strain is met.
4) Minimum time step is met.

(Chatla, 2012)., This criterion differentiates failure due to tensile fiber mode, compressive fiber mode, tensile matrix mode and compressive matrix mode based on Chang/Chang failure criterion. The stress interactions leading to laminate failure are coupled in all failure modes other than compressive fiber mode. If the failure has occurred in all of the laminate layers, then the element is deleted (Krishnamoorthy, 2009).

This model is used for thin shells only. The LS-DYNA MAT54 material model is of interest for large full-scale structural damage simulations because it is a relatively simple material model, which requires minimal input parameters. Not only does this reduce the computational requirement of the simulation, but it also reduces the difficulty and amount of material testing necessary to generate input parameters. In addition to material properties of the composite material listed on Table 4.8. Other user defined parameter for MAT 54/55 are listed below as stated on the literature (Mahadevan & Liu, 1996).

Table 4.8. MAT54 additional user input definitions and required experimental data

Variable	**Definition**	**Value**	**Unit**	**Description**
DFAILT	Max strain for fiber tension	0	[-]	Disabled to control elements' deletion by time step only
DFAILC	Max strain for fiber compression	0	[-]	Only activated if DFAILT is non zero
DFAILM	Max strain for matrix straining in tension and compression	0	[-]	Only activated if DFAILT is non zero
DFAILS	Max shear strain	0	[-]	Only activated if DFAILT is non zero
SOFT	Crush front strength reducing parameter	0.8	[-]	Default value
SOFT2	Optional transverse softening reduction factor	0	[-]	Not used
EFS	Effective failure strain	0	[-]	Default value
ALPHA	Shear stress non-linear term	0	[-]	Default value
TFAIL	Time step size criteria for element deletion	1E-07	[s]	Element is deleted if time step is less than 1E-7
FBRT	Softening factor for fiber tensile strength after matrix failure	0	[-]	Default value
YCFAC	Softening factor for fiber com pressive strength after matrix failure	2	[-]	Default value
BETA	Weighing factor for shear term in tensile fiber mode	0	[-]	Default value
SLIMT1	Factor to determine the minimum stress limit after stress maximum (fiber tension)	0.01	[-]	Small but non-zero residual strength is assumed after tensile failure to avoid numerical instabilities
SLIMC1	Factor to determine the minimum stress limit after	0.375	[-]	Recommended

	stress maximum (fiber compression)			
SLIMT2	Factor to determine the minimum stress limit after stress maximum (matrix tension)	0.10	[-]	Recommended
SLIMC2	Factor to determine the minimum stress limit after stress maximum (matrix compression tension)	1.00	[-]	Recommended
SLIMS	Factor to determine the minimum stress limit after stress maximum(shear)	1.00	[-]	Recommended
SOFT	Crush front strength reducing parameter	0.8	[-]	Recommended
TSIZE	Time step for automatic element deletion	1E-07	[s]	Element is deleted if time step is less than 1.7E-8
ERODS	Maximum effective strain for element failure. If lower than zero, element fails when effective strain calculated from the full strain tensor exceeds ERODS	0	[-]	Default value
SLIMT1	Factor to determine the minimum stress limit after stress maximum(fiber tension)	0.01	[-]	Small but non-zero residual strength is assumed after tensile failure to avoid numerical instabilities
SLIMC1	Factor to determine the minimum stress limit after stress maximum (fiber compression)	0.375	[-]	Recommended
SLIMT2	Factor to determine the minimum stress limit after stress maximum (matrix tension)	0.10	[-]	Recommended
SLIMC2	Factor to determine the minimum stress limit after stress maximum (matrix compression tension)	1.00	[-]	Recommended
SLIMS	Factor to determine the minimum stress limit after stress maximum(shear)	1.00	[-]	Recommended

In general, the material model definition MAT 54/55 listed under Table 4.7 and Table 4.8 fails under any of the category listed below:

1. Constitutive properties: *RO, EA, EB, EC, PRBA, PRCA, GAB, GBC, GCA, KF*

2. Local materials axes: *AOPT, XP,YP, ZP, A1-A3, MANGLE, V1-V3, D1-D3*

3.Shear weighing factors: *ALPH, BETA*

5.Damage factors: *SOFT, FBRT, YCFAC*

6.Materials Strengths: *XC, XT, YC, YT, SC*

7. Failure criterion selection: *CRIT*

4. Deletion factors: *DFAILM, DFAILS,TFAIL, DFAILT, DFAILC, EFS*

4.4.2 The section definition

Since the thickness of the bumper beam which is considered is very small comparing to its all length, a shell section is used to model the beam. The shell elements are formulated by ELFORM=2 (Belytschko-Tsay elements), because it gives better results with bending stress. Rectangular cross section is used as cross section of the beam which is superior in load carrying capacity compared to circular and trapezoidal beam (SayaliMankar, 2018). It also provide good fitting space with the existing TWV frame structure when making modification. Different thicknesses of carbon fiber composite bumper beam are taken into consideration to achieve the effect of thickness on impact performance of the bumper system.

Laminate notation

Considering a laminate manufactured using unidirectional (UD) plies, the layup notation is described as shown on Figure 4.25.

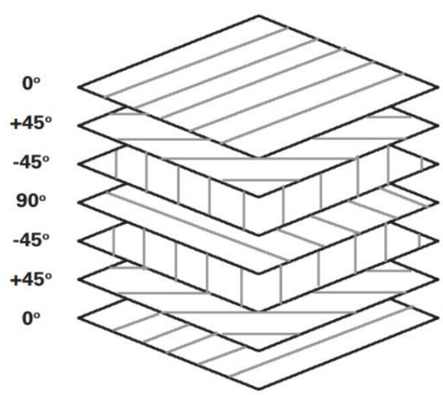

Figure 4.25. Fiber lay-up orientation Starting at the top surface (0/+45/-45/90/-45/+45/0)

So the first important thing to note when designing a laminate of composite material is to consider the stacking sequence of plies and to define the appropriate symmetry and balance of the stack. For example, the stack shown in the above Figure, to eliminate any tendency to bend Or warp it is both symmetric about the mid plane and also balanced (an equal number of +45° & -45° plies), which reduces shear coupling (Gurit Holding AG, 2000).

For this paper, a bumper beam with 7 layers and fiber orientation of [0, ±30, ±60, and 90] taken which is considered to be good (Basavaraju, 2005). The ply angles (fiber orientation) and thicknesses were defined at each integration point in the. In LS-DYNA this can be set in three different ways or input card, these are by using:

- *SECTION_SHELL/_TSHELL
- *PART_COMPOSITE (TSHELL)
- *ELEMENT_SHELL_COMPOSITE

On this paper ply angles and thicknesses were defined at each integration point in the *SECTION_SHELL/_TSHELL input card. Another point to note is unlike metals, the mechanical properties of the composite is dependent of its fiber direction meaning that they produce different results when tested in different of its fiber direction meaning that they produce different results when tested in different directions. This means that at the design stage, it is important to be aware of both the magnitude and the direction of the applied loads on the composite. Since fibers have their highest mechanical properties along their lengths, rather than across their widths. This leads to the highly anisotropic properties of composites .When correctly accounted for, these anisotropic properties can be very advantageous since it is only necessary to put material where loads will be applied, and thus redundant material is avoided (Gurit Holding AG, 2000).

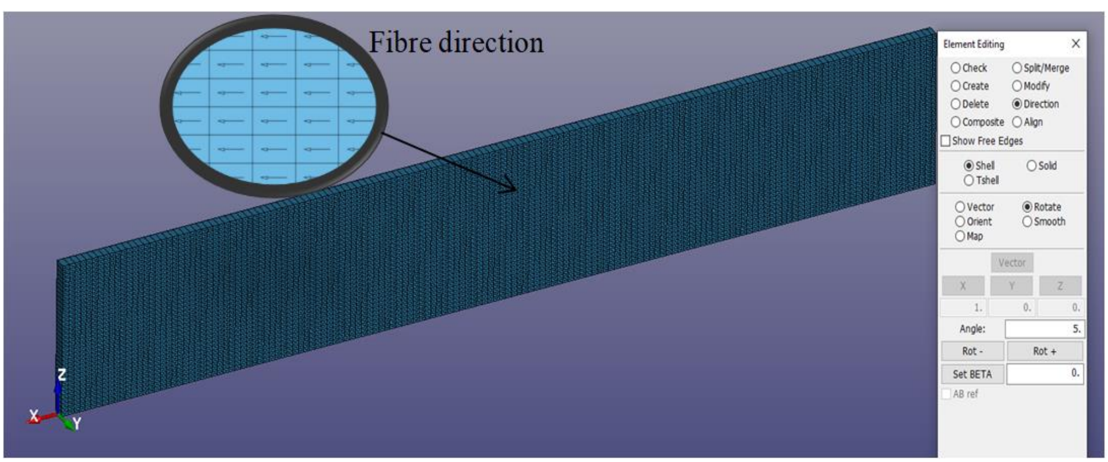

Figure 4.26. Beams fiber orientation

on LS-DYNA the fiber direction can be adjusted by using tool called element editing ,under this tool the fiber initial orientation can be arranged in such way that it can give the desired strength. As shown in the figure 4.26, since the load will be applied on the transverse y direction so that in order to get the required strength of the composite when the load is applied, the fiber is oriented on the longitudinal x direction. As a result the fiber is stronger on the longitudinal direction and less stiff normal direction.

Boundary conditions

The different boundary settings for testing each of the bumpers (front, rear and side) are represented by LS-DYNA's cards as follows:

INITIAL_VELOCITY_GENERATION was used to define the velocity of the moving components. *CONTACT_AUTOMATIC_SINGLE_SURFACE_ID, used to define contact between the beam and support and CONTACT_AUTOMATIC_ SURFACE _SURFACE_ID between the beam and the impactor (in case of front and rear impact) or rigid wall (in case of side impact),as recommended by the user manual in formulation involving crashworthiness analysis (Manual & Ii, 2012).

1. The CONTROL_TERMINATION time is set as 0.1 s, Settings of several control cards are also necessary to be addressed in composite beam material test are;

2. CONTROL_ACCURACY, INN=4:

The invariant node numbering for shell and solid elements are toggled on. The orientation of the material coordinate system and thus response of orthotropic shells can be very sensitive to in-plane shearing deformation and hourglass deformation, depending on how the element coordinate system is established. Setting INN=4 minimize the sensitivity of updating of the orientation of the material coordinate system, as the material coordinate system is automatically updated following the rotation of element coordinate system.

2. CONTROL_BULK_VISCOSITY, Q1=0, Q2=0, TYPE=-2:
The shell bulk viscosity may aid stability in compressive mode of response.
3. CONTROL_SHELL, LAMSHT=1:

The laminate shell theory corrects for the incorrect assumption of uniform constant shear strain through the thickness of the shell.

4. CONTROL_HOURGLASS, IHQ=4, QH=0:

Hourglass modes are non-physical, and zero energy mode of deformation for non-fully-integrated elements, therefore producing no Stress and strain. Type 4 offers stiffness based hourglass deformation modes, aiming to minimize nonphysical stiffening of the response and at the same time effectively inhibiting hourglass modes (Mahadevan & Liu, 1996).

6. DATABASE_EXTENT_BINARY.

- For composite material models, stresses (and strains) will be written in the material coordinate system rather than the global coordinate system if CMPFLG (and STRFLG) is set to 1 in *DATABASE_EXTENT_BINARY .this is Useful option for post processing of fiber and matrix stresses.
- Set MAXINT in *DATABASE_EXTENT_BINARY to the total number of through-thickness integration points in your composite shell. By default, stresses only at the top, bottom, and middle integration points are written.
- Set NEIPS to 6**,** this help to track modes of failure in each integration point of or track the damage parameter in MAT_054 (LSTC, 2012).

Side bumper beam test

Side beam considered as one of important safety component which strengthen the side members of the TWV and helps on lowering the degree of injures to occupants during side collision. Under this section, bumper beam with carbon fiber composite unidirectional IM7/8552 material is designed for different thickness. Rectangular cross section used for the bumper beam having maximum bending stiffness to other cross section as suggested by (SayaliMankar, 2018) The thickness of the side bumper beam that were considered are 4.5, 5, 5.5, 6, 6.5 and 7.2 mm .the reason for starting from 4.5mm thickness is that when the material thickness was lowed from this value it showed some kind of faller mode. Among the listed ones, the best material thickness is selected based on parameters like, load carrying capacity, Stress energy absorption capacity and reduction in displacement.

The boundary conditions and the setups used are discussed below. The test consists of three components, these are the supports (red colors), bumper beam (blue) and rigid pole (black). The pole is represented by a rigid body, and discretized by solid elements. The beam and its supports utilizes single-layered modelling approach, where only one layer of shell elements (Because the thickness of the bumper beam, is much smaller than the other dimensions) is implemented for efficiency. The components are mainly mashed with quadrilateral elements with fewer triangular one and totally consists of 18199 elements and 19430 nodes. MAT 20 (mat-rigid) is used for simulation of the rigid pole, and mat 24 (MAT_PIECEWISE_LINEAR_PLASTICITY) used for the supports of the beams.

The test procedure follows the same procedure used in the full crush test of the TWV. The supports were arranged or set up in the same manner as point where the modification was made on TWV. The same distance that was set between the TWV and rigid pole was also set for the bumper beam and the side pole. The support together with the bumper beam moving with 25km/h was collide with the rigid pole, see Figure 4.27.

- The rigid pole degree of freedom is all fixed (DOFs=0).
- The moving beam and its supports are fixed in all DOFs except for the moving direction.

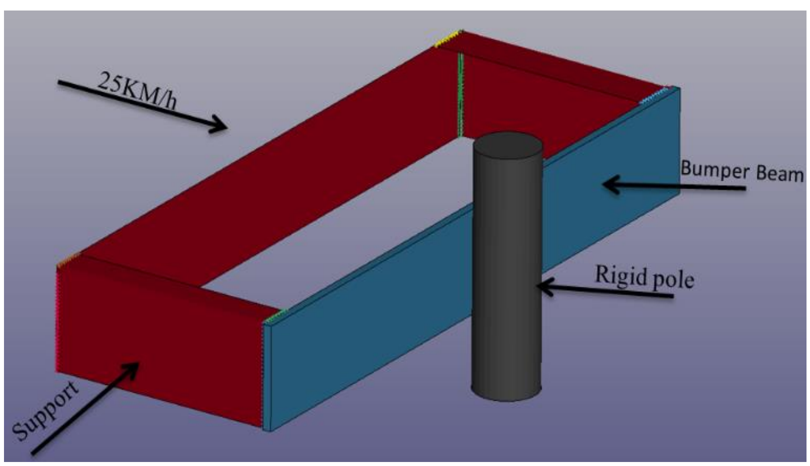

Figure 4.27. Side bumper test set up

Rear bumper test

Using the same principle and methodology used in side beam, selection of a suitable for carbon fiber composite bumper beam is made. Here for rectangular hallow section of rear bumper, thickness of, 7,8,9 and10mm are taken into consideration to study the effect of thickness on

Rear bumper at event of rear impact .at the event of rear crush, the bumper should protect the engine, fuel tank, and exhaust systems as well as other safety related components. The boundary condition and set ups used to test the rear bumper is listed on figure 4.28.

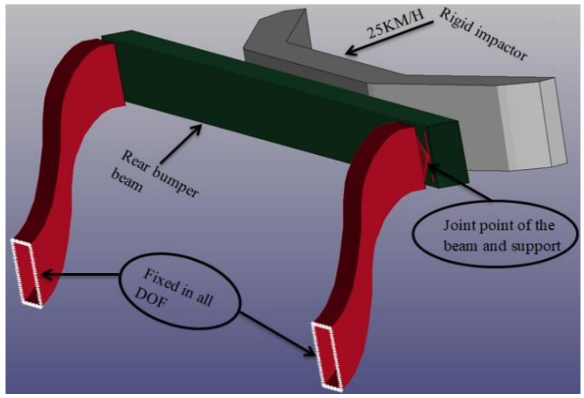

Figure 4.28. Rear bumper test

The test consists of three components, these are the supports (red colors), bumper beam (green) and rigid impactor (black). The setups of the supports are the same as the modification arrangement made on the rear at of TWV. The impactor, as a steel structure, was modelled with rigid solid impact elements and Material type 20 (mat-rigid) is assigned using LS-DYNA. The supports are assigned as deformable structure is so called "MAT type 24"A, Piecewise Linear Isotropic model. Usually in all finite element study constraints plays a major role. Bumper beam supports are constrained at both the ends in all degree of freedom using BOUNDARY_SPC_SET and also the beam and the support is joined together using CONSTRAINT_NODAL_RIGID_BODY (CNRB) keyword available in LS-DYNA as shown in Figure 1. The total length of the beam is equal with the distance between the two rear wheel which is 900mm, and also have 30mm width and 60mm. The thickness of the beam is varied from 7mm to 10mm.The components are mainly mashed with quadrilateral elements with fewer triangular one and totally consists of 63204 elements and 65758 nodes. According To (Hu et al., 2015), the mass of impactor should be Equal to the whole vehicle; thus, a gross mass 280 kg was given to the impactor . Also the same mass was rigidly given to the two supports of the beam using ELEMENT_MASS_PART in order to simulate the TWV mass. The test procedure follows the same procedure used in the full crush test of the TWV. The supports were arranged or set up in the same manner as point where the modification was made on TWV. The same distance that was set between the TWV and rigid pole was also set for the bumper beam and the

Side pole. The impactor moves 25km/h and will hit or collide with the stationary TWV structure.

Front bumper test

For any vehicle, front bumper is the most critical part which protect the occupants and the vehicle parts by deforming and absorbing much of the impact energy. For TWV a type of bumper beam shown Figure 4.29 is mounted on the front part so that at event of crush it absorb the impact energy together with the front tire cover. Using the analysis method used in previous section different bumper thickness are considered and based parameters such as deformation, force and internal energy best material thickness is selected.

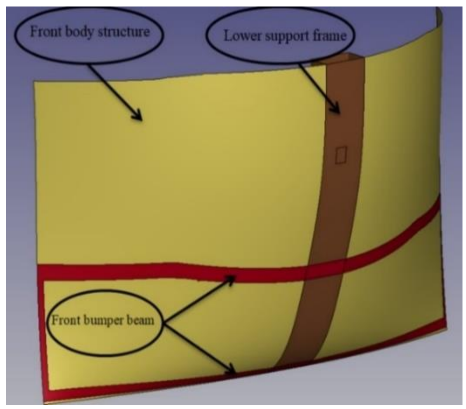

Figure 4.29. Front bumper

Figure 4.30 shows the reduced front structure of the TWV that saves simulation time when determining the best thickness of front bumper beam. The rescued model consist of half of the front body structure, front portion of the lower frame support and front bumper beam. The boundary condition or set up used were shown in Figure 4.30:

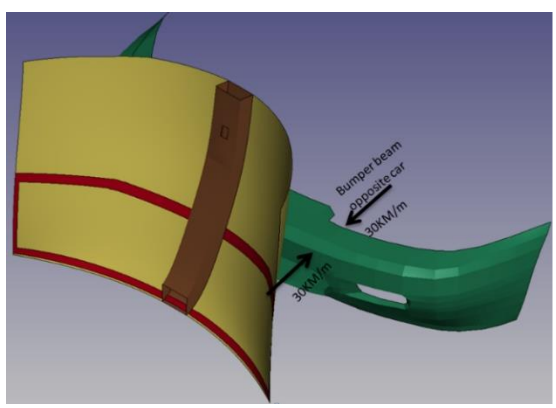

Figure 4.30. Front bumper test set up

In addition to component reduction of TWV, the structure of the opposite car is reduced and left with bumper beam only. According to gb17354-1998 (Hu et al., 2015), to simulate the total mass, the same mass was rigidly given to the two reduce model using ELEMENT_MASS_PART. Therefore, the meshed reduce model totally consists of 115635 elements and 116243 nodes with much quadrilateral and fewer triangular elements .the total length of the front bumper beam is equal with the front track of the TWV. The thickness of the beam is varied from 6 mm to 11 mm. The test procedure follows the same procedure used in the full crush test of the TWV. The same distance that was set between the TWV and car structure was also set for the reduced models. Both moves with same velocity of 25km/h and then they collide with each other.

The results of the above method used were discussed on the next chapter called result and discussion. The result of existing, modified and the bumper beam were listed and discussed one by one.

CHAPTER FIVE
RESULTS AND DISCUSSION

5.1 Introduction

On this chapter the results of the simulation of frontal, side, rollover and rear crush of TWV is reported and comparative analysis carried out between the modified and existing method is also made. In addition, the detail discussion on the results is presented. But before dive into the report or result, the verification method for LS-DYNA simulation results are discussed below.

I. Result and discussion of existing model

5.2 Frontal collision results

5.2.1 The analysis of the whole vehicle's distortion.

The simulation result of frontal crush where a car moving with velocity of 30 km/h will collide with TWV which is moving in opposite side of car at the same velocity is presented and discussed. Figure 5.1 shows the distortion of the whole vehicle structure and the response of dummy at the time 100 ms.

As it can be observed from the graph at t=0.025s, the first part of the TWV which is in contact with the opposite car and deformed the mudguard (tire cover) of front tire. After this point as the simulation time increase and reach 0.05s, the contact area increases, as a result the car hit the front structure and the steering of TWV, and both parts starts to deform progressively and have generated plastic deformation. When the time reaches 0.075s, the car hits the lower support frame

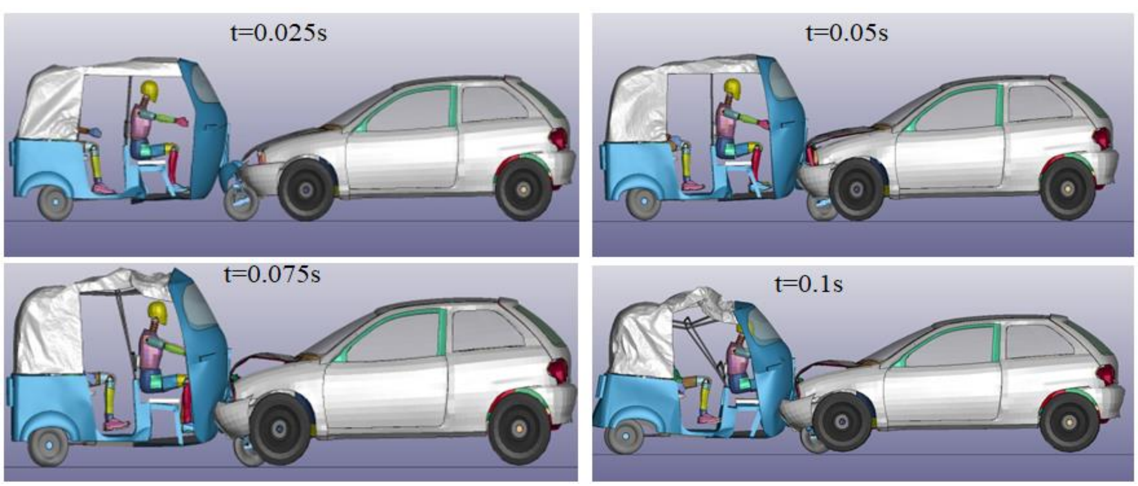

Figure 5.1. Sequence of front crush event

(chassis) of the TWV, since the chassis of the TWV is relatively stiffer than the car front bumper so the car starts to deform together with TWV. At final stage, the front tires of the car leave the ground and jump it to the TWV. As result the inner structure of the TWV deforms and high deformation at front structure occurs.

Figure 5.2. Real accident (a) vs FEA modeling accident (b)

Figure 5.2 show the FEA simulation of TWV vs the real crush. As it can be seen from the graph the simulation result is much similar with the real crush. The fact that the windscreen of the FEA model is not broken is that the material model of the FEA windscreen is not glass. So that there is no breakage at the windscreen. In addition, the real crush of TWV shown on the image is a little bit offset from the front, whereas the FE is full frontal.

5.2.2 Analysis of the Dummy Response

The response of dummy in the process of crash is shown in Figure 5.3. At initial time the dummies are positioned with their appropriate position and as the vehicle starts to move and collide with the car the time of 0.024s the dummy's back begins to leave the their original position and move forward with its neck a little bending; when the time is 0.048s, the vehicle's deformation rises and dummy keeps moving forward at their bend position , the head of driver trend to decline, and the back of the passenger bend backward and then moves forward and also their the arms moves forward and their legs begins to bend as well; when the time is 0.075s, the vehicle's deformation keeps rising, the dummy as a whole slides forward, and lift up from their position, and the legs bend with a larger range; when the time is 0.115s, the front of the vehicle deforms seriously.

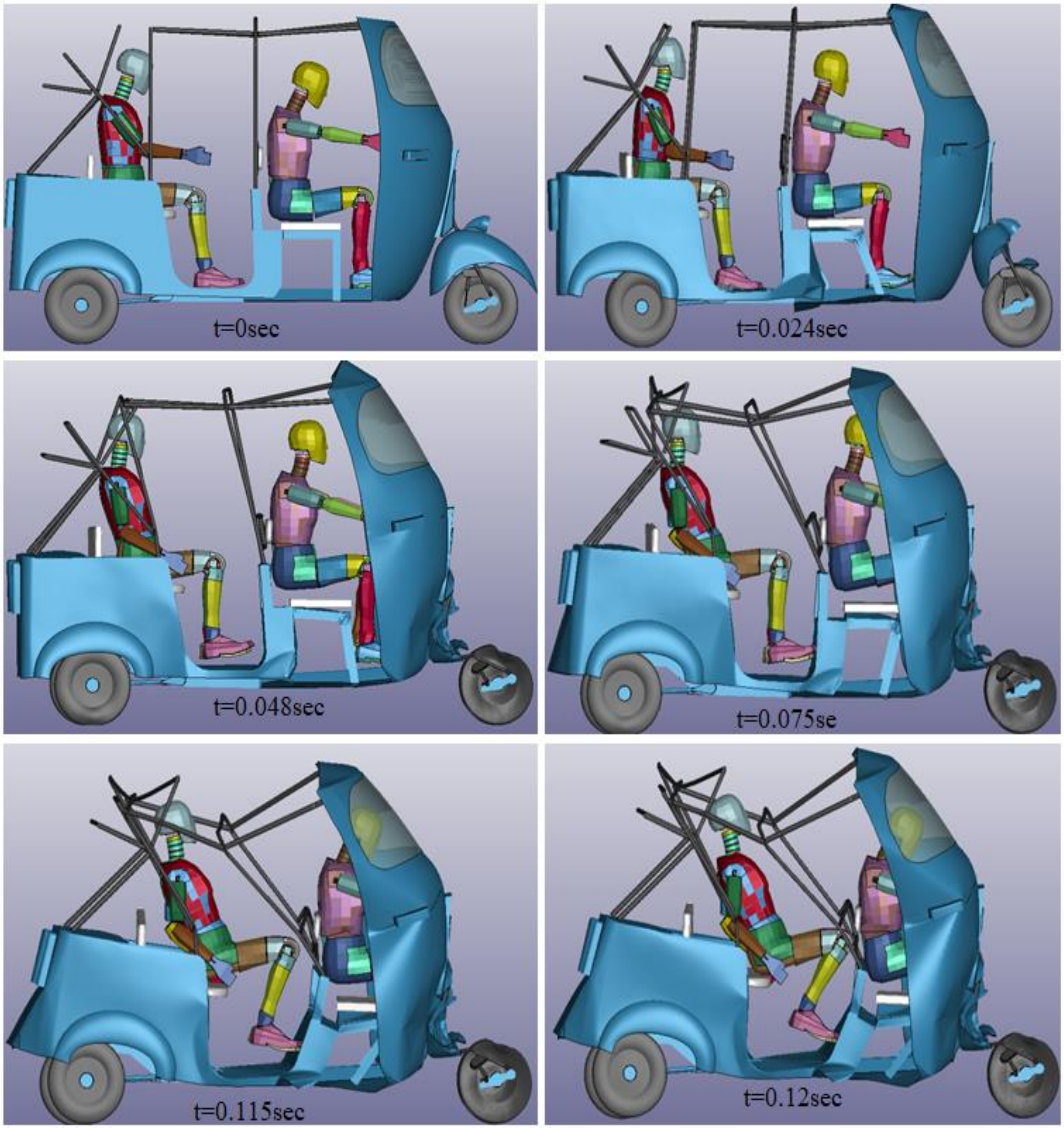

Figure 5.3. Occupant's response during front crush

The dummies slide out and move forward and the leg of the passenger and the knee tend to collide highly with the body and the body gets deformed; when the time is 0.12s, the body keeps crouching; the head of the driver declined and crashes, the leg of the passenger and the knee of the driver hits the vehicle body. In case this case (velocity of 30 km/h), both the driver and the passenger have a very high probability of suffering serious head and upper leg (femur) injuries.

The knees of passengers and the driver impact inner surfaces of the vehicle as shown on Figure 5.4.

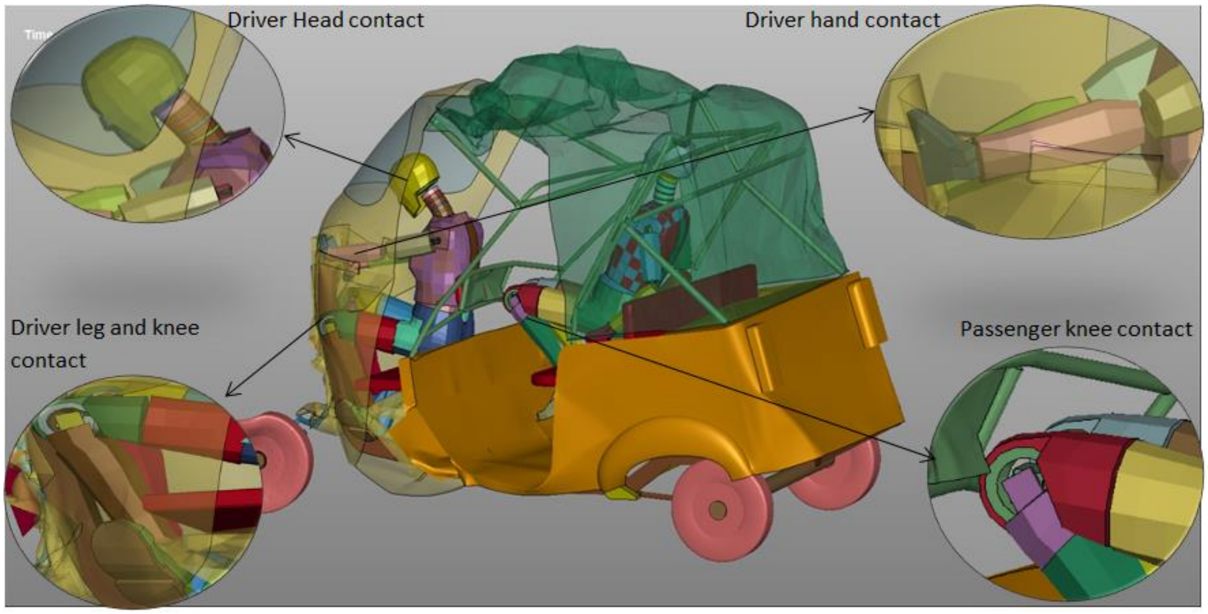

Figure 5.4. Occupants contact area with the TWV

To reduce the injuries at contact areas shown on Figure 5.4, it is possible to provide paddings at areas such as knee and Head contact points. Injury severity can be reduced by providing less stiff impact surfaces at the contact point for the passengers and with similar modifications in the driver cabin windshield area. Provision of lap belts does not seem to benefit either the driver or the passenger however, provision of lap and shoulder belts for both the driver and the passenger show major safety benefits. Enabling shoulder belts would require inclusion of load bearing structures for anchoring of the shoulder belts which is not present in current models (S. mukherjee et al., 2007).

5.2.3 Total Energy-balance graph

Figure 5.5 shows how the energy balance during the test. According to Law of Conservation of energy, Energy can neither be created nor be destroyed, but it can be converted from one form of energy to other form. Applying the same principle to crash analysis, the amount of kinetic energy lost during impact must be converted to other forms of energy such as internal energy, sliding energy and hour glass energy. From Figure 2.1 it can be seen that, initially the kinetic energy which is high at the start of the impact is equal with the total energy with value equal to 42.5 kJ and as the crush event starts to take place the kinetic energy of the system starts to slowly getting decayed and converted to other forms of energy and then finally reaches to 13.8 kJ of energy. From this difference, it can be observed that 28.7 kJ of energy is absorbed and converted to internal energy, sliding energy and hour glass energy.

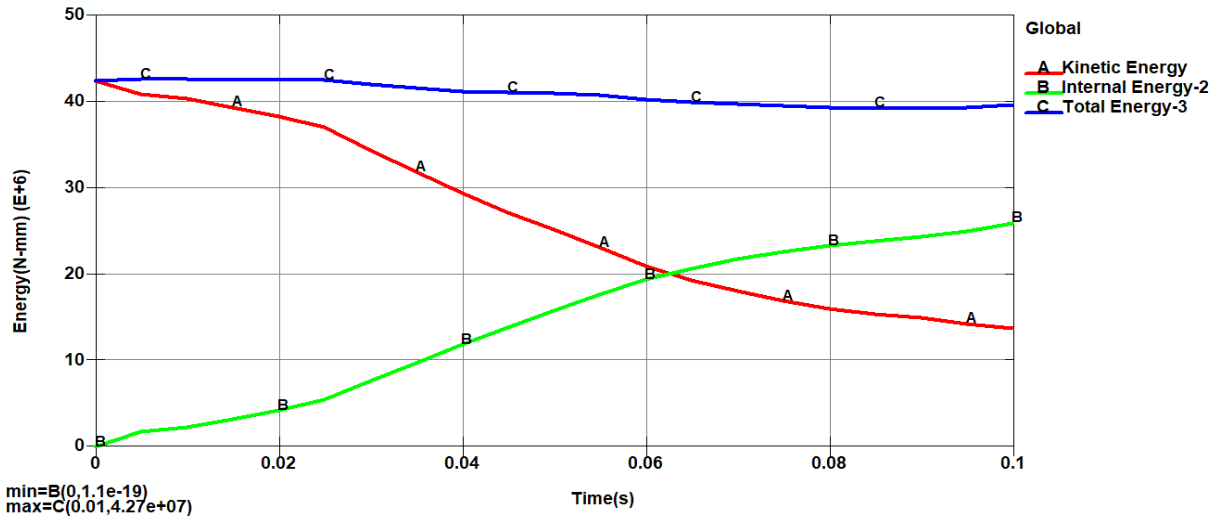

Figure 5.5. Energy balance curve

Among this 26 kJ 0r 90% of energy is converted in the form of internal energy as shown on Figure 5.6 and the remaining 10% energy is dissipated in the form of sliding, hourglass energy

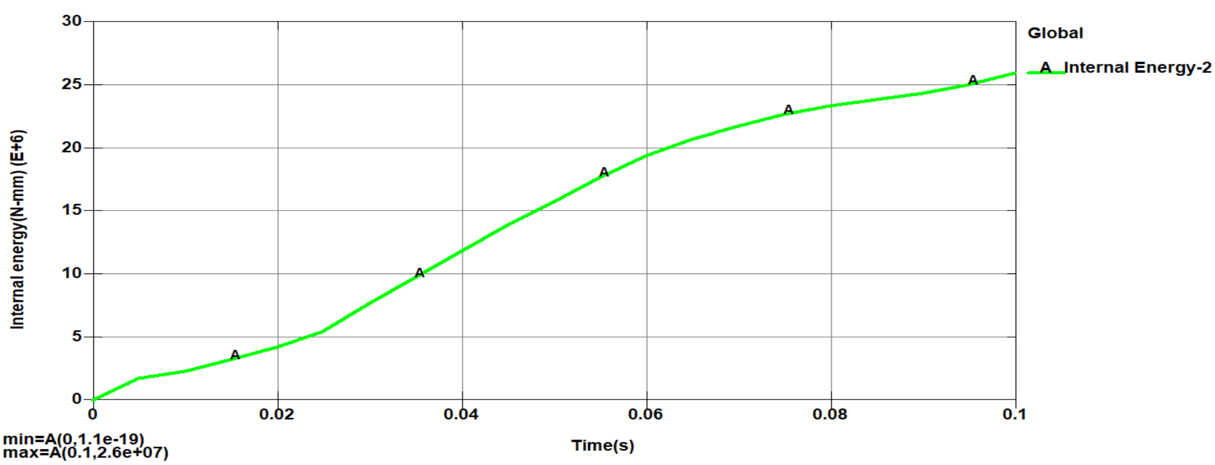

Figure 5.6. Total internal energy

5.2.4 Energy absorbed by the vehicle parts

Energy absorbed by TWV is shown on Figure 5.7 The energy graph shows the total internal energy absorbed by each of the vehicle parts. The sum of total internal energy absorbed by the vehicle parts are equal with 14.7 kJ, which is 51.23% of energy dissipated from the whole system.

Among the parts, the most of the energy of the impact is absorbed by the front structure, rear structure and the mainframe. The maximum internal energy is obtained from the front structure with value of 6.85 kJ, this is due to that the collision first take place between the front structure and high impact force is transferred on it and this will lead to high deformation of the part. Minimum value is from the axle, foam and engine, since they are modeled using the rigid material model so no deformation imposed on them. Other parts like rear structure, roof supports, main frames, steering system and tires have 2.32 kJ, 0.411 kJ, 2.02 kJ 1.47 kJ, and 1.21 kJ of internal energy respectively.

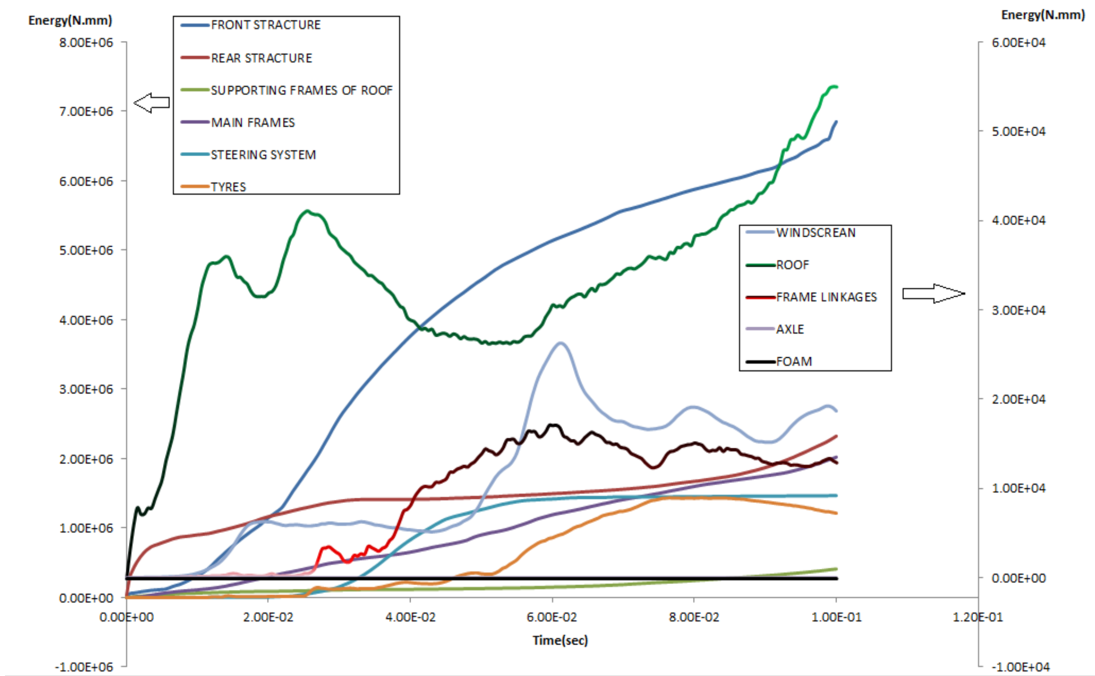

Figure 5.7. Energy absorbed by TWV

Generally, the front have which have shown large folding deformation takes effects in absorbing the energy. It causes the excessive stress surpassing the material bend stress greatly, so it can result in greater plastic deformation at the same, it can absorb the impact force mostly. At the same time, some amount of deformation is transferred to the rear, roof support and inside the driver cabin. In other hand the rear tires, foams and axles haven't shown deformation. This is due to that the parts are modeled with rigid material model but even if they are rigid, the kinetic energy of the TWV decrease and the stress which effects on rear part of the TWV comes down, and resulted in less deformation.

5.2.5. Force between the vehicles

The contact for between the TWV and the car is shown on Figure 5.8

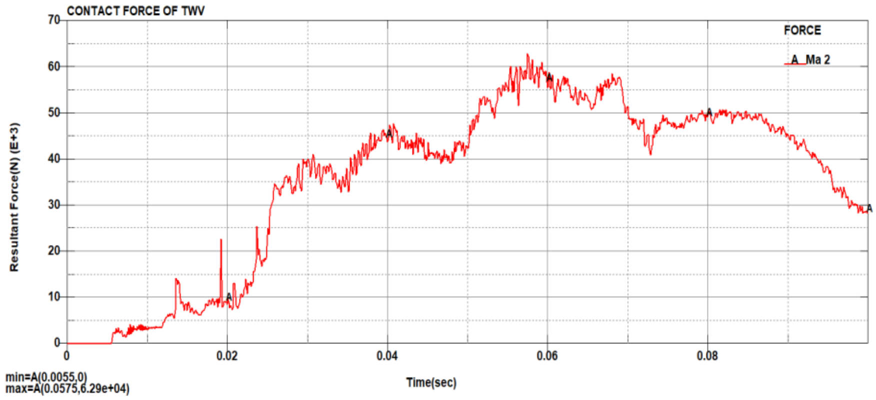

Figure 5.8. Contact force between TWV and car

As shown on 5.8, the contact force pulse data shows one peak force at 57.5 ms. This peak force is due to the high contact force as the car is fully in contact with the TWV main frame. (Srikanth & Prakash, 2009) stated the simulation result of the contact force for frontal crush of TWV at speed of 20 km/h and 48 km/h was 47 kN and 270 kN respectively this value is quite similar to the result presented here, in which the maximum contact force at speed of 30 km/h is 62.9 kN.

5.2.6 The Change of the Whole Vehicle's structure

Figure 5.9 shows the method used for measuring the distortion.

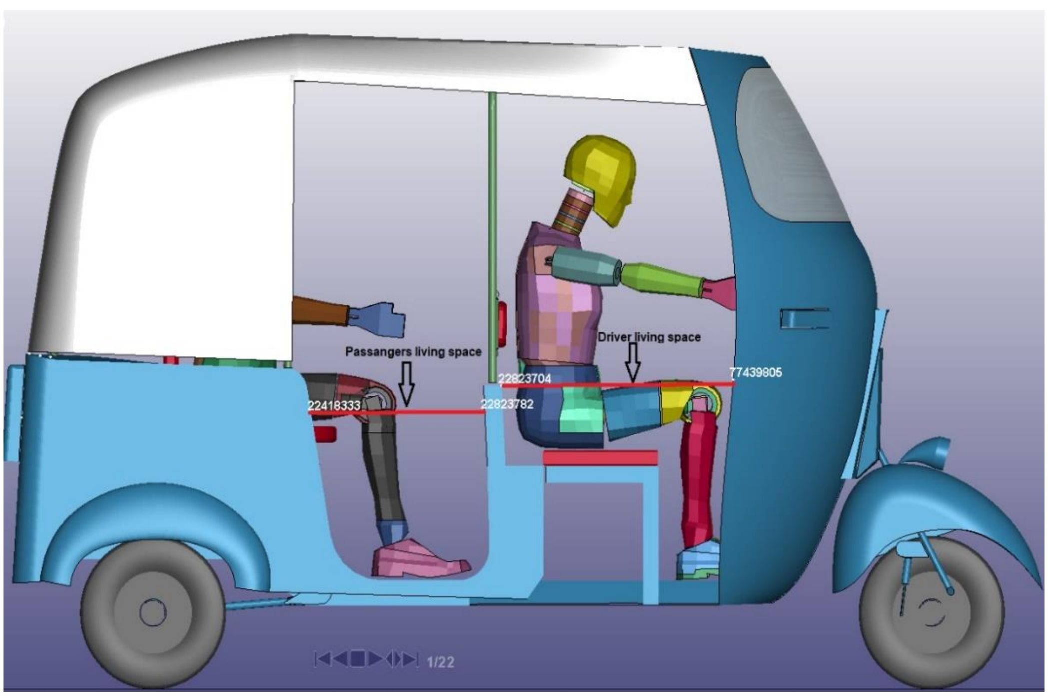

Figure 5.9. Vehicle deformation measuring points

In LS DYNA displacement is obtained by measuring the relative distance between two nodes So to measure the change in displacement of the driver compartment we take two nodes (node id 22823704 relative to node 77439806), for the passenger compartment node no 22418333 relative to 22823782 as Shown on Figure 5.9. From that we can know the maximum displacement on node 22823782 relative to node 22418333 in X direction is about 32mm and it elongates the compartment Figure 5.10, This displacement is not enough to pose crisis to the living space of passenger, but in the driver component which is between node 22823704-77439785 there is no survival space in which the Maximum relative displacement is 308 mm and the compartment get compressed Figure 5.11. This show that the crashworthiness of the TWV vehicle at event of front crush is not good.

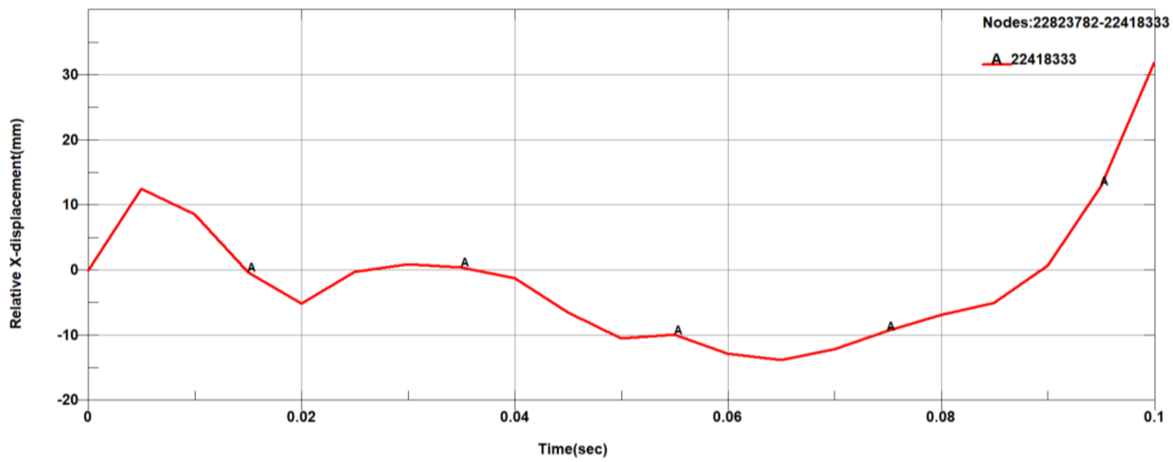

Figure 5.10. Displacement of passenger’s compartment

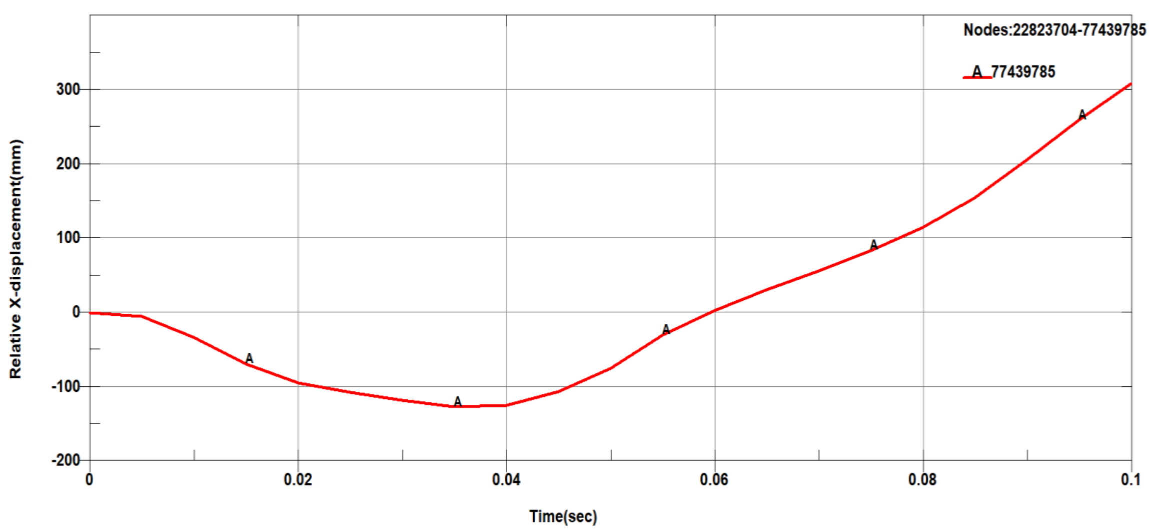

Figure 5.11. Displacement of driver compartment

5.2.7 Velocity of the component TWV

To analyze the change of speed of varying vehicle section, we take the front most (tire cover), front, middle and back section in all four point (node 77010472, node 87007300, 17216209 and node 22643439 respectively). As the Figure 5.12 shows, initially the vehicles velocity for the TWV is given negative initial velocity of 8.3 m/s in horizontal, the speed on node 77010472 (tire cover) falls down the most quickly because it is the point where the first impact contact occur, and reach maximum velocity of 16 m/s at time 0.01 ms it has come down and then up which shows the rebounding of the part. The speed on node 87007300 (front structure) initially starts to move with constant velocity of 8.3 m/s until the body starts to deform and then increases its speed without rebounding effect and finally reach same velocity with node 87007300. Node 166579 (a point in the rear of the vehicle) falls down both to zero at about time 64 ms, but it has reversal speed after falling down to zero, this reflects the phenomena that the vehicle would generate rebound after crash.

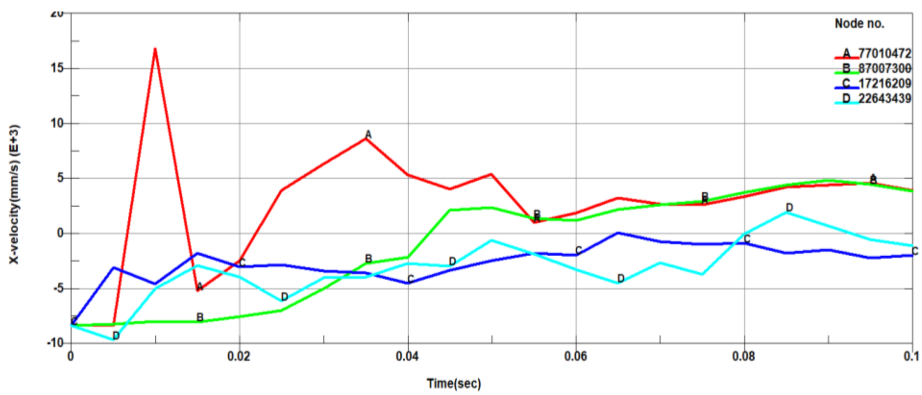

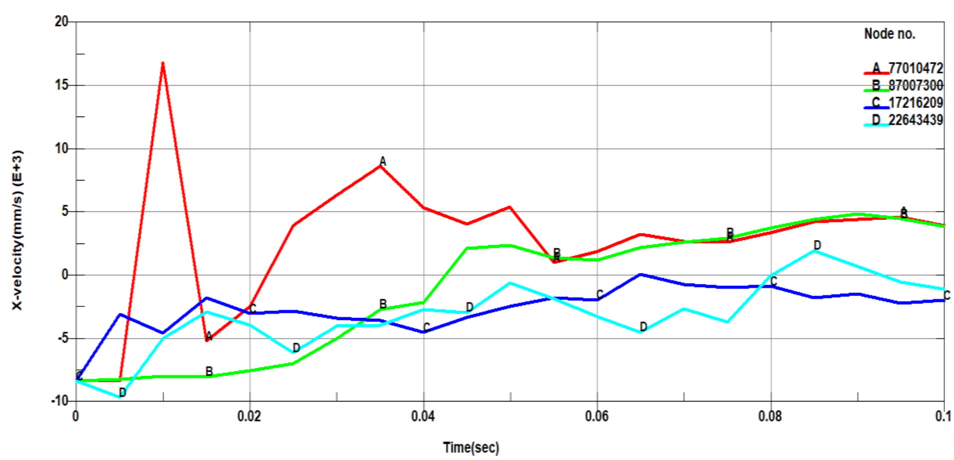

Figure 5.12. Velocity of the component TWV

5.2.8 Verification

Energy ratio

From the energy balance curve it has been seen that the system energy is not fully conserved and this is due to zero energy form of some elemnts.so it may be noted that, all the processes in this universe are irreversible and some losses are always included which deviates energy ratio slightly from one. This can be observed in the energy ratio graph.

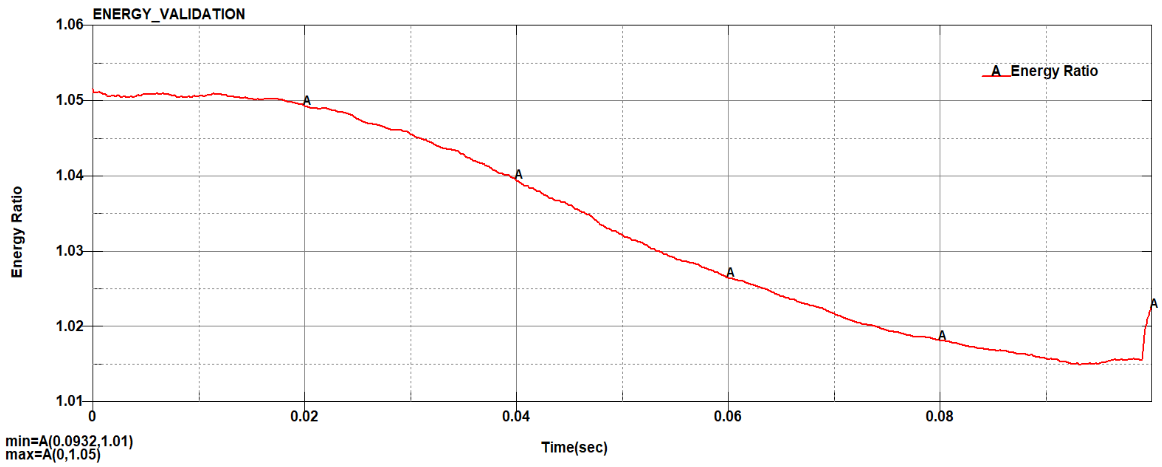

Figure 5.13. Verification: energy ratio

As it is discussed at the start of this chapter, to be accepted the energy ratio value should be 1.00 +/- 0.07. As it ca be seen in Figure 5.13, the simulation produce maximum value of 1.05 energy ratio and this value is approximately one with an error of 0.05% which is acceptable.

5.3 Side pole collision

5.3.1 Dummy and structure response

The overall sequence of events during a side impact are shown on the Figure 5.14. It shows the response of the structure and the occupants to the side pole collision. As it is seen in the Figure 5.14, when the collision process starts the vehicle and the occupants starts to move in sideways. the whole process takes 0.1 s, at initial stages only small deformation of vehicle and movement (like neck, leg and shoulder) of occupants is observed until the time reaches 0.45 s. after this point, the force of impact increase as contact between the vehicle and pole increase as a result the occupants and the vehicle body starts to respond with the same amount in which visible movements of occupant and damage of vehicle body is observed at t=0.6s.

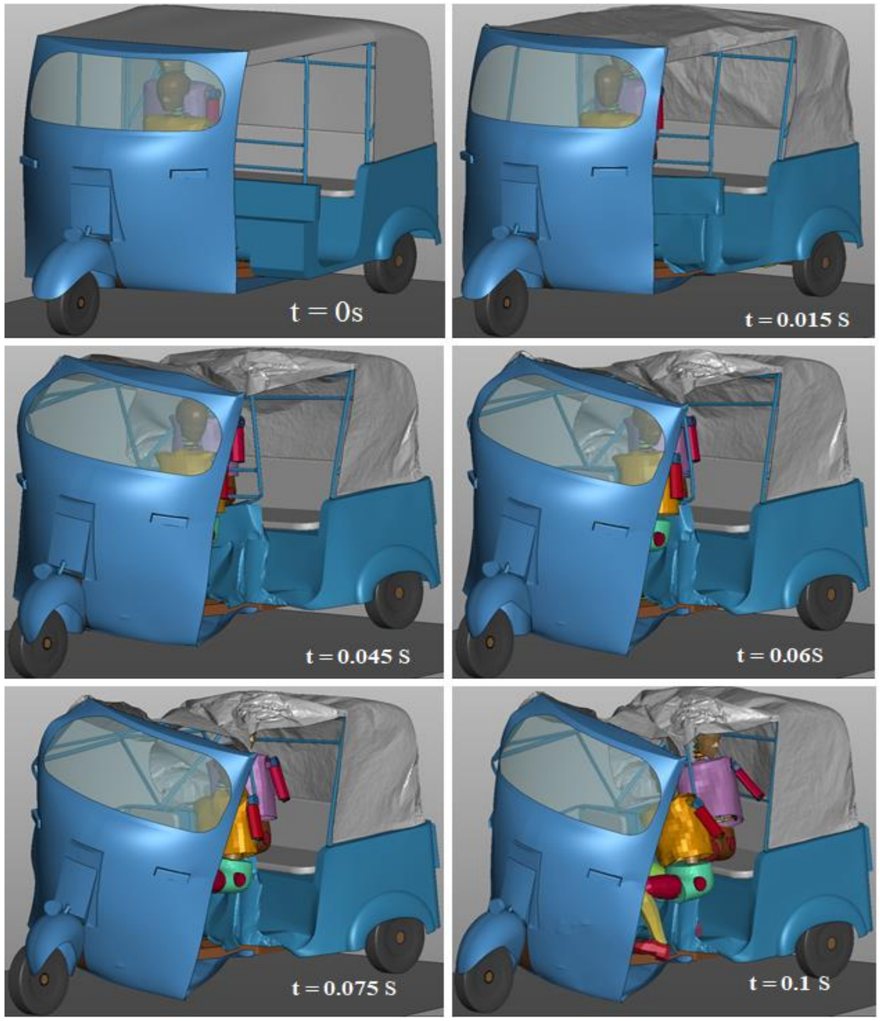

Figure 5.14. Sequence of side pole collision

Then when the time reaches 0.075S, significant damage to the rear and fronts structure, roof supports and lower support is observed and due to this TWV body is distorted to much.in addition to the structure ,the occupants are starts to move towards the side pole, as a result the driver slides out of the TWV as there is no side doors and the passenger which is initially in opposite side of the pole is move toward the pole and this shows that when TWV is occupied with three passenger, there is high probability of collision of the passenger to each other and the risk of injury increase as well. At the fill stage of the simulation(t=0.1s), the vehicles is no more protecting the driver from external objects as a result the driver slide out of the vehicle and hit the pole as shown on the figure. This result in high degree of injury to the driver body especially around its shoulder and also the passenger is fully travelled through the compartment. This mean that any one of the passenger have the probability to thrown away from the vehicle which will result in more sever condition. The contact areas, deformed position and critical points of the occupants during the collision process is shown on the Figure 5.15.

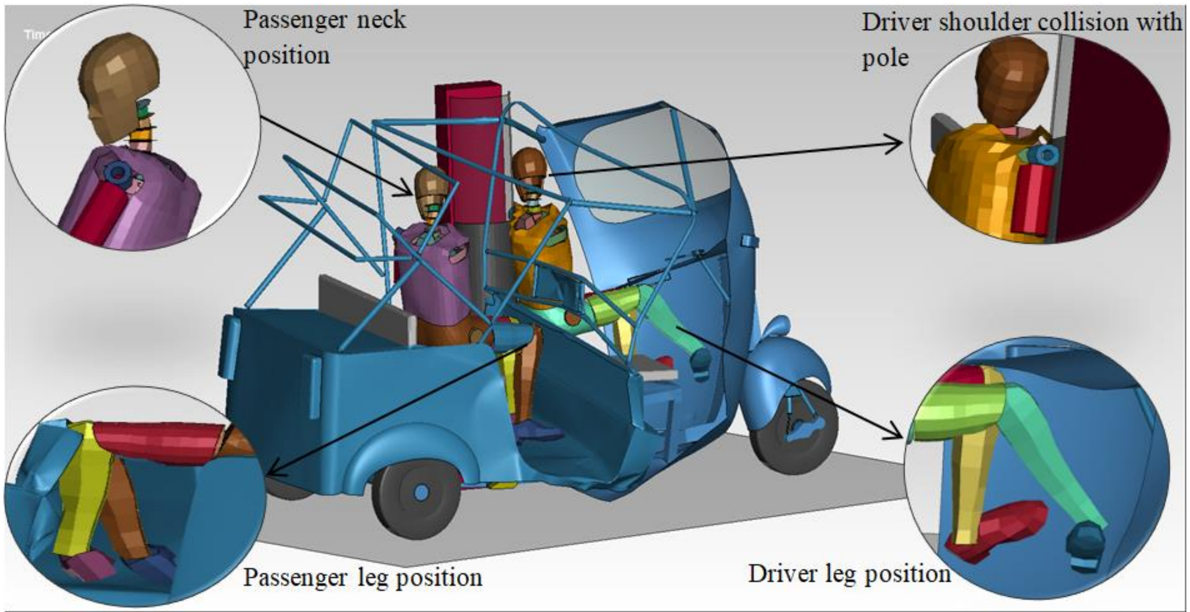

Figure 5.15. The dummies contact with the TWV

As it can be observed on the Figure 5.15, the legs of both the driver and passengers have on twisted position. This result in serious injuries of legs and also the force of the necks and shoulders will put them in higher risk.

5.3.2 Intrusion into the vehicles

Intrusion into the TWV is obtained by measuring the relative displacement of the node where there is no deformation with the node at another side where the deformation is more.

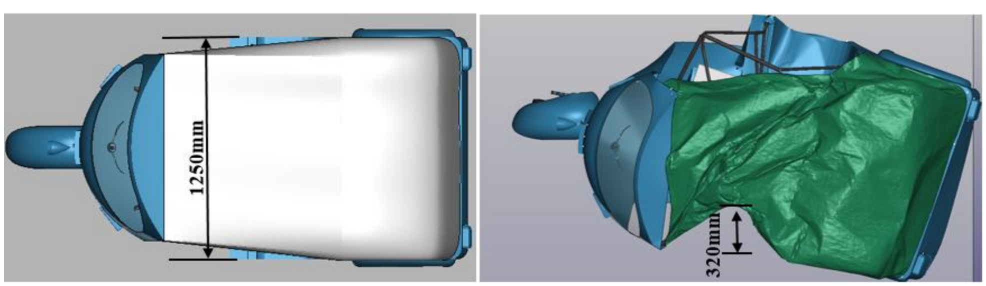

(a) (b)

Figure 5.16. The original (a) and deformed (b) TWV vehicle structure

From Figure 5.16, shows the un-deformed and the final deformation of the TWV before and after impact with the rigid pole. As it can be seen, from the original width of the TWV, due to the side crush the side structure of the vehicle deformed 320 mm and remain with 930 mm space. This space is not enough space to protect the occupants as the deformation (intrusion) value is high as indicated in Figure 5.16

5.3.3 Displacement

As shown on figure 5.17, the maximum deformation is equal with 345mm.

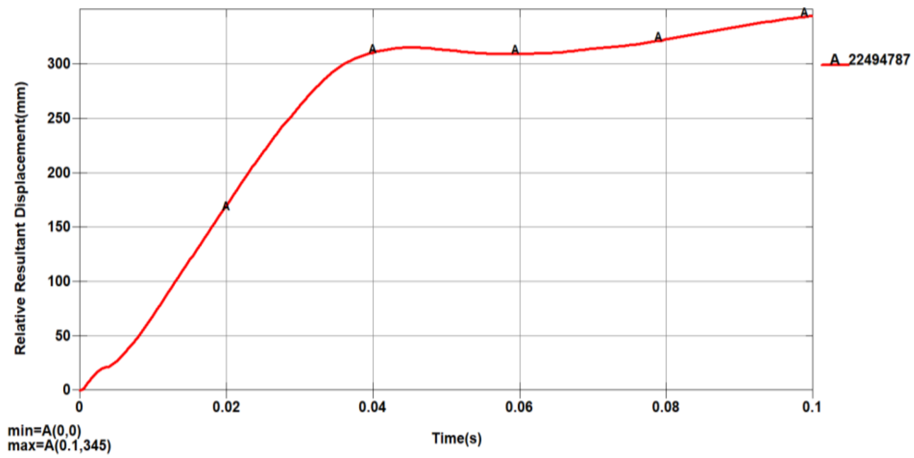

Figure 5.17. Displacement

Most of the deformation process takes place until 0.04s and after this point only little deformation is observed. This is because initially the pole is in contact with the low stiff vehicle structure. So the deformation increase linearly until the vehicle structure collapsed and reaches the lower vehicle structure which is relatively stiffer. After this point the force of impact is decreased as a result only less deformation are observed.

5.3.4 Energy balance curve

The energy versus time plot of the total system is shown in Figure 5.18. As it is shown the total energy of the system remain constant for the whole simulation with value equal to the initial kinetic energy which is 14.9 kJ. on another hand the kinetic energy of the whole system starts to decrease as the collision process starts and converted into internal energy which is increasing starting from the 0 energy. Most of the internal energy is gained due to the deformation of the structure. After 0.06s little deformation is observed, as a result the energy graph of the K.E and I.E become flat. The final kinetic energy is equal with 3.64 kJ and this can be interpreted as 24.4% of the initial kinetic energy or total energy. So, we can conclude that 11.26 kJ or 75.6 % of total energy (initial K.E) is converted to other forms of energy such us internal energy, hourglass energy, sliding energy or other forms.

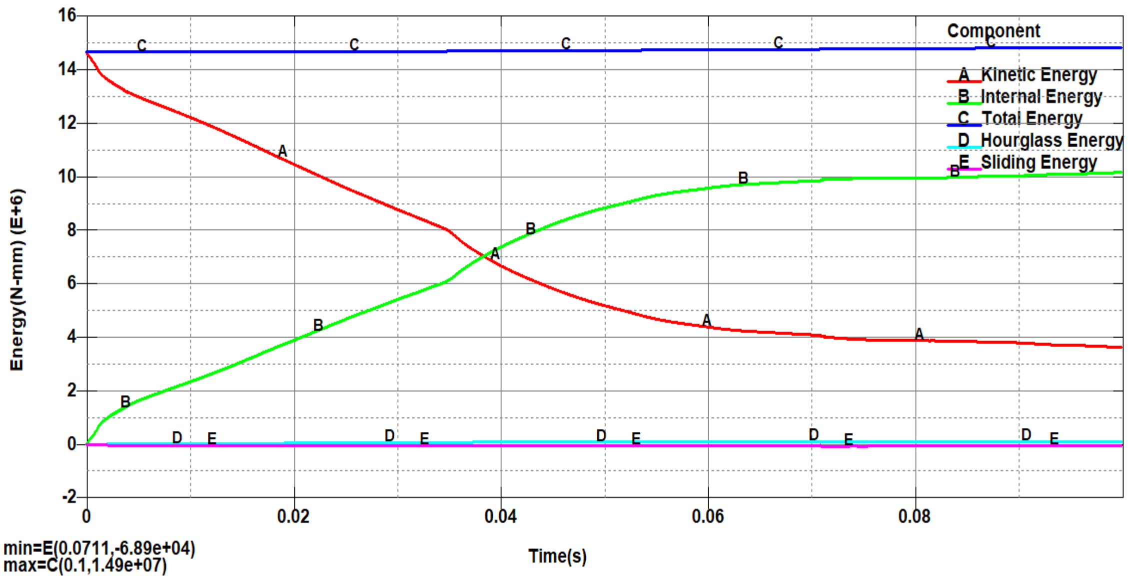

Figure 5.18. Side collision energy balance

Among this the internal energy is accounts for 10.2 kJ of energy which is 68% the total energy and 90.5 % of the converted K.E, and reaming values are in the form of hourglass energy, sliding energy and other energy with value of 0.0366 kJ ,0.132 kJ and 0.8914 kJ respectively. The total energy graph is shown on the Figure 5.19.

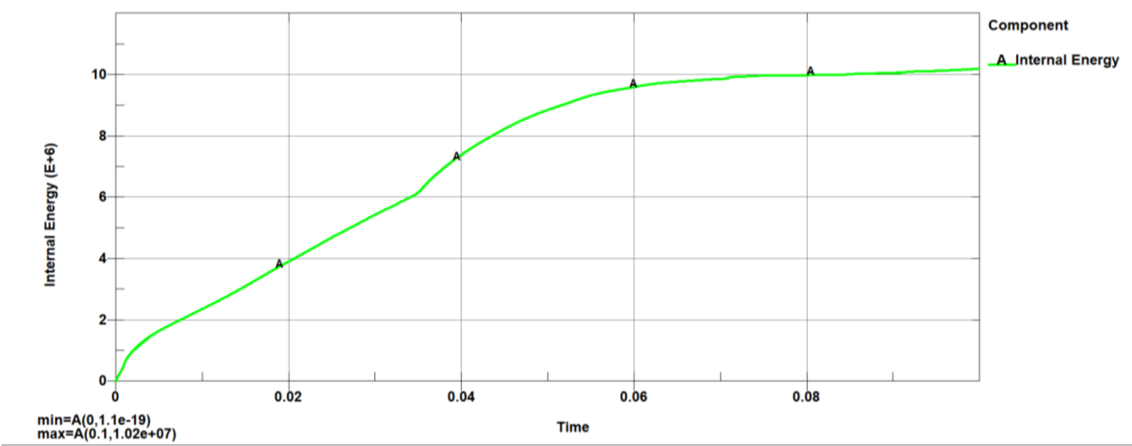

Figure 5.19. Side collision total Internal energy

5.3.5 Energy absorbed by TWV Vehicle

From the total energy absorbed by the whole system, the energy absorbed by the TWV structure is presented on the Figure 5.20. The graph shows the energy absorbed by the TWV structure. The energy value indicated on the primary axis (left vertical axis) shows the TWV parts with the highest energy absorption such as rear body structure, roof support frame, main lower frame and front body structure and the secondary axis (right vertical axis) the one with lower absorption of energy.

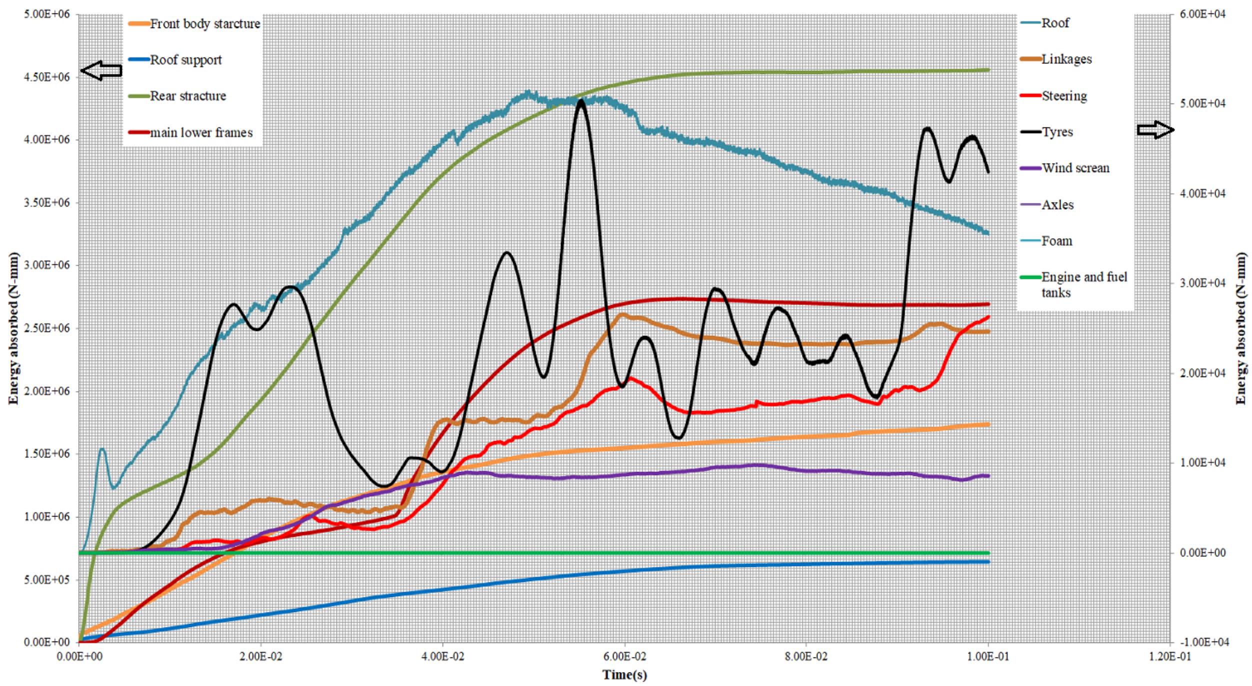

Figure 5.20. Energy absorbed by TWV components during side collision

The total amount of energy absorbed by the TWV is equal with 9. 50301kJ.This shows that 93% of the total amount of energy is absorbed by the TWV structure. Among this 47% of the energy (4.75 kJ) is obtained by the deformation of rear body structure. This is quite easy to predict because the pole have direct contact with the side structure. In addition to the rear body structure the lower frame which support the rear structure have absorbed maximum of 2.72 kJ of energy which is 28% of total absorbed energy. Since after the deformation of the rear structure the deformation take place on the main lower frame as there is no energy absorbing member which protects the frame. This can affect the whole structure of the vehicle because most of the vehicle components are mounted on the frame. The other part which is subjected more deformation is the front structure, it have maximum energy absorption value of 1.61 kJ (16% of total I.E of TWV).This is due to the force of impact transferred from the rigid pole to rear structure then to the front structure, as a result the drivers and occupants are subjected to high risk of injury. Another most significant energy is absorbed by the support of the roof which has direct contact with the rigid pole. They absorbed maximum of 0.618 kJ or 6.5% of total I.E of TWV. The remaining 2.5% (0.152) of energy is absorbed the parts shown on the right vertical axis of Figure 5.20. Among this roof, linkage, steering, tire, and windscreen absorbed 0.045, 0.0233, 0.0164, 0.021 and 0.00981 kilo joule of energies respectively. Since axle, foams and axles are modelled using rigid material so they do not show any deformation. As a result they will remain parts 0 energy absorption.

5.3.6 Contact force

The contact force between the TWV and the rigid pole is shown in the Figure 5.21. Initially the contact force is almost zero until the time reaches 0.01s. After this point the force starts to increase and shows some fluctuations. The fluctuations are due to the transient (time dependent) behavior of the simulation as a result the force on element is not always constant. The maximum force occur when the pole is directly in contact with the more stiff structure of the TWV such as the lower frame structure and also fully in contact with the dummies. At this point the vehicle is highly damaged and as well as the occupants.

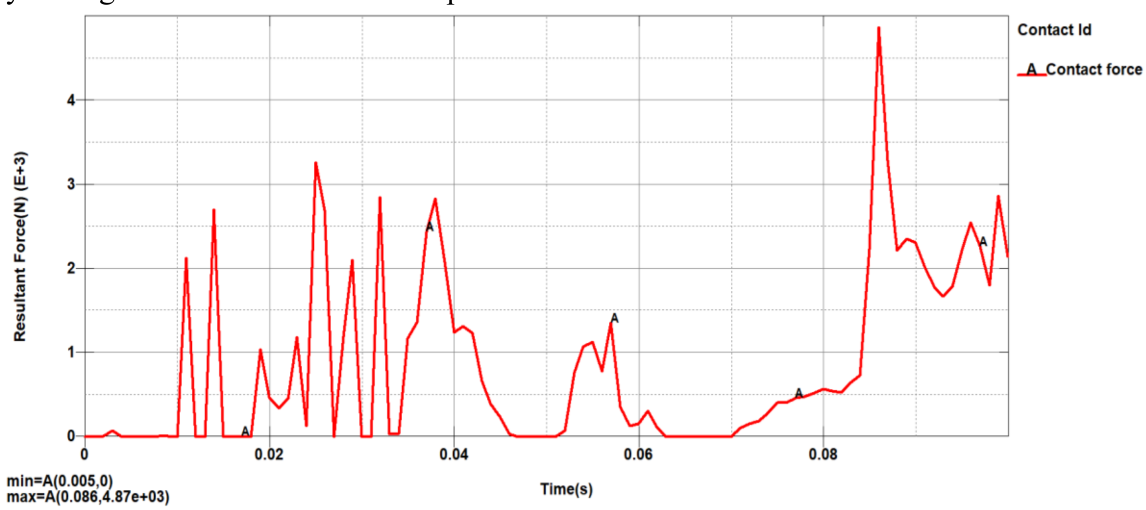

Figure 5.21. Contact force between the pole and TWV

The higher the force of impact the more damaged to the occupants and driver. The force impact is reduced by introducing deformable elements on the structure. Otherwise stiff elements will increase the force as the contact time of less.

5.3.7 The resultant velocity

The resultant velocity shows in Figure 5.22. Initially the velocity is 6.5 m/s and as the collision starts the resultant velocity reduces and reaches final value of 1.84 m/s. This shows that plastic deformation occurred on the TWV since the coefficient of restitution is low.

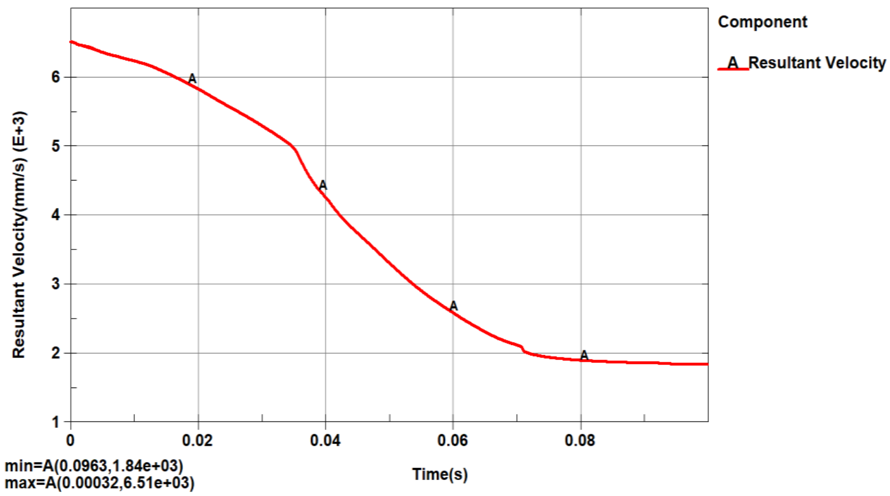

Figure 5.22. Resultant velocity

5.3.7 Verification

Energy ratio graph

As it can be seen on Figure 23, for the 0.1 s simulation the energy ratio value varies between 1.048 and 1.0466 which is within the range of acceptable value.

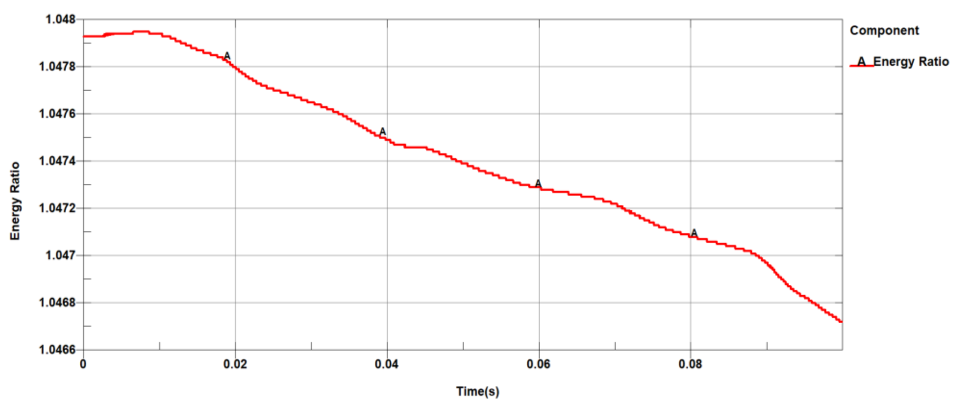

Figure 5.23. Validation: energy ratio

Ratio of TE/HE

Through analyzing the energy curves, the validity of the finite element model can also be determined using the ratio between the total energy to hourglass energy. Hourglass energy can cause a zero-energy model. If the hourglass Energy is less than 5% of the total energy, the finite element model is reliable In the above graph the hourglass energy graph is shown on the right hand vertical axis vs time and the total energy graph is shown in the left hand vertical axis vs time.as it can be seen the maximum value of hourglass is equal to 0.32 kJ and the total energy is equal with 14.9 kJ.

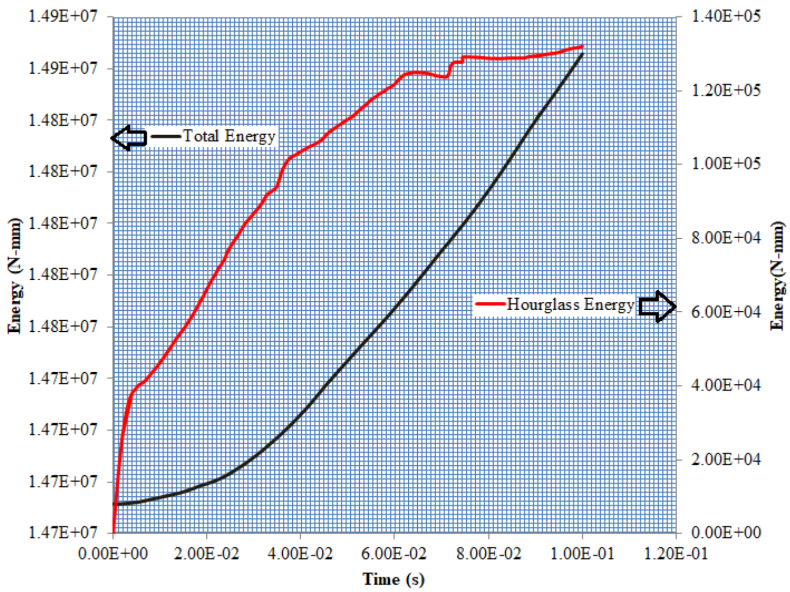

Figure 5.24. Verification: ratio TE/HE

Dividing this two gives 0.021 (2.1 %) Because the hourglass energy is too small, i.e HG < 5% it can be concluded that the result is reliable.

5.4 Rear crush collision results

5.4.1 The simulation responses of the cars

The simulation responses of the cars can be observed in Figure 5.25. The simulations of TWV with dummies inside show us that there is a significant damage to the cars at rear crush events. Thus, one can also observe the occupants to be significantly affected by the crash. As the crush scenario starts to take place there is little deformation to the vehicle and less effects on the occupants, as the time of collision goes on the speed of the MDB decreased and the lost kinetic energy starts to convert to the internal energy. This can be seen as the deformation on the vehicle progressively shown at time of 0.045,0.06.when t=0.09,the vehicle starts to rotate outward and significant damage starts to occur to vehicle as well as the occupants, the rear components of the vehicle (the fuel tank, engine and other will be starts to damaged. As it reaches t=0.125s, the rotates of the TWV to outward increases and the occupants head starts to move in to back and amore sever condition occur to the vehicle. At the last stage, the occupants head fully rotated and their foot and whole body will be affected by the inertia force and the vehicle fully damaged at the back and the contact force created between them creates sever damage. Other details are discussed in the next topics

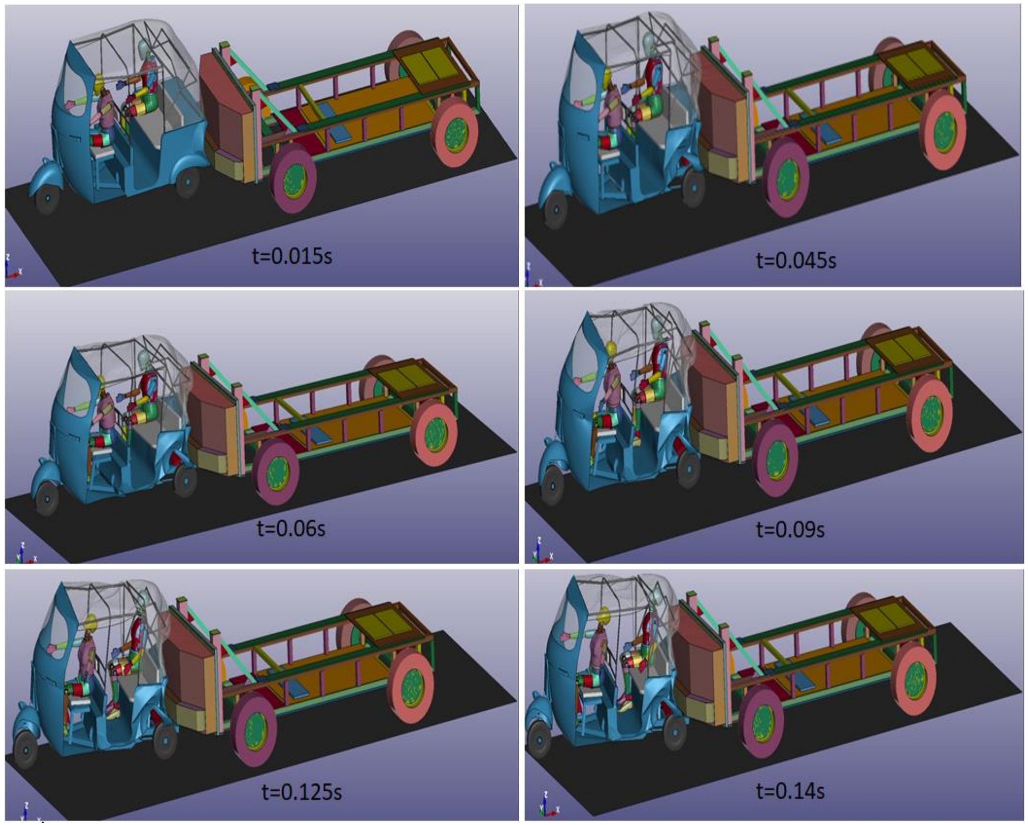

Figure 5.25. Rear crush TWV Simulation at different time seconds.

5.4.2 Structural analysis (The maximum overall intrusion)

To evaluate the structural responses of the models, the LS-PrePost has been utilized used for post-processing.

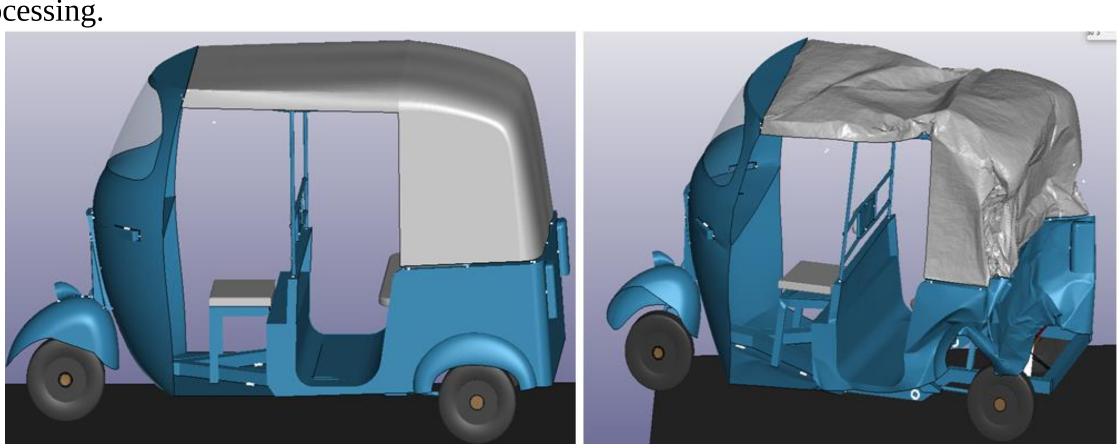

(a) (b)

Figure 5.26. The TWV before (a) and after (b) rear end collision.

Figure 5.27. Maximum overall intrusion.

Two nodes are selected on the front and the rear bumpers and simulated to identify the maximum intrusion. The nodes are selected with keyword *IDENT and the distance between the nodes is found out using *MEASUR keyword. The structural response of the TWV before and after the crash is shown in Figures 5.26 a and b. and also Figure 5.27. The relative distance between two nodes (one from front and other from rear structure) is measured at the initial and final state. The longitudinal initial distance of the selected point before the collision start is around 1829.43 mm but after last state it result in 1523. The resultant displacement between the two nodes vs. time graph shown on Figure 5.28.

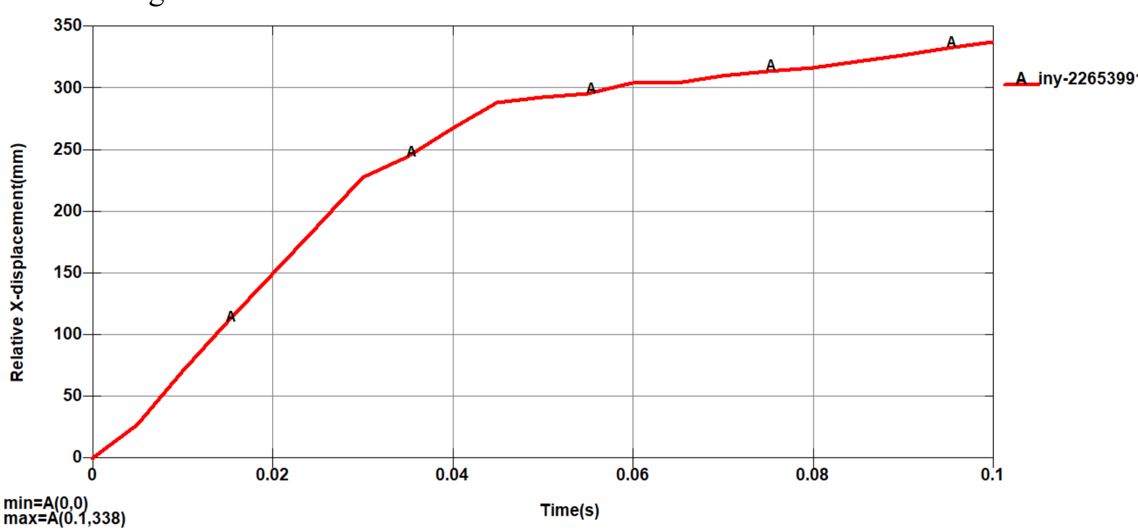

Figure 5.28. Longitudinal relative displacement

From the displacement graph we can see that the vehicle is subjected to maximum of 338 mm of intrusion at 0.1s.

This intrusion value will show that the rear components of the vehicle which are mounted on the main frame are damaged.

5.4.3 Occupant responses of rear impact simulations

The occupant responses for the rear impact simulations which are obtained by reconstructing the test with an occupant (Hybrid III 5th percentile dummy) is shown on the Figure 5.29. The responses can be seen by making some of TWV parts transparent. The collected results include, the screenshots of the simulation are taken for every 0.03s to observe the responses of the occupant inside the car. The aim of this section is to show the occupant in the car being

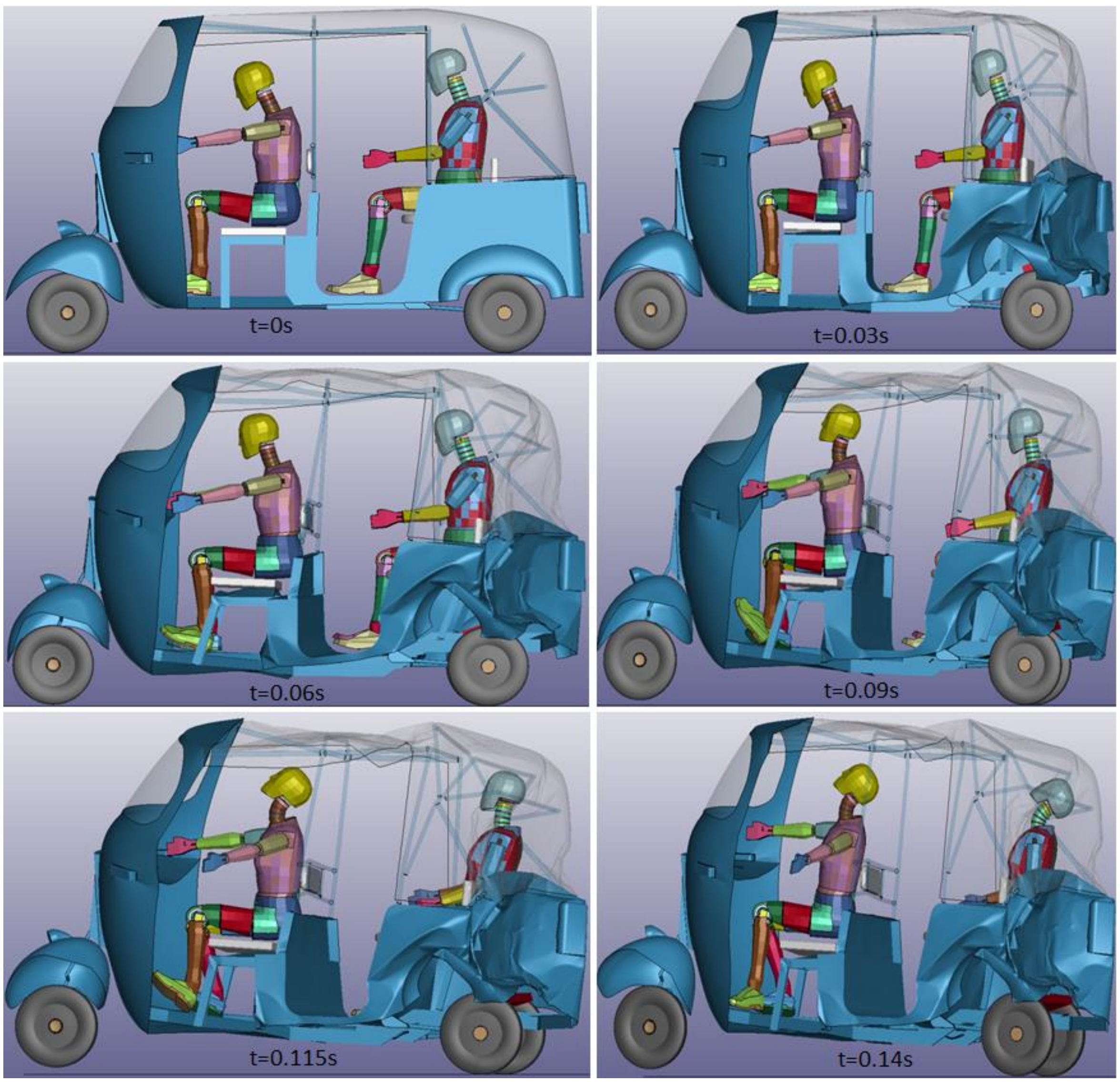

Figure 5.29. Occupant responses of rear impact simulations

Pushed against the seat as the loads act on the neck, causing significant injury. The responses recorded for the dummies (driver and passenger) for about 0.14s were shown on Figure 5.29. we can see that the occupants will not show any motion until 0.06s and this due to that the vehicle is not in direct contact with the dummies. When t=0.09s the driver starts to receive a little impact to his body, due to this his hand and foot starts to move from their original position and also the back of the passenger bends backward. As t=0.115, the occupants starts to feel high impact force due to this the head, leg and neck starts to bend highly, although the passenger starts to feel high impact from the back as result his back and hands bends a lots. At final stage, the driver and the occupants Experiences a significant rear-ward motion as the impact occurs causing injury to the neck, leg and their backs.

Neck injuries are the most common type of injuries to the occupants in rear-end collision. due to the pushing effect of the MDB, as THE VECHILE starts to accelerated forward it causes the occupant's torso to be pushed BACKWARD. The head lags the torso therefore suddenly accelerating and reaching its permissible limit. This neck motion is called an "hyper-extension" and when it protracts, it is called a "flexion"(Vedantam, 2018). Figure 5.30 shows the mechanism of "hyper-extension" the driver and the passenger at event of rear-end collisions.

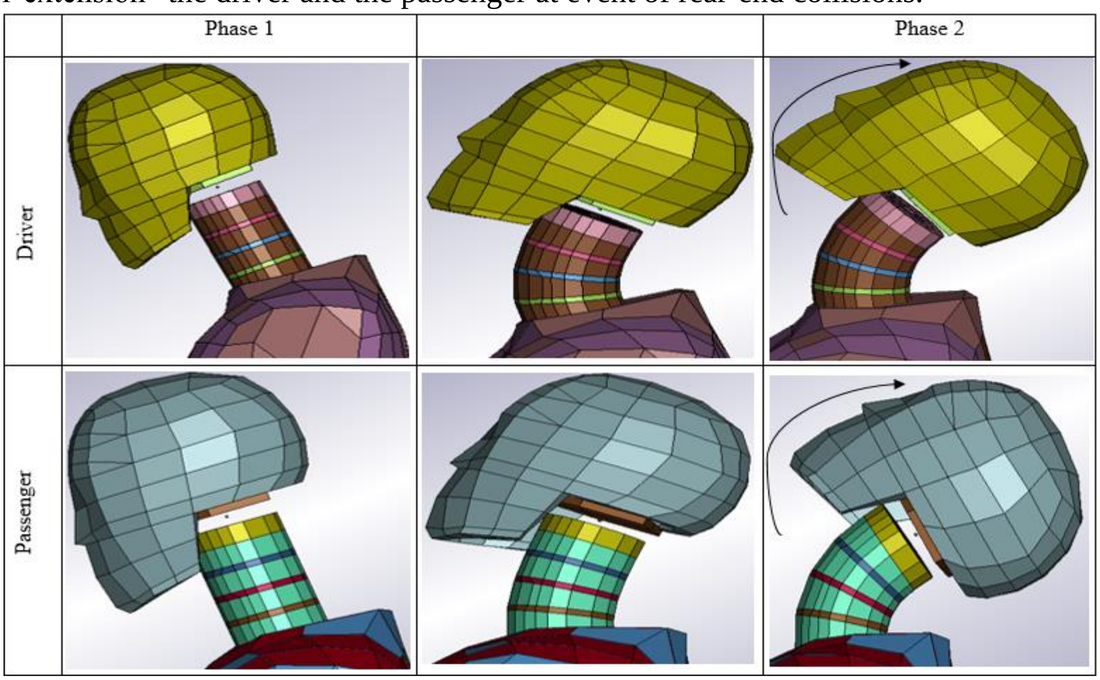

Figure 5.30. "hyper-extension" of the driver and the passenger

5.4.4 Energy balance

The energy balance for a typical rear crash is shown in the Figure 5.31. It can be observed that the total energy remains approximately constant throughout the 0.1s. The conversion of KE to IE has happened within 0.08s, beyond which the curve remains flat. Initially the kinetic energy is 52.5 kN, this energy is starts to decrease and converted to internal energy, sliding and, other energy.at final state, the kinetic energy is 37.6 kN (71.7% of initial value) and this shows that 28.3% energy is lost in the form of other energies.

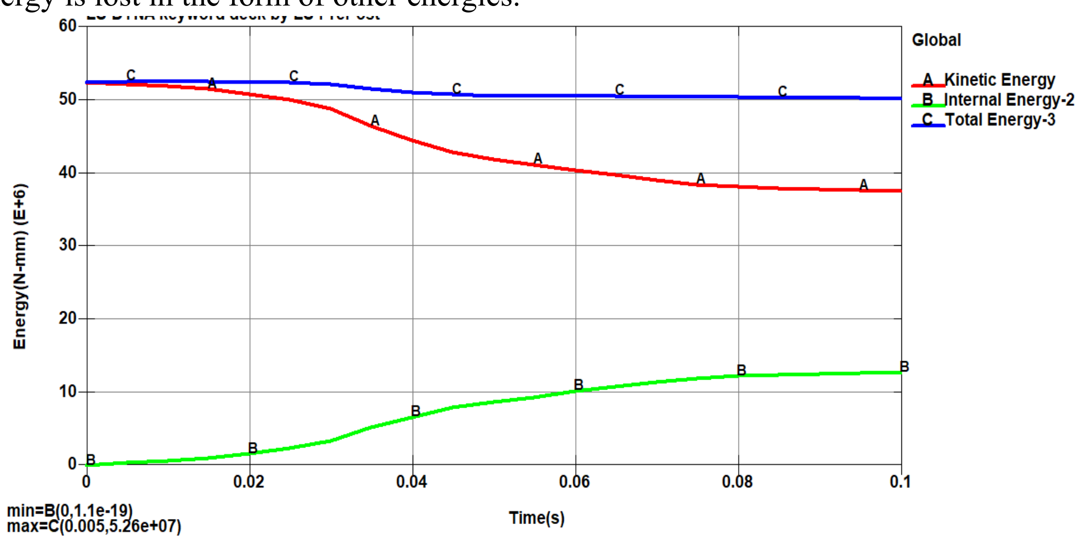

Figure 5.31. Rear crush Energy balance curve.

The final internal energy is equal with 12.7 kJ which covers 84% of the lost energy and the sliding and energy and other energies have 0.148 kJ (0.9% lost kinetic energy) and 2.252 kJ (14% lost kinetic energy), respectively.

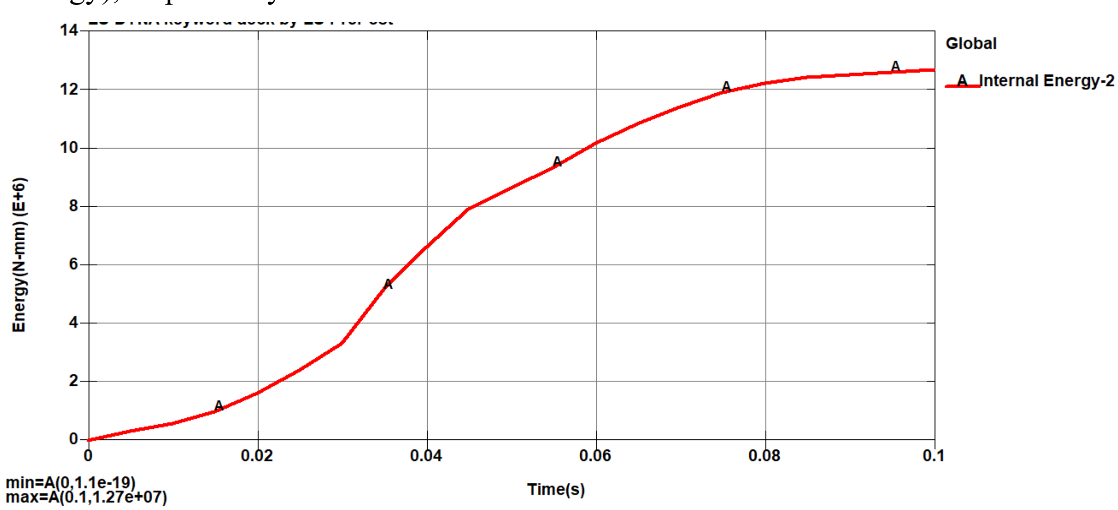

Figure 5.32. Rear crush internal Energy.

The above graph shows the total internal energy absorbed by the whole components during the collision process.

5.4.5 Energy absorbed by TWV parts

Energy absorbed by the TWV components are shown on Figure 5.33. The graph shows the energy absorbed by TWV parts with vertical primary (left) axis and secondary (right) axis versus time graph. The left vertical axis shows parts with highest energy absorption and the right side axis shows parts with less energy absorption.

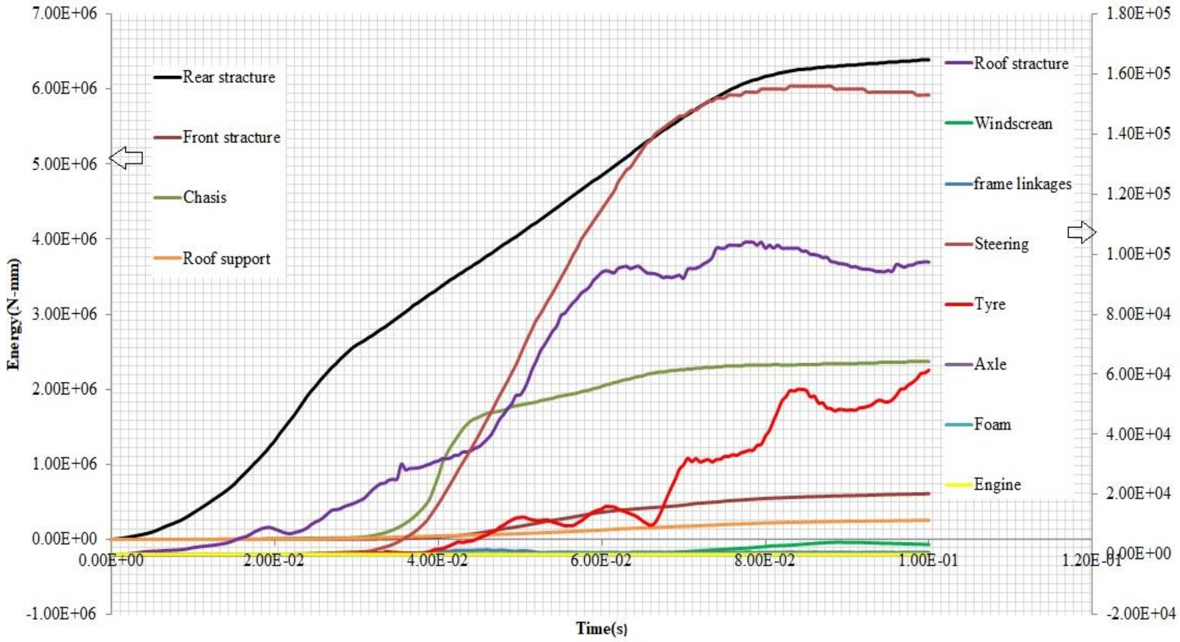

Figure 5.33. Energy absorbed by TWV parts.

Total energy absorbed by the TWV is 9.7 kJ which is 76.5% of the total internal energy. As it is indicated most of the energy is absorbed by rear structure, front structure, chassis and roof supports. This parts are totally accounts for 9.624 kJ (99% total energy absorption of the TWV parts) absorbed of energy. The rest of parts listed on the right side (roof structure windscreen frame linkages tire axle, foam and engines) absorbs only 7% of the total. This is because some of the parts are far from the collision contact point and the rigid material model. This results in no or less deformation. In general the rear structure is a part with highest energy absorption and it accounts generally most of the energy is absorbed by the rear structure with 6.39kJ. this is obvious as the rear structure is collision contact point and result in large deformation. To protect the critical rear parts such as gas cylinders, fitting rear bumper might be considered as solution.

5.4.6 Force Pulse

Figure 5.34 shows the barrier unfiltered force-time pulse, in rear impact the maximum value of collision force happens 0.037s with force value of 109 kN. After this point the force will completely slows down due to decrease velocity of the MDB and completely becomes flat after 0.1s. This value is relatively small as compared to frontal collision (Srikanth & Prakash, 2009) and this is due to the boundary condition created between the MDB and TWV will produce less momentum as compared to the boundary condition between the TWV and rigid wall.

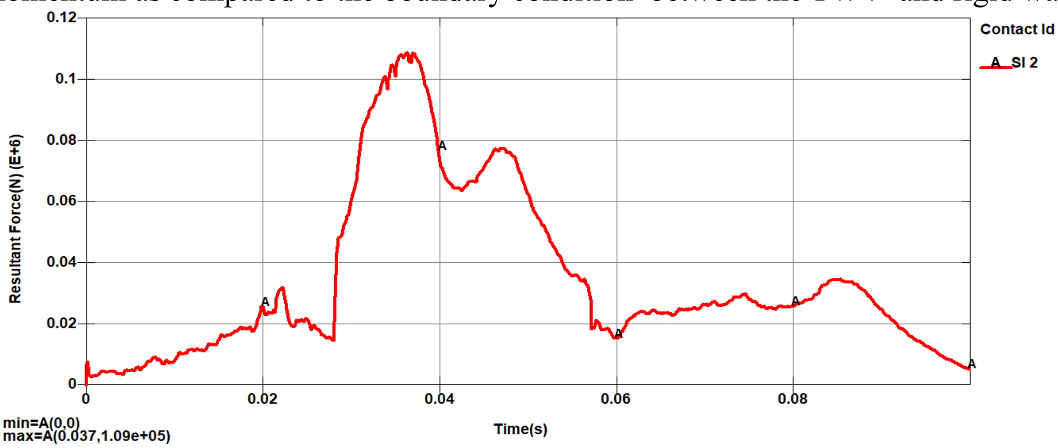

Figure 5.34. Contact force between MDB and TWV.

5.4.7 Vehicle Velocity

The resultant velocity of the MDB and TWV is shown in the Figure 5.35.

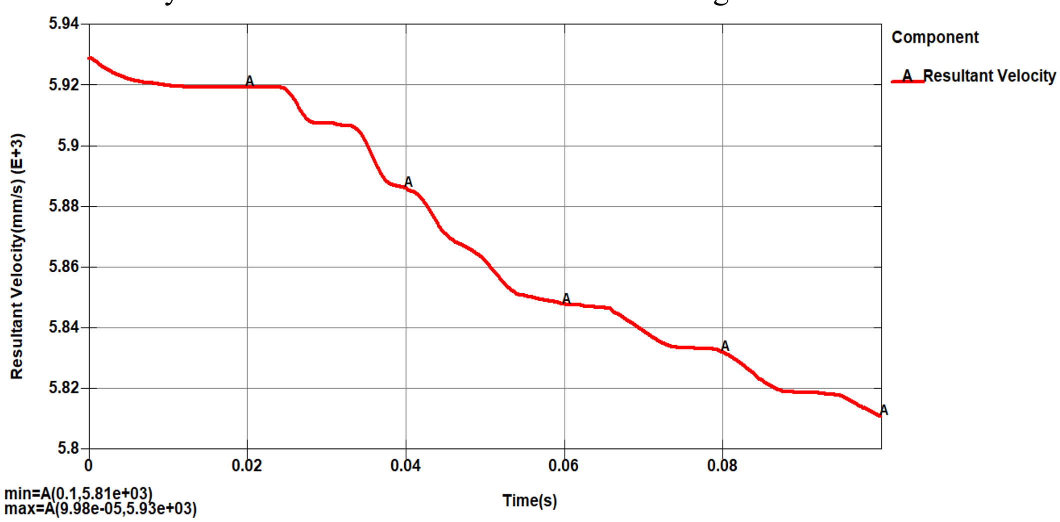

Figure 5.35. Resultant velocity

The resultant velocity get reduced from the initial maximum value (which in turn gets converted to internal energy).

5.4.8 Verification

Energy ratio

The above values are validated by the energy ratio, which is equal with the ratio of the total energies to the sum of other energies. From the energy ratio, it can be observed that the maximum and minimum energy ratio is less than 1. So the results are in the acceptable range.

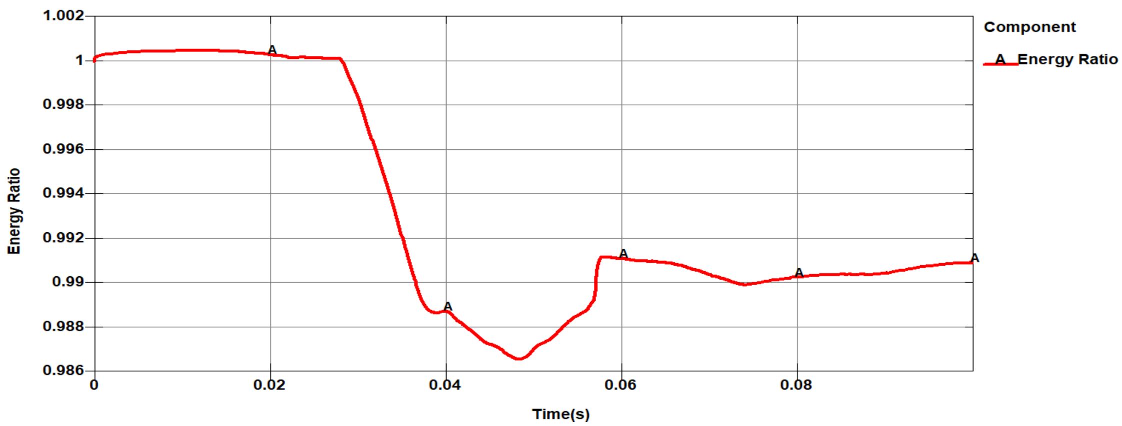

Figure 5.36. Verification: Energy ratio

5.5 Roof crush test

5.5.1 Resultant displacement

The total resultant displacement of the TWV for 127 mm movement of the plate is shown on the Figure 5.37.

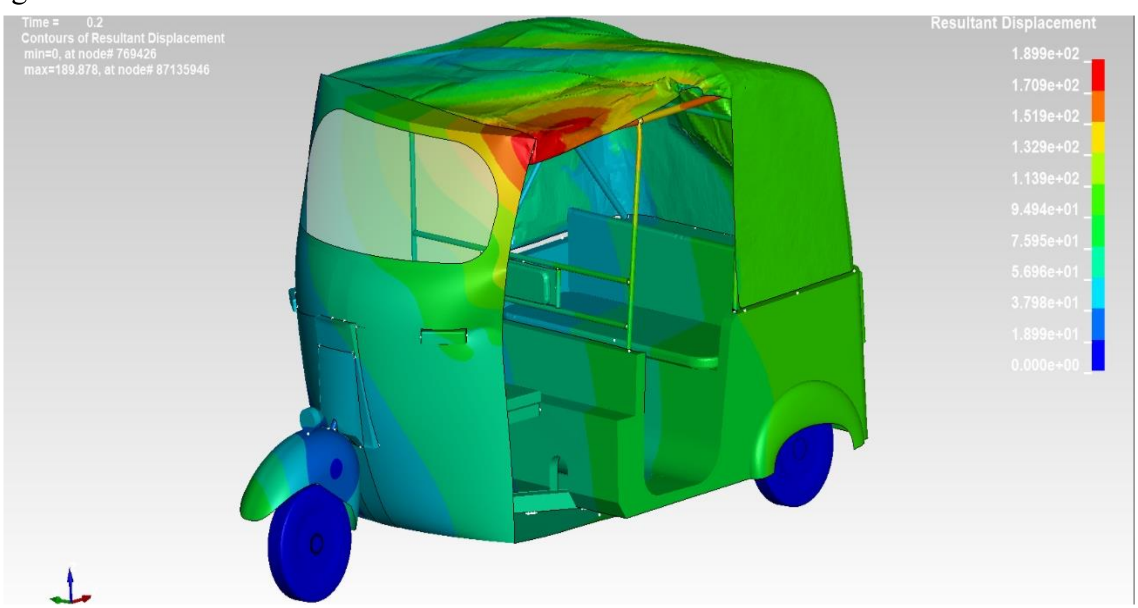

Figure 5.37. Resultant displacement of TWV at event of roof crush

As it can be seen the vehicle displaces 189 mm. Since the tire is fixed in all DOF as a result it displaces 0 displacement. The maximum displacement is observed at contact areas. However this is not the main determinant factor for the required roof strength of the TWV. The main parameter which determines the strength of the roof is its resistance or reaction force to the rigid plate.

5.5.2 Resistance force

The resisting force developed by the body structure is as shown in the Figure 5.38.

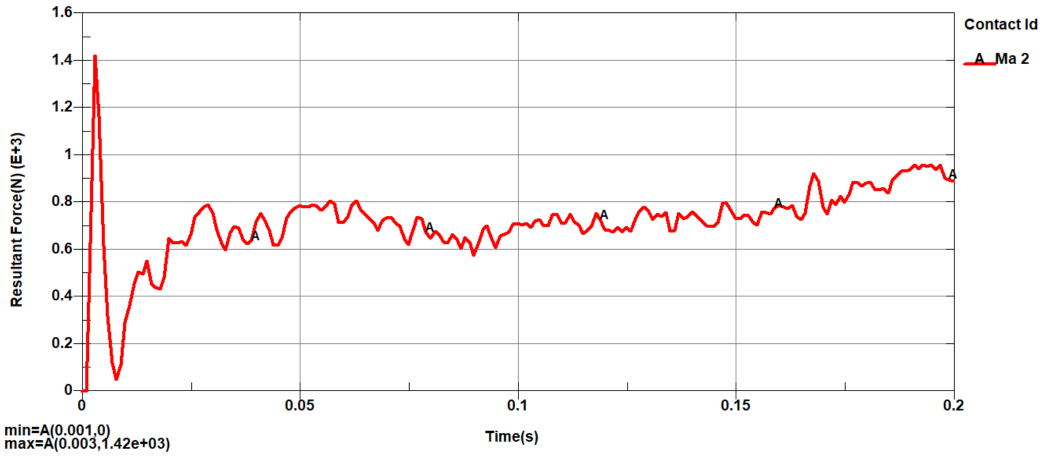

Figure 5.38. Resistance force of the roof structure

The maximum reaction resultant force of the TV structure is 1420N. As per the Standard of FMVSS 216 (Roof crush resistance, Passenger vehicle), the reaction forces must be higher than 1.5 its curb weight said to be a good car body.

5.5.3 Force vs deformation

The TWV produces the maximum force as the plate moves 1.28 mm shown on Figure 5.39.

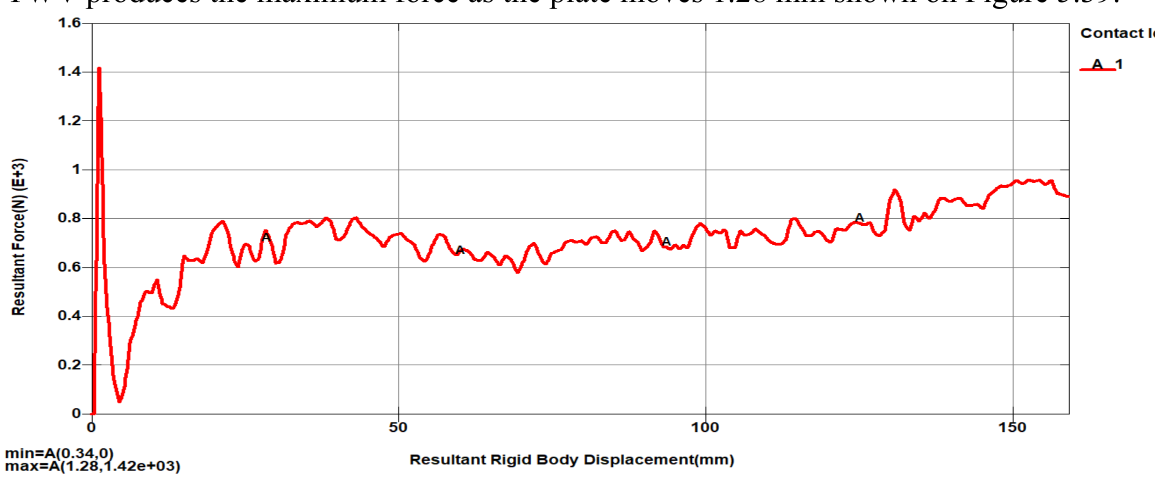

Figure 5.39. Resistance Force vs deformation

5.5.4 Strength determination of the roof

This can be determined by using strength to weight ratio as follow:

The curb force of the TWV structure is calculated as, $F = m \times g$

$Curb\ weight\ of\ the\ car: 280\ kg\ \ thus\ F_C = (280 \times 9.81)N$

$$F_C = 2{,}746.8N$$

Strength to weight ratio (SWR)

The TWV roof structure should withstand a force 4 times the unloaded vehicle weight prior to roof crush by 127 mm or 5 inch according to the FMVSS 216.

$$SWR = \frac{F_R}{F_C}$$

Where F_R, is the reaction force of the TWV structure to the plate Displacement from Figure 5.39. The maximum force of reaction is equal with 1420 N.

$$SWR = \frac{1420}{2{,}746.8}$$

SWR=0.51

This value can be compared to IIHS rating system for strength to ratio ranges. As it can be seen from the Figure 5.40. The calculated value fails under poor region. This mean that the TWV roof have no ability to protect the occupants at events of rollover accidents.

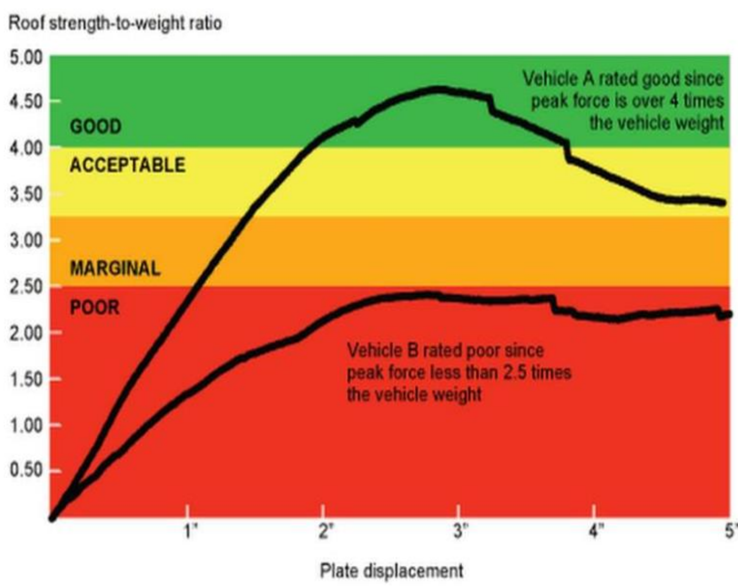

Figure 5.40. IIHS rating system for strength to ratio.

5.6 Side beam Simulation results

The result for different thickness of bumpers are represented in graphs at regular interval of time as shown below. Judgments were going to be made by observing the impact analysis results like force, stress, displacement (deformation) and strain values.

5.6.1 Deformation

The deformation values are obtained by measuring the relative displacement from two nodes (one at the right or left end of the beam and the other at middle of the beam). With this measurement the value of deformation graph for different thickness of the beam was shown below.

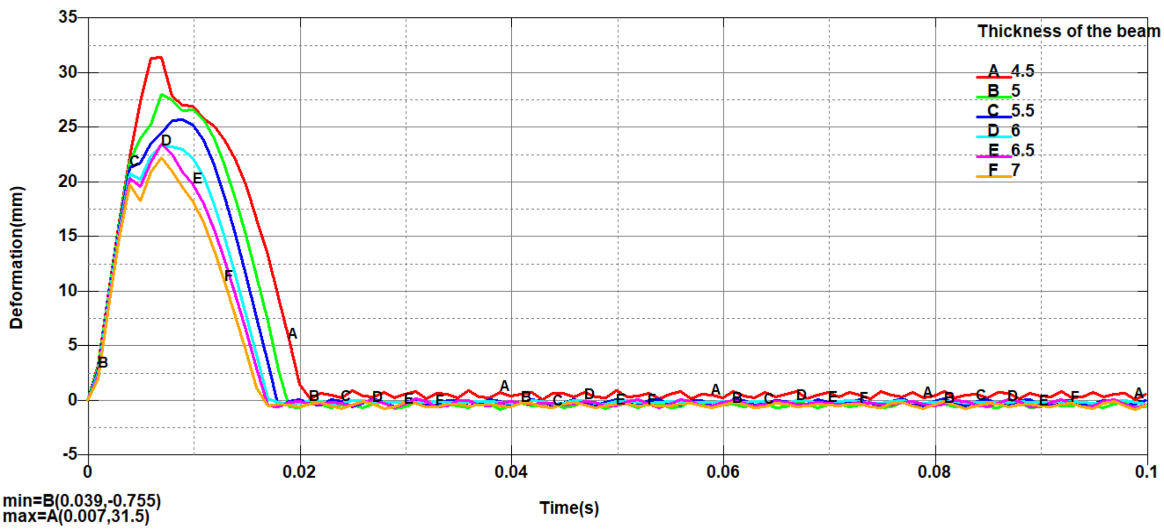

Figure 5.41. Deformation for Side bumper beam is 4.5, 5.0, 5.5, 6.5, and 7.5 mm thickness

The thickness of the bumper beam is 4.5, 5.0, 5.5, 6.5, and 7.5 mm as shown in Figure 5.41. As we can see in this Figure 5.41, as the thickness of the beam increases from 4.5 mm to 7 mm, the maximum deformation of the beam decreases and the rate of decrease becomes also less with the increase of thickness. This does mean that abeam with less thickness is always better because more deformation means that there is probability of intrusion to the vehicle main compartments.

5.6.2 Energy absorption

On another hand, as it can be seen in Figure 5.42, the higher deformation of the beam leads to more absorption of energy of the composite beam. The maximum amount of energy absorbed by the beam is reduced as the thickness become increased.

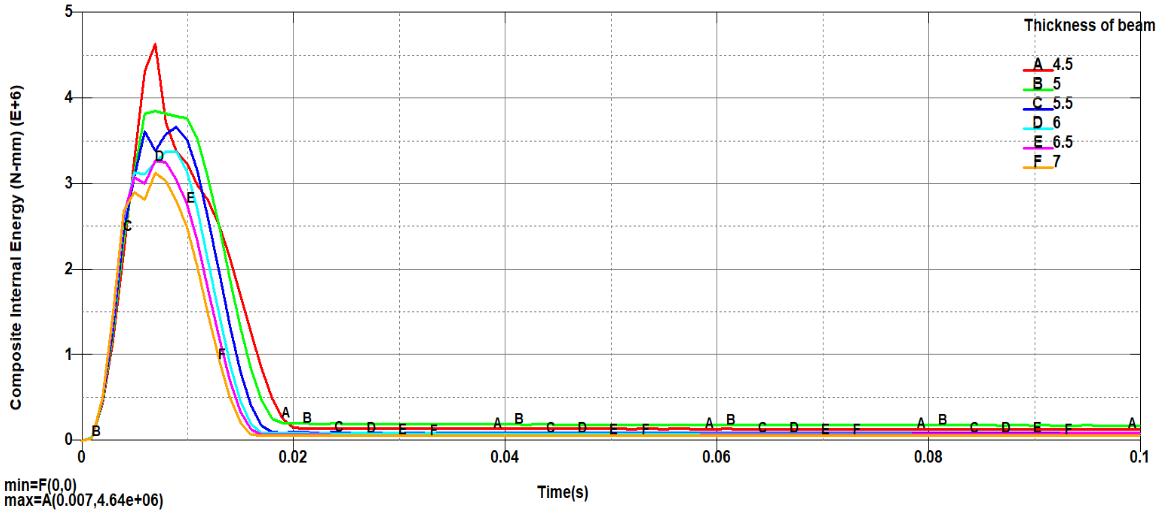

Figure 5.42. Energy absorption for side bumper beam

5.6.3 Impact force

Although maximum impact force between rigid pole and side bumper beam increase with the increase of thickness. This is obvious that with increase in thickness the mass of the beam increases as a result, high impact force is produced. Contributes as shown in Figure 5.43.

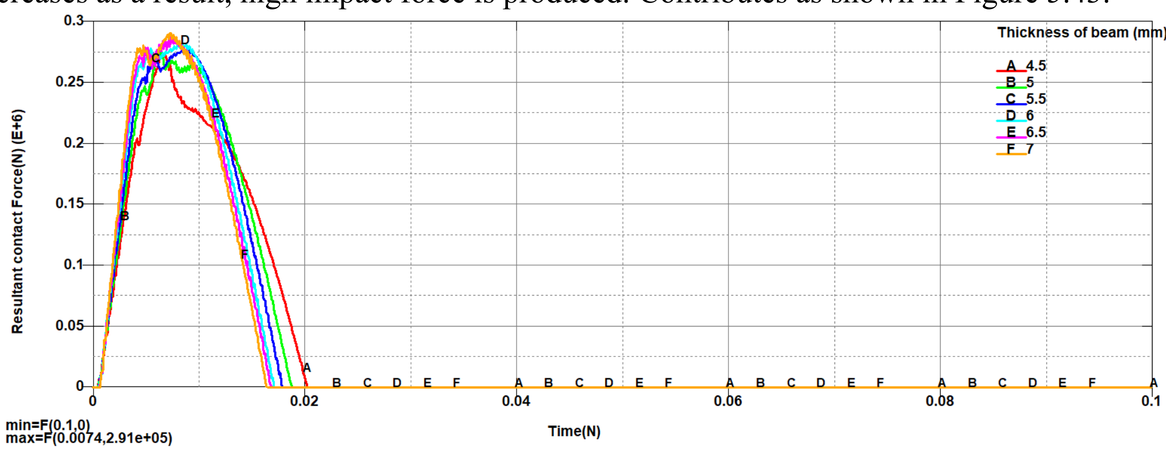

Figure 5.43. Impact force for Side bumper beam

But that does not mean that beam with smaller thickness is better because the stress on the on the beam increases with the use of less thickness. Therefore, from the above results it can be concluded that neither abeam with less thickness nor with higher thickness is better, rather it depends on the application it is required for. The main purpose of this investigation is to select a lightweight side bumper beam without sacrificing the impact behavior. From the viewpoint of impact performance, among the listed thickness taking the average value provides improved the level of performance relative of other for the body parts and passengers of TWV. Therefore, the bumper beam with 6mm thickness is better. The van mosses equivalent stress, and displacement graph of the selected beam is shown below.

5.6.4 Effective von Moises stress

As it is indicated on the Figure 5.44, the maximum stress value is equal to 3781 mpa. The composite material strength and failure criteria is determined based on Chang-Chang failure criterion. If the failure has occurred in all of the laminate layers, then the element is deleted (Krishnamoorthy, 2009). Since there is no dilatation of element was reported when running the simulation so based on that assumption the beam is safe.

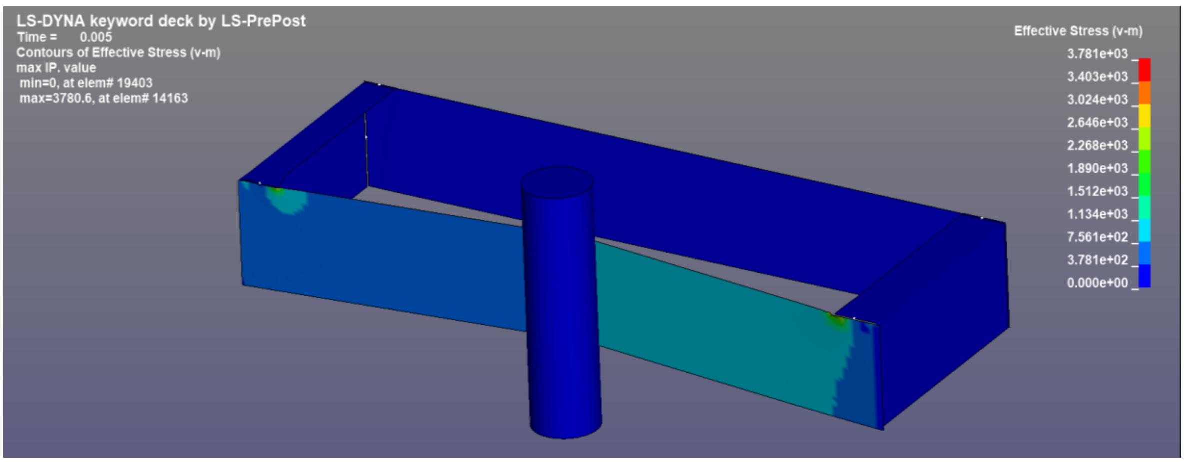

Figure 5.44. Effective von mosis stress

5.6.5 Resultant displacement

As it is indicated on the counter plot, the maximum resultant deformation of the beam is 32mm at node 9479.

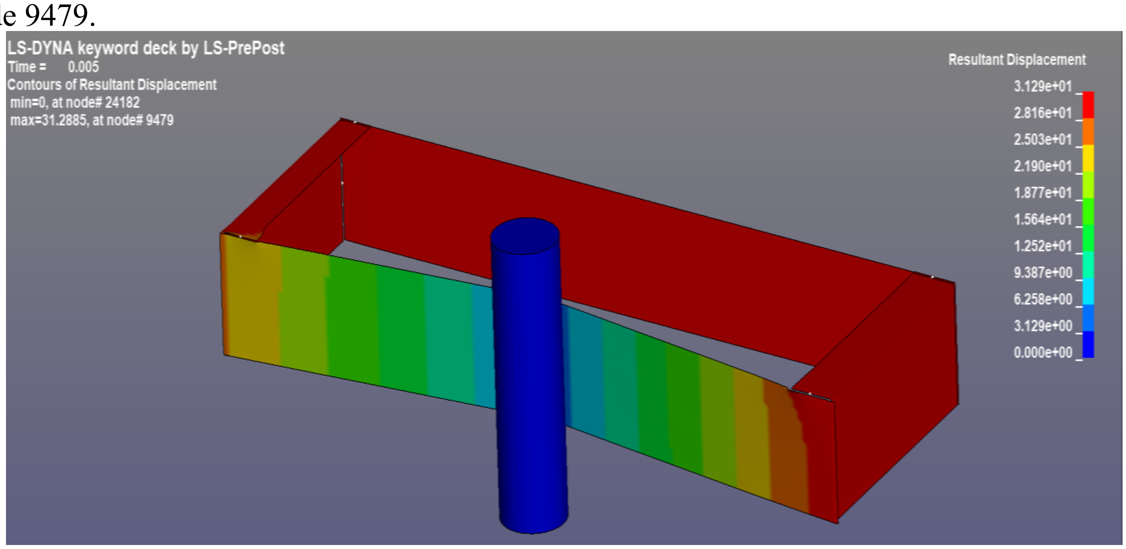

Figure 5.45. Resultant displacement

Deformation of the bumper produce changes in energy absorption the beam. With this deformation the intrusion is very less and the force of impact is gradually increase but he damage on the will be less as compared to the existing, see Figure 5.45.

5.7 Rear bumper beam

The result for different thickness of bumpers are represented in graphs at regular interval of time as shown below. Judgments were going to be made by observing the impact analysis results like force, stress, displacement (deformation) and strain values.

5.7.1 Deformation

The deformation value is obtained by measuring the relative distance between two nodes .So to observe the deformation of the bumper beam ,as a reference point the node whose deformation is the biggest in the bumper beam is taken relative to another node (undeformed). The deformation versus time diagram is shown in Figure 5.46. For each thickness the maximum deformation occur at t=0.025s, and after this point the beam rebound a little bit and then stays constant without change after t=0.045s. The behavior of the beam is called plastic deformation in which the beam will note get back to its original position. In this configuration, the ideal would be that the beam doesn't rebound after crashing meaning that the whole energy has been absorbed and therefore the velocity change is the lowest possible.

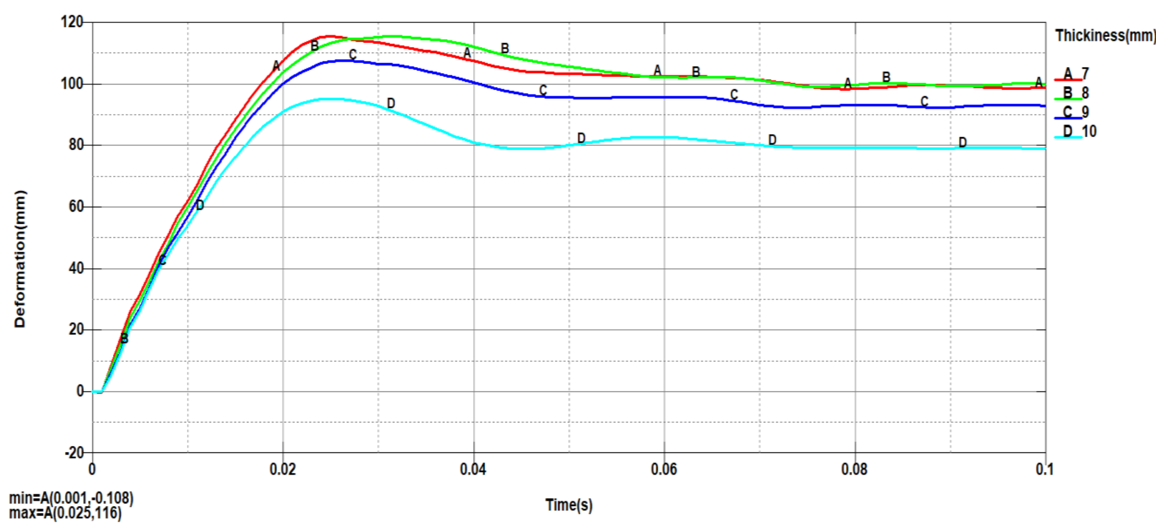

Figure 5.46. Deformation rear bumper beam is 7, 8, 9, and 10 mm thickness

Among them maximum deformation occur when the thickness is 7mm and the minimum occurs at thickness of 10mm. This indicate that with increase in thickness of the beam there is small the reason for this situation is that the stiffness of carbon fiber composite beam is increase with increase in thickness.

5.7.2 Impact force

A beam with higher thickness is not always better because, as the thickness increases the force between the impactor and rear bumper beam increase. As shown on Figure 5.47, Using beam with higher thickness increases force transferred to the other vehicle part and occupants and produces more damage. The increase in force is due to the stiffness of the beam as the impact contact time between the beam and impactor is reduced as the thickness of the beam increase, as a result higher contact force is obtained at higher thickness.

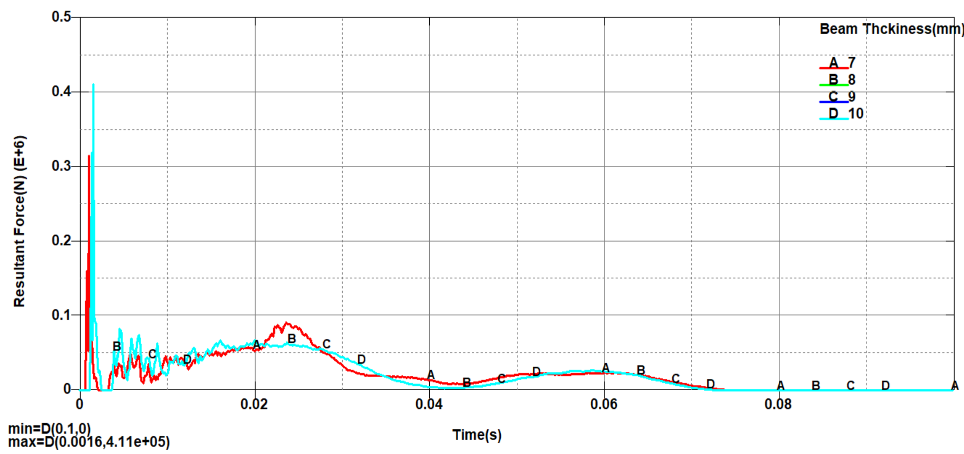

Figure 5.47. Impact force for rear bumper beam is 7, 8, 9, and 10 mm thickness

5.7.3 Energy absorbed

In addition to the force, with less deformation the energy absorbed by the also less as shown on Figure 5.48, as a result the energy transferred to the vehicle parts and occupants increases.

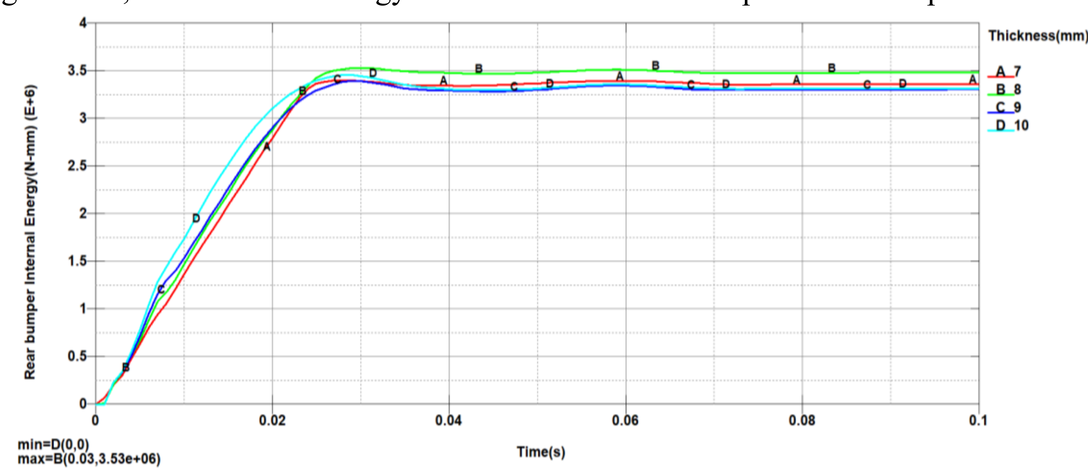

Figure 5.48. Internal energy for rear bumper beam is 7, 8, 9, and 10 mm thickness

So in order to achieve those aims the beam should be stiff and absorbed most energy with little deformation so that it reduce damage and intrusion in to the TWV. So here priority is given to strength and deformation. Even if the force increases with the use of higher thickness but the rate of increasing is very small, as a result for the rear bumper abeam with 10mm thickness will provide the required performance (create a survival cell around the occupants reducing intrusion). The couture plot of the beam with selected thickness is shown on the next section.

5.7.4 Resultant displacement

The resultant displacement of the bumper beam is shown in Figure 5.49.

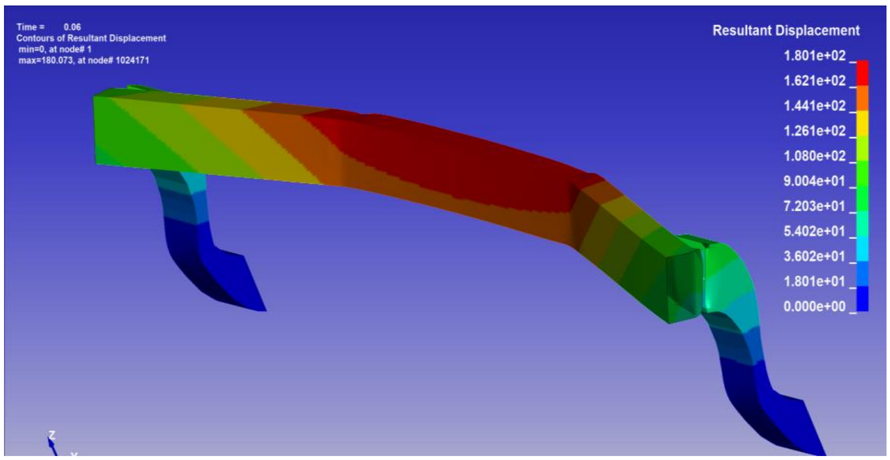

Figure 5.49. Counter of Resultant displacement of rear bumper

As it is indicated on the counter plot the maximum resultant displacement or deformation of the beam is 180 mm at node 1024171. This value is enough to reduce the intrusion of the impactor in to the rear compartments. Deformation of the bumper also produce changes in energy in the energy absorption of the collisions. Even if there is intrusion the force of impact is gradually decreased by the beam and the damage on the rear compartment at intrusion point will be minimized.

5.7.5 Effective von-Moises stress

On this paper as it is mentioned in the previous section , For composite material the material strength and failure criteria is based on, the material strength and failure criteria is determined based on Chang-Chang failure criterion. If the failure has occurred in all of the laminate layers, then the element is deleted (Krishnamoorthy, 2009), since there is no element dilatation is shown during the simulation so we can say that the beam is safe under the given condition.

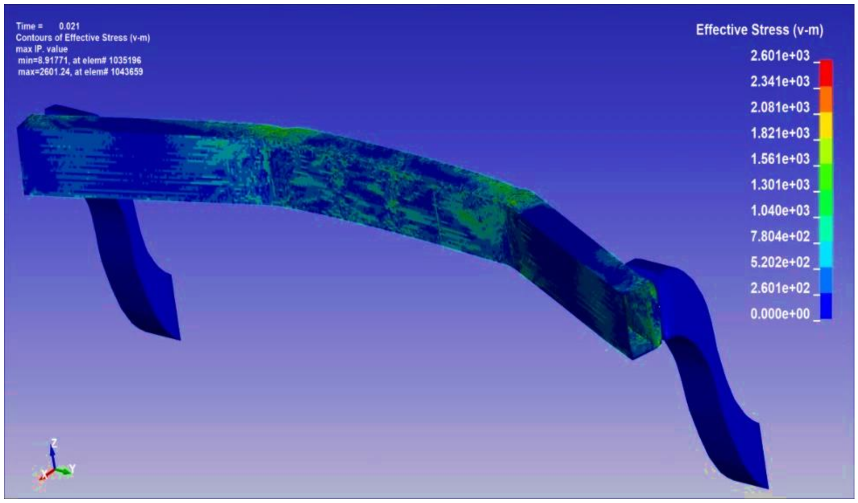

Figure 5.50. Rear bumper Effective von-Moises stress

The maximum stress occur at element 1043659 with value of 2601 mpa, see Figure 5.50.

5.8 Front bumper beam

Under this section the impact behavior of different thickness of front bumper beam is analyzed based on parameters like force, displacement (deformation). Based on the above studies , the deformation and energy absorbed have direct relation, so it is enough to study the energy absorbed in terms deformation The thickness considered were 6, 7, and 8 mm.the result of the simulation were discussed below.

5.8.1 Deformation

As it is discussed in previous section, the behavior follows the same pattern in which the deformation decreases as the thickness increases.

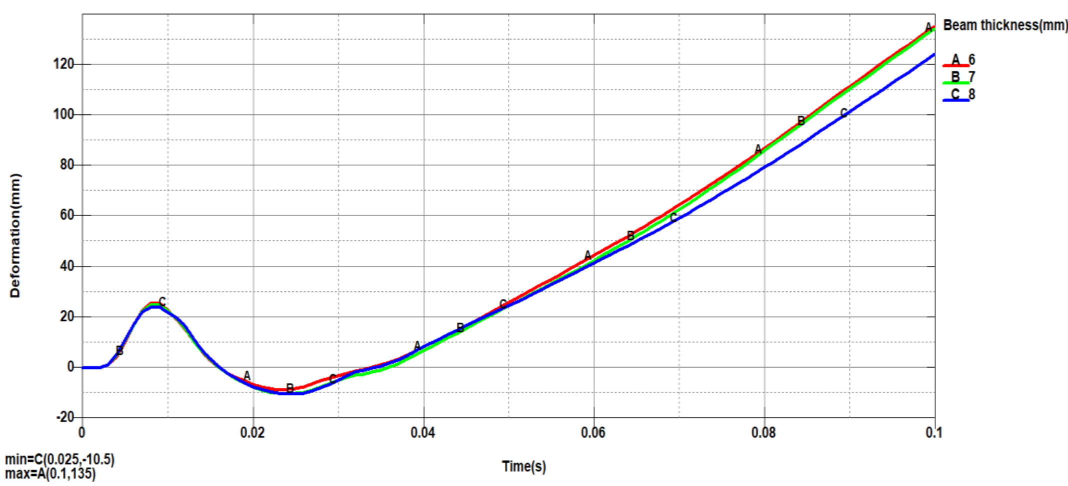

Figure 5.51. Deformation for front bumper beam thickness of 6, 7, 8

Initial until t=0.003 there is no deformation until the collision phenomena occurs, then the collision starts to occur and the structures were subjected to deformation as shown on Figure 5.51.

5.8.2 Impact force

The up and down effect observed on the graph shown the compression and elongation effects occurs between the measuring nodal points of the beam. From the deformation it can also concluded that the energy absorbed by bumper beam in decreases with more deformation and decreases with les deformation.in another word the increase in thickness of the beam results in less deformation and energy absorption.

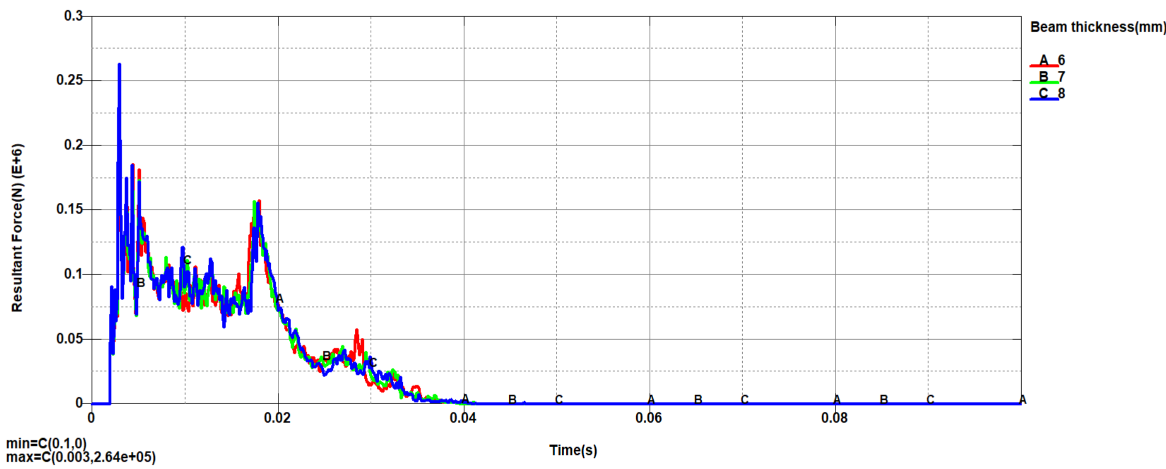

Figure 5.52. Resultant force for front bumper beam thickness of 6, 7, 8

Another phenomenon to look at was the force of impact in relation with the above values (deformation and absorbed energy). The contact force vs. time graph is shown in Figure 5.52 .the graph reveals that as the thickness increases the force of impact increases. The maximum peck force (26.4kN) occur when the bumper thickness 8mm.This behavior is obvious as the stiffness of the beam increases with increase in thickness of the front beam.so generally looking at the above result it can beam concluded that the increases in thickness results in less deformation, less energy absorption and high contact force.

5.8.3 Effective von Moises stress

The effective van mosis stress of the front structure is shown on Figure 5.53. The maximum stress on the structure is equal with 2604mpa.The strength of composite fiber and matrix for Tensile and compressive strength is determined using Chang-Chang failure criterion.

It uses the ratio of the maximum stress to the material tensile or compressive strength.

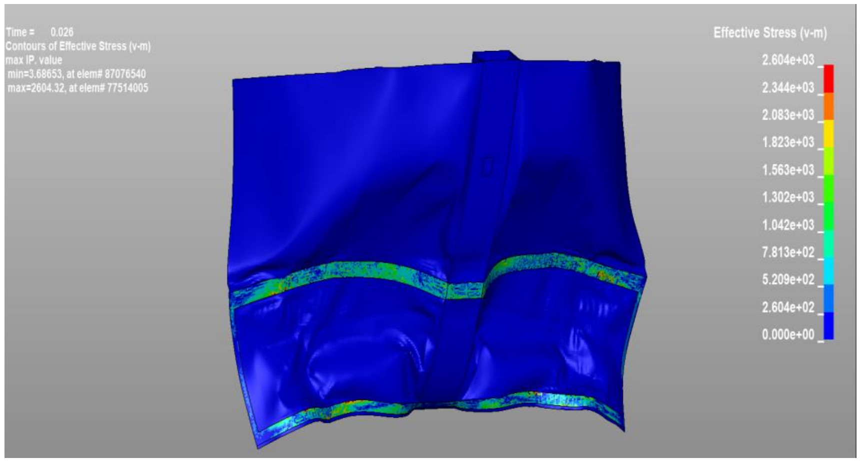

Figure 5.53. Effective von Moises stress of front bumper

If the value is >1, failure destruction occurs, and if the value is <1, no failure destruction occurs (Schweizerhof, n.d.). In LS-DYNA when analyzing composite material ,the material strength and failure criteria is based on the material strength and failure criteria is determined based on Chang-Chang failure criterion. If the failure has occurred in all of the laminate layers, then the element is deleted (Krishnamoorthy, 2009). Since no dilatation of element is reported during the running of the simulation, so that it can be concluded that the beam is safe.

5.8.4 Resultant displacement

The Resultant displacement of the front structure is shown on Figure 5.54

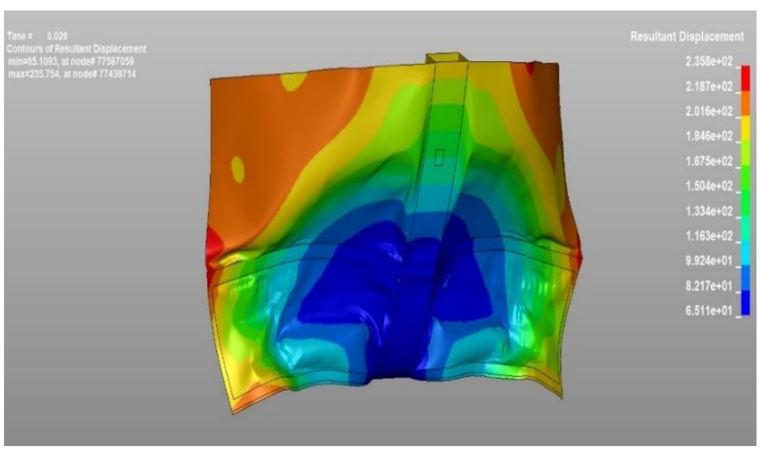

Figure 5.54. Resultant displacement

From the couture plot it can be seen that the maximum resultant displacement of the structure is equal to 235 mm.

II. Result and discussion of Modified TWV

5.9. Side pole collision

5.9.1 Intrusion into the vehicles

The intrusion into the modified TWV model due to the side pole collision shown on Figure 5.55 Intrusion obtained by measuring the relative displacement between two nodes of the model.

D=997mm

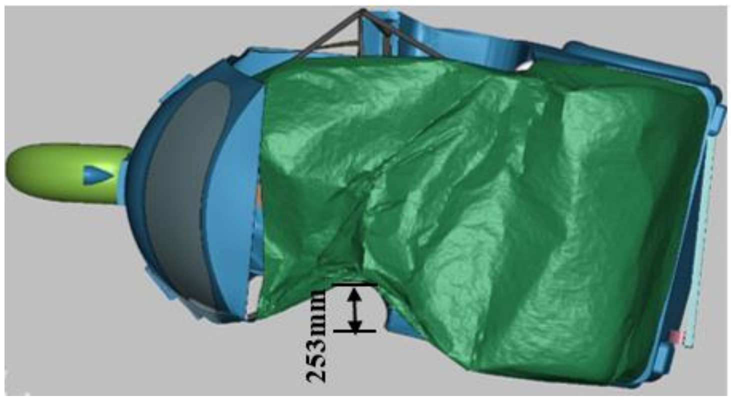

Figure 5.55. Side Intrusion into the vehicles

From Figure 5.55 shows the un-deformed and the final deformation of the TWV before and after impact with the rigid pole. As it can be seen, pole intrude 132 mm in to the modified model. The original width of the TWV in lateral direction is 1250 mm. This shows that the modified model remain with 997 mm space on lateral direction

5.9.2 Displacement

The resultant displacement of the modified model in lateral direction is shown on Figure 5.56.

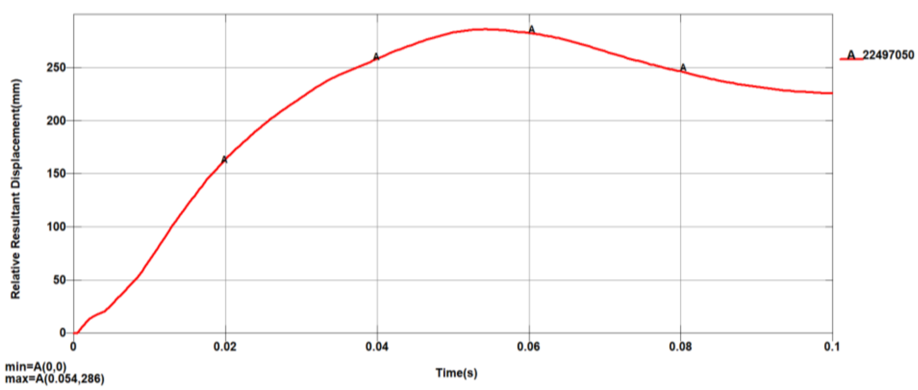

Figure 5.56. Displacement of Modified TWV model vehicle

As shown on the graph the maximum displacement is equal with 286 mm. The maximum deformation occur at 0.055s and after this point the deformation decrease. This is due to the reduction on speed of the TWV rebounding and the contact between stiff elements. Although after this point the force of impact is decreased as a result only less deformation are observed

5.9.3 Energy balance curve

The energy versus time plot of the total system is shown in Figure 5.57. As it is shown the total energy of the system remain constant for the whole 0.1s simulation with value equal to the initial kinetic energy which is 14.8 kJ. On the another hand the kinetic energy of the whole system starts to decrease as the collision process starts and converted into internal energy which is increasing starting from the 0 energy. Most of the absorbed energy is due to the deformation of the structure. The little jump in K.E and I.E energy AT T=0.092s is due to the additional movements of the modified TWV during rebounding. After this point little deformation is observed, as a result the energy graph of the K.E and I.E become flat. Energy such us internal energy, hourglass energy, sliding energy or other forms.

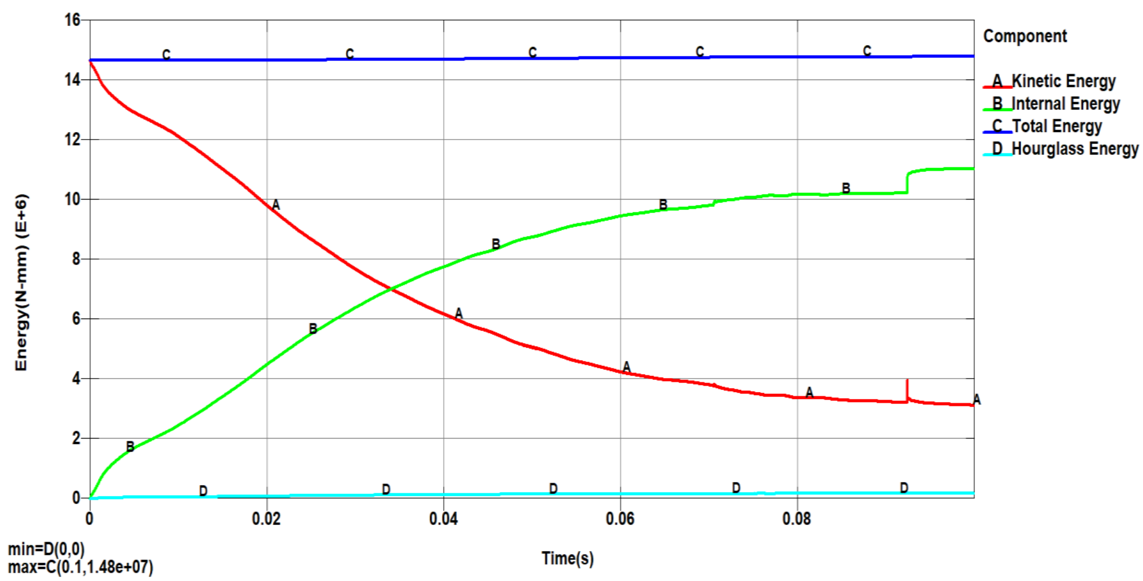

Figure 5.57. Energy balance of modified TWV model vehicle at event of side collision

At 0.1s the kinetic energy value is equal with 3.13 kJ and this indicate that 11.67 kJ kinetic energy is lost and converted in to other forms of energy such as I.E, H.E and others. The total energy graph is shown on the Figure 5.58. As indicated on the graph 11kJ of energy is in the form of internal energy .this mean that internal energy takes 94 % of the dissipated or lost KE. the remaining 0.67 kJ of energy is in the form of hourglass and sliding energy.

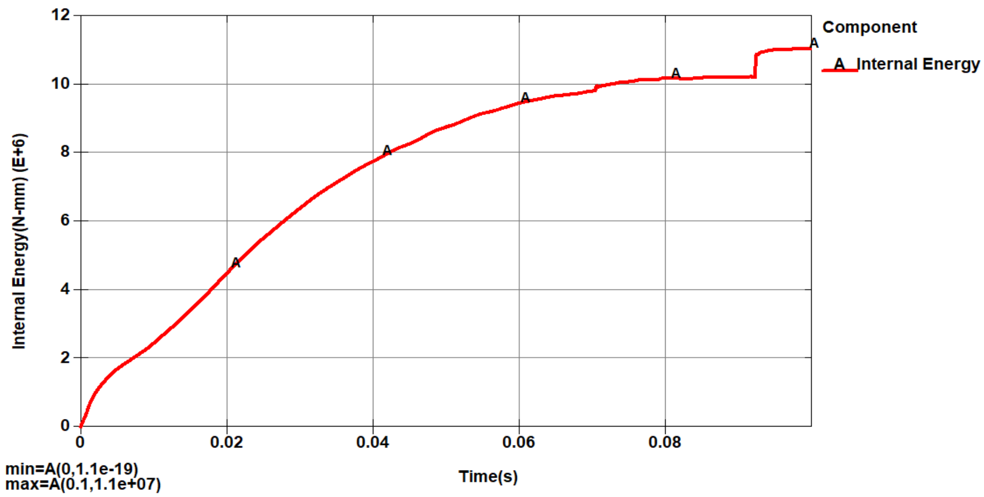

Figure 5.58. Internal energy of modified TWV model vehicle at event of side collision

5.9.4 Energy absorbed by TWV Vehicle

From the total energy absorbed by the whole system, the energy absorbed by the TWV structure is presented on the Figure 5.59.

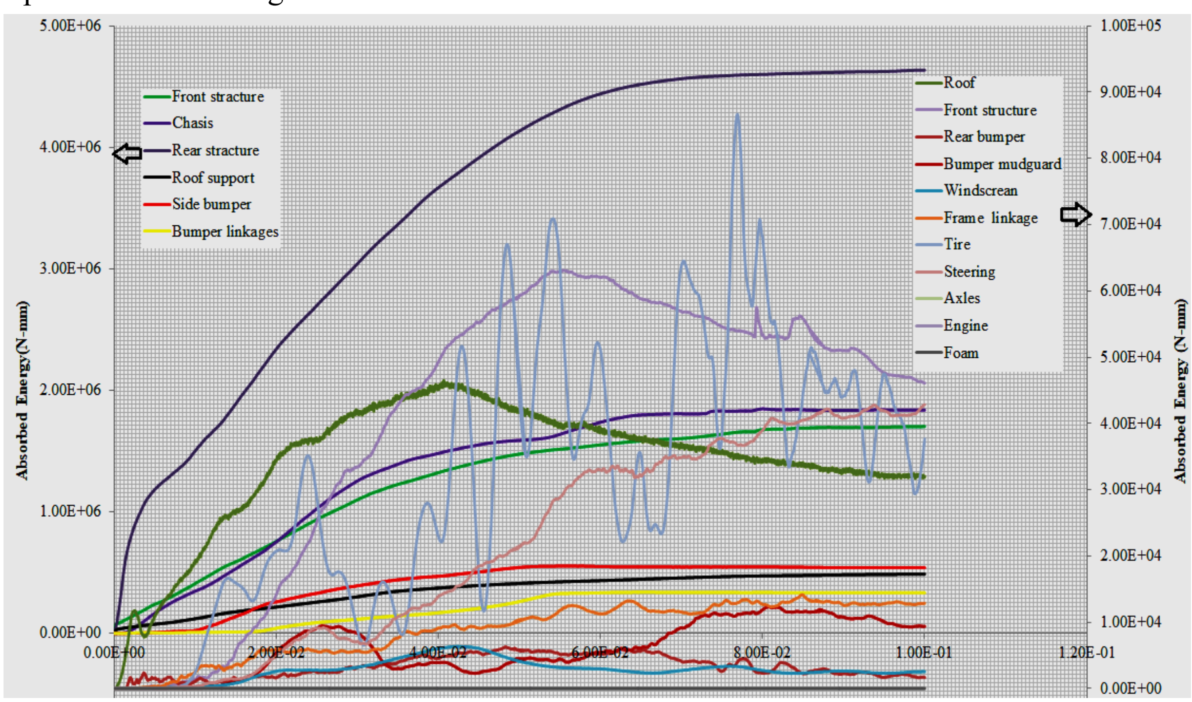

Figure 5.59. Energy absorbed by TWV Vehicle at event of side collision

on the Figure 5.59, the primary axis (left vertical axis) shows the TWV parts with the highest energy absorption such as rear body structure, roof support frame, main lower frame and front body structure and the secondary axis (right vertical axis) shows the parts with lower absorption of energy. The total amount of energy absorbed by the TWV is equal with 9.7207kJ.this shows that most of the energy is absorbed by the TWV structure. Among the parts which are listed under primary (left) axis are absorbed 98% .the side structure is the part with highest energy absorption with value equal to 4.64 kJ and others parts such as front structure, chassis, roof support side bumper and bumper linkages have value of 1.7 kJ,1.84 kJ,0.486 kJ,0.0461 kJ and 0.033 kJ respectively.

Totally the bumpers absorbs 0.9302 kJ and this accounts 9% of the total energy absorbed by the TWV. The side bumpers absorbed much of energy among the bumpers with value equal to 0.54 kJ. This is quite easy to predict because the pole have direct contact with the side structure. In addition the front bumper linkages, rear bumper and bumper mudguard accounts 0.046 kJ, 0.00167 kJ, 0.33 kJ and 0.00938 kJ respectively with less deformation. The other part which is subjected more deformation is the front structure, it have maximum energy absorption value of 1.7 kJ. This is due to transfer of impact other parts are subjected to less deformation so that less absorption of energy. Since axle, foams and axles are modelled using rigid material so they do not show any deformation. As a result they will remain parts 0 energy absorption.

5.9.5 Contact force

The contact force between the TWV and the rigid pole is shown in the Figure 5.60. Until the time reaches 0.01s there is fluctuation force.

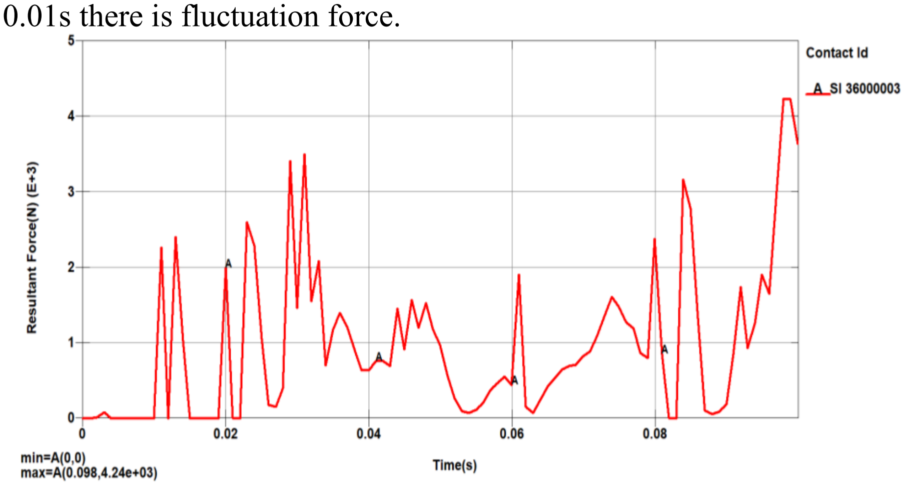

Figure 5.60. Contact force between the side pole and TWV

After this point the force starts to increase and shows some fluctuations. As mentioned on previous section the fluctuations are due to the transient (time dependent) behavior of the simulation. The maximum resultant force occur at t=0.097s with value equal to 4.24kN. This value is maintained only for 0.001 s and then drops down higher force of impact may because more damaged to the occupants and driver.

5.9.6 The resultant velocity

The resultant velocity shows in Figure 5.61. Initially the velocity is 6.5 m/s and as the collision starts the resultant velocity reduces and reaches final value of 1.84 m/s. This shows that plastic deformation occurred on the TWV since the coefficient of restitution is low.

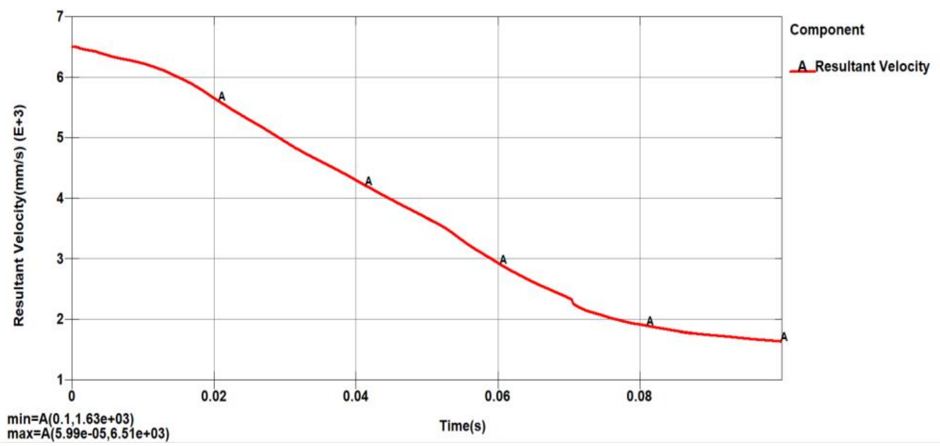

Figure 5.61. Resultant velocity

5.9.7 Verification

Energy ratio graph

Figure 5.62 shows verification value using energy ratio

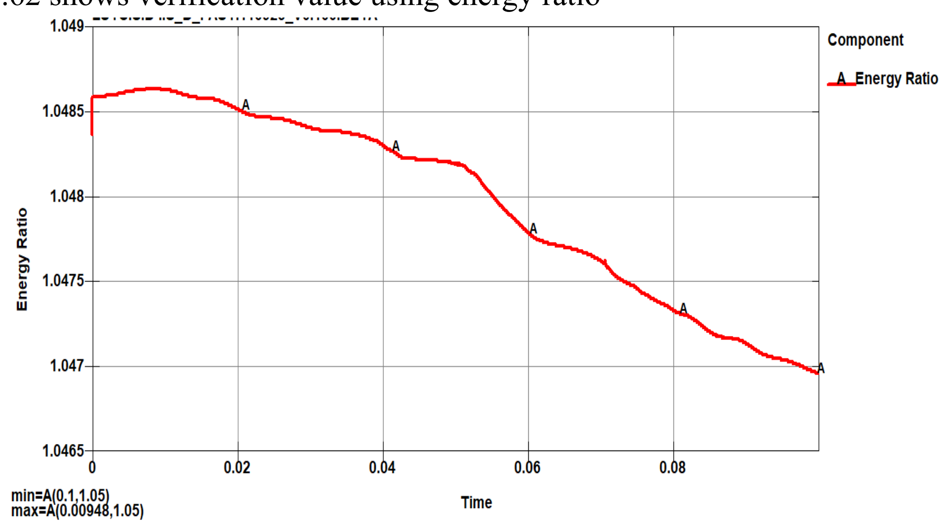

Figure 5.62. Verification: Energy ratio

As it can be seen on Figure 5.62, for the 0.1 s simulation the energy ratio value varies between 1.048 and 1.0465 which is within the range of acceptable value.

Ratio of HE/TE

Another means for validating the FEA result is the ratio between the total energy to hourglass energy .as indicated on the graph the energy graph of the hourglass energy is shown on the right vertical axis vs time and the total energy is the left vertical axis vs time. The maximum hourglass energy is equal with 0.16 kJ and the total energy is 14.85 kJ. The ratio between this values (*HE/TE*) is less than 5%. If the hourglass Energy is less than 5% of the total energy, the finite element model is reliable.

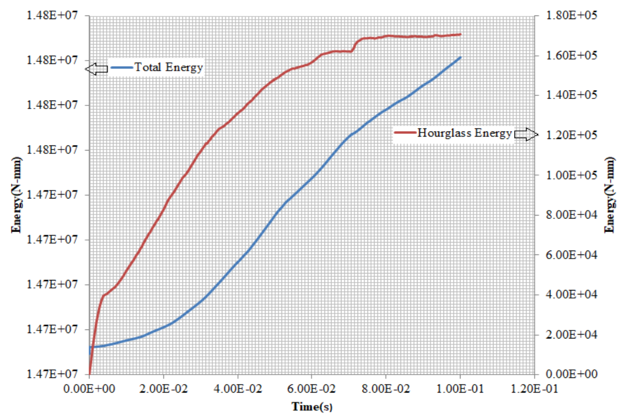

5.9 Rear crush

5.10.1 Structural analysis (The maximum overall intrusion)

The structural response of the modified TWV after rear crash is shown in Figures 5.64.

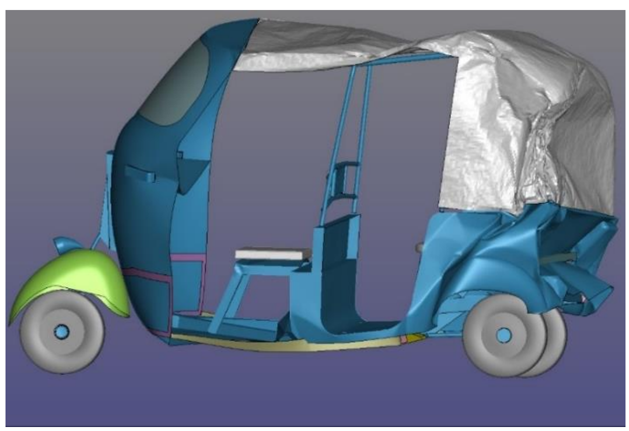

Figure 5.64. Modified TWV the maximum overall intrusion at event of rear crush

As shown on the Figure 5.64, the rear structure of the vehicle is deformed together with the rear bumper. There is no much structural deformation rather than the rear structure and this is due to less intrusion at the rear structure and bumper resistance. The initial longitudinal distance of the selected point before the collision 1829.43mm but after crush it remains with state it result in 1645 mm at t=0.1s.

5.10.2 Displacement

The result of the relative distance measured between two nodes (one from front and other from rear structure) is shown on Figure 5.65.

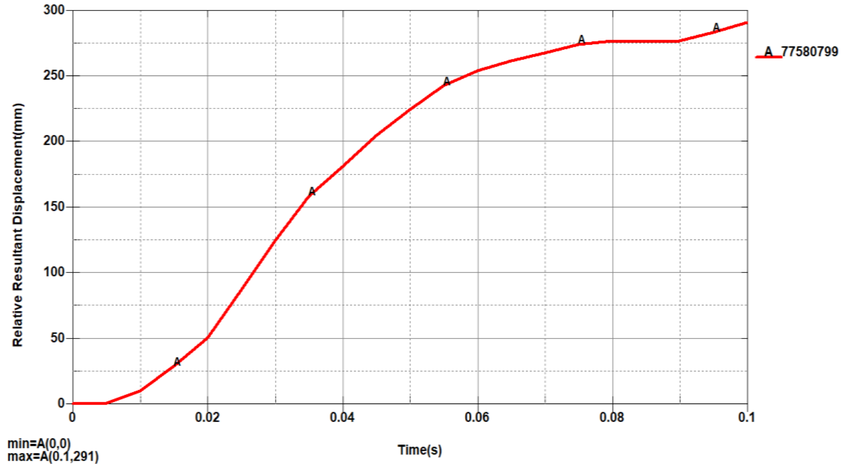

Figure 5.65. Modified TWV displacement at event of rear crush

From the graph we can see that the vehicle is subjected to maximum intrusion of 291mm. The deformation increases linearly up to 0.07 and after this point the graph changes its shape to flat due to reduction of the velocity.

5.10.3 Energy balance

The energy balance for a typical rear crash is shown in the Figure 5.66. The total energy of the system remains constant for the whole simulation

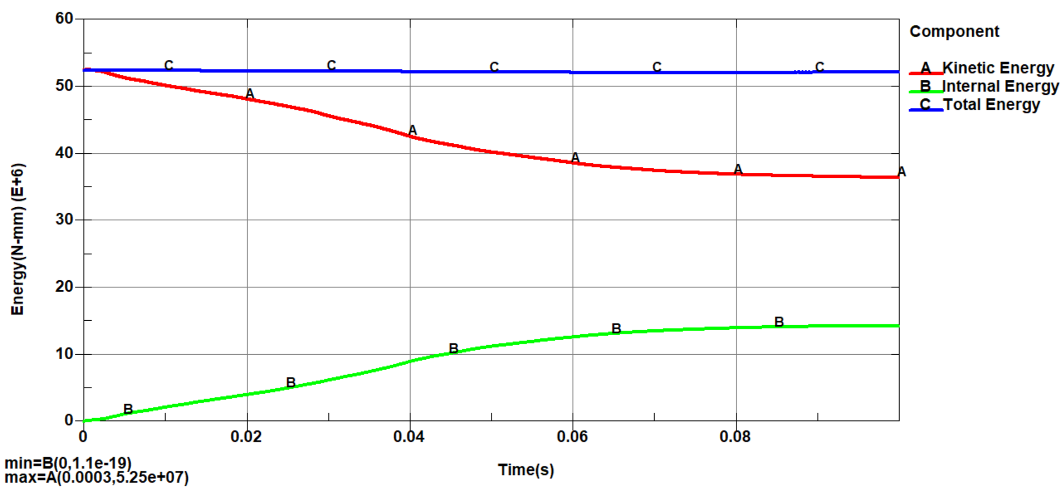

Figure 5.66. Modified TWV energy balance at event of rear crush

Until the time reaches 0.08s, some portion of the kinetic energy is converted to internal energy and after that the conversion process stops and both graph will be flat. Initially the kinetic energy is 52.5 kJ. This energy is starts to decrease and converted to internal energy, sliding and, and other energy.at final state, the final kinetic energy is equal to 36.5 kJ (69.5% of initial value) and this shows that 29.5% energy is lost in the form of other energies.

The final internal energy is equal with 14.3 kJ which covers 89.3% of the lost energy and the sliding and energy and other energies have 1.7 kJ (10% lost kinetic energy).

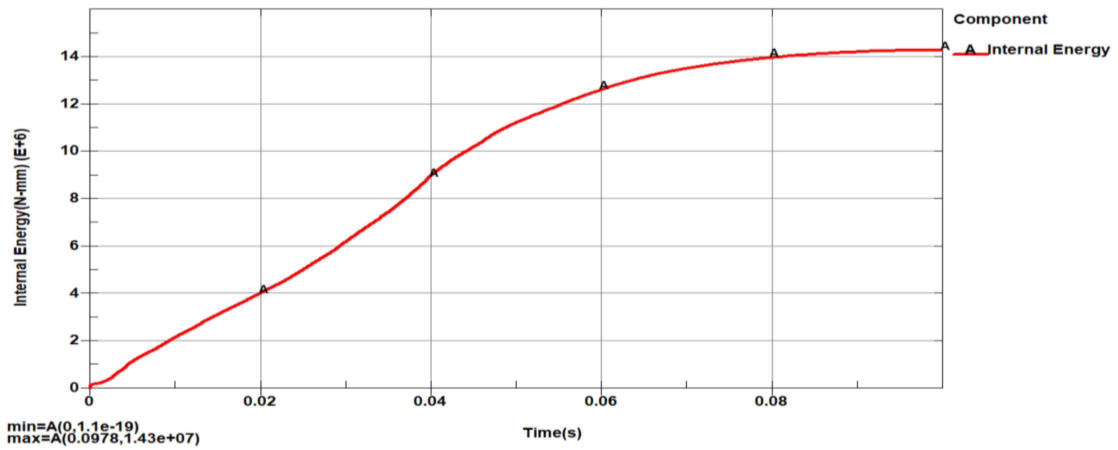

Figure 5.67. Modified TWV internal energy at event of rear crush

The above Figure 5.67 shows the total internal energy absorbed by the whole components during the collision process.

5.10.4 Energy absorbed by TWV parts

The energy absorbed by the TWV components are shown on Figure 5.68, the graph shows the energy absorbed by TWV parts with vertical primary (left) axis and secondary (right) axis versus time graph. The left vertical axis shows parts with highest energy absorption and the right side axis shows parts with less energy absorption.

Totally the bumpers or modifications absorbs 4.13 kJ and this accounts 32.5% of the total energy absorbed by the TWV. The rear bumper support linkages absorbed much of energy among the bumpers with value equal to 3.64 kJ. The rear bumper also accounts 0.345 kJ, this mean that the rear bumper together with its linkage absorbed much energy. In addition to the above, the side bumper, front bumper and bumper mudguard accounts 0.128 kJ, 0.0124 kJ, and 0.00856 kJ respectively with les deformation.

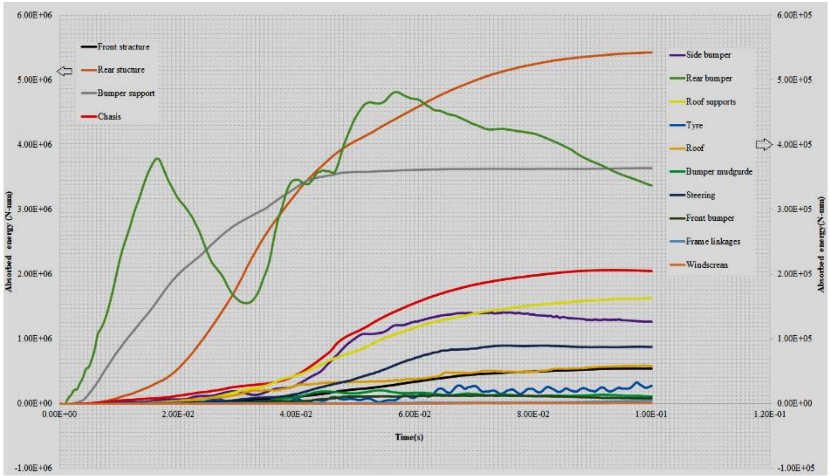

Figure 5.68. Modified TWV parts absorbed energy at event of rear crush

In general the rear structure is a part with highest energy absorption and it accounts generally most of the energy is absorbed by the rear structure with 5.41 kJ and then followed by the bumpers 4.13 kJ.

5.10.5. Force Pulse

The impact force vs pulse shown on Figure 5.69, in the maximum value of collision force happens at the 0.04s with force value of 85kN. After this point the force will completely decreases velocity of the MDB decreases.

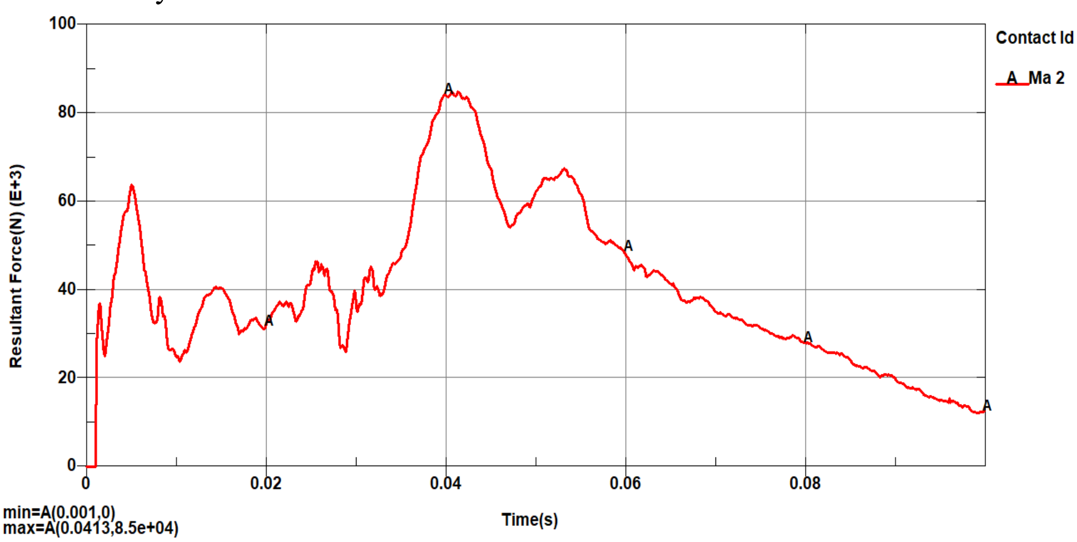

Figure 5.69. Modified TWV contact force at event of rear crush

5.10.6. Vehicle Velocity

The resultant velocity of the MDB AND TWV is shown in the Figure 5.70.

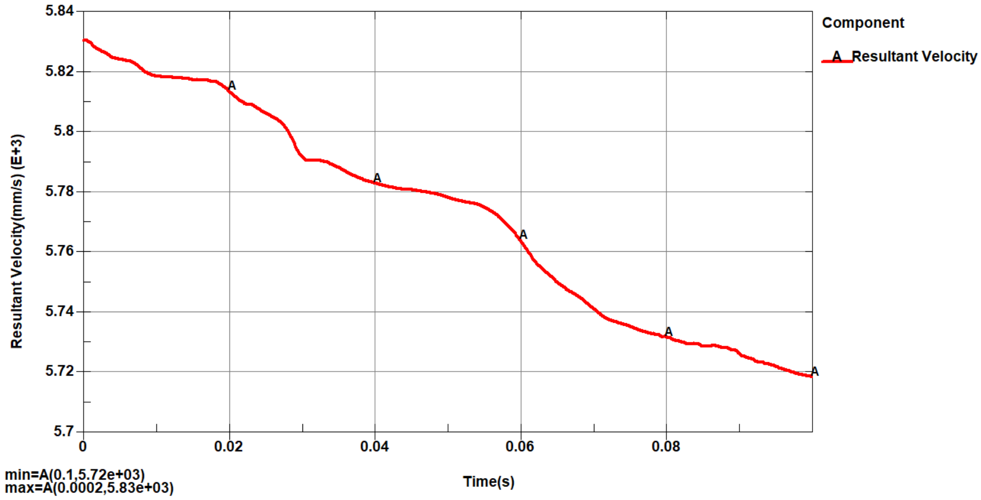

Figure 5.70. Modified TWV resultant velocity at event of rear crush

Initial the velocity time vs curve show the velocity of the MDB. As the collision process starts the velocity of MDB decreases and starts to push the TWV. As a result the motion of TWV created.

5.10.7 Verification

Energy ratio

The above values are validated by the energy ratio, which is equal with the ratio of the total energies to the sum of other energies. From the Figure 5.71, it can be observed that the energy ratio value ranges between 1 and 0.992. This range is within 1+/- 0.07. So the results are in the acceptable range.

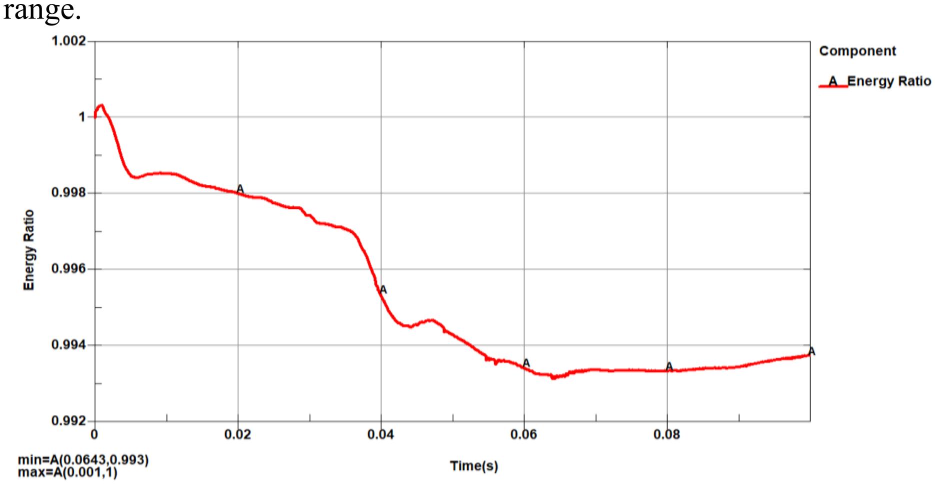

Figure 5.71. Modified TWV energy ratio at event of rear crush

5.10 Front collision

5.11.1 The analysis of the whole vehicle's distortion

The simulation result of modified model TWV frontal crush is presented and discussed. On Figure 5.72 and Figure 5.73. The Figure shows the distortion of the whole vehicle structure and the response of dummy at the time 0.1 s. On the modified initially the dummies are fitted with belts, and the front structure of TWV have bumper mudguard and bumpers. As it can be observed from the graph at t=0.025s, the first part of the TWV which is the mudguard (tire cover) starts to deform and absorbed energy and the dummies starts to show a little motion by moving backwards. As the collision event continues at t = 0.005s,the car front bumper reaches the front body structure of the TWV and deforms the steering linkages. At this time the occupants starts to experience the collision effect more as a result their body parts such as legs and spinal cord starts to move and hit seats. Due to the collision of the dummies with the inner parts of the TWV the inner structures starts to deform as shown at t=0.0075s. At these time the car will also hit the front portion of the chassis of TWV, as the chassis is more stiff then other parts of TWV, more energy is starts to transfer and this leads to jump effect of the car into the TWV. At final stage (t=0.1s), the jumping of the car on to the TWV continues, as a result the front tires of the TWV moves under the car front whereas the rear portion jump up. On another hand due to the seat belts the rear passenger is restrained with in its original position only with a little movement whereas the driver experience more impact force as it is relatively near to the collision area but due to the seat belts and the modification the movement and collision with the inner parts of the vehicle is limited

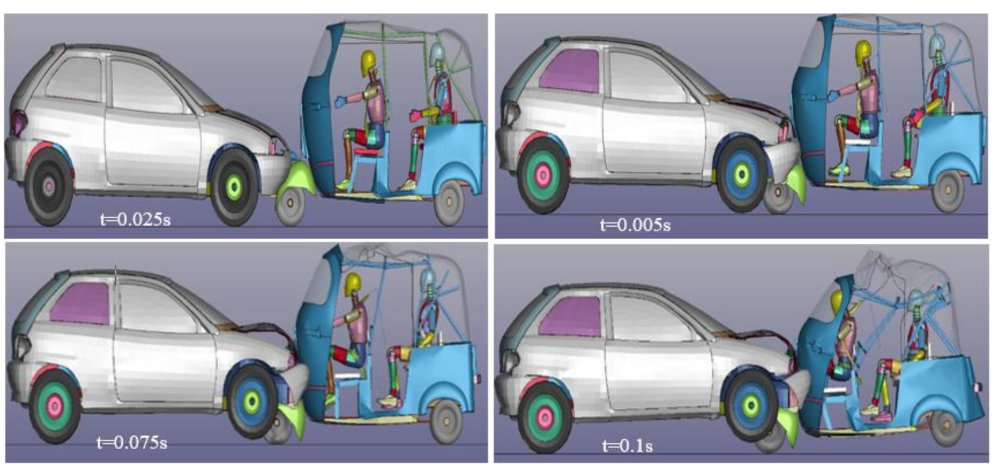

Figure 5.72. Sequence of front crush event

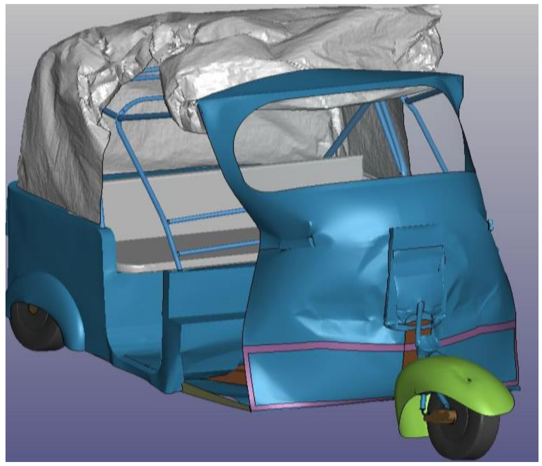

Figure 5.73.The appearance of the modified TWV at final state

5.11.2 Energy balance curve

The energy versus time plot of the total system is shown in Figure 5.74. As it is shown through the simulation the Conservation of energy principle is obeyed in which the amount of kinetic energy lost during impact is converted to other forms of energy such as internal energy, sliding energy and hour glass energy. An the total energy graph remain approximately constant .initially the kinetic energy is equal with total energy with value equal to 42.72 kJ but as the vehicles starts motion the KE value decrease and get converted into internal energy and other forms. As a result at final state it reaches energy value equal to13.1 kJ this indicate that 69.3 % of kinetic energy is lost and converted in to other forms of energy.

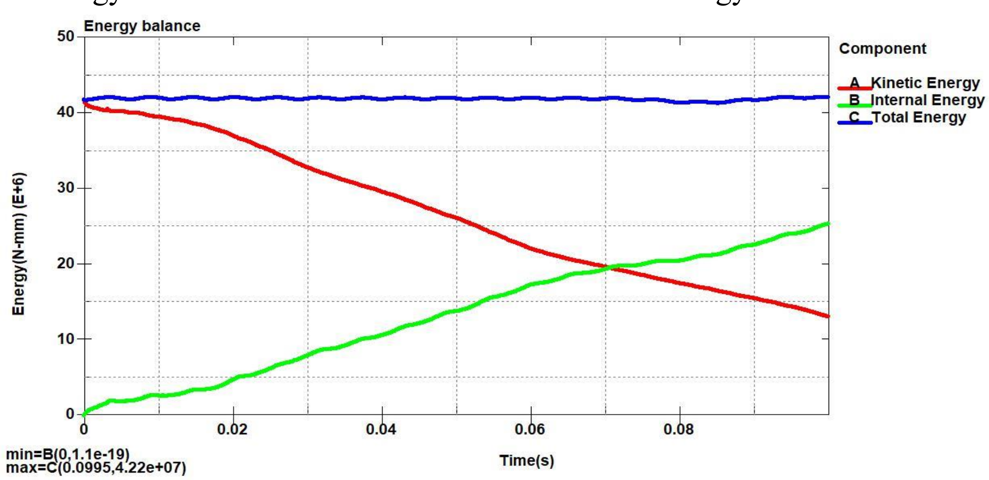

Figure 5.74. Modified model energy balance curve

Among the lost kinetic energies 25.4 kJ (85%) of energy is in the form of internal energy as shown Figure 5.75.

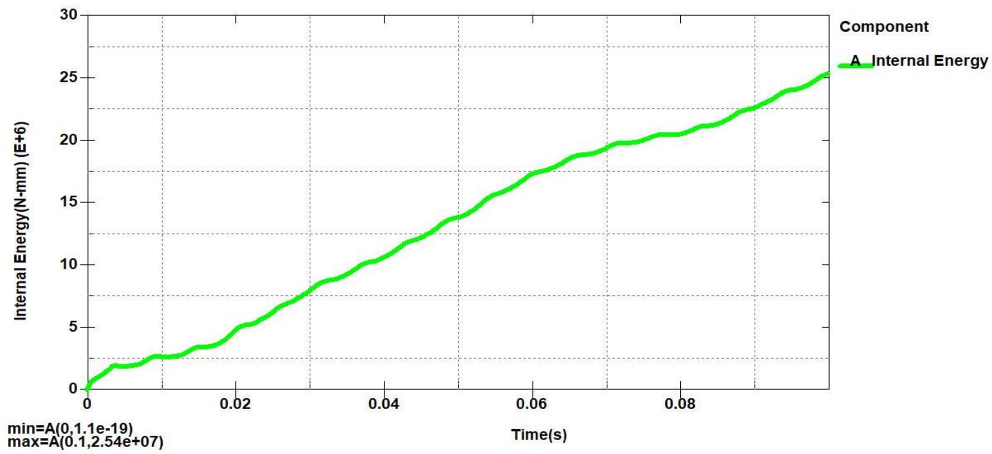

Figure 5.75. Modified model internal energy

5.11.3 Energy absorbed by modified TWV parts

Figure 5.73 shows the energy absorbed by the whole system, among the total the parts of the modified TWV contributes13.61 kJ of absorbed energy .this covers 53% of the total energy absorbed by the whole system. Figure 5.76 Show the energy absorbed by TWV parts with primary and secondary axis versus time. As indicated the parts listed under primary axis absorbed much of energy by covering 99.5% of the energy absorbed by TWV parts. The front structure (windscreens and front structure body) is responsible for most of the energy absorbed as it is very near to the collision contact area. It absorbs 4.74 or 33% of energy absorbed by TWV parts. The rest of the energy is absorbed by mudguard and front bumper, roof and support

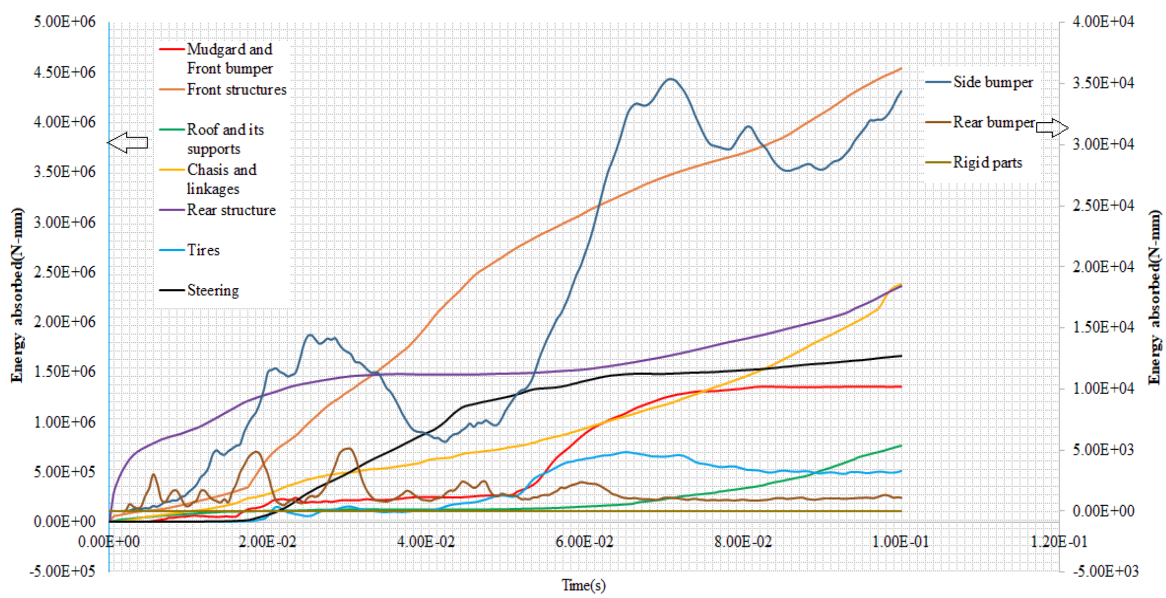

Figure 5.76. Energy absorbed by modified TWV parts

structure, chassis, rear structure tires and steering with 1.35kJ, 0.736 kJ, 2.38 kJ, 2.37 kJ, 0.515 kJ, 0.0344 kJ, 0.00103 kJ and 1.66 kJ of energy respectively. The modified front bumper and the mudguard absorbed 9% (1.35 kJ) of the total energy absorbed by TWV. This significantly helps on reducing the energy which is likely to be transferred to the occupants. They also reduce the deformation of the front structure the parts which are listed on the left axis or secondary axis have very less contribution in absorbing energy at event of front collisions .the rigid part includes the engine, foam and axles. This parts are the only parts with zero deformations due to the material model used for the simulation.

5.11.4 Displacement

Here the same method used with the existing model is applied to determine the Displacement of the drive and the passenger compartments. The longitudinal displacement of the passenger and driver compartments obtained by measuring shown on Figure 5.77 and Figure 5.78 respectively. From that we can know the maximum longitudinal displacement of the passenger compartment is about 12.6 mm as shown on Figure 5.77.

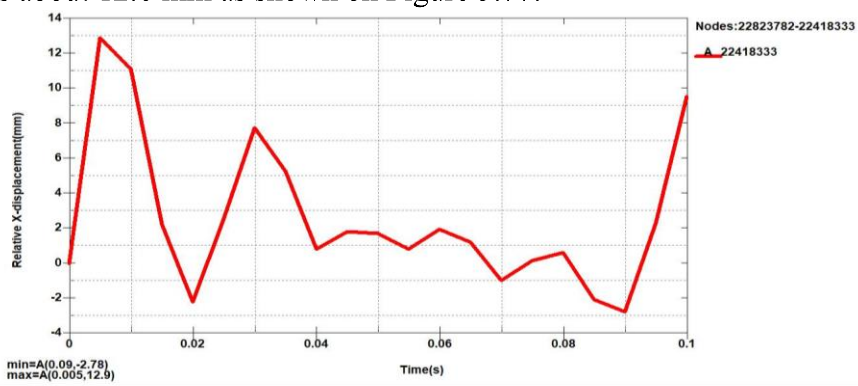

Figure 5.77. Displcement of Passanger compartment

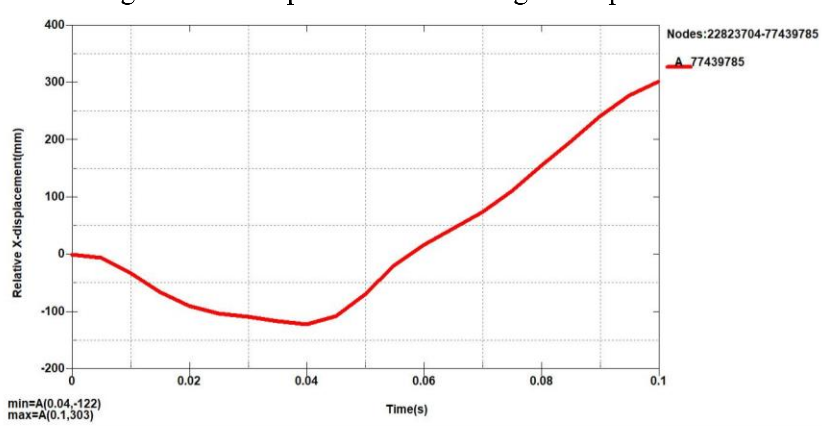

Figure 5.78. Displcement of driver compartment

It the fluctuation the elongation and compression or the back and forth movement of the compartment. This displacement is not enough to pose crisis to the living space of passenger. Maximum displacement of the driver compartment shown on Figure 5.78 is equal to 303 mm. This leads to the compression of the room. This show that the modified TWV driver compartment needs additional improvement at event of front crush.

5.11.5 Contact force

The contact force between the car and modified TWV is shown on Figure 5.79. As shown the Contact force pulse data shows one peak force at 0.06 s. This maximum peak force is equal to 68.7kN. This force is due to the high contact force occurred as the car is in contact with the front portion of the chassis of TWV and jump in to it.

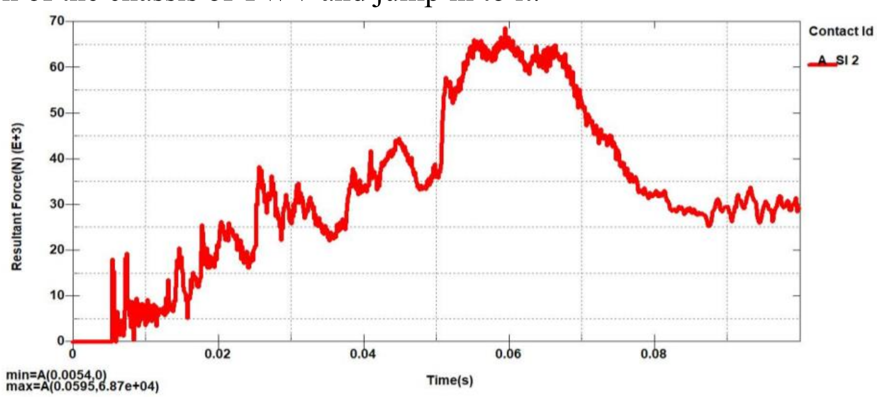

Figure 5.79. Modified TWV contact force

5.11.6 Resultant velocity

The resultant velocity of the whole system is shown on Figure 5.80. As it is shown the velocity before the start of the collision is equal to 2.82m/s but as it is indicates as the collision process

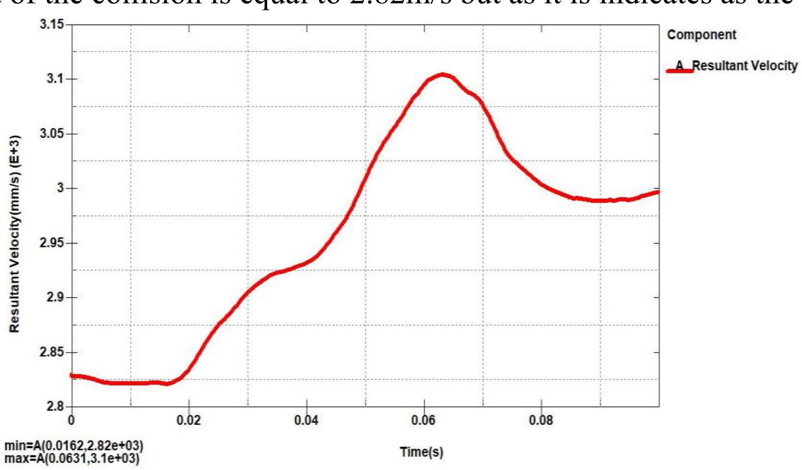

Figure 5.80. Resultant velocity

starts to take place the initial velocity value get increased and reaches final value of 3.1 m/s this maximum velocity value occur at appoint where maximum force occurs.

5.11.7 Verification

The above obtained values are verified by the energy ratio and ratio of TE/HE, the graphs are presented as follow:

Energy ratio

The energy ratio of the whole system is presented on Figure 5.81, the energy ratio value varies between 1.03 and 1.035. This value in the range stated by (Pezzucchi, 2016), so it is acceptable.

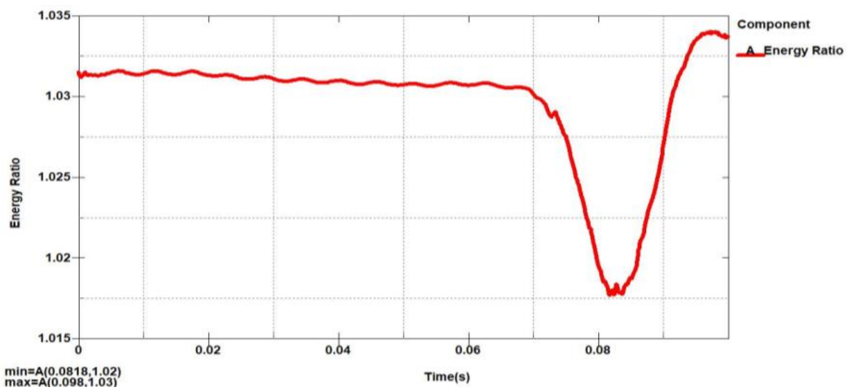

Figure 5.81. Energy ratio

Ratio of TE/HG

As it can be easily seen from Figure 5.82, the value of hourglass energy is very less as compared

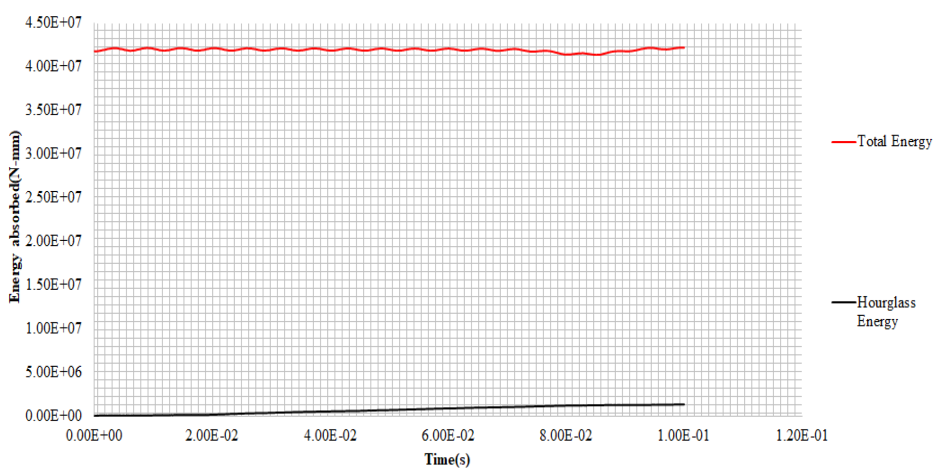

Figure 5.82. Ratio of HE/TE

To the total energy. The ratio resulted in 0.032 or 3%. According to the definition stated on (Gulavani et al., 2014), since the energy ratio is less than 5% so there results are acceptable.

5.11 Comparison between the existing and modified model of TWV

Under this section the crash worthiness ability of the existing and modified model will be compared. The comparison parameters are:

- The structural response,
- Displacement(Deformation)
- Energy absorption ability
- Force of impact

For each of the crush scenarios the comparisons are presented as follow.

5.12.1 Front crush

Structural and dummy response

Figure 5.83 shows the structural and dummy response of the existing and modified TWV for 0.1S.

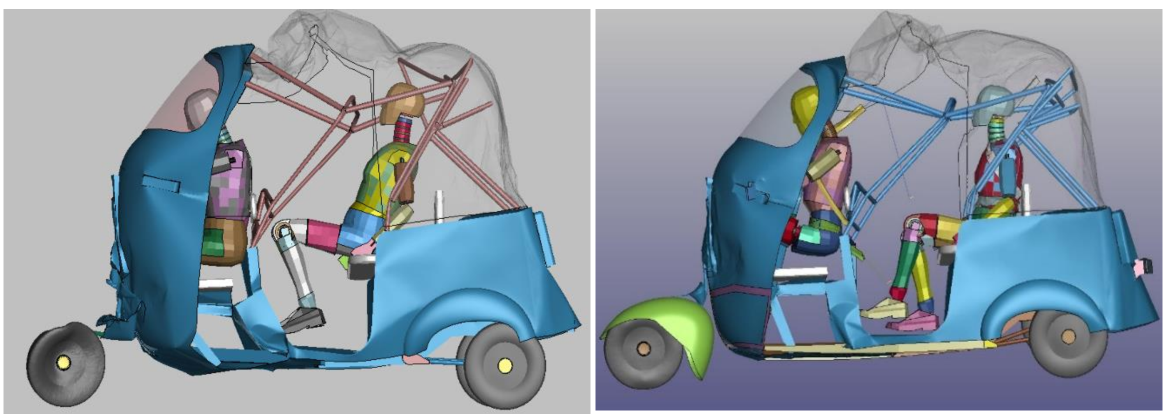

Figure 5.83. Structural and dummy response of the existing (a) and modified model (b)

As shown on Figure 5.83 At t= 0.1s, The dummies inside the existing model tends to move forward in hit the inner structure of the vehicles whereas the dummies inside the modified model move little bit as they are restrained by seat belt as indicated on Figures 5.83 b. The structural deformation of the existing TW vehicles looks more as compared to the modified for example the mudguard (tire cover) of the existing model damage to much whereas the very less for modified one. Generally the structural response and occupant's safety of the two TWV were determined by comparing the deformation of the occupant's living space remains after collision Figure 5.84 and Figure 5.85, Compares the structural deformation of the passenger and occupant living space the models respectively.

As shown on Figure 5.84, Maximum deformation occur at the existing passenger compartment with 31.9 mm but the modified model deformed with less value equal to 16 mm this indicate that the modified model provide better survival space and living place for the passenger at event of front crush.

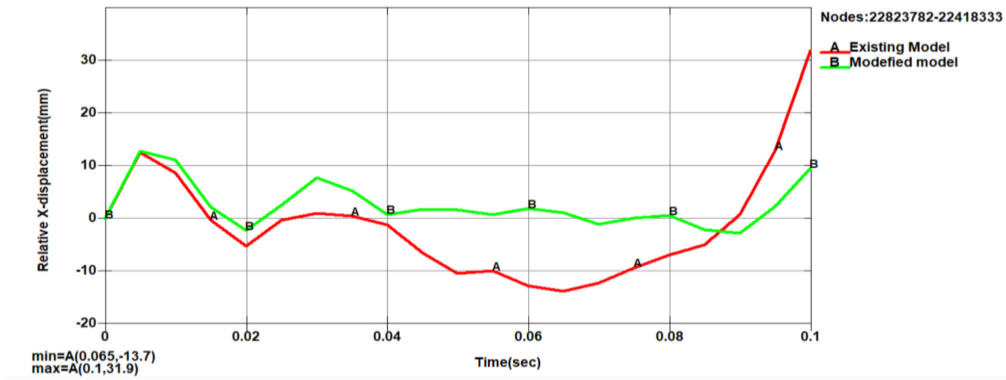

Figure 5.84. Passenger compartment displacement

The displacement of passenger compartment is shown on Figure 5.85. As shown, with the modified model the deformation is less whereas with the existing one it is more. The existing model deforms maximum of 308mm, and the modified produce 303 mm .This indicates during front crush, modified model provide better protection as comparing to the existing model.

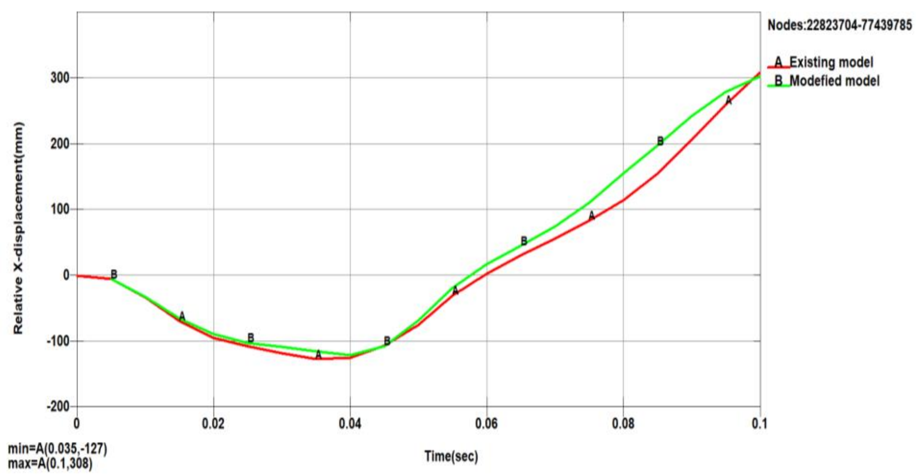

Figure 5.85. Driver compartment displacement

Internal energy

The total energy absorbed by the existing and modified model is shown on figure.as it can be seen the maximum amount of energy is absorbed during the existing model. This is due to the thickness of bumper beam used for the modification were more thicker, as a result they deformed less and produces less absorption. Their difference in absorption is 0.6 kJ. The absorption capacity of the modified model can be increased by decreasing the bumper beam thickness.

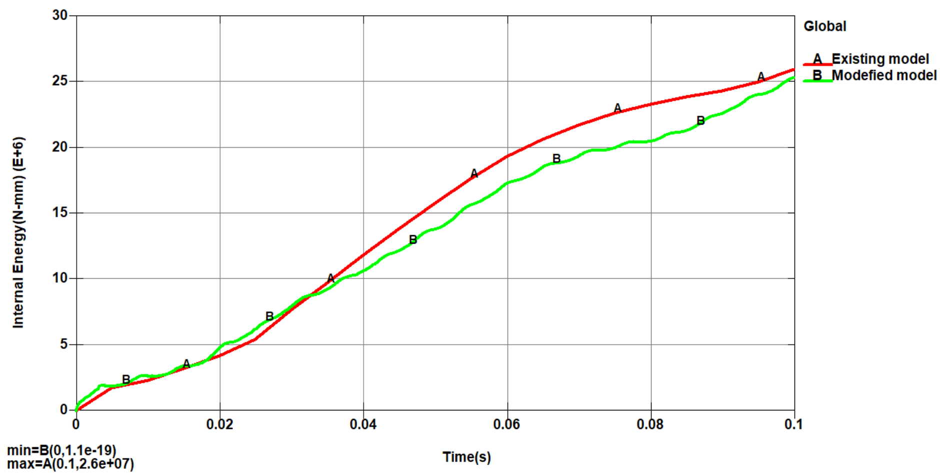

Figure 5.86. Internal energy of modified and existing model

Force of impact

In addition to internal energy, the force of impact for the existing model is better as shown on F igure 5.86. The maximum impact force occur on the modified model is equal to 68.7kN, whereas the existing produced 62.9 kN. This is also the stiffness of the bumper beam.

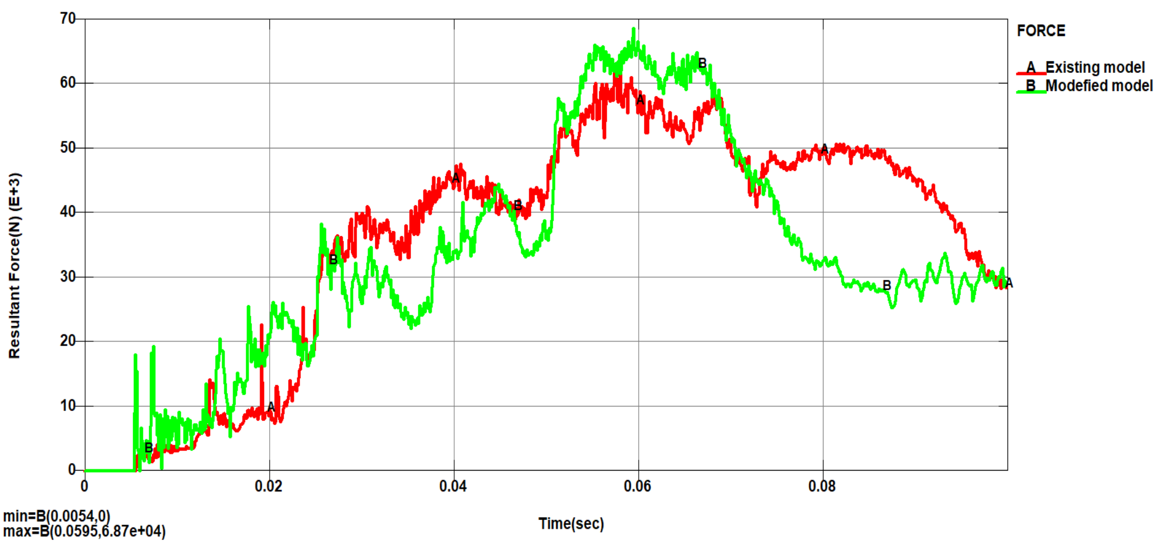

Figure 5.87. Force of impact for modified and existing model

The effect of the less energy absorption capacity and high force of impact of the Modified TWV model is improved by the use of less thickness bumper beam. However, the fact that the occupants inside the modified TWV were fitted with seat belt the injuries occurred is less as compared to the existing one.

5.12.2 Side crush

Structural response

Figure 5.88 shows the structural response of the existing and modified TWV for 0.1S. The parameter used to compare the structural response is the occupant's living space remains after collision

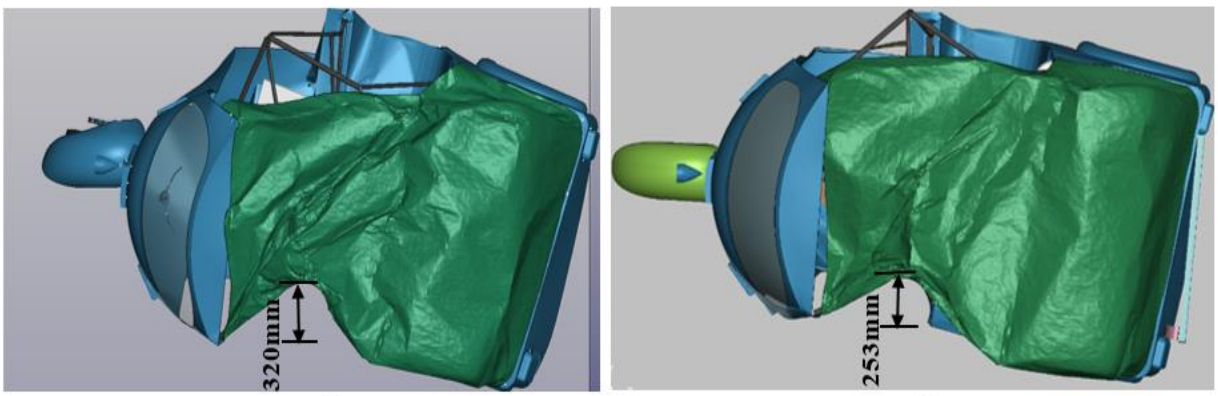

a b

Figure 5.88. Comparison of structural response

Figure 5.88 (a) shows the space remain for the existing model and b shows for the modified one. The pole intrude 320 mm in case of existing model and 253 mm in case of modified one. The original lateral spacing of the modeled before collision is 1250 mm. Subtracting the intruding distance from the original width will give as the remaining space the existing and modified TWV model remain with 930 mm and 997 mm respectively. This shows that the modified model have remain with more living space after side pole collision.

Displacement

The deformation results the existing and modified model is shown on Figure 5.89. The red line shows the displacement of the existing TWV and the green line indicate the modified model. The maximum deformation for existing model and modified model is equal to 345 mm and 286 mm respectively. It is clear that the maximum deformation occurs on the existing model For the modified model the maximum deformation occur to earlier at 0.055s and the decrease. whereas in case of the existing model the deformation increase linearly. This shows that there is reduction on energy in duration of 0.1s for the modified model.

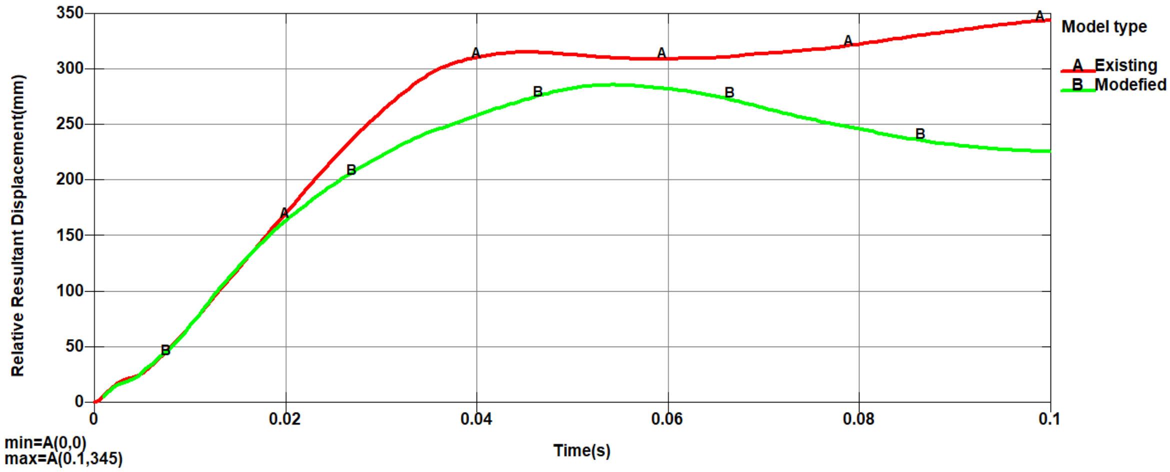

Figure 5.89. Comparison of displacement

Force of impact

The contact force between the TWV and the rigid pole is shown in the Figure 5.90. The red line indicates existing model and the green one shows the modified model force of impact.

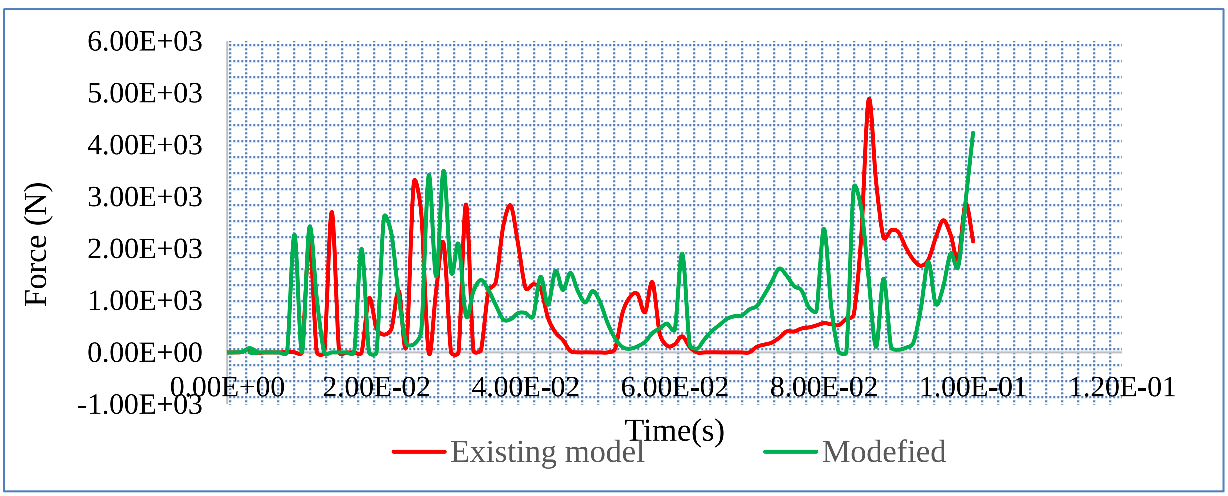

Figure 5.90. Comparison of force of the existing and modified TWV at event of side collision

As it is shown on the graph the maximum impact force occur at the existing model with value 4870N. The force on the modified model is equal to 4240 N and their difference equals 630 N. this much difference in force can create more momentum to the vehicle as a result the vehicle is highly damaged. Higher force of impact may cause more damaged to the passengers and the driver. So it can be concluded that the modified model will decrease the impact force on the driver as well as the occupants.

Energy absorption

The absorption ability of the modified and existing model is shown on Figure 5.91. Since the same conditions are applied in simulation of both models so that their energy absorption capacity of the models are determined by using the total internal energy graph.

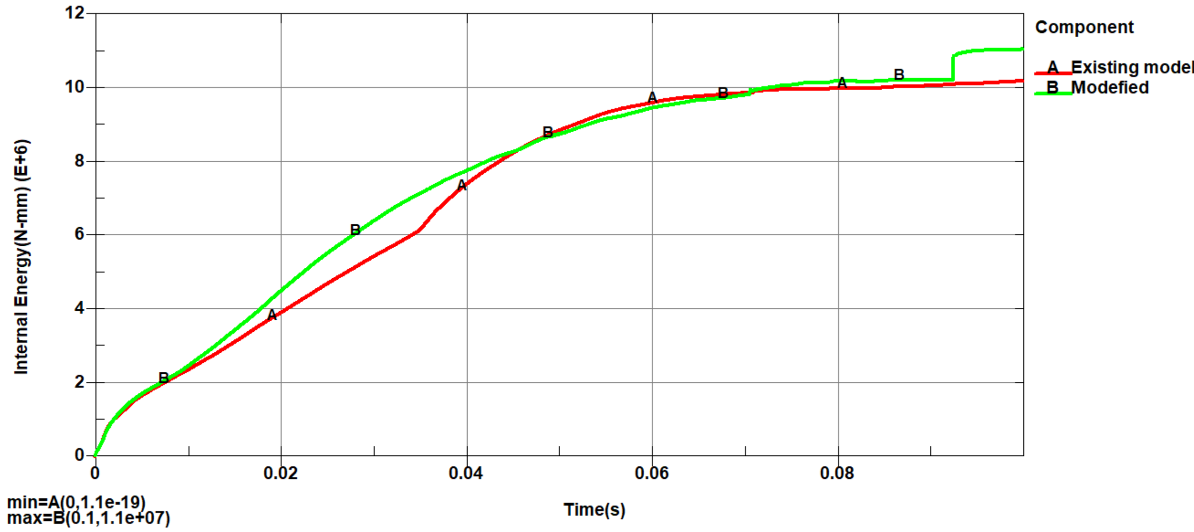

Figure 5.91. Comparison of internal energy

The models internal energies are shown with green (modified) and red lines (existing). As it is indicated on the graph among them maximum amount of kinetic energy is absorbed in case of modified model with value equal to 11kJ of internal energy. The existing model remain with 10.2 kJ. This show that for the same condition, the modified model have the ability to absorb more kinetic energy with less deformation. This helps in reducing the energy transferred to the occupants of TWV.

5.12.3 Rear impact

Structural response

The structural response of the modified and existing model to the rear crush event is shown Figure 5.92.For both cases, the remaining living space at final state (t=0.1s) is directly measured by taking two nodes at the front and rear point of the structure. As shown on the Figure 5.92 a and b, the structural deformation of the existing model is more as compared to the modified one. On the existing TWV model (Figure 5.92 a), the impact energy produced was transferred to the front structure and cause deformation in the front structure whereas in case of the modified model (Figure 5.92 b) the energy is absorbed more before transferring in to the front parts so that no deformation is observed at the front parts. To express the structural deformation numerically, the models are measured on the longitudinal direction in which the existing model remain with 1523 mm and the modified with 1624 mm. Their difference is equal to 101 mm. This mean that under the same condition, the rear structure of the existing TW vehicle is deformed more than the modified. This allows more intrusion in to the engine and other rear components and compartments. Since the rear structure of the modified TW vehicle model is deformed after the deformation of the rear bumper as a result it deforms less as compared to the existing i.e produces less intrusion.

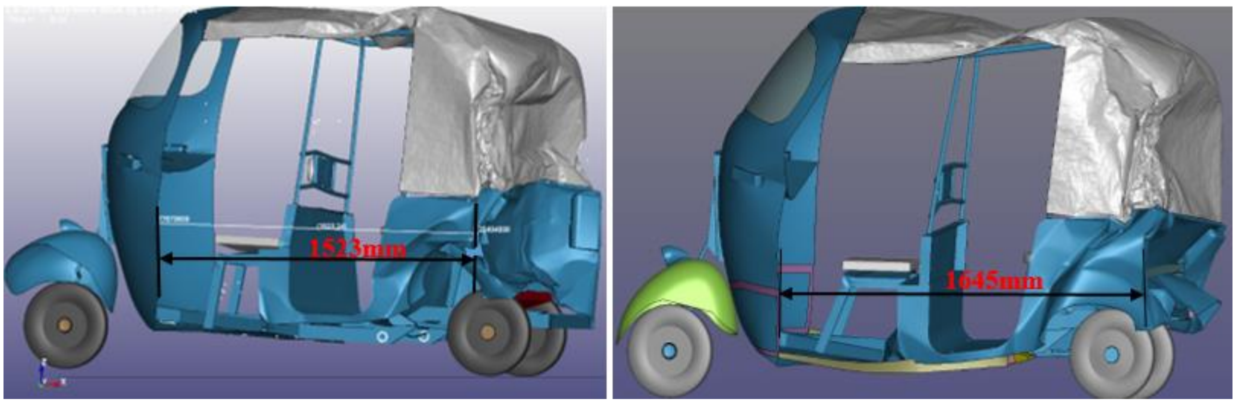

(a) (b)

Figure 5.92. Comparison of structural response

Deformation

The result of the longitudinal relative displacement measured between two nodes (one from front and other from rear body structure) is shown on Figure 5.93. The red line indicates the displacement of existing model and the green line implies the modified model. As show on the graph the existing model is subjected to maximum intrusion of 338 mm in longitudinal direction whereas the modified model shows maximum of 235mm.this shows that for the same condition. The modified model have high capacity of resisting deformation as compared to the existing one. Since deformation is measured by selecting nodes from rear body structure (excluding the rear bumper), modified model shows 0 deformation until the time reaches t=0.001s, this is because until t=0.1s the bumper is deforming in place of rear structure. This improve the protection of the rear components including the rear body structure. On another hand in case of the existing model when collision occurs there is no component to protect the rear body structure, so the body structure is the part which is responsible for protection of the parts in case of collision. As a result when collision occur at rear end TWV

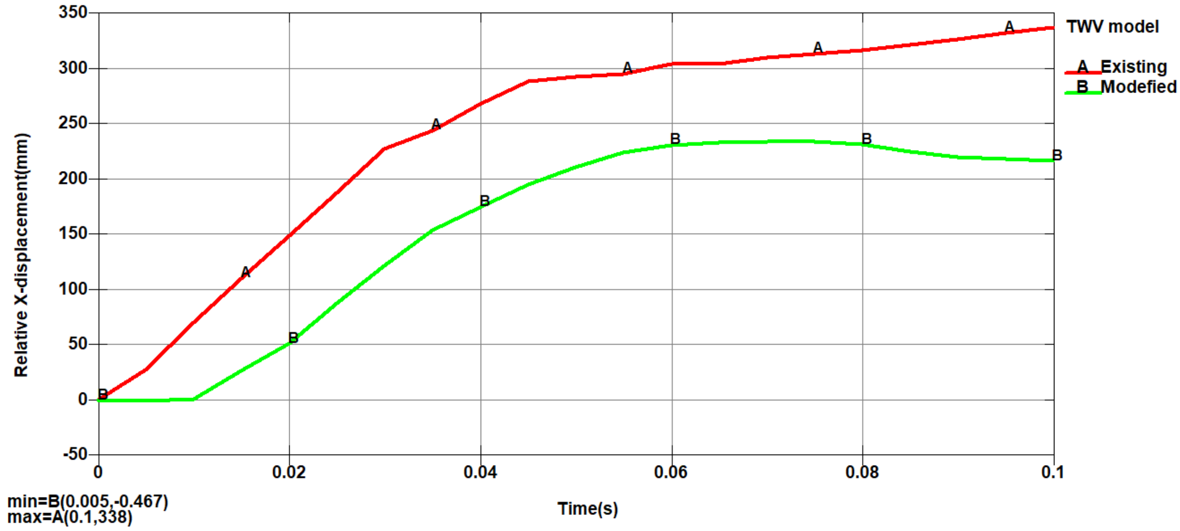

Figure 5.93. Comparison of longitudinal displacement

High deformation will immediately take places even with less impact force. So it can be concluded that when considering deformations the modified model is much better that the existing model.

Force of impact

The impact force is one of the measure of the injuries likely to happen on the occupants due to the collision. Less force of impact means that less energy is transferred to the occupant and higher force value means more damage is likely to happen.

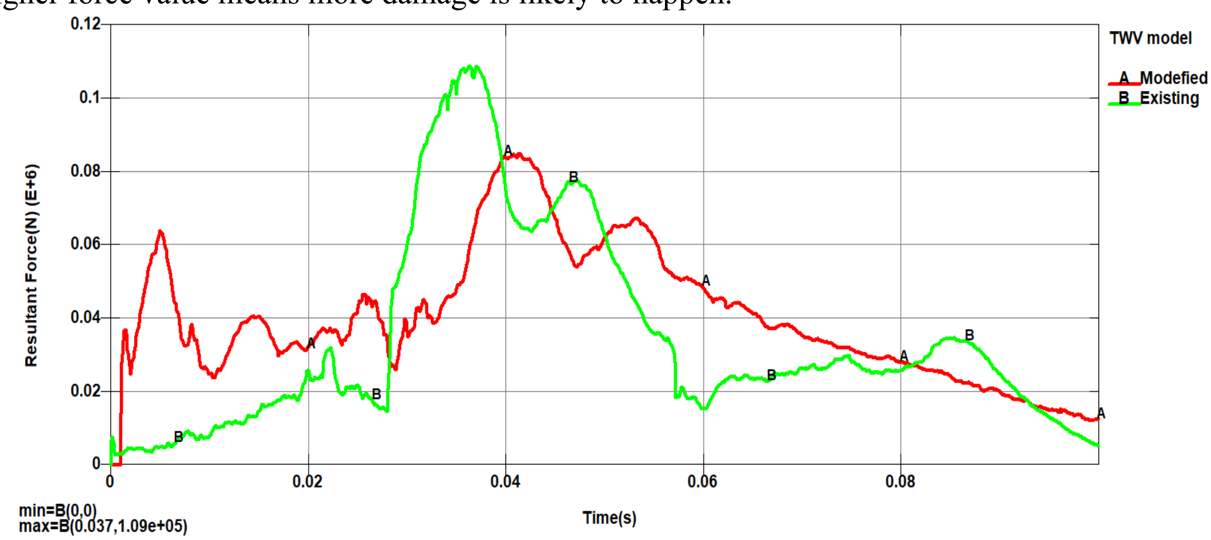

Figure 5.94. Comparison of resultant force

Figure 5.94 shows the impact force vs time for the existing and modified model. The modified model is indicated by red line and the existing with green color. As shown on the graph, for rear impact the modified model have maximum force value of 85 kN at t=0.45. On another hand the existing model produces maximum value of collision force equal to 109 kN , at t=0.037s. After this point the force will completely slow down.

This value is relatively high as compared to the existing model. The obtained force difference is equal to (0.024KN), which means that with the use of modified model, 0.024 KN of force is reduced from the vehicle body and occupants. With this much difference there will be a high chance of survival for the occupants as well as the vehicle parts. So here it can be concluded that when the existing and modified twv model were tested under the same condition, the modefied model relatively produces the desired less force, where as the existing model produces the undesired high impact of force.so that the modefied model is better when considering force of impact.

Internal energy

Internal energy is one of the main criteria to determine the crash worthiness of the vechile.it gives information about how much of energy (kinetic energy for this case) is absorbed by deformation of the vehicle. This helps in decreasing the impact energy which is likely to be transferred and cause problem to the occupants. Figure 5.95 Shows the energy absorbed by the existing model and modified model.as indicated on the graph, the final internal energy of the

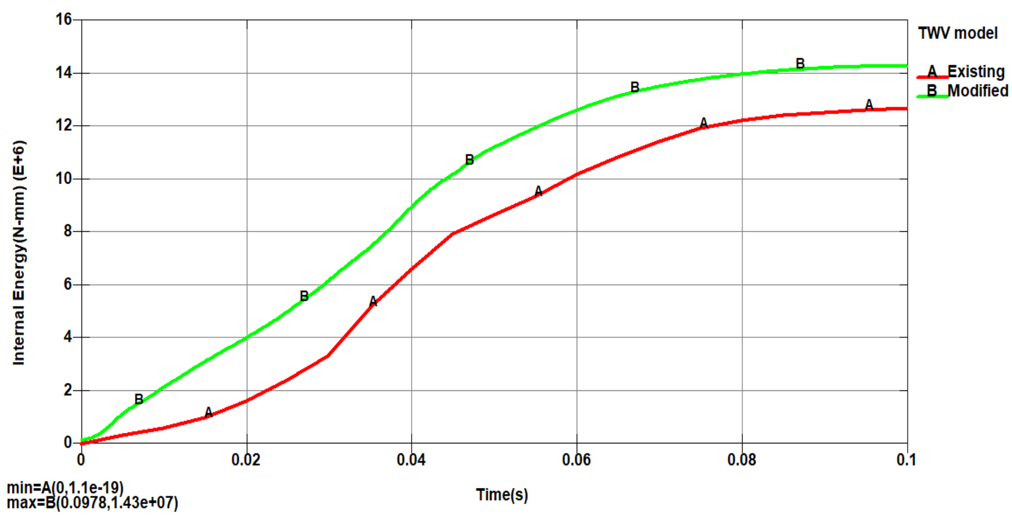

Figure 5.95. Comparison of internal energy

Existing model indicated using red line is equal with 12.7 kJ which covers 84% of the lost kinetic energy whereas the modified model absorbs 14.7 kJ of energy which converts 89% of the kinetic lost energy.

This indicate that the modefied model absorbe more energy as compared to the exsting model. This due to the bumpers fitted at the rear and side of the modefied twv.this componets will absorbe energy with less deformation. So finaly it can be colcluded that the modefied model produces the requred high energy absorbation capacity.

Generally, the comparison made between the existing and modified three wheeler vehicle model is summarized on the Table 5.1. For the front collision case the passenger compartment displacement is used for comparison of the Deformation. Vehicle with a good crashworthiness structure will absorbed more energy with less deformation and impact force. As it can be seen on the Table 5.1 the result of the deformation, impact force and energy absorption of the modified model is better in condition of side and rear collision than that of the existing three wheeler vehicle. But in case of front collision the energy absorption of the modified model is less that the existing, and also the force of impact is more. This is due to the usage of thicker bumper beam at the front. The effects of the above disadvantages of the modified model is over comes by the application of seat belt which restrained the motion of the occupants. So that it can be concluded that modified model have better crashworthiness performance in each of crush scenarios as compared to the existing model.

Table 5.1. Results of the beam

	Front beam	Rear beam	Side beam
Maximum Deformation	130mm	80mm	27mm
Maximum Impact force	0.17kN	0.41N	0.27N
Maximum Energy absorption	3.2kN	3.5J	3.25J
Maximum Resultant displacement	235mm4	180mm	32mm
Von Moises stress	2604mpa	2601mpa	3781mpa

The results of the beam which are mounted on as a bumper on the TWV structure were summarized on Table 5.1.

Table 5.2. Summary of compression between existing and modified TWV model

		Existing TWV model	Modified TWV model
Front head on collision	Maximum deformation(mm)	32	16
	Maximum Impact force (kN)	62.9	68.7
	Maximum Internal energy(kJ)	26	25.4
Side pole collision	Maximum deformation(mm)	345	286
	Maximum Impact force(kN)	4.87	4.24
	Maximum Internal energy(kJ)	10.2	11
Rear end collision	Maximum deformation(mm)	338	235
	Maximum Impact force(kN)	109	85
	Maximum Internal energy(kJ)	12.7	14.3

CHAPTER SIX
CONCLUSION AND RECOMMENDATION

6.1 Conclusions

This research was to establish FEA model of an auto rickshaw to improve the crashworthiness of existing TWV through a series of different impact simulations. This study clearly states the problems exist on TWV at event of different crush scenarios. It also shows the occupant response at event of different collision configurations. Thus, several standards and regulations are used to computationally analyze the crashworthiness of the current TWV. The front, side, rear and frontal collision of the existing TWV is analyzed. In addition, based on the results obtained from the existing model an attempt was made to modify the structural crashworthiness of the vehicle and occupant safety. As a result, the modified TWV has improved crashworthiness features and better occupant's safety protections. Key findings are summarized as follows:

In case of side collision;

- The structure of the modified model has produced more living space than that of the existing model by only deforming 250 mm whereas the existing model deformed 320 mm this shows that at event of side collision the modified model provides more protection to the occupants and the vehicle sensitive parts.

- The force produced due to the collision of the vehicle in to the pole is less for the modified model. A reduction of 630N force was obtained by the implementation of the modifications. The reduction of contact force resulted in reduced rate of transferred impact energy to the occupants.

- The modified model also absorb more energy than the exiting model. It absorbed additional 0.8 kJ energy.

In cases of rear collision

- Since the modified model is fitted with rear bumper, so it reduces intrusion in to the rear compartment of the vehicle. It deformed less with 102mm difference, as a result 30% more protection was obtained for rear parts such as fuel tank and engine.

- The rear bumper is made up with composite material and this lead to a more absorption of energy with less deformation. Totally the energy absorption of TWV was increased with amount of 1.6 kJ. As a result less energy is transferred to the occupants with use of modified model.
- With the use of modified model, the force of impact was reduced by 22%, consequently the occupants inside the modified model experience less injures as comparing to the existing TWV.

In case of front collision

- The modified model shows better protection by deforming less as compared to the existing model, it doubles the driver living space or compartment after collision, although for the driver it improves the compartment space by providing additional 10mm space after collision.
- On another hand, the total energy absorbed by the existing is more for existing model, in addition the force of impact is also less. This is due to the thickness of bumper beam used for the modification were thicker, as a result they deformed less and produces less absorption and high impact force as compared to the existing one. The existing model provide 8.4% less force and 2.3% more energy absorption. The absorption capacity of the modified model can be increased by decreasing the bumper beam thickness.
- The effect of the less energy absorption capacity and high force of impact of the modified TWV model is improved by the use of less thickness bumper beam. However, the fact that the occupants inside the modified TWV were fitted with seat belt the injuries occurred is less as compared to the existing one.

In addition to the above finding the roof of the existing model was analyzed for roof crush strength and the result indicted that the roof structure of the TWV is poor to protect the occupants at event of rollover crushes.

6.2 Recommendation

Based on the studies done on this paper the following points are recommended:

- It can be observed that with little modification the safety of the current TWV can be modified, so that the owners and manufacturers shall implement some of the safety developments concepts discussed on this paper to improve the crash worthiness of the TWV.
- As the study shows even with less speed the TWV has causing more sever damages, so it is better if the government and concerning bodies implement the crash and safety regulation for TWV which were mostly used for car segment.

6.3 Recommendation for future work

Considering the extensive review of the existing research limitations and results the motivations for future research are suggested as follows:

- The present work evaluated the crash behavior of existing three wheeler vehicles by considering the response of occupants and this work can be extended to evaluating the injuries levels to occupants at different crush scenarios
- This work does not include the effect of rear impact on rear components of the TWV such as fuel tank, so the effect of rear collision on rear components of the vehicle can be studied.
- In addition, on this study the improvement of the roll over resistance of TWV is not accomplished, so the modification of TWV roof structure at event of roll over can be made.

Research Fund Acknowledgment

This research project is funded by Adama Science and Technology University under the grant Number ASTU/SM-R/320/21, Adama, Ethiopia.

REFERANCE

A. Chawla, s. Mukherjee, d. Mohan, jasvinder singh, n. R. (1997). *Crash simulations of three wheeled scooter taxi (tst) a.*

Alex ogana. (2009). *Nhtsa and iihs crash test scores explained.*. Https://www.autoevolution.com/news/nhtsa-and-iihs-crash-test-scores-explained-4239.html

Ambati, t., srikanth, k. V. N. S., & veeraraju, p. (2012). Simulation of vehicular frontal crash-test. *International journal of applied research in mechanical engineering*, *1*, 262–267. Https://doi.org/10.47893/ijarme.2012.1047

Asefa, f., assefa, d., & tesfaye, g. (2014). Magnitude of, trends in, and associated factors of road traffic collision in central ethiopia. *Bmc public health*, *14*(1), 1–11. Https://doi.org/10.1186/1471-2458-14-1072

Babu, a. D., rajesh, k., & tech, m. (2020). *Impact analysis of an automobile bumper*.

Basavaraju, d. H. (2005). *Design and analysis of a composite beam for side impact*. *December*.

Belts, c. S., makes, w., & different, t. (2021). *4 types of car seat belts what makes them different 4 types of car seat belts – what makes them*. 1–7.

Cassia, r. De, araújo nunes, m. A. De, & s. Oliveira, a. B. De. (2015). Numerical simulation of roof crush test for assessing passenger damage in rollover situation: rops device evaluation. *International journal of engineering science & advanced technology*, *5*(3), 160–170.

Chatla, p. (2012). Ls-dyna for crashworthiness of composite structures. *Aerospace engineering*, *master*, 101.

Chawla a, m. S. And m. D. (2020), *3 wheeler*. 2002–2004.

Chawla, a, mukherjee, s., mohan, d., kumar, r., & gavade, t. (2001). Fe simulation studies of a three-wheeled scooter taxi. *Mechanical engineering*.

Chawla, anoop, mukherjee, s., & mohan, d. (2001). Impact biomechanics in two wheeled and three wheeled vehicles. *Simulation*, 110016–110016.

Cheng, z. Q., thacker, j. G., pilkey, w. D., hollowell, w. T., reagan, s. W., & sieveka, e. M. (2001). Experiences in reverse-engineering of a finite element automobile crash model. *Finite elements in analysis and design*, *37*(11), 843–860. Https://doi.org/10.1016/s0168-

874x(01)00071-3

Dange, m. V, buktar, r. B., & raykar, n. R. (2015). Design and analysis of an automotive front bumper beam for low-speed impact. *Iosr journal of mechanical and civil engineering ver*, *12*(2), 2320–2334. Https://doi.org/10.9790/1684-12241727

Datti, d. H., nallamothu, r. B., mitiku, g., siraj, a., & fentaw, g. (2021). Design and analysis of front axle of truck at different driving conditions. In *recent advances in sustainable technologies* (pp. 195-206). Springer, singapore.

Desapriya, e. (2011). Vehicle safety standards. *Traffic safety*, 201–222.

Driverseducationusa.com. (2021). *What forces are involved in a crash ?* 1–2.

Dynasupport.com, p. (2021). *2 . Detecting penetrations 3 . Initial penetration 4 . Need for penetration-free simulation model at first cycle 5 . Default treatment to the handle initial penetrations in node / segment contact 6 . Advantages and disadvantages of the default initial pen*. 1–5.

Elmardi suleiman khayal, o. M. (2019). Literature review on the history of bajaj rickshaw vehicles. *Global journal of engineering sciences*, *3*(2). Https://doi.org/10.33552/gjes.2019.03.000560

Enawgew, d. (2013). *Addis ababa institute of technology addis ababa , ethiopia strength analysis of three wheeled vehicle ' s chassis and body frame assembled in ethiopia by a thesis submitted to school of mechanical and industrial engineering presented in partial fulfillmen*.

Eromo, b. (2017). *School of mechanical , chemical and material engineering improvement of structure and body of three wheeler vehicle a thesis submitted in partial fulfillment of the requirements for the award of the degree of master of science in automotive engineering by*.

For, g., & vehicle, a. (2021). *Guidelines for authorizing vehicle*. 1–4.

Friedman, k., & hutchinson, j. (2009). Review of existing repeatable vehicle rollover dynamic physical testing methods. *Asme international mechanical engineering congress and exposition, proceedings*, *16*, 51–59. Https://doi.org/10.1115/imece2008-68751

Gehre, c., vetter, d., & appel, h. (2001). Protection of the lower extremities in two and three wheelers with safety cell. *17th international technical conference on the enhanced safety* *of vehicles*, 1–8. Http://www-nrd.nhtsa.dot.gov/pdf/nrd-01/esv/esv17/proceed/00200.pdf

Georgiou, g., & zeguer, t. (2018). On the assessment of the macro-element methodology for full vehicle crashworthiness analysis. *International journal of crashworthiness*, *23*(3), 336–353. Https://doi.org/10.1080/13588265.2017.1328723

Global road safety partnership. (2007). Drinking and driving: a road safety manual for decision-makers and practitioners. *Alcohol world*, *14*(1), 1–149.

Guha, s., dbhalsod, d., & krebs, j. (2011). *Lstc hybrid iii 50th fast dummy*.

Gulavani, o., hughes, k., & vignjevic, r. (2014). Explicit dynamic formulation to demonstrate compliance against quasi-static aircraft seat certification loads (cs25.561) -part i: influence of time and mass scaling. *Proceedings of the institution of mechanical engineers, part g: journal of aerospace engineering*, *228*(11), 1982–1995.

Gurit holding ag. (2000). Guide to composites. *Available in url: http://www. Netcomposites. Com/ …*, 74. Http://www.gurit.com/guide-to-composites.aspx

Haslegrave, c. M. (1974). Dummies for crash testing motor cars. *Applied ergonomics*, *5*(3), 153–160. Https://doi.org/10.1016/0003-6870(74)90352-4

Hollowell, w. T., gabler, hampton c. Stucki, sheldon l. Summers, s., & hackney, j. R. (2009). Updated review of potential test procedures for fmvss no. 208. *Updated review of potential test procedures for fmvss no. 208*, *15*(1), 5–19.

Hu, y., liu, c., zhang, j., ding, g., & wu, q. (2015). Research on carbon fiber-reinforced plastic bumper beam subjected to low-velocity frontal impact. *Advances in mechanical engineering*, *7*(6), 1–15. Https://doi.org/10.1177/1687814015589458

Inani, s., & bisen, a. M. (n.d.). *Aesthetical body design of three wheeler e-rickshaw*.

Jeong, s. B., yi, s. I., kan, c. D., nagabhushana, v., & park, g. J. (2008). Structural optimization of an automobile roof structure using equivalent static loads. *Proceedings of the institution of mechanical engineers, part d: journal of automobile engineering*, *222*(11), 1801–1811. Https://doi.org/10.1243/09544070jauto855

Karanam, v. M., & ghosal, a. (2013). Studies on the wobble mode stability of a three-wheeled vehicle. *Proceedings of the institution of mechanical engineers, part d: journal of automobile engineering*, *227*(8), 1200–1209. Https://doi.org/10.1177/0954407012469498

Kokate, v. L., uttekar, s. S., karandikar, p. B., & holmukhe, r. M. (2020). Retrofitting of auto rickshaw to e-rickshaw - a feasibility study. *2020 1st international conference on power, control and computing technologies, icpc2t 2020*, *january*, 229–234. Https://doi.org/10.1109/icpc2t48082.2020.9071492

Krishnamoorthy, s. K. (2009). *Co py rig ht by am or py rig ht by*. 1–13.

Krishnamoorthy, s. K., kopp, g., german, f., concepts, v., & tel, s. (2011). *Co py rig ht by am or e co py rig ht am or*. 1–9.

Kumar, k. N. K., raja, a., chander, p. R., reddy, y. M. M., & vivekananda, k. (2019). Design evaluation & improvement analysis of vehicle structural crashworthiness using cae in iihs frontal crash test. *International journal of engineering and advanced technology*, *9*(1), 1575–1582. Https://doi.org/10.35940/ijeat.f8597.109119

Kunle, m. A., farah, m. J., ahmed, a. /hakim, & mohamed. (2019). *Auto rickshaw impacts with pedestrians - a computational analysis of post- collision kinematics and injury mechanics a thesis submitted to cardiff university for the degree of doctor of philosophy by*. *September*.

Kweon, y.-j. (2020). *Evaluation of fmvss no . 216a , roof crush resistance , upgraded standard*. *216*.

Lefer, b., & rebolloso, i. (2012). *Car-to-truck frontal crash compatibility*. Http://publications.lib.chalmers.se/records/fulltext/160351.pdf

Liu, y. P. (2013). Simulation of vehicle's frontal crash with dummy inside. *Advanced materials research*, *760–762*(iccsee), 1244–1249. Https://doi.org/10.4028/www.scientific.net/amr.760-762.1244

Livermore, & corp, software, t. (2021). *Ls-dyna*. 1–5.

Ljungberg, m., nybacka, m., & gómez, g. G. (2015). *- n pr on ly iew ot di s tr ibu - n iew on ly pr ot for di s tr ibu tio n*. *2*(1). Https://doi.org/10.4271/2020-28-0490.ragul

Ls-dyna support site. (2021). *Welcome to the ls-dyna support site*. 10–11.

Lst, v., is, c. S. I. D. I., beta, d. V, & maurath, c. (2009). *Lstc sid - iis - d finite element model*.

Lstc. (2012). *Modeling of composites in ls-dyna*. 1–12. Http://ftp.lstc.com/anonymous/outgoing/jday/composites/mat_comp.pdf

Mahadevan, s., & liu, x. (1996). Optimization of composite structures for reliability requirements. *6th symposium on multidisciplinary analysis and optimization*, 162–167. Https://doi.org/10.2514/6.1996-3999

Mama gasu, a. (2019). Evaluation of road traffic accidents in moyale town, oromia regional state, ethiopia. *International journal of transportation engineering and technology*, *5*(1), 1. Https://doi.org/10.11648/j.ijtet.20190501.11

Manual, k. U. S., & ii, v. (2012). *Keyword user ' s manual volume ii: vol. Ii* (issue february).

Mukherjee, a. . C. & s. . (2003). Projects of the simulation & control group (a . Chawla & s . Mukherjee). *Group*, 1–7.

Mukherjee, s., mohan, d., & gawade, t. R. (2007). Three-wheeled scooter taxi: a safety analysis. *Sadhana - academy proceedings in engineering sciences*, *32*(4), 459–478. Https://doi.org/10.1007/s12046-007-0035-5

Nhtsa crash test - consumer reports. (2021). *Nhtsa crash test 101*. 1–4.

Nilesh dhole, v. Y. And g. O. (2012). Certification by analysis of a typical aircraft seat. *12th international ls-dyna users conference*, *2*, 1–12. Http://www.dynalook.com/international-conf-2012/automotive22-a.pdf

Nsw.gov.au/topics/government. (2021). *Modifed and non-standard vehicles*. 1–8.

Osendorfer, h., & rauscher, s. (2001). The development of a new class of two-wheeler vehicles. *17th international technical conference on the enhanced safety of vehicles*, 1–10. Http://www-nrd.nhtsa.dot.gov/pdf/nrd-01/esv/esv17/proceed/00055a.pdf

Patil, s. J., ashoka, t., tavildar, r. K., & kulkarni, a. A. (2018). *Roof crush resistance of passenger vehicle*. *3*(6), 200–204.

Predictive engineering goods, c. (2020). *The advanced simulation tool for nonlinear , linear , dynamic , and static analysis ls-dyna*. 1–16.

Rahman, a., & babu, d. P. (2019). *Simulation of car frontal fascia during crash using ls-dyna*. *8*(07), 616–622.

Redscan. (2017). What is a penetration test? *Redscan blog*, *mar*, 1–10. Https://www.redscan.com/news/what-is-a-penetration-test/

Sayalimankar. (2018). *Comparative evaluation of steel and composite side impact beams at low speed impact abstract :* *4*(5), 57–61.

Schweizerhof, k. (n.d.). *Crash_composites_paper.pdf*.

Sheldon, a. (2018). *Co py ht by am or py rig by am or*.

Singh, h. (edag i. . (2012). Mass reduction for light-duty vehicles for model years 2017-2025 final report. *Report no. Dot hs 811 666*, *august*, 582.

Srikanth, k. M., & prakash, r. V. (2009). Assessing the structural crashworthiness of a three-wheeler passenger vehicle. *The 2nd international conference on research into design.*, 152–159.

V.teja, j.goutham raj, k. R. (2019). *Design and analysis of car roof crush*. *09*(2), 1–8.

Vadysinghe, a. N., herath, b., kasun, m., katugaha, d., & piyarathna, c. (2018). Injury patterns and causes of death among occupants of three-wheelers succumbed to their injuries from road traffic accidents in sri lanka. *International journal of medical toxicology and forensic medicine*, *8*(2(spring)), 55–64. Https://doi.org/10.22037/ijmtfm.v0i0.20803

Vedantam, r. (2018). *Automotive rear-end crash simulations according to fmvss 310r for evaluation of structural damage and prediction of occupant potential injuries through linear regression*. *December*.

Waghmare, s. A. Deshmukh, p. D. Kulkarni, s. S. (2013). Roof crush analysis for improving occupant safety. *International journal of advanced engineering research and studies*, *216*(216), 1–5. Http://www.technicaljournalsonline.com/ijaers/vol iii/ijaers vol iii issue i octber december 2013/371.pdf

Wang, t., & li, y. (2015). Design and analysis of automotive carbon fiber composite bumper beam based on finite element analysis. *Advances in mechanical engineering*, *7*(6), 1–12. Https://doi.org/10.1177/1687814015589561

Xu, t., sheng, x., zhang, t., liu, h., liang, x., & ding, a. (2018). Development and validation of dummies and human models used in crash test. *Applied bionics and biomechanics*, *2018*. Https://doi.org/10.1155/2018/3832850

Yadav, s., & pradhan, s. K. (2014). Investigations into dynamic response of automobile components during crash simulation. *Procedia engineering*, *97*, 1254–1264. Https://doi.org/10.1016/j.proeng.2014.12.404